CHEMICAL CHARACTERIZATION AND QUANTIFICATION OF ORGANIC AEROSOLS: ADDRESSING STORAGE EFFECTS AND PEROXIDE QUANTIFICATION

Inauguraldissertation

zur
Erlangung der Würde eines Doktors der Philosophie
vorgelegt der
Philosophisch-Naturwissenschaftlichen Fakultät
der Universität Basel von

Julian Resch

2024

Genehmigt von der Philosophisch-Naturwissenschaftlichen Fakultät auf Antrag von:

Prof. Dr. Markus Kalberer (Erstbetreuer)

Prof. Dr. Moritz Lehmann (Zweitbetreuer)

Prof. Dr. Alexander Vogel (Externer Experte)

Basel, 17.09.2024

Prof. Dr. Marcel Mayor (Dekan)

CHEMICAL CHARACTERIZATION AND QUANTIFICATION OF ORGANIC AEROSOLS: ADDRESSING STORAGE EFFECTS AND PEROXIDE QUANTIFICATION

Dissertation submitted for the degree of Doctor in Philosophy

Julian Resch

Supervised by Prof. Dr. Markus Kalberer
Co-supervised by Prof. Dr. Moritz Lehmann
External expert Prof. Dr. Alexander Vogel

2024

In gratitude to my parents.

Acknowledgements

First and foremost, I would like to express my immense gratitude to my supervisor, Markus Kalberer, for giving me the opportunity to conduct my Ph.D. in his group and for his unwavering support, guidance, patience, and mentorship. From the numerous times I knocked on his door with questions about science and chemistry, which he always took the time to answer thoroughly, to the opportunity and trust to work independently in our LC-MS lab, and his warm welcome, introduction, and explanations of the swiss way of life. I also want to thank him for believing in me, even though I had a background in physics and chemistry was not my expertise. I truly could not have asked for a better supervisor, and I hope many students after me will appreciate how great an opportunity it is to work alongside him.

I also want to thank Moritz Lehmann for being my second supervisor and Alexander Vogel for being my external expert. Thank you for finding the time to read my thesis and attending my Ph.D. defense.

Furthermore, I want to thank the entire atmospheric science group at the University of Basel. Without their help, I would not have managed to finish my Ph.D., and it would not have been as fun and enjoyable. I especially want to thank the Post-Docs who worked with me during this time, Kate Wolfer and Kangwei Li. I believe it is their guidance and collaboration that has brought me to where I am and has enabled me to conduct the research for this thesis.

A very special thank you goes to my Ph.D. peers Alexandre Barth and Battist Utinger, who were there from the beginning of this journey and with whom I could always engage in fruitful discussions. I also enjoyed all the non-science-related conversations we had, the time spent during lunch breaks (in or outside the Rhein), blasting music in the lab, and the fun outside of work. I am happy to have shared my time with such great friends. I would also like to thank Julia Bechter, who worked on her Master's thesis with me and whom it was a great pleasure to mentor. Additionally, I am very grateful to Rita Manohar for her help from before my first day until the end. You are truly the heart of this group and the glue that holds it together.

Special thanks also go to my friends outside academia who have supported me throughout, from my studies back home in Vienna to my Ph.D. here in my new home, Basel. Even though none of them ever had a clue what I did, they were always

there to encourage me to keep going. Thank you, Thomas Kreuzhuber, for being my brother from another mother and such a great best friend. I would also like to thank my girlfriend, Lea Sarina Lang, for her patience, support, and love during this time.

Last but not least, I would like to thank my family, especially my parents, Stephanie and Armin Resch. I can't put into words how much you mean to me and how grateful I am for you. You have enabled me to do everything I ever dreamt of and have always been great role models along the way. None of this would have been possible without your unconditional support and love. Thank you from the bottom of my heart.

Abstract

Organic aerosols are crucial constituents of atmospheric particulate matter, significantly influencing the Earth's climate and human health. Despite extensive research, large uncertainties remain in the molecular-level chemical characterization of aerosols, particularly regarding the effects of sample storage during offline analysis and the quantification of specific compounds, such as organic peroxides. This dissertation addresses these challenges through two main objectives: characterizing the effects of storage conditions and time on the molecular-level chemical composition of aerosol samples and developing a novel method to identify and quantify individual peroxides in aerosols.

To evaluate the effects of storage conditions on the chemical composition of aerosols, β-pinene secondary organic aerosol (SOA), naphthalene SOA, and urban atmospheric aerosol were collected on filters and investigated. To characterize temporal changes in aerosol composition, all samples were extracted and analyzed immediately, or stored as aqueous extracts or filters for 24 h, 1 week, 2 weeks, or 4 weeks at either +20°C, -20°C, or -80°C. Analysis was conducted using ultra-high-performance liquid chromatography-high-resolution mass spectrometry (UHPLC-HRMS). Targeted and non-targeted data analysis combined with principal component analysis were used to identify changes in composition over time. The study highlights that all samples should be kept frozen as soon as possible after sampling to best retain their chemical composition compared to the fresh collected samples. In contrast, storage of both aqueous extracts and filters at room temperature led to significant compositional changes even at short storage times of only 1 day. In cases where immediate frozen storage is not possible, authors should mention in detail how the samples were stored and how much time passed between collection and analysis to reduce uncertainties.

The significant compositional changes observed in samples stored at room temperature (i.e. +20°C) were further investigated and characterized. β-Pinene SOA filter and extract samples show distinct temporal concentration changes for monomers and oligomers. In aqueous SOA extracts a significant increase is observed for monomers, while dimers decay at the same time. The inverse can be seen on filters, a strong and persistent increase for dimers, while many of the monomers decrease. Additionally, new dimer compounds are formed over time in SOA samples stored on filters. These observed trends are proposed to be due to hydrolysis

of dimers in aqueous extracts, and a continuous formation of oligomers in SOA formed through reactions of monomers on filters. Further experiments were done to confirm dimer formation through esterification of monomers. It is important to consider such on-filter reaction artifacts when detailed composition of organic aerosol is studied. These continuous reactions of SOA components over days and weeks on filters can also mimic dark aging particle phase processes in particles with low-water content in the ambient atmosphere over their entire lifetime. Such long-term experiments of many days are not possible with conventional laboratory chamber studies.

The second main objective of this thesis shifts the focus away from storage effects to the quantification of peroxides, which have been identified as an important class of SOA components contributing to aerosol toxicity and new particle formation. Despite their importance, there are large uncertainties about their contribution to the mass of SOA. One source of uncertainty may be the differences in detection methods, such as iodometric titration, which is often used to determine the total peroxide concentration in aerosol samples. A major drawback of such methods is the inability to identify and quantify individual peroxide concentrations in organic aerosol. Therefore a novel high-performance liquid-chromatography (HPLC) in-column derivatization method is presented to identify and quantify individual organic peroxides in SOA through chemiluminescence of luminol catalyzed by cytochrome c. Three different sample types were measured: commercially available peroxide standards, samples generated through liquid-phase ozonolysis of α-Pinene and 3-Carene, and laboratory generated SOA from α-Pinene, 3-Carene, naphthalene, and a 3-Carene and naphthalene mix. The results presented highlight the methods capability of differentiating between different samples. All samples are additionally analyzed by traditional iodometry with UV-Vis to obtain a total peroxide concentration. A clear linear correlation is observed between the HPLC chemiluminescence method and iodometry for peroxide quantification. This allows for quantification of individual peaks in the chromatograms. A unique cross-product peroxide peak in the 3-Carene/naphthalene mix SOA is identified and quantified to contribute 5.5% of the total peroxide concentration, illustrating the additional complexity when several SOA precursors are oxidized simultaneously, as is the case in the ambient atmosphere.

Zusammenfassung

Organische Aerosole sind wesentliche Bestandteile des atmosphärischen Feinstaubs, die das Klima der Erde und die menschliche Gesundheit erheblich beeinflussen. Trotz umfangreicher Forschungsarbeiten bestehen nach wie vor grosse Unsicherheiten bei der chemischen Charakterisierung von Aerosolen auf molekularer Ebene, insbesondere hinsichtlich der Auswirkungen der Probenlagerung während Offline-Analysen und der Quantifizierung bestimmter Verbindungen, insbesondere organischer Peroxide. In dieser Dissertation werden diese Herausforderungen durch zwei Hauptziele angegangen: Charakterisierung der Auswirkungen von Lagerungsbedingungen und -zeit auf die chemische Zusammensetzung von Aerosolproben auf molekularer Ebene und Entwicklung einer neuen Methode zur Identifizierung und Quantifizierung einzelner Peroxide in Aerosolen.

Um die Auswirkungen der Lagerungsbedingungen auf die chemische Zusammensetzung von Aerosolen zu bewerten, wurden β-Pinen sekundäre organische Aerosole (SOA), Naphthalin SOA und urbanes atmosphärisches Aerosol auf Filtern gesammelt und untersucht. Um zeitliche Veränderungen in der Aerosolzusammensetzung zu charakterisieren, wurden alle Proben extrahiert und sofort analysiert oder als wässrige Extrakte oder Filter für 24 h, 1 Woche, 2 Wochen oder 4 Wochen bei entweder +20°C, -20°C oder -80°C gelagert. Die Analyse erfolgte mittels Ultra-Hochleistungs-Flüssigkeitschromatographie mit hochauflösender Massenspektrometrie (UHPLC-HRMS). Gezielte und nicht gezielte Datenanalyse in Kombination mit der Hauptkomponentenanalyse wurden verwendet, um Veränderungen in der Zusammensetzung im Laufe der Zeit zu erkennen. Die Studie unterstreicht, dass alle Proben so schnell wie möglich nach der Entnahme eingefroren werden sollten, um ihre chemische Zusammensetzung im Vergleich zu frischen Proben bestmöglich zu bewahren. Die Lagerung sowohl von wässrigen Extrakten als auch von Filtern bei Raumtemperatur führte jedoch selbst bei kurzen Lagerungszeiten von nur einem Tag zu erheblichen Veränderungen der Zusammensetzung. Auf der Grundlage dieser Ergebnisse wird empfohlen, die Proben so bald wie möglich nach der Probenahme einzufrieren. In Fällen, in denen dies nicht möglich ist, sollten die Autoren detailliert angeben, wie die Proben gelagert wurden und wie viel Zeit zwischen der Entnahme und der Analyse vergangen ist, um Unsicherheiten zu verringern.

Die signifikanten Veränderungen in der Zusammensetzung, die bei Proben beobachtet wurden, die bei Raumtemperatur (d.h. +20°C) gelagert wurden, wurden weiter untersucht und charakterisiert. β-Pinen SOA-Filter- und -Extraktproben zeigen deutliche zeitliche Konzentrationsänderungen bei Monomeren und Oligomeren. In wässrigen SOA-Extrakten ist ein deutlicher Anstieg der Monomere zu beobachten, während die Dimere gleichzeitig abnehmen. Bei Filtern ist das Gegenteil zu beobachten: ein starker und anhaltender Anstieg der Dimere, während viele Monomere abnehmen. Darüber hinaus werden in SOA-Proben, die auf Filtern gelagert werden, im Laufe der Zeit neue Dimerverbindungen gebildet. Es wird angenommen, dass diese beobachteten Trends auf die Hydrolyse von Dimeren in wässrigen Extrakten und die Bildung von Oligomeren zurückzuführen sind, die durch Reaktionen von Monomeren auf Filtern entstehen. Weitere Experimente wurden durchgeführt, um die Bildung von Dimeren durch Veresterung von Monomeren zu bestätigen. Es ist wichtig, solche Reaktionsartefakte auf Filtern zu berücksichtigen, wenn die detaillierte Zusammensetzung von organischem Aerosol untersucht wird. Diese kontinuierlichen Reaktionen von SOA-Komponenten über Tage und Wochen auf Filtern können auch die Prozesse der dunklen Alterung der Partikelphase in Partikeln mit geringem Wassergehalt in der Umgebungsatmosphäre über ihre gesamte Lebensdauer nachahmen, was mit herkömmlichen Laborkammerstudien nicht möglich ist.

Das zweite Hauptziel dieser Arbeit verlagert den Schwerpunkt von den Lagereffekten auf die Quantifizierung von Peroxiden, welche als eine wichtige Klasse von SOA-Komponenten identifiziert wurde, die zur Aerosoltoxizität und zur Bildung neuer Partikel beitragen. Trotz ihrer Bedeutung gibt es grosse Unsicherheiten bezüglich ihres Beitrags zur SOA-Masse. Eine Quelle der Unsicherheit können die unterschiedlichen Messmethoden sein, wie z. B. die iodometrische Titration, die zur Bestimmung der Gesamtperoxidkonzentration in Aerosolproben verwendet wird. Ein grosser Nachteil solcher Methoden ist die Unfähigkeit, einzelne Peroxidkonzentrationen in organischem Aerosol zu identifizieren und zu quantifizieren.
Daher wird eine neuartige Hochleistungs-Flüssigkeitschromatographie (HPLC) In-Säulen-Derivatisierungsmethode vorgestellt, mit der einzelne organische Peroxide in SOA durch Chemilumineszenz von Luminol, das durch Cytochrom c katalysiert wird, identifiziert und quantifiziert werden können. Es wurden drei verschiedene Probenklassen gemessen: handelsübliche Peroxidstandards, Proben die durch Flüssigphasen-Ozonolyse von α-Pinen und 3-Caren erzeugt wurden, sowie im Labor

erzeugtes SOA aus α-Pinen, 3-Caren, Naphthalin und einer Mischung aus 3-Caren und Naphthalin.
Die vorgestellten Ergebnisse unterstreichen die Fähigkeit der Methode, zwischen verschiedenen Proben zu unterscheiden. Alle Proben werden zusätzlich durch traditionelle Iodometrie mit UV-Vis analysiert, um eine Gesamtperoxidkonzentration zu erhalten. Für die Bestimmung der Peroxidkonzentration lässt sich eine klare lineare Korrelation zwischen der HPLC-Chemilumineszenz Methode und der Iodometrie gemessen mit UV-Vis herstellen. Dies ermöglicht die Quantifizierung der einzelnen Peaks in den Chromatogrammen. Ein einzigartiger Kreuzprodukt-Peroxid-Peak in der 3-Caren/Naphthalin-SOA Mischung wurde identifiziert und quantifiziert, dieser macht 5.5% der Gesamtperoxidkonzentration aus.

Contents

Chapter 1

Introduction

The following chapter will describe the definition of aerosols, their characteristics, their formation mechanisms, and why they are of interest. Secondary organic aerosol and the processes leading to secondary organic aerosol formation in the atmosphere will be discussed in more detail. Furthermore, a detailed overview of the chemical composition of aerosols and the different analytical techniques available to characterize their molecular level chemical composition is presented. Finally an outline, motivation, and aim for this thesis is given.

1.1 Aerosol

Aerosols are defined as a two-phase system consisting of either solid or liquid particles suspended in a carrier gas.[1] Aerosols can be characterized by several different properties, such as physical parameters, origin, formation process, and chemical composition. Atmospheric aerosol, also termed particulate matter (PM), is important due to its impact on climate through scattering and absorbing of solar radiance, influence on cloud formation, visibility, atmospheric reactivity, and human health. The most recent IPCC report highlights that human activities are responsible for global warming through emissions of greenhouse gases, which are partly masked by aerosol cooling. There still remain large uncertainties regarding the contribution of clouds and aerosols to understanding the Earth's radiation energy budget.[2, 3, 4, 5, 6]
Additionally, negative health effects of air pollution have been demonstrated by the results of epidemiological studies where exposure to increased levels of PM could directly be linked to cardiovascular and respiratory diseases such as asthma and lung cancer, as well as increased mortality.[7, 8] The most prominent study on the correlation between air pollution through aerosol particles (i.e. $PM_{2.5}$) and mortality

is the six-city study by Dockery *et al.* [9]. These results have been reinforced by several similar follow-up studies.[10, 11] While these studies draw a correlation for long-term exposure and chronic diseases, short-term exposure can also have acute severe negative effects on human health. A well-known example of such an event is the London smog event in 1952, where a strong correlation between SO_2 concentration (a major emission product of coal burning) and increase of mortality in greater London was observed.[12]

The most important physical parameter to characterize aerosol particles is size, which is given as aerodynamic particle diameter. They can range from sizes as small as a few nm to more than 100 µm with lifetimes in the atmosphere of a few seconds to weeks.[1] The idealized size distribution of atmospheric aerosol particles, as given in Figure 1.1 (from Buseck and Adachi [13]), can be grouped into different modes. The nucleation mode with particles ranging from 1 to 10 nm in size, which are typically formed by nucleation through clustering of gas phase molecules and ions. The Aitken- (~ 10 to 100 nm) and accumulation-mode (100 to 1000 nm) particles, which are formed by coagulation and condensation of nucleation-mode particles or particles from combustion sources, as well as particles formed in the atmosphere by photochemical reactions of volatile organic compounds (VOCs) and oxides of nitrogen in the presence of strong sunlight (more on oxidation of VOCs in Chapter 1.2). Coarse mode particles (≥ 1 µm) generally result from mechanical processes such as abrasion and re-suspension, they also contain dust, large salt particles from sea-spray, and pollen among others, these larger size particles contain most of the mass of atmospheric aerosol.[1, 13, 14, 15, 16, 17]

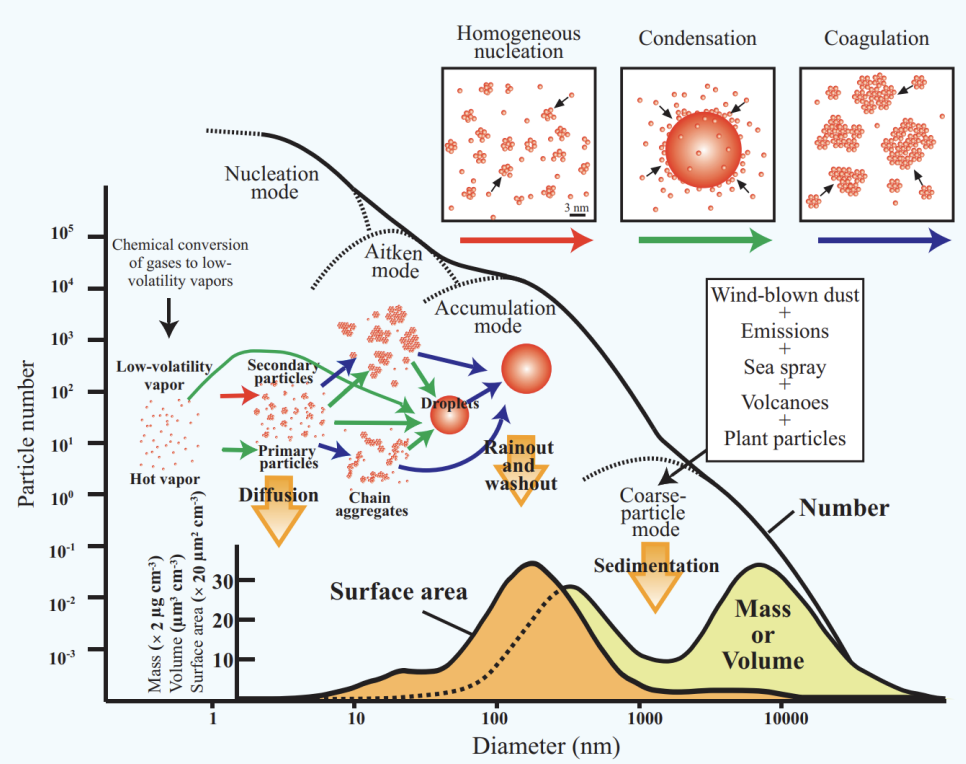

Figure 1.1: Idealized size distribution of atmospheric aerosol particles for various parameters (number, mass, volume, surface area), including the different modes. Illustrations of the formation and removal mechanisms as well as the sources. From Buseck and Adachi, 2008.[13]

Aerosols can be of either primary or secondary type. Primary describes aerosols that are directly emitted into the atmosphere, such as dust, sand, smoke, and sea spray among others. Secondary aerosol on the other hand is generated through gas to particle-phase conversion either through condensation or nucleation of gas-phase compounds.[1, 18] Furthermore, aerosols can be from either biogenic or anthropogenic sources. The former being particles arising from natural sources, such as sea-spray, dust, wildfires, bioaerosol such as pollen, and volcanoes, while the latter refers to sources like cooking, combustion of fossil fuels, wood, and other biomass. Once airborne, particles can change their size and composition by coagulation with other particles, evaporation or condensation of vapor species or chemical reactions (e.g. oxidation, which leads to particle aging) or by activation into fog and cloud droplets.[1, 15]

Due to the different sources and processes of aerosols in the atmosphere, their chemical composition is highly complex and also spatially and temporally extremely variable around the world.[19] Aerosols often consist of an organic and an inorganic fraction. The inorganic fraction containing inorganic salts (e.g. ammonium nitrate,

ammonium sulfate, sodium chloride), mineral dust, metals, soot, and water. While organic material significantly contributes to the total fine aerosol mass from around ~ 20-50% at continental mid-latitudes and as high as 90% in forested areas. It is estimated that there are far more than 10'000 different organic compounds in the atmosphere with different oxidation stages and functional groups, most of them being in the particle phase.[15, 20, 21, 22, 23] Figure 1.2 (from Zhang *et al.* [21]) shows the different compositions of aerosols across the northern hemisphere, highlighting the high organic content (green) across the different locations.

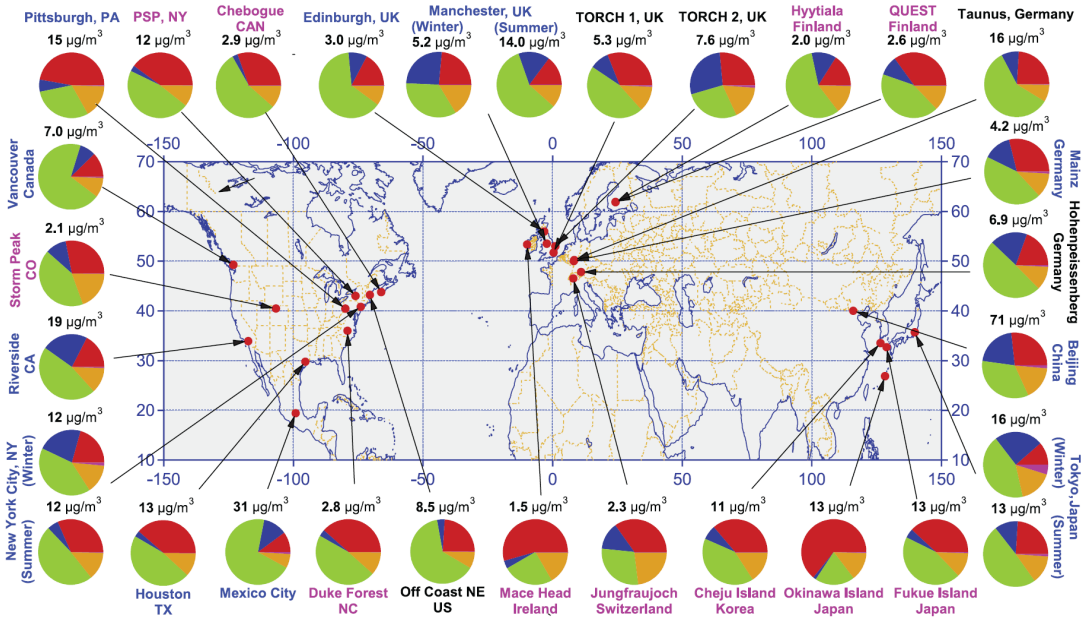

Figure 1.2: Composition of aerosol in winter and summer in the northern hemisphere using aerosol mass spectrometry (AMS). Organic (green), sulfate (red), nitrate (blue), ammonium (orange), and chloride (purple). From Zhang et al., 2007.[21]

1.2 Secondary Organic Aerosol

Globally, most of the organic aerosol (OA) can be attributed to secondary organic aerosol (SOA) emitted form both anthropogenic and biogenic sources.[2] As a result, SOA significantly contributes to the Earth's radiation balance through absorption and scattering of solar radiation and by altering cloud properties.[24]

The atmospheric oxidation of VOCs can create products with low volatility which condense into the particle phase, forming SOA. In order for this to happen there are two participating separate steps: the formation of low-volatility compounds (depending on the gas-phase chemistry of the precursor vapor) and the partitioning

between the gas and particle phase (a physio-chemical process depending on the interactions of compounds in both phases). As organic gases undergo oxidation by oxidants present in the atmosphere such as the hydroxyl radical ($^{\bullet}OH$), ozone (O_3), and the nitrate radical ($^{\bullet}NO_3$), their resulting oxidation products accumulate. The presence of these oxidants is dependent on the time, during daytime the oxidation is attributed to both $^{\bullet}OH$ and O_3, while nighttime chemistry is dominated by both O_3 and $^{\bullet}NO_3$.[15, 25, 26] The main VOCs accountable for SOA formation in the atmosphere are isoprene, monoterpenes (e.g. α-pinene, β-pinene, 3-carene, limonene), aromatic compounds, and long chain alkanes.[22, 25, 27, 28]

Common atmospheric processes, taking place in both the gas- and particle phase, that lead to a decrease in volatility include functionalization and oligomerization. The oxidation of an organic molecule leads to the addition of functional groups, such as hydroxyl (-OH), carbonyl (-C=O), hydroperoxy (-OOH), carboxyl (-C(O)OH), and ester (-C(O)OR). Products containing such functional groups are more polar and less volatile and are therefore more likely to condense into the particle phase.

Oligomerization describes the process of linking monomeric compounds forming longer chain molecules such as dimers, trimers, and higher order oligomers. Such accretion reactions lead to an increase of the carbon number per molecule which significantly lowers the vapor pressure. The particle phase oligomerization pushes the gas-particle phase equilibrium of the aerosol towards the particle phase, which leads to further growth through condensation of other oxygenated compounds. Such low volatility compounds are often linked to new particle formation (and therefore SOA formation) in the atmosphere.[2, 3, 15, 18, 29, 30, 31, 32, 33]

The processes described above (i.e. oxidation of organics in both the gas- and particle-phase and the oligomerization) can be described by the general term of aging. Generally, the aging of aerosols will alter their composition and properties. For example, in the particle-phase the photolabile compounds like aldehydes and ketones will absorb radiation and fragment, while unsaturated hydrocarbons will more likely react with oxidants such as $^{\bullet}OH$, which will lead to further oxidation and therefore changing their chemical functionality once again.[34, 35, 36] Understanding these aging processes has been a large focus of aerosol research in the last years.[17, 37, 38, 39, 40, 41, 42, 43, 44, 45, 46, 47]

1.3 Chemical Composition and Analysis

The following chapters aim to give a short overview of the different chemical compositions of aerosols and how they are measured. The different analytical tools used to characterize the composition are discussed as well.

1.3.1 Chemical Composition

In an atmospheric context, quantifying the rate of compositional transformation and aging of aerosols is necessary for using molecular markers to identify aerosol sources and obtaining a better understanding of aerosols' role in environmental processes.[48, 49] The detection of such tracer compounds in ambient SOA samples can also suggest identities of their respective VOC precursors and oxidants.[50, 51] Some of the most prominent markers include compounds such as levoglucosan, mannosan, and galactosan (biomass burning aerosols), 2-methyltetrols and its derivatives (isoprene SOA), cis-pinonic and cis-pinic acid, 3-methyl-1,2,3-butanetricarboxylic acid (MBTCA), and pinyl-hydroxypinonyl- and pinyl-diaterpenyl esters (α-/β-pinene fresh and aged markers respectively).[32, 47, 52, 53, 54, 55, 56, 57, 58, 59]

The composition of SOA also greatly affects many of the chemical, optical, and physical properties. For example, while the ability of SOA particles to act as cloud condensation nuclei certainly depends on size (which to some degree is also a function of chemical composition through e.g. particle growth), it is also affected by the presence of organic material affecting the hygroscopicity and the mixing state.[60, 61, 62] The optical properties of organic aerosol are strongly dependent on the chemical composition, while both mineral dusts and black carbon (BC) have been recognized as efficient light absorbing agents for a long time [63, 64], many studies suggest that light-absorbing organic matter (OM), often referred to as "brown carbon" (BrC), can also strongly absorb light at shorter visible and ultraviolet wavelengths, accounting for ~ 20% of the solar absorption of carbonaceous aerosols globally. SOA has also been identified to have light absorbing effects and therefore has been attributed as a source of atmospheric BrC.[65, 66, 67, 68, 69]

Despite the chemical composition of SOA being so important, as the understanding of processes involving organic compounds in the atmosphere depends on how well these compounds are identified, it still remains poorly understood on a molecular-level due to the complexity and variability of SOA. Over the last decades, mainly due to advances in analytical techniques and a large increase of research activities on this

subject, investigations have unveiled numerous previously unknown compounds in SOA. Examples being: organosulfates and their nitrated derivatives (nitrooxy organosulfates), high molecular-weight (MW) compounds such as oligomers, humic-like stubstances (HULIS), highly oxidized multifunctional molecules (HOMs), and short-lived organic species such as Criegee intermediates (CIs) and organic peroxy radicals (see Ref. [52], and references therein). Besides the importance of SOA for atmospheric chemistry and climate as describes above, these recent advances have also led to the detection of toxic properties of certain compounds, such as the class of particle-bound reactive oxygen species (ROS), referring to oxygen-containing molecules with one or more unpaired electrons, such as H_2O_2, $^{\bullet}OH$, superoxide radical (O_2^{-}), and organic peroxides.[47, 70, 71]

Determining the chemical composition of organic aerosol largely relies on different analytical measurement techniques. A summary of different analytical techniques corresponding to their ability to detect a certain fraction of the total organic mass of atmospheric samples versus their ability to identify the molecular structure of a compound, given as the "I factor", is presented in Figure 1.3 (from Nozière *et al.* [52]). The I represents the number of possible molecules matching the measurement by the analytical technique, where I = 1 is full unambiguous identification. If only one of two or more isomers can be detected then the I = 2 or more accordingly. The analysis of SOA mixtures can easily reach I ≥ 100 or higher.[52]

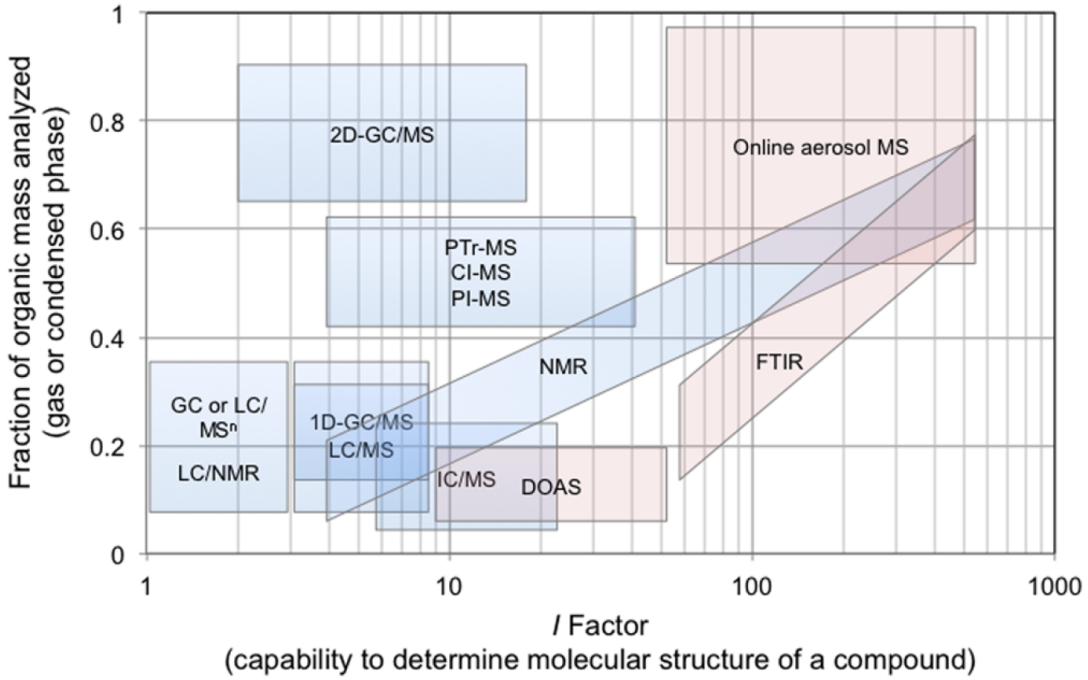

Figure 1.3: The most abundant analytical techniques and tools used to characterize atmospheric organic compounds as a function of their I factor and the fraction of organic mass characterized by the technique. The coupling of two techniques significantly decreases the I. Frequently the techniques are coupled to some sort of chromatography, the techniques coupled to or capable to couple to chromatography are given in blue, the others are given in red. From Nozière et al., 2015.[52]

1.3.2 Analytical Tools

In general the main analytical techniques used to characterize aerosol composition can be separated between optical spectroscopy, mass spectrometry, and other methods such as NMR. These methods will be discussed in the following paragraphs, examples and their advantages as well as disadvantages for detailed chemical composition analysis are given.

Spectroscopic Methods

Spectroscopic methods include Ultraviolet-Visible (UV-VIS) absorption spectroscopy, Fourier-Transform Infrared spectroscopy (FTIR), Nuclear magnetic resonance (NMR) spectroscopy, fluorescence spectroscopy, and Raman spectroscopy, among others. These methods are able to provide information on the following characteristics of samples: functional groups and their concentration, optical properties (such as the absorption or scattering of light), analyte quantification, and the

detailed chemical composition through NMR spectroscopy (if the sample quantity is high enough).

These analytical tools are important and provide information about the overall composition and properties of aerosol samples. Their downside is that either this information is only given for bulk aerosol properties, which hinders detailed molecular-level characterization (i.e. I ≥ 100 or even 1000), or involves extensive non-automated data analysis. This is not ideal for organic aerosol samples due to their high complexity and the resulting high time and cost investment necessary to identify targeted individual compounds.[52, 72, 73]

Chemical derivatization methods such as different oxidative potential (OP) assays, iodometric titration, alkylation, and silylation are used for quantification and to increase the identification capability for certain classes of compounds within different methods.

In the field of atmospheric chemistry derivatization methods have frequently been coupled with GC-MS to analyse aerosol composition. Examples include derivatization with reagents such as PFBHA (O-2,3,4,5,6-pentafluorobenzyl)-hydroxyamine), MHA (O-methylhydroxylamine hydrochloride), or BSTFA (N,O-bis(trimethylsilyl)trifluoroacetamide) to convert polar into less polar compounds, i.e. the sylilation through reaction of BSTFA with carboxyl and hydroxyl groups or the oxime formation through reaction of PFBHA with carbonyls, which can then be measured with GC-MS. This allowed for detection and quantification of e.g. oxidation products of isoprene, cyclohexene, and other oxygenated species in organic aerosol.[52, 74, 75, 76, 77]

Quantification and enhanced identification capability can also be achieved by coupling of liquid chromatography (LC) and derivatization methods with pre- or post-column injection. Little applications of chemical derivatization with LC have been used in the field of atmospheric chemistry, such methods are more commonly used in the fields of amino acid detection, peroxide and especially hydrogen peroxide detection, and the fragrance industry, among others. A detailed list of analytes detected by derivatization methods is given in Jones *et al.* [78] and Jones *et al.* [79].[80, 81, 82, 83] In general, such derivatization methods are capable of improving detection sensitivity, selectivity and, compound identification.[84]

Mass Spectrometry

Mass spectrometry (MS), have been at the forefront of analytical tools used to identify SOA composition, as it allows for effective detection, identification, and in some cases quantification of a broad range of chemical species with high resolution and

sensitivity. Several reviews have been written in the last years describing the evolution and capabilities of mass spectrometry in atmospheric chemistry, the following chapter will aim to summarize the most important parts.[52, 72, 85, 86, 87, 88, 89, 90] In mass spectrometry the three essential steps to proper separation and identification of analyte molecules are sample introduction, ionization, and mass to charge (m/z) ratio separation and detection.

The ionization methods can be divided into hard and soft ionization. Hard ionization, such as electron ionization and laser desorption/ionization methods, leads to stronger fragmentation of compounds. While fragmentation can be useful in individual compound detection in cases of rather simple samples, the data interpretation of fragmentation patterns for complex samples, such as SOA, can be challenging or even impossible. Soft ionization methods, such as chemical ionization, photoionization, and the frequently used electrospray ionization (ESI), on the other hand lead to less fragmentation which is advantageous for the identification of analyte molecules in complex samples. A major downside of all ionization techniques is the uncertainty regarding ionization efficiency, which makes quantification without adequate standards impossible.

The m/z analyzers generally include either Time-of-Flight (TOF), Quadrupole Ion Trap, Orbitrap, or Fourier-transform ion-cyclotron-resonance (FT-ICR) detectors. A detailed explanation of Orbitrap mass spectrometry will be given in Chapter 2.2.2, the other detector types will not be discussed in detail. Differentiation between them can be made in regard to the mass resolving power and mass accuracy of the instruments. These parameters are used to describe the performance of a mass analyzer. The mass resolving power (R, see eq. 1.1) of an instrument defines its ability to separate two ions of two different m/z values and is usually given as the ratio of the mass of a detected ion with respect to its peak width at half maximum (Δm):

$$R = \frac{m/z}{\Delta m} \tag{1.1}$$

The mass accuracy of an instrument, usually expressed in part per million (ppm), is defined as its ability to measure a mass near its theoretical mass. It is given as (see eq. 1.2)

$$\Delta m/z = \left(\frac{m/z_{exp} - m/z_{the}}{m/z_{the}} \right) \times 10^6 \tag{1.2}$$

where m/z_{exp} is the experimentally measured mass and m/z_{the} is the theoretical mass.[52, 91]

Instruments with high mass accuracy and high resolution are capable of detecting and separating thousands of ions in ranges of only a few 100 *m/z*. Often the *m/z* can be determined with such high accuracy enabling molecular formula assignment and reaching desirable low I factors. In order to achieve even lower I factors, mass spectrometry measurements are done after chromatographic separation through gas- (GC) or liquid-chromatography (LC), the combination of these techniques is termed gas-/liquid-chromatography coupled to mass spectrometry (GC/LC-MS) respectively. Another multi-dimensional technique which is capable of characterizing complex organic aerosols, by separation of both volatility and polarity, is GCxGC-MS. GC separation has been crucial for detecting and quantifying (semi-)volatile organic compounds and their oxidation products in both laboratory studies and in the atmosphere.[74, 92, 93, 94, 95, 96]

More on liquid-chromatography, and especially (ultra)high-performance liquid chromatography ((U)HPLC) in Chapter 2.2.1. Additionally, tandem MS (MS/MS or also MS^n) can be performed to lower the I factor of a measurement technique. In MS/MS measurements a specific peak detected in the first mass separation is selected and then a second analysis of this mass is performed by fragmenting the selected ion, after all other masses are removed between the steps. These fragmentation patterns can give additional information about the structure of the parent compound. The combined use of LC and MS/MS (LC-MS/MS) allows for unambiguous identification of compounds (see Figure 1.3). LC enables the separation of isomers (i.e. compounds with the same *m/z* but structural differences) and reduces the adduct formation during ESI due to less concentrated analyte being infused into the MS, which is a big advantage over direct infusion measurements. [52, 72, 88]

Finally, the last distinction between MS techniques for the chemical analysis of SOA can be made between real-time measurements, often called online measurements, and offline techniques, where sampling and sample preparation steps are performed prior to analysis. Online techniques, such as aerosol mass spectrometry (AMS), offer high time resolution of aerosol composition and enable simultaneous measurement of particle size distributions. These methods are ideal for studies where high temporal resolution is important, such as field studies or studies of brief events such as new particle formation, and where the analysis of average compositions of aerosols are of interest. The major drawback in analysis of detailed chemical composition with the AMS are: (1) the thermal/ionization-induced decomposition and fragmentation artifacts, which make identification of the parent compounds nearly impossible, and (2) the low mass resolving power of the TOF mass analyzers usually deployed in the instruments ($R \approx 4000$)[97], which makes unambiguous assignment of SOA

compounds impossible at I factors often in the ≥ 100s.[52, 72, 86, 87] A promising approach for the use of online methods to study the detailed chemical composition of aerosols by using extractive electrospray-ionization coupled to an Orbitrap has recently been developed.[98] The use of soft ionization and high resolution mass spectrometry (HRMS) should be able to advance our understanding of the formation and evolution of atmospheric aerosols on a molecular level, but this will need further development and refinement of the technique before it can become a mainstream instrument to use.

Offline MS techniques, such as direct infusion HRMS, GC-MS, 2D-GC-MS, and LC-HRMS, have improved our fundamental knowledge of aerosol chemistry, molecular-level composition and atmospheric aging significantly. They offer superior mass resolving power ($R \approx 10^{5-6}$) and often allow close to unambiguous identification and mass assignment of molecular compounds in aerosol samples with low single-digit I factors, especially if additional separation methods and MS/MS measurements are conducted (see above).[52, 85, 87, 88, 89] In this thesis no direct infusion measurements were done, therefore studies conducted will focus on sample analysis after chromatographic separation, enabling lower identification factors. Offline methods require sample collection, usually done on filters (PTFE or quartz fibers), followed by subsequent sample extraction and analysis. An advantage of this is that the filters can easily be collected on remote sites without intense labor or the need to relocate analytical instruments. Furthermore, a collected filter usually supplies enough material to be used for different types of analytical methods. The biggest disadvantage of offline measurements, apart from the low time resolution, is the offline aspect itself. The sampling, the storage, and the extraction can all have effects on the results obtained through analysis and alter the chemical composition significantly. A number of studies have investigated some of the potential offline analysis artifacts such as; condensation and evaporation of vapors during sampling, gas-phase artifacts (e.g. gaseous VOC residuals) and oxidants (e.g. O_3, OH, NO_3) can continue to react with the particles on the filters for measurements in absence of denuders, the effects of different filter materials (i.e. quartz vs. PTFE membrane filters) on composition, the difference due to different extraction methods (i.e. sonication vs vortexing, concentrating by freeze-drying vs N_2 drying), the effects of different extraction and reconstitution solvents (i.e. Methanol (MeOH) vs. Acetonitrile (ACN) vs Dimethyl Sulfoxide (DMSO) vs. Water).[99, 100, 101, 102, 103, 104, 105, 106, 107] All of these studies show that offline analyses are prone to some sort of collection, extraction or analysis artifact. An important aspect of offline analysis that has been neglected in literature in the last decades is the storage of offline, and especially filter, samples.

Although there are several factors, such as temperature, sample type, and time of storage, which may potentially influence the chemical composition of aerosols on filters, little investigation has been done in this regard. Often, in publications little or no information is given on the duration or temperature of storage, making it hard to assess the actual chemical composition of the samples during the time of collection.

1.4 Aim of this Thesis

This thesis focuses on two main topics; characterizing molecular-level changes occurring during storage of aerosol samples frequently used in offline measurements and the development of a novel method to quantify individual peroxides after chromatographic separation through in-column derivatization with a reagent. Chapter 2 aims to give an overview of the theory of the instrumentation and methods used in this thesis.

As described above, detailed chemical analysis is necessary to further improve our understanding of SOA and its effect on both the environment and human health. This detailed analysis often requires offline measurement techniques, which include the collection of aerosol on filters that are then often stored for extensive periods of time before extraction and analysis. At the commencement of this work there was no literature information on the effects such storage conditions have on aerosol samples. Therefore, Chapter 3 of this thesis aims to investigate this uncertainty regarding storage effects over extended periods of times on the chemical composition of aerosol particles using UHPLC-Orbitrap MS. The study investigates three different types of aerosol samples, one biogenic SOA, one anthropogenic SOA, and atmospheric aerosol. Both principal component analysis (PCA) and time series of individual compounds are used to analyze the temporal behaviour of the sample composition of samples stored at different temperatures as aqueous extracts or as filter samples. Significant changes between samples stored at room temperature vs. < 20 °C are observed. Recommendations for future studies where detailed chemical characterization of aerosol is measured with offline methods are given.

The observed differences between samples stored as filters or aqueous extracts at room temperature motivated the study presented in Chapter 4. Upon further analysis of the large dataset available for β-Pinene SOA samples, an explanation for the observed differences was given. Both untargeted analysis of the LC-MS data and targeted analysis of previously in literature identified dimer esters show that there are two contrasting effects happening during storage. In aqueous solution a decomposition of dimers leads to an increase of compounds over time in the

monomer region, while on filters the inverse can be seen, an increase in dimer formation over time. This study highlights previously unidentified continuous dark chemical processes which affect the chemical composition of SOA samples over time. Furthermore, it is proposed that the storage of SOA on filters might mimic dark aging particle phase processes of SOA in particles with low-water content in the ambient atmosphere over days and weeks. Such long processing times are typically not accessible with aerosol-base methods, hence it could be used in future studies to investigate longer aging times.

Chapter 5 of the dissertation shifts the focus away from storage effects of offline analysis to the quantification of peroxides, motivated by the reasons outlined in Chapter 1.3. Due to the lack of ability of conventional peroxide analysis methods to quantify individual peroxides rather than obtain a peroxide value for the bulk sample, a novel method to quantify peroxides in aerosol samples after liquid chromatographic separation using in-column derivatization with luminol catalyzed by cytochrome c is presented. Three different sample types were measured: commercially available peroxide standards, samples with a complex mixture of peroxides generated through liquid-phase ozonolysis of α-pinene and 3-carene, and laboratory generated SOA from α-pinene, 3-carene, naphthalene, and a 3-carene and naphthalene mix. The results highlight the method's capability of identifying clear differences in the peroxide profile of different organic aerosol samples. All samples are additionally analyzed by iodometry with UV-Vis to obtain a total peroxide concentration. A clear linear correlation can be made between the total luminol chemiluminescence from the HPLC in-column derivatization method and total peroxide concentration quantified by iodometry with UV-Vis. This allows for identificaiton and quantification of individual peaks, such as a unique cross-product peroxide peak in the 3-carene and naphthalene mix SOA. This peak was found to contribute 5.5% of the total peroxide concentration.

Chapter 6 concludes this dissertation by discussing the knowledge gained from assessing the storage effects of offline techniques and individual peroxide quantification. It also comments on future work related to the detailed chemical characterization of SOA and the potential of combining peroxide quantification with identification methods.

Chapter 2

Methodology

The following chapter describes the theory of the instrumentation and methods used in this PhD project to generate SOA in the lab, measure the detailed chemical composition of aerosol samples, how to analyze the data obtained, and the methods and instrumentation used to quantify peroxides in aerosols. Detailed descriptions of the exact experimental methods and conditions used in this work are given in the Chapters 3, 4, and 5.

2.1 Oxidation Flow Reactors and the Organic Coating Unit

This Chapter will briefly describe the organic coating unit (OCU), as presented in detail in Keller *et al.* [108], and give an overview of how oxidation flow reactors (OFRs)[109, 110, 111, 112] work in producing SOA. Most of our understanding of SOA formation from VOC precursors comes from laboratory chamber experiments.[2] These chambers are often large, rarely transportable, and require both time and money to operate. OFRs have been developed as a complement to these traditional chambers, and they offer a faster, portable and more economic approach to studying oxidation of VOCs, while minimizing wall effects due to much shorter residence times. They provide a highly oxidizing environment, which simulates atmospheric aging processes ranging from a day to several days in a few minutes in the laboratory. Their volume can range from several 0.05 to >100 L resulting in a residence time ranging from seconds to minutes.[112] In order to produce SOA from a precursor VOC, the gas-phase VOC is added to an airflow. This airflow is irradiated with UV light with Ozone generating mercury lamps with emission line wavelengths at λ = 185 nm and/or 254 nm. Different versions of OFRs exist, depending on the wavelengths

available from the UV lamps.[112] Since the OCU has mercury lamps with both 185 and 254 nm, this version is discussed. The UV light will produce Ozone from the photolysis of O_2 according to the following simplified mechanism:[15]

$$O_2 + h\nu \rightarrow O + O \qquad \lambda \leq 240\,\text{nm}$$
$$O + O_2 \rightarrow O_3$$

Furthermore, OH radicals are also produced in OFRs through the following mechanism, where the the photolysis of O_3 produces both ground-state (O) and excited singlet ($O(^1D)$) oxygen atoms. The ground-state O combines rapidly with O_2 to form O_3 again, this is a null cycle. The excited singlet oxygen on the other hand can react with H_2O to form 2 OH radicals, as shown below:[15]

$$O_3 + h\nu \rightarrow O_2 + O(^1D) \qquad \lambda \leq 310\,\text{nm}$$
$$O(^1D) + H_2O \rightarrow 2OH$$

Both of these oxidants, i.e. O_3 and OH, will then react with the VOC to form SOA as previously mentioned in Chapter 1.2.
The OCU is an automated OFR with a humidifier, automated systems for dosing VOC precursor substances, and control electronics. The OCU is operated under continuous flow conditions and enables a stable continuous output of SOA particles and mass. This allows for very reproducible collection of samples, as described in the publications by Keller *et al.* [108] and Resch *et al.* [113]. This stability and reproducibility is essential for the measurements conducted during this thesis. Furthermore, the OCU enables the production of both low and high SOA concentrations. High concentrations are ideal for collecting high amounts of SOA mass, which is often necessary in laboratory studies. The disadvantage of high concentrations is that the produced SOA particles might not reflect atmospheric SOA conditions due to increased partitioning of gas phase products into the particle phase. An additional advantage of the OCU is its capability to use two different VOCs and mix these in order to produce SOA mixtures. The SOA output of the OCU can then be collected on filters for further analysis.

2.2 Liquid Chromatography coupled to Mass Spectrometry

As discussed in Chapter 1.3, LC-MS is widely used in the field of aerosol science because of its ability to reach very low I factors and to characterize (highly) oxidized organic compounds. The following chapter will present both the UHPLC and the Orbitrap individually, as well as explain how the obtained data can be analyzed.

2.2.1 Ultra High Pressure Liquid Chromatography

In chromatography, separation of analytes occurs due to their varying affinities for the mobile and stationary phases. In liquid chromatography both the stationary and the mobile phase can be adjusted according to the compound of interest, while only the stationary phase can be modified in GC.
An LC system consists of the following components, as seen in Figure 2.1: a solvent reservoir (containing the mobile phases), solvent delivery pumps, a sample injector with an injection valve (often connected to a temperature controlled auto sampler, not depicted) and a column containing a stationary phase. The basic working principle of an LC can be explained by the following steps: a liquid mobile phase (solvent) carries the injected sample to the column where the compounds adsorb onto the surfaces and desorb in discrete bands. The separated compounds are then transported to the detector with the solvent flow. The resulting detector signal can then be plotted against time, and these results are known as a *chromatogram*. More on data analysis in Chapter 2.2.3. (U)HPLCs are advanced types of LCs that are capable of operating under higher pressure, they consist of the same components and operate under the same working principle.

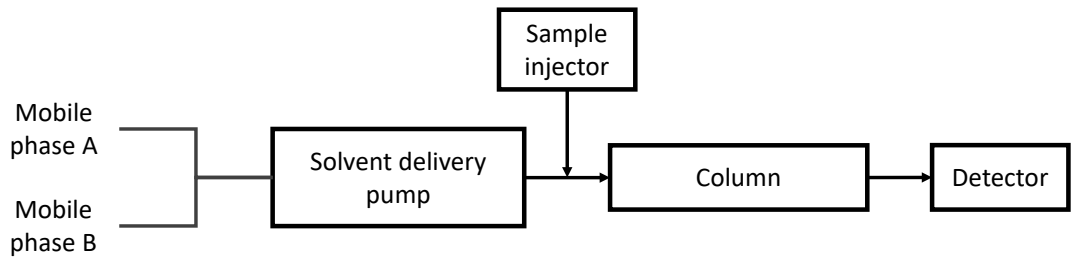

Figure 2.1: Schematic of the main components of an LC, containing two mobile phases, a solvent delivery pump, a sample injector and the column. The detector is not part of the LC.

Developing a method to obtain adequate chromatographic separation requires understanding of how the separation is affected by the following factors such as the type of column, the solvents, the flow rate, the temperature, and so on. The crucial factors being the selection of an appropriate column and mobile phases. LC columns can differ in stationary phase, length, and diameter, all affecting the separation efficiency.

The most widespread types of chromatographic modes and columns are reversed-phase chromatography (RPC, a nonpolar stationary phase and a mobile phase mixture of water plus organic solvent), normal-phase chromatography (a polar stationary phase and a mobile phase mixture of less-polar organic solvents), hydrophilic interaction chromatography (HILIC, similar to RPC but used for samples that are highly polar, which would not retain in RPC), Chiral chromatography (enantiomers are separated in specific chiral columns), and Ion-exchange chromatography (stationary phase with charged sites and a mobile phase with ions of opposite charge), among others. RPC is the most common used LC technique as it allows for the separation of a wide range of polar and nonpolar solutes in complex samples.[52, 88, 114, 115]

Typically water, methanol, and acetonitrile are used as mobile phases in reverse-phase chromatography. Often acids such as formic or acetic acid are added to the mobile phase to enhance the ionization efficiency of the EIS prior to MS detection. The stationary phase in RPC columns is usually composed of ligands (e.g. alkyl chains, phenyl, and cyano) attached to small particles (e.g. silica, porous polymers, and metal-oxide particles). The most common combination being alkyl chains attached to silica particles. The silica particles usually range from <2 to 5 µm in diameter. With the capability of LCs, and especially (U)HPLCs, to work under higher back-pressures, smaller particles have been used in the stationary phase. This use of smaller particles results in a higher surface area for interactions between analytes and the stationary phase, which significantly improves the resolution of the separation process. Additionally, the higher back-pressure generated enhances the efficiency of the chromatographic process, allowing for faster flow rates and reduced analysis times. The attached alkyl chains also differ in length between C_3 to C_{18}. With increasing chain length, the hydrophobic interactions between the analyte and the stationary phase increase, therefore increasing the attraction forces towards smaller and more water-soluble analytes. When analytes are injected into the column, they will be retained by the Van der Waals forces and the hydrophobic interactions with the particles of the stationary phase. With increasing organic solvent content in the mobile phase (i.e. decreasing the polarity of the mobile

phase), the analytes will eventually elute due to decreasing affinity for the nonpolar stationary phase as nonpolar analytes are better solvated by the less polar mobile phase. The composition of the mobile phase can be kept constant (isocratic elution) or deliberately changed during the method (gradient elution) to increase the organic content of the mobile phase over time, leading to an order of elution of more polar compounds eluting before nonpolar ones.[114, 116, 117] In this work only methods with a gradient elution were used.

2.2.2 High Resolution Orbitrap Mass Spectrometry

Following chromatographic separation and ionization, the samples are detected by a mass spectrometer. As explained previously in Chapter 1.3, high resolution MS is the preferred detection method for detailed chemical characterization of complex aerosol samples. In this chapter the components and working principle of Orbitrap mass spectrometers, and especially the Thermo Scientific™ Q Exactive™ Orbitrap™ (Thermo Fisher Scientific™, Switzerland) which was used in this work, will be discussed. Figure 2.2 shows the schematic of the Q Exactive™ Orbitrap™ components.

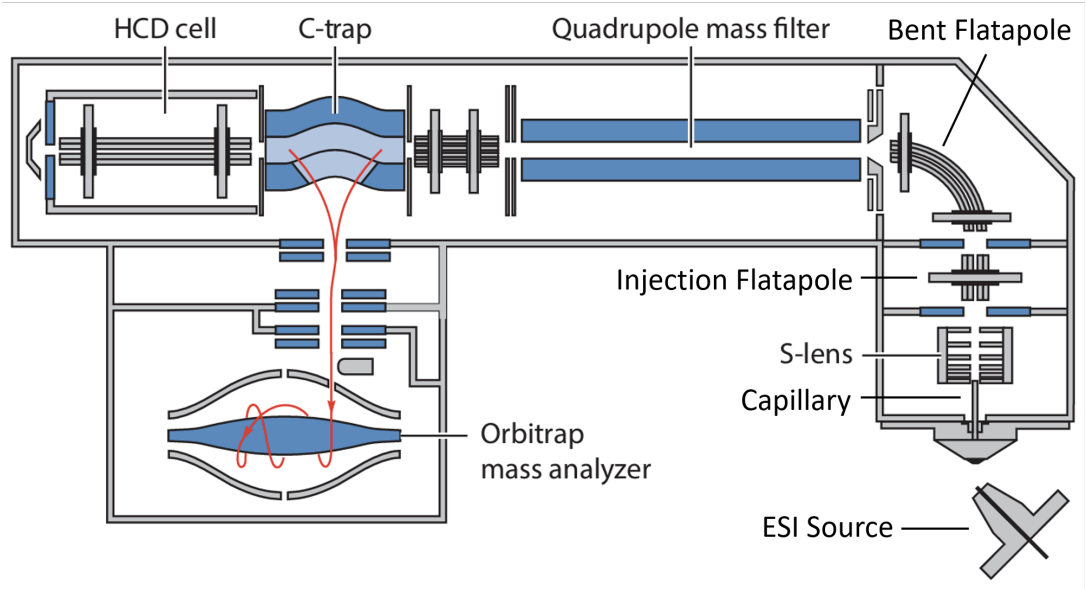

Figure 2.2: Schematic of the Q Exactive™ Orbitrap. The sample is ionized in the ESI source. The ions then pass through the capillary, S-lens, injection flatapole, bent flatapole, quadrupole, and c-trap before being measured in the Orbitrap. A detailed description of each component is given in the main text. Figure adapted from Eliuk and Makarov, 2015.[118]

The whole system after the ESI source is under vacuum to reduce collisions of ions with other molecules in the gas phase. After ionization in the ESI Source, the sample

passes an ion transfer capillary into the S-lens (an ion transmission device consisting of electrodes) where the ions are focused. The injection flatapole is a square array of flat metal electrodes which acts as a further ion focusing device. In the bent flatapole the ions are guided through a right angle to the Quadrupole. The bent flatapole acts as an ion transmission guide where the neutral particles are finally removed, as they do not follow the electric field in the bend. The ions are then guided into the quadrupole, which consists of two pairs of electrically connected rods. RF and DC voltage are supplied to these rods and the voltages are ramped during scans. The voltages applied are equal in amplitude and sign between the pairs, but opposite in sign for the other pair. The applied voltages determine the range of mass-to-charge ratios to be transmitted through the quadrupole mass filter to the nitrogen gas-filled curved linear trap (C-trap). Upon entering the C-trap the ions loose their kinetic energy through collisions with nitrogen collision gas (bath gas) and they're collected near the center of the C-trap. The voltages applied to the ends of the C-trap provide a potential well along its axis and lead tightly focused packets of ions to the Orbitrap mass analyzer. The axially symmetrical Orbitrap consists of a spindle-shape central electrode with two bell-shaped outer electrodes, which employ an electric field to capture and confine the ions inside. The electric field between the electrodes varies as a function of position along the longitudinal axis of the inner spindle (z-axis), due to the nonparallel surfaces of the coaxial electrodes, reaching a minimum at the point of greatest separation between the two electrodes (i.e. the center). The ion packets are then injected at a nonzero position along this z-axis (see Figure 2.3).

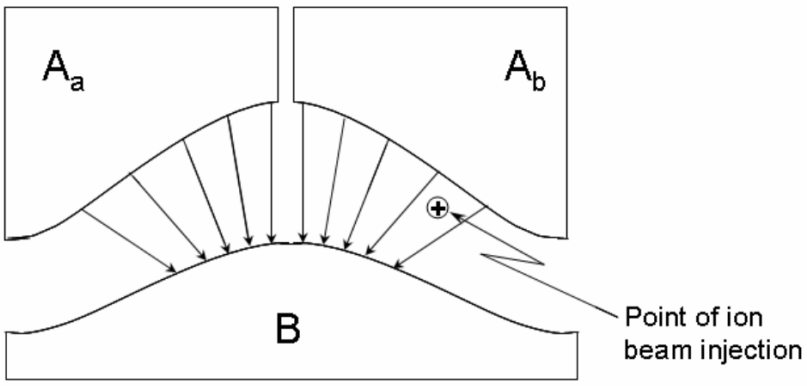

Figure 2.3: Cross-section of the Orbitrap electrodes (the outer electrodes (A_A + A_B) and the inner electrode (B)) and the inhomogeneous electric field. The ion beam is injected at a 90° angle from the plane of the page. Figure from Watson and Sparkman, 2007.[91]

Due to the inhomogeneous electric field, the ions oscillate axially around the inner electrode, and because of the nonparallel field vectors the electric field causes

mass-dependent oscillations of the ions along the z-axis. The frequency ω of these oscillations is given as a function of the ions m/z and an instrumental constant k as presented in equation 2.1:

$$\omega = \sqrt{\frac{z}{m} \times k} \tag{2.1}$$

Using fast Fourier transform these frequencies of oscillation are then transformed into mass spectra. Some advantages of the Orbitrap opposed to other types of mass analyzers are the simplicity and size of the device, the high resolving power, and no need for cryogen as in FT-ICR while having comparable performance. Disadvantages of most high-resolution mass spectrometers, including the Orbitrap, include the high cost of the instruments and the low pressure required due to the mean-free path of the ions being ~100 km.[91]

2.2.3 Data Analysis

As mentioned above LC-MS is an excellent tool to separate and identify individual compounds in a complex SOA sample. This chapter will briefly discuss the structure of the data obtained, data presentation and interpretation, and methods for targeted and untargeted analysis. An example of a LC-MS spectrum is presented in Figure 2.4, displaying the Chromatogram through Retention time (RT, the time between the sample injection and the appearance of the compound in the MS) and Intensity, and the underlying m/z mass spectra.

In principle there are three main ways of displaying chromatograms; Total Ion Current Chromatogram (TIC), Base Peak Chromatogram (BPC), and Extracted Ion Chromatogram (EIC). The difference between them being what information is extracted from the mass spectra. In a TIC the intensity of all measured ions across the entire m/z range is summed up, a BPC displays the intensity of the most intense peak at every RT, and in an EIC one m/z value of interest is selected and monitored. In complex samples the TIC often provides limited information due to the simultaneous elution of multiple analytes, hence oftentimes the BPC is displayed because of the reduced background intensity and the resulting improved visualization of eluting major compounds as individual peaks. When analysis focuses on specific targeted compounds, then EIC are used to identify and quantify the compound through detection of the peak area. EICs are the main tool for targeted analysis of individual ions, they can either be extracted from the data using commercial software such as Xcalibur™ (Thermo™ Scientific) or free software packages for R

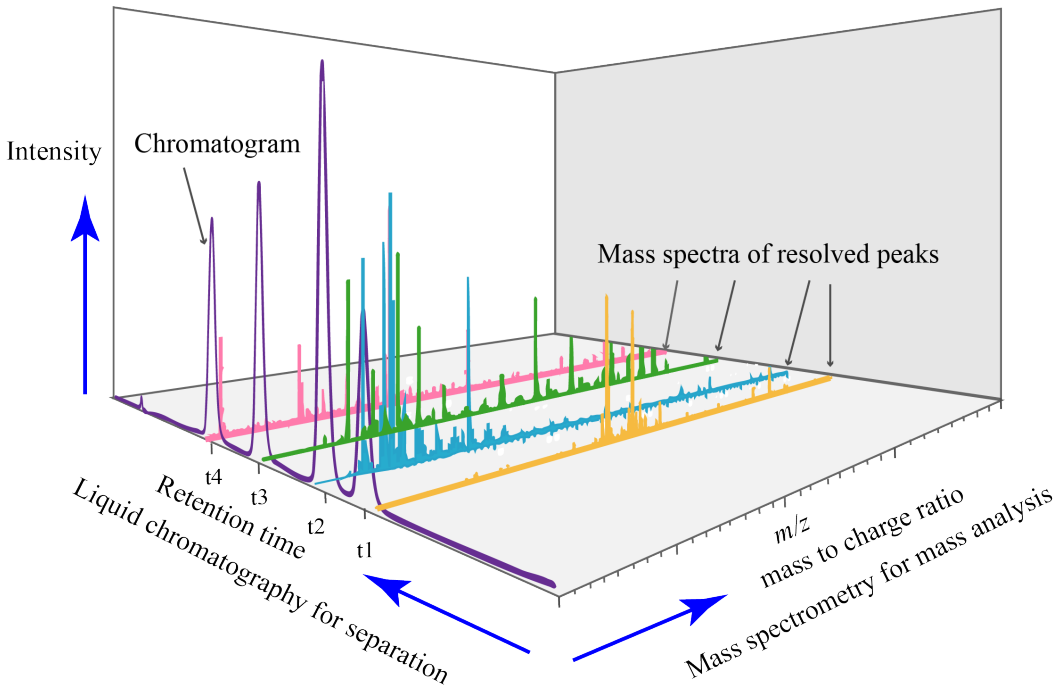

Figure 2.4: Example of a 3D LC-MS spectrum of each resolved peak. The chromatogram is displayed through the x- and y-axis with the retention time of the different eluting chromatographic peaks and their corresponding signal intensity (displayed in purple). Each point in the chromatogram has a corresponding mass spectra of the *m/z* values. Credit: Daniel Norena-Caro, 2017.[119] Reproduced under the Creative Commons CC0 1.0 Universal Public Domain Dedication license.

(R Core Team, Austria) such as PeakPantheR.[120] With high enough resolution the mass tolerance can be below 5 ppm to allow for annotation of the chemical formula of ions. Unambiguous identification of the structure is only possible if there is only one isomer in the EIC, as explained in Chapter 1.3, or through further analysis with techniques such as LC-MS/MS to identify or compare fragmentation patterns between the sample and standards. The only way of accurate quantification with ESI-LC-MS is through comparison of both the retention time and peak area of the compound in the sample and a previously injected standard of the same compound. During this thesis, the LC-MS was not used for quantification.

Due to the large amounts of data generated by LC-MS, it is often necessary to use an untargeted analysis approach to gain a more comprehensive understanding of sample composition. There are several different commercial and free software tools for untargeted peak detection, in this work only the XCMS package [121, 122, 123] in R 4.2.1 (R Core Team, Austria) in RStudio 2022.07.01 (Boston, MA, USA) was used and will be discussed in more detail (see Appendix Chapter E for a version of the R script used). When using any type of free software, the first step is always converting

raw data files into another type of format, which can be used for further processing. Here the raw data files were converted into mzML format using the ProteoWizard (MSConvert, version 3) software.[124] Once in the correct format the data can be imported into the XCMS script. A short summary of the steps done are given in the following paragraph. After import of the data, peak detection is run after specifying certain parameters such as a minimum threshold for peak intensity, peak width and deviation of *m/z* values between individual samples. If necessary, a retention time correction can be run if the samples were run over extended periods of time and the chromatographic conditions changed or RT shifts are observed in this time span. At this time it is necessary to introduce metadata about the sample set including sample information such as: name, date of collection, date of extraction, sample type, etc. The peaks will then be aligned and grouped between the different samples. Finally, the data is exported into a .csv file including the *m/z* and RT value for each peak detected for all of the samples in the dataset. This information can then be used for further data processing and visualization. In this work mainly R, Python[125], and SIMCA® 17 (Sartorius, Germany) were used for further statistical analysis and data treatment, details are given in Chapters 3 and 4.

2.3 Methods to Identify and Quantify Peroxides in Aerosols

Due to their high reactivity and oxidation potential, peroxides have been associated as major contributors to health risks of aerosols.[73, 126, 127] They are also crucial in the overall oxidation scheme of VOCs in the gas phase, and in the formation of SOA, as it is believed that they can contribute significantly to the mass of SOA, ranging from < 1% to > 80% depending on SOA type.[55, 128, 129, 130] This large range is most likely also attributable to differences in detection methods and therefore reflects the uncertainty of our knowledge of peroxides in SOA. This was an additional motivation for the work done in Chapter 5. The following chapter will present current methods to quantify and detect peroxides in aerosol samples, differing between bulk measurements (which obtain a total peroxide concentration value for the sample) and a newly developed method which allows for differentiation between individual peroxides.

2.3.1 Total Peroxide Detection

Several methods have been used to quantify peroxides in aerosols. These methods include electrochemical reduction [131], fluorescent detection of a derivatized fluorescing dimer produced through the derivatization of peroxides [82, 132, 133, 134], and the most common method of iodometric titration (also called iodometry).[71, 135, 136, 137] As iodometry is used in the scope of Chapter 5, it will be discussed here in more detail.

The basis for the method is the reaction of organic peroxides with potassium iodide (KI). In an acidic medium iodide ions (I^-) reduce an organic peroxide to its corresponding alcohols, releasing iodine (I_2):

$$R_1OOR_2 + 2I^- + 2H^+ \rightarrow R_1OH + R_2OH + I_2 \tag{2.2}$$

With R_1 and R_2 being H or any alkyl group. In an excess of I^- the I_2 instantly forms triiodide (I_3^-)[138]:

$$I_2 + I^- \rightarrow I_3^- \tag{2.3}$$

The produced triiodide forms a yellow to orange colored solution, whose characteristic absorption can be measured using UV-VIS spectroscopy. Several studies have applied iodometry to quantify peroxides in SOA samples of different kinds. The first quantification of the peroxide content in SOA from the ozonolysis of terpenes using iodometry was presented by Docherty *et al.* [130]. In short, the method consisted of the extraction of SOA sample filters, the subsequent storage in airtight microreaction vials where the solution was purged with N_2 to remove O_2, and the addition of KI. The samples were then allowed to stand for 1h. The absorbance was then measured at 470 nm. Many other studies have quantified peroxides based on this method.[55, 139, 140, 141] The maximum absorption peaks of I_3^- are at 287 and 351 nm, with extinction coefficients of 40,000 and 26,400 $M^{-1}cm^{-1}$, respectively. I_2 has two maxima at 260 and 460 nm.[142] Therefore 350 nm is often selected due to the maximum absorption of I_3 and the minimum of I_2.[143, 144, 145] Alternatively both 420 and 470 nm have been used. Even though the absorption is smaller at these wavelengths, there are less optical interferences due to organic solvents, and it allows for higher concentrations of peroxides present in samples.[55, 130, 136, 137, 139, 146, 147]

The main disadvantages of this traditional iodometric method are; the different reactivities towards some organic peroxides such as *tert*-butyl hydroperoxide (t-BuOOH), the necessity to work in anaerobic conditions (or atleast degassing of the solvents

used) due to the reactivity of I^- with O_2, and the reaction times needed of at least one hour and often much longer to complete the reaction.[130, 136, 137, 147] There have been attempts to reduce these disadvantages through adaptions of the method. For example Mertes *et al.* [136] presented a novel instrument where extraction, reaction, and measurement of the samples are performed in an oxygen-free environment, as well as the implementation of a longer optical detection cell to increase the photometric sensitivity. They still require reaction times of > 1 h, and even observe incomplete reaction for t-BuOOH after 5 h. Alba-Elena *et al.* [137] recently presented a new microwave-assisted iodometric method, where the reaction is accelerated by microwave radiation, with the advantages of a faster reaction time (< 1 min), applicability in the presence of oxygen, and no sensitivity differences between different peroxide types. In the scope of this thesis iodometry was conducted using the classical method with the primary focus of quantifying the total peroxide content of samples after 24 h and measuring the absorbance at 361 nm, due to the samples being in acetonitrile.[148] The total peroxide content was then used to compare and calibrate our developed method for individual peroxide quantification as explained in Chapter 2.3.2. The extended time which is needed to complete the reaction (i.e. > 1h, except if microwave-assisted, which is not combinable with LC) makes iodometric methods unpractical for measurements of previously separated individual peroxides, as in post-column derivatization LC techniques, where the reaction needs to be completed within < 1min to be compatible with LC peak resolution.

2.3.2 Individual Peroxide Detection

Quantification of the total organic peroxide content in samples allows for comparison of organic peroxide concentrations in different types of aerosols and their chemical evolution for different conditions. However, it does not provide molecular level information of organic peroxides, which is crucial to understanding the sources of peroxides and their effects on the atmosphere.[71] Chromatography-based methods are capable of identifying individual organic peroxides and isomers in a complex sample. A method recently developed by Zhao *et al.* [144], where pre-column derivatization of samples with potassium iodide leads to altered chemical profiles that can be analyzed by LC-MS, where the disappearance of certain peaks enables identification of peroxides in complex aerosol samples.[144] Although the pre-column derivatization is destructive to the sample and does not enable quantification of the specific compounds. Because both the identification and the quantification of peroxides in complex aerosol samples is of interest in atmospheric chemistry, a method

to detect peroxides by post-column derivatization with an HPLC was adapted and is described in more detail below and in Chapter 5.[83] This combination of chromatographic separation and post-column derivatization should enable quantification of individual peroxides and one compound that has been used as a derivatization agent to detect H_2O_2, lipid peroxides, hydroperoxides, and organic peroxides is luminol in the presence of a catalyst. Luminol chemiluminescence (CL) has been used in many chemical and environmental applications in the fields of blood detection in forensic, amino acid and antioxidant detection, peroxide contamination in waste water and the fragrance industry, among many others.[149, 150, 151, 152, 153, 154] To date, no such method has been applied in the field of atmospheric chemistry.

Luminol Chemiluminescence

The reaction mechanism of luminol oxidation and chemiluminescence needs alkaline pH and a catalyst. The reactions are presented in Figure 2.5 and are explained in the following text. Luminol (LH_2) is deprotonated to form the luminol monoanion (LH^-) (reaction 1), which is then oxidized by the catalyst and the oxidant to the luminol radical ($L^{-\bullet}$) (reaction 2). The reaction pathway of the catalyst with the oxidant depends on the oxidant itself, the native catalyst is oxidized from (Porf)Fe(III)$^+$ to either (Porf)Fe(IV)-OH$^+$ with H_2O_2, (Porf)Fe(IV)=O$^{\bullet+}$ with peroxyacids, and to (Porf)Fe(IV)-OH$^+$ with subsequent formation to (Porf)Fe(IV)=O$^{\bullet+}$ with hydroperoxides. After oxidation, the $L^{-\bullet}$ can either undergo dismutation to the diazaquinone L and react with a ($O_2^{\bullet-}$) (reaction 3 and 4), or recombine with a superoxide to form the α-hydroxy hydroperoxide ($LOOH^-$) (reaction 5). This α-hydroxy hydroperoxide decomposes into the excited 3-aminophthalate* (3-APA*) under N_2 formation (reaction 6 and 7). Upon returning to the ground state (3-APA), the excited 3-APA* emits light with a maximum at 425 nm (reaction 8).[155, 156, 157, 158]
Several different catalysts are available for this reaction, which can be divided into three categories: nanoparticles (e.g. gold nanoparticles), transition metals (e.g. Iron(II), Copper (II)), and bio-based (e.g. horseradish peroxidase (HRP), hemoglobin, and cytochrome c (Cyt c)) catalysts. Bio-based catalysts are often used due to their high sensitivity, rapid reaction, and availability. For the work conducted in this thesis Cyt c (a small water-soluble heme protein found in the membranes of mitochondria across all eukaryotic organisms) was chosen as a catalyst for the organic peroxide detection.[83, 159, 160] Cytochrome c has several advantageous properties compared to other catalysts such as its activity over a wide pH range, its high thermal stability, its high catalytic activity, and its biological activity at high concentrations of organic solvents.[161, 162]

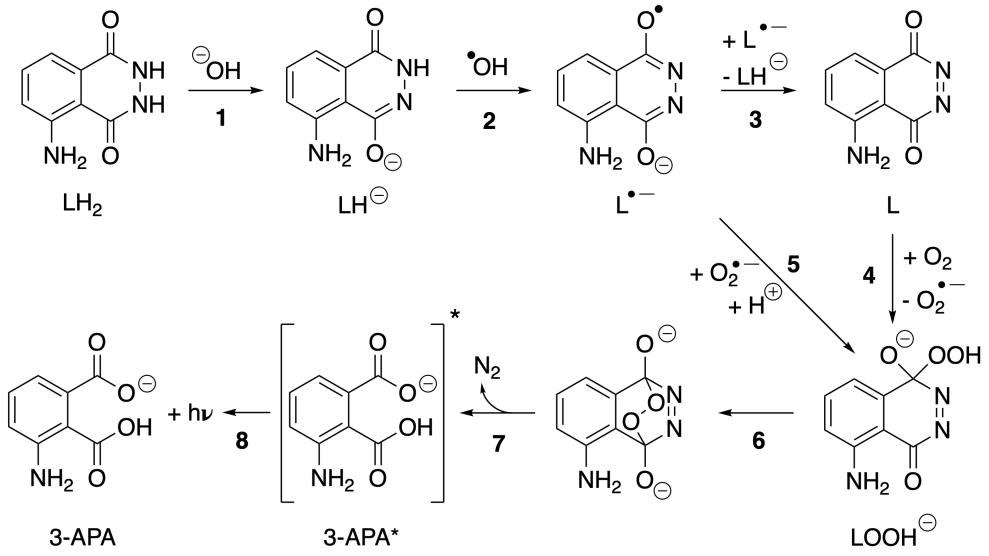

Figure 2.5: Reaction mechanism of the luminol oxidation and chemiluminescence.

To better understand the catalytic chemical reaction of luminol with peroxides, it would have been advantageous to use either Iron(II) or Copper(II), but these were excluded due to their precipitation when stored in solution. Any form of insoluble particles in an HPLC system will lead to pressure spikes or blockage of the column or the tubing and therefore must be avoided.

Post-Column/In-Column Derivatization

In classic post-column derivatization LC systems the reagent solution is induced to the sample flow through a t-piece followed by some sort of dead volume, often with several 100 µL to enable proper mixing and reaction.[78, 163] This increase of dead volume leads to unwanted peak broadening in the chromatogram, greatly decreasing the separation performance. Here we use a novel in-column derivatization (ICD) frit as introduced by Jones *et al.* [78] and Manwaring *et al.* [164], see Figure 2.6.[165] In this ICD system the derivatization reagent flow is introduced at a 45° angle to the flow direction through the column. This results in a reduction in dead volume to approx. 1 µL and increased mixing, which is highly advantageous with modern HPLC columns and applications. The biggest disadvantage of this novel ICD method being the limited availability of the column fitting and the fact it has only been trialled on a limited range of derivatization products. In our application the derivatized product can then directly be measured by the detector connected to a 12µL flow-through cell cuvette (CUV). A schematic of the setup used in these experiments is given in Figure 2.7.

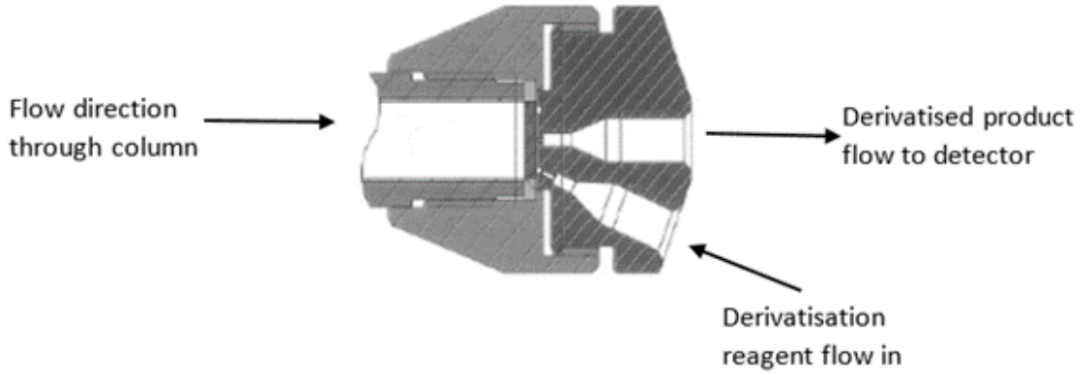

Figure 2.6: Schematic of the in-column derivatization (ICD) column fitting. The derivatization reagent flow in introduced at a 45° angle against the flow direction from the column. Figure from Manwaring et al., 2023.[164]

Due to the chemiluminescence of the luminol reaction the emitted photons can easily be measured by a Photomultiplier Tube, which detects photons and converts them into a measurable electrical signal. This has the advantage of not needing any sort of excitation wavelength as in fluorescent methods and a reduced background signal due to the fact that the derivatized sample will not emit any light if no peroxides are present. The main disadvantage of chemiluminescence being the short-lived time dependant luminescence, which requires prompt detection.

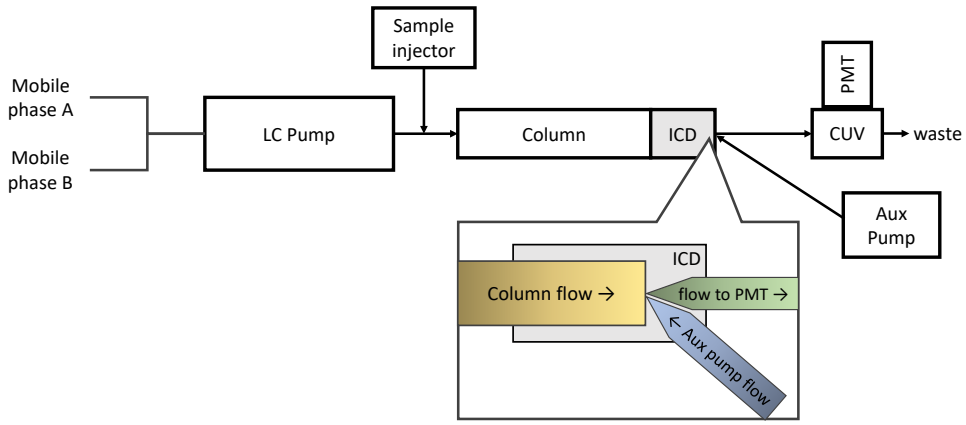

Figure 2.7: Schematic of the LC in-column derivatization (ICD) setup used to detect individual peroxides through luminol chemiluminescence. The LC pump delivers the sample flow to the column and the ICD frit, where it is mixed with the derivatization reagent (luminol/cytochrome c solution) supplied by the auxiliary (Aux) pump. The resulting chemiluminescence signal is then detected by a Photomultiplier Tube (PMT) connected to a 12 µL flow-through cell cuvette (CUV).

When developing or applying novel methods it is necessary to characterize the effects of different variables on the results. In the scope of this work the following parameters were tested: the flow rate of both the LC and the auxiliary pump supplying the luminol solution, the mixing ratios of these flows, the temperature of the column, the concentration of the solution including the luminol and the cytochrome c concentrations, and the pH of the buffer solution. Once the optimal conditions were identified three different types of samples were measured: commercially available peroxide standards, samples with a complex mixture of peroxides generated through liquid-phase ozonolysis of α-pinene and 3-carene, and laboratory generated SOA from α-pinene, 3-carene, naphthalene, and a 3-carene and naphthalene mix also containing complex mixtures of peroxides. The peak areas of the different chromatograms were compared to the standard iodometric titration method to show the quantification ability of the presented method. More details are presented in Chapter 5.

Chapter 3

Effects of Storage Conditions on the Molecular-Level Composition of Organic Aerosol Particles

Julian Resch, Kate Wolfer, Alexandre Barth and Markus Kalberer

Department of Environmental Sciences, Unversity of Basel, Klingelbergstrasse 27, 4056 Basel, Switzerland

Published in Atmospheric Chemistry and Physics, 23, 9161-9171, 2023.[113]
DOI: 10.5194/acp-23-9161-2023
`https://acp.copernicus.org/articles/23/9161/2023/`

Abstract

A significant fraction of atmospheric aerosol particles, which affect both the Earth's climate and human health, can be attributed to organic compounds and especially to secondary organic aerosol (SOA). To better understand the sources and processes generating organic aerosol particles, detailed chemical characterization is necessary, and particles are often collected onto filters and subsequently analyzed by liquid chromatography–mass spectrometry (LC–MS). A downside of such offline analysis techniques is the uncertainty regarding artifactual changes in composition occurring during sample collection, storage, extraction and analysis. The goal of this work was to characterize how storage conditions and storage time can affect the chemical composition of SOA generated from β-pinene and naphthalene, as well as from urban atmospheric aerosol samples. SOA samples were produced in the laboratory using an aerosol flow tube and were collected onto PTFE filters, whereas ambient samples were collected onto quartz filters with a high-volume air sampler. To characterize temporal changes in SOA composition, all samples were extracted and analyzed immediately after collection but were also stored as aqueous extracts or as filters for 24 h and up to 4 weeks at three different temperatures of +20, -20 or -80 °C in order to assess whether a lower storage temperature would be favorable. Analysis was conducted using ultra-high-performance liquid chromatography–high-resolution mass spectrometry (UHPLC–HRMS). Both principal component analysis (PCA) and time series of selected compounds were analyzed to identify the compositional changes over time. We show that the chemical composition of organic aerosols remained stable during low-temperature storage conditions, while storage at room temperature led to significant changes over time, even at short storage times of only 1 d. This indicates that it is necessary to freeze samples immediately after collection, and this requirement is especially important when automated ambient sampling devices are used where filters might be stored in the device for several days before being transferred to a laboratory.

3.1 Introduction

Organic aerosol (OA), and especially secondary organic aerosol (SOA), constitutes a large fraction of atmospheric fine particulate matter ($PM_{2.5}$) and has been shown to exert effects on both the climate and human health [2, 3, 166]. The complexity of organic matter on the molecular level, representing thousands of different compounds, requires detailed and sensitive chemical characterization in order to

identify the sources or atmospheric processes generating the organic material [167]. Highly detailed chemical analysis can be hard to achieve with online measurement techniques [52, 168], and instead offline analysis (most commonly mass spectrometry) is necessary, where it is common for aerosol particles to be collected onto filters and analyzed at a later point in time in the laboratory.

Although offline methods enable very detailed chemical characterization and accurate quantification, they are prone to multiple sample collection, work-up and storage artifacts, which have the potential to alter the particle composition significantly, and thus they confound the characterization of the original particle composition in the atmosphere. These influences have been discussed previously in the literature, including the use of different filter substrates, extraction methods and different storage times and conditions. Several studies (e.g., [104, 105]) have explored the differences in aerosol composition between samples collected on quartz and PTFE membrane filters and have identified significant gas-phase adsorption artifacts, especially on quartz filters. These differences prevent the direct comparison of results between different studies, particularly where the filter materials used are not described. Other studies have examined differences in extraction methods, with the notable observation that sonication causes H2O2 formation in aqueous extracts (e.g., [102, 103]). This is a particularly major problem for chemical characterization, as it triggers further reactions in the extracts, creating side products (which may themselves also be present in atmospheric particles), and therefore leading to differences in results if not taken into consideration, while vortex extractions largely avoid such artifacts [103]. A study by Roper et al. (2019) [106] compared different extraction methods of individual $PM_{2.5}$ filters and observed significant differences in the concentrations of elements and polycyclic aromatic hydrocarbons (PAHs). More recently, Wong et al. (2021) [107] investigated the effects of water versus acetonitrile as extraction solvents on the chemical composition of SOA during storage for 1–2 d and identified concentration changes for some components.

All of these studies show how small differences in sample collection, extraction and storage can lead to different results and therefore highlight how important it is to characterize such potential artifacts in organic offline analysis measurements and carefully report sample work-up conditions.

In addition, in multiple studies where aerosol particles are analyzed for their detailed organic composition, samples are stored on filters or as solvent extracts for a considerable amount of time, and analyses are sometimes performed months or even years after the initial sample collection. The total storage time is often only indirectly or not at all recorded, which makes the assessment of the nature and extent of

potential artifacts impossible. Extended storage on filters at room temperature may, for example, occur during automated sampling of high-volume samples. Storage conditions were often developed and evaluated for particle characterizations other than detailed organic molecular-level analysis, where extended storage has no significant effect (e.g., for total carbon, gravimetry, metal or inorganic ion analysis) [169, 170, 171]. However, if such filters are also used for detailed organic compositional studies, then caution is needed to avoid unintended and unaccountable alteration of particle composition before analysis.
In this study we aimed to identify the effects of different storage conditions and times on the molecular-level composition of organic aerosols using ultra-high-performance liquid chromatography–high-resolution mass spectrometry (UHPLC–HRMS). We characterized the changes occurring in organic aerosol particles collected onto offline filter samples and stored as filters or as extracts at different temperatures from room temperature to -80 °C and for different time periods, from immediate analysis to 4-week storage time. We collected and characterized both laboratory-generated SOA particles and ambient atmospheric aerosol samples from an urban location.

3.2 Materials and Methods

3.2.1 Chemicals

β-Pinene (99 %), cis-pinonic acid (98 %), camphoric acid (99 %), 4-hydroxybenzoic acid, naphthalene (≥ 99.7 %), 1,2-naphthoquinone (97%) and pimelic acid (98 %) were all obtained from Sigma Aldrich (Merck, Switzerland). Optima LC-MS grade water, methanol, acetonitrile, formic acid and acetic acid were obtained from Fisher Scientific (Switzerland). $PM_{2.5}$ ambient samples were collected on 150 mm Pall Tissuquartz membrane filters (VWR, Switzerland). SOA samples were collected on 47 mm PTFE membrane filters with a 0.2 µm pore size (Whatman, Merck, Switzerland).

3.2.2 Filter Sample and Collection and Extraction

In this study laboratory-generated SOA and ambient samples were collected and characterized to cover a wide range of organic aerosol components.
Two precursors, β-pinene and naphthalene, representing natural and anthropogenic sources, were used to generate SOA particles via O_3 and OH oxidation with a compact

aerosol flow tube, the "organic coating unit" (OCU) [108]. The detailed setup for SOA generation, concentrations and masses deposited onto the filters is presented in the Appendix B Supplement (Figure B.1 and Table B.1). Five filter samples were collected for each SOA type and storage condition to assess reproducibility. Prior to particle collection, each filter was cleaned in order to remove residual organic products from manufacture by rinsing with LC–MS-grade methanol and air-dried in the fume hood.

Ambient PM2.5 samples were collected with a Digitel DH-77 high-volume air sampler fitted with a $PM_{2.5}$ inlet (Digitel, Switzerland). The urban sampling site was on the roof of a building at 20 m height above street level at Klingelbergstrasse 27, Basel, Switzerland. Prior to sampling, each quartz filter was baked out for 6 h at 550 °C in order to remove residual organics and to ensure reproducibility; cleaned filters were stored at -80 °C and were wrapped in aluminum foil and in an airtight plastic storage bag until use. High-volume ambient aerosol samples (HVASs) were collected at a flow rate of 500 L min^{-1} for 24 h. The exposure area of each filter was 169.7 cm^2.

An overview of all samples collected and the time between collection and extraction and analysis is given in the Appendix B Table B.2. All samples were stored in the dark and at temperatures of +20 °C (hereafter referred to as room temperature), -20 or -80°C and were analyzed either immediately or after storage times of up to 44 d. Due to the large number of samples and LC–MS analyses it was not possible to analyze all samples after the exact same number of days.

The filter extraction of SOA and ambient samples differed due to the difference in the properties of the filter material, PTFE for SOA and quartz for ambient. The extraction procedure was partially adapted from the method described in Keller et al. (2022) [108] and adapted for this study as described below for SOA samples. Deviations of the method for ambient samples are indicated in parentheses.

Each filter was cut into equal quarters (for ambient filter samples five 1 cm punches were used), placed into 2 mL Eppendorf safe-lock tubes (Eppendorf, Switzerland), and placed in a freezer (i.e., -20 or -80 °C) or extracted immediately. For extraction, 1.500 mL extraction solvent (1 : 5 water : acetonitrile (ACN) *v/v*) was added to the safe-lock tube using Eppendorf Research® plus 200 and 1000 µL pipettes (Eppendorf, Switzerland), and then the samples were vortexed at maximum speed (2400 rpm) for 2 min each and placed on a Fisherbrand™ open-air rocker (Fisher Scientific, Switzerland) for 30 min (post-extraction, ambient samples were additionally put in a centrifuge for 10 min at 12 000 rpm to separate the quartz filter slurry from the liquid sample). A total of 1.500 mL of the sample extract was then pipetted into an empty Eppendorf tube to remove the filter material (for ambient samples 1.0 mL of

the sample extract was transferred to an empty Eppendorf tube using a 5 mL gastight glass Hamilton syringe and a PTFE 0.45 µm pore size syringe filter (Agilent Technologies, Switzerland) in order to avoid larger particles from being transferred into the LC, a common source of blockages). The samples were then placed into a benchtop rotary evaporator (Eppendorf Basic Concentrator Plus, Eppendorf, Switzerland), and extracts were dried for 2 h at 45 °C in vacuum concentrator alcohol (V-AL) mode until complete dryness was reached; this process was conducted in batches where necessary. Samples were then reconstituted with 500 µL (ambient samples with 400 µL in order to further concentrate the samples) reconstitution solvent (1 : 10 ACN : water *v*/*v*) and vortexed again for 90 s before they were split into five aliquots of 100 µL (ambient samples: 80 µL) in amber LC–MS vials with 150 µL glass inserts. These were then either stored for the times stated in Appendix B Table B.2 or placed directly in the LC autosampler for analysis.

3.2.3 UHPLC-MS Analysis

Liquid chromatography was conducted using the Thermo Vanquish Horizon UHPLC with a binary pump and split sampler (Thermo Fisher Scientific, Reinach, Switzerland). The Waters HSS T3 UPLC column (100 mm × 2.1 mm, 1.8 µm, Waters AG, Baden, Switzerland) was used at a temperature of 40 °C and a flow rate of 400 µL min^{-1}. Water and 10 mM acetic acid (mobile phase A) and methanol (mobile phase B) were used as mobile phases at the following gradient in a 30 min method: 99.9 % A from 0–2 min, a linear ramp-up to 99.9 % B from 2–26 min; 99.9 % B was held until 28 min and was then switched to 99.9 % A for column re-equilibration from 28.1–30 min. To clean up between sample injections and to prevent carryover, a needle wash using 1 : 4 ACN : H2O (with 0.1 % acetic acid) was performed for 15 s prior to each sample injection. Additionally, a seal wash of 1 : 10 methanol : water (with 0.1 % formic acid) was used. To ensure system suitability, the stability of the signal intensities and retention times over multiple weeks of analyses, and batch correction where necessary, an HPLC gradient test mix injection consisting of phenol, uracil and a mixture of parabens (Sigma Aldrich, Merck, Switzerland) was run daily.

An Orbitrap Q Exactive Plus (Thermo Fisher Scientific, Switzerland) was used for mass spectrometric detection in negative electrospray mode. The following instrument parameters were used: spray voltage 3.5 kV, sheath gas flow 60 a.u., auxiliary gas flow 15, sweep gas flow 1, capillary temperature 275 °C and auxiliary gas heater temperature 150 °C. The scan parameters were set to full MS, a scan range of *m*/*z*

85 to 1000, a resolution of 70 000, an automated gain control (AGC) target of 3 × 106 and a maximum injection time of 25 ms. The mass spectrometer was calibrated daily using the Thermo Scientific Pierce Negative Ion Calibration Solution (Fisher Scientific, Switzerland). Additionally, a standard mix consisting of camphoric acid, cis-pinonic acid, 4-hydroxybenzoic acid, 1,2-naphthoquinone and pimelic acid was run at concentrations between 10 ng mL^{-1} and 0.01 mg mL^{-1} in order to obtain the calibration curves of compounds with atmospheric relevance and which were also used along with the HPLC gradient test mix in order to monitor the stability of the signal intensity and retention times (see Appendix B and Table B.3). Cis-pinonic acid and 1,2-naphthoquinone were additionally used for annotation.

In total 810 (270 per sample type) LC–MS injections were run, including repeats and excluding blanks and conditioning runs. Raw data files were converted to mzML format using ProteoWizard (MSConvert, version 3) software [124]. LC–MS data analysis was performed in R 4.2.1 (R Core Team, Austria) in RStudio 2022.07.1 (Boston, MA, USA) using the XCMS package for untargeted peak detection [121, 122, 123] and the peakPantheR [120] package for targeted feature extraction. For the untargeted analyses, the XCMS centWave algorithm was used for peak detection on the centroided data in order to produce a table of *m/z* retention time (RT) pairs, henceforth referred to as features. All reported features are assumed to be the deprotonated (i.e., singly charged, $[M–H]^-$) species unless otherwise indicated. Additional in-house scripts using R and Python were used for post-processing data analysis.

To observe variation and trends in the large datasets produced, principal component analysis was used, as this method easily illustrates the dominant sources of variation in multivariate data. Multivariate statistical analysis was performed with SIMCA® 17 (Sartorius, Germany); model performance was evaluated using R^2 values as a measure of proportion of variance explained by the model and using the Q^2 value, which estimates the predictive power of the model through 7-fold cross-validation using randomly selected test/train subsets taken from the whole dataset. Hotelling's T^2 statistic was used to estimate potential outlier samples in the principal component analysis (PCA) scores relative to the whole dataset using the multivariate probability distribution. The ggplot2 package [172] in R was used to plot the PCA score plots from the SIMCA data. Python [125] implemented in Spyder IDE 5.1.5 [173] with the Matplotlib [174] and NumPy [175] packages was used for time series plots. Error bars in the time series plots using the peak area represent the total relative uncertainty of ±20 %. This was calculated as the sum of the following individual uncertainties: the standard deviation of the UHPLC-MS injection repeats, which was 4 %; the standard deviation of the detected peak area for specific features of the filter sample repeats,

which was 13 %; and the variation due to the filter extraction procedure, which was calculated from the immediately extracted samples and which was as high as 23 %.

3.3 Results and Discussion

The main focus of this study was to evaluate the potential effects of storage conditions, i.e., time, temperature and storage on filter versus extract, on the concentration of organic aerosol components in laboratory-generated SOA and ambient urban aerosol. The samples were analyzed with UHPLC-Orbitrap MS, and peak areas of all detected peaks in each chromatogram were compared using multivariate statistical analysis to identify overall trends. In addition, the peak areas of the most intense peaks in the base peak chromatogram (BPC) for each sample type were investigated in more detail.

3.3.1 Laboratory-Generated SOA from β-Pinene

β-Pinene was chosen as a representative biogenic precursor for SOA [2]. In order to reduce the large number of total features detected and to remove potential interferences from non-informative noise and background peaks, a peak intensity filter was set to 7×105 (equivalent to 0.12 % of the highest peak intensity in the sample); hence only features with a peak intensity higher than this value were considered for further analysis. This led to 4735 features being detected for each of the 270 β-pinene SOA samples analyzed (excluding blanks); this figure is comparable with previous studies, with a similar number of features being detected in ambient $PM_{2.5}$ samples using LC–MS characterization [176].

The PCA score plot of principal components (PCs) 1 and 2 (Figure 3.1) using non-normalized peak intensities shows that for samples stored as extracts and filters, the key parameter to ensuring stable sample composition over weeks was the storage temperature. The samples immediately extracted and analyzed on the day of collection represent the freshest samples available, and the tight clustering of these indicates the stability between different filters and the reproducibility of the aerosol generation and extraction. Both frozen sample types demonstrated little deviation in the multivariate space from the fresh samples, which confirmed the initial assumption that keeping both extracts and filters at cool temperatures best preserves the chemical profile for at least several weeks as represented by the peak intensity

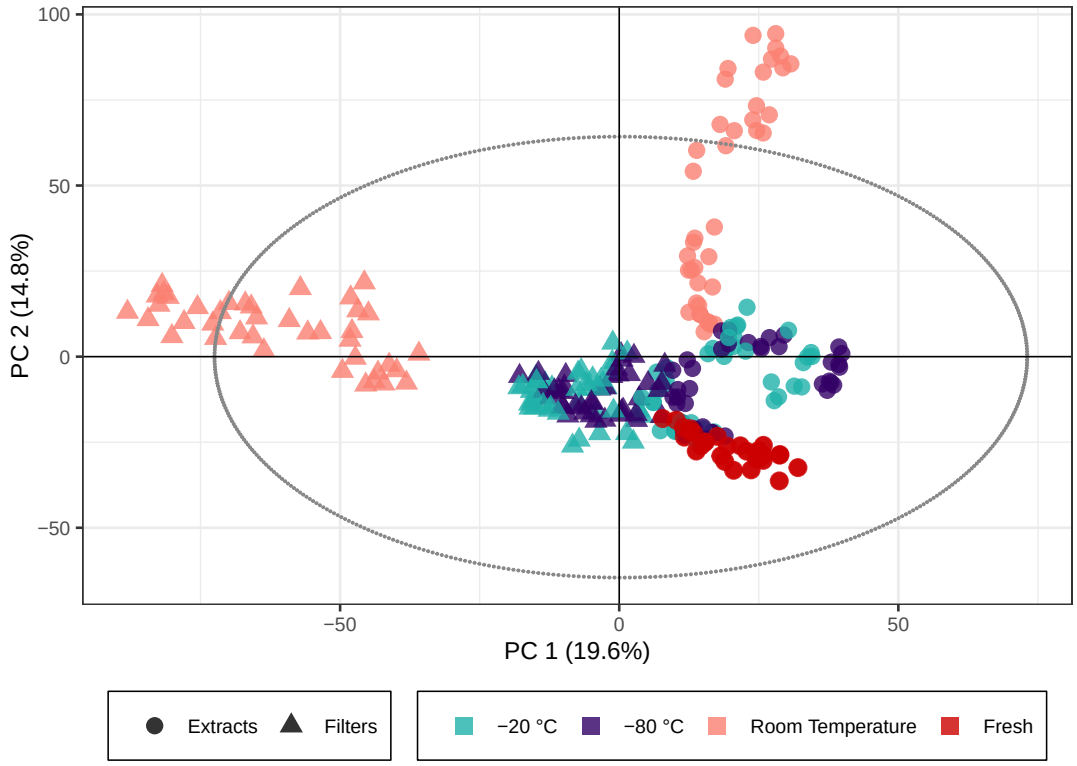

Figure 3.1: PCA score plot of the β-Pinene SOA samples. The colors represent the storage temperature, and the directly analyzed (i.e. fresh) samples and icons indicate the storage type. Hotelling's T^2 ellipse (95 %) is represented by the dotted line. $R^2X[1]$ is 0.196, $R^2X[2]$ is 0.148, $Q^2[1]$ is 0.190, and $Q^2[2]$ is 0.176.

for SOA samples. For $\log_{10}(x)$ normalized peak intensities, the PCA score plot is presented in Appendix B Fig. B.3. The same trend can be seen with the exception of the extracts stored for 4 weeks, where the overall composition also starts to deviate significantly from the fresh samples.

In contrast, samples kept at room temperature drift away from the fresh samples in the PCA model, indicating a change in composition. Samples stored as filters or extracts at room temperature displayed a different behavior in PC1 and PC2 (PC1 giving the biggest variance for the filters and PC2 for the extracts). This suggests that there is a significant difference between samples that are extracted immediately and ones that are kept as filters at room temperature. For these room temperature samples, there is a clear temporal trend over the storage time of about 4 weeks: the longer the samples were kept at room temperature, the larger the deviation from the fresh samples (see also Appendix B Fig. B.2, displaying the storage time for each data point). Both the filters and the extracts stored at room temperature for 2 and 4 weeks surprisingly unveil signals outside of Hotelling's ellipse representing the 95 % limit of the multivariate probability distribution for the dataset, indicating that if the

sample set was unknown, these samples might be qualified as outliers. The filters and extracts stored at room temperature seem to change their overall composition most significantly during the first days of storage because the biggest change per day seems to occur at the beginning of the storage time (Appendix B Fig. B.2).

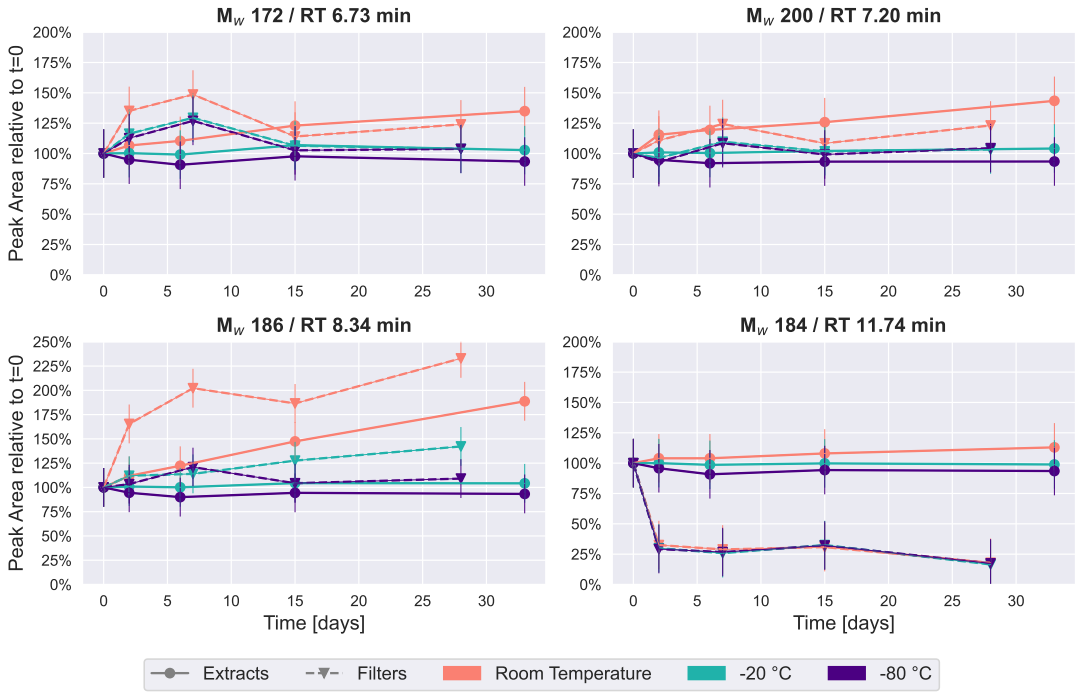

Figure 3.2: Time series plots of the four most intense peaks in the β-pinene SOA samples over a period of 4-5 weeks. Especially for room temperature storage conditinos, the concentration of some of these four compounds changes considerably.

The four most intense peaks in the base peak chromatogram (see Appendix B Fig. B.4) of the immediate extracts were chosen as representative of how the relative concentration of individual chromatographic peaks change over time under the different storage conditions. Figure 3.2 illustrates these temporal trends, sorted by retention time, where each point represents the average of two repeated analyses of each of the five filters collected (i.e., the average of 10 UHPLC-MS analyses). All four compounds or isomers of these have been identified in previous studies as carboxylic acids in SOA from gas-phase oxidation of α-pinene/β-pinene [37, 54, 58], and we tentatively confirmed the M_w 184 (detected as *m/z* 183.1027, $C_{10}H_{15}O_3$) peak at 11.74 min to be cis-pinonic acid through comparison with an authentic standard. The time series plots show a similar trend to the PCA results: the samples kept at -20 or -80 °C demonstrated the highest stability, where peak areas are also mostly within 25 % of the values detected in the freshly analyzed samples for M_w 172 (detected as *m/z* 171.0663, RT 6.73 min, $C_8H_{11}O_4$), M_w 200 (detected as *m/z* 199.0976, RT

7.20 min, $C_{10}H_{15}O_4$) and M_w 186 (detected as *m/z* 185.0819, RT 8.34 min, $C_9H_{13}O_4$). This clearly indicates that storing the samples at -20 °C or below conserves samples sufficiently to prevent significant changes to the highest-intensity peaks.
In contrast, for features with M_w 172, 186 and 200, the extracts and filters at room temperature demonstrated noticeable increases over time (Figure 3.2). This observation seems to contradict the hypothesis that compounds decay during storage. However, a possible explanation for this increase in these prominent features in the monomeric mass region might be a decomposition of oligomers (i.e., compounds with 11 or more carbon atoms). Since it is assumed there is limited oxidation chemistry occurring during storage, it is unlikely that the concentration of these compounds increased due to oxidation reactions, which is the dominant formation pathway of these compounds in the atmosphere. One class of oligomers frequently described in the literature is dimer esters [40, 177, 178]. The hydrolysis of dimer esters in samples stored in aqueous solution results in an increase in the intensity of the precursor monomers as decomposition products (i.e., compounds with 10 or fewer carbon atoms) [144], which in our case would be the carboxylic acids discussed here. A time series analysis of the dimer ester M_w 388 (detected as *m/z* 387.0759, $C_{18}H_{28}O_9$) [40] is given in Appendix B Fig. B.5. This compound showed a clear decrease over time for samples stored as extracts at room temperature, and it might therefore be one of the compounds decaying in the sample, causing the observed concentration increase in compounds presented in 3.2.
An exception to this trend is cis-pinonic acid (M_w 184, RT 11.74 min), which had little temperature dependency, but the signal dropped by about 75 % for the samples which were kept on the filters, whereas it remained relatively stable in immediately extracted samples. Previous studies have observed similar results, where cis-pinonic acid demonstrated different behavior in comparison with the rest of the dataset, i.e., with a desorptive loss upon purging spiked filters with clean air [54] or a decrease in acetonitrile and an increase in water over time [107].
Overall, the results for β-pinene SOA demonstrate that samples, both extracts and filters, kept at temperatures of -20 °C or below exhibited good stability of signal intensity over time, emphasizing that for studies conducting detailed offline analysis of SOA, composition samples should immediately be frozen after collection until analysis. However, these results also indicate that at least some compounds change over time, even under these low-temperature storage conditions, and the impacts of these artifacts on quantitative and compositional analyses must be considered.
For samples kept at room temperature, there were clear and significant temporal changes in the signal intensity for many features as illustrated in Figure 3.1 and

Figure 3.2, and samples stored for a day or longer at room temperature before analysis should not be considered for detailed chemical characterization.

3.3.2 Laboratory-Generated SOA from Naphthalene

Naphthalene SOA (a representative anthropogenic aerosol; [179]) samples were analyzed analogously to the β-pinene samples. A total of 5640 peaks with an intensity higher than 7 × 105 (equivalent to 0.19 % of the highest intensity in the sample) were detected in 269 analyses.

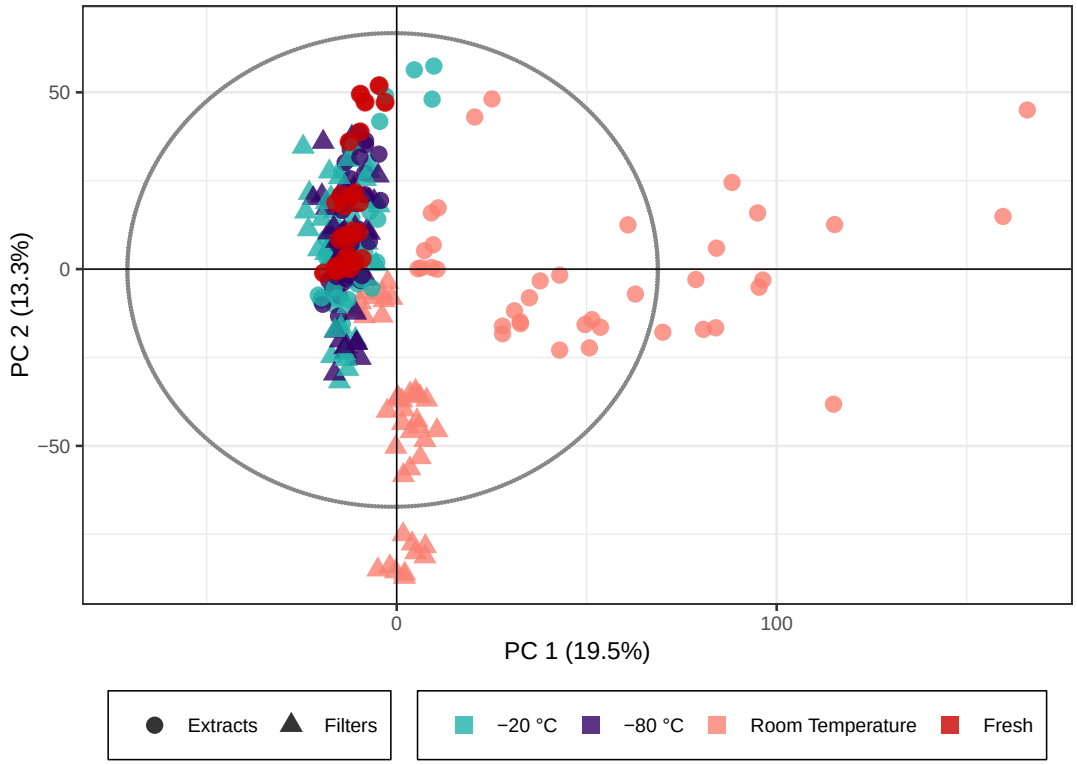

Figure 3.3: PCA score plot of the naphthalene SOA samples. The colors represent the storage temperature, and the directly analyzed (i.e. fresh) samples and icons indicate the storage type. Hotelling's T^2 ellipse (95 %) is represented by the dotted line. $R^2X[1]$ is 0.195, $R^2X[2]$ is 0.133, $Q^2[1]$ is 0.135, and $Q^2[2]$ is 0.153.

The PCA score plot for naphthalene SOA in Figure 3.3 displayed similar overall trends using the non-normalized peak intensities as for β-pinene SOA (see Figure 3.1). The generation of naphthalene SOA particles in the flow tube is slightly more unstable than for β-pinene; therefore the spread of fresh samples was higher across the five filter repeats as compared with the β-pinene samples. Similar to β-pinene SOA, the naphthalene samples kept frozen at -20 or at -80 °C exhibited closer profiles to the immediately analyzed samples and deviated little beyond the spread of the

freshly extracted samples in the PCA model. For the room temperature samples there was a clear trend of variation associated with storage time for the extracts, which showed the largest variation in PC1, and for the filters, which showed the largest variation in PC2. This similarity with the β-pinene samples again indicates that the overall composition of the SOA samples stored for 2-4 weeks at room temperature deviated significantly from the immediately analyzed samples and that the influence of the extract and filter storage results in very different compositional changes. The samples kept at room temperature for 2–4 weeks fell outside Hotelling's T^2 ellipse (see Appendix B Fig. B.6), again indicating that relative to the other samples, they have differing profiles and much larger variance across their features. The PCA score plot with $\log_{10}(x)$ normalized peak intensities is given in Appendix B Fig. B.7 and shows the same trends for all three temperatures as the score plot for the non-normalized peak intensities.

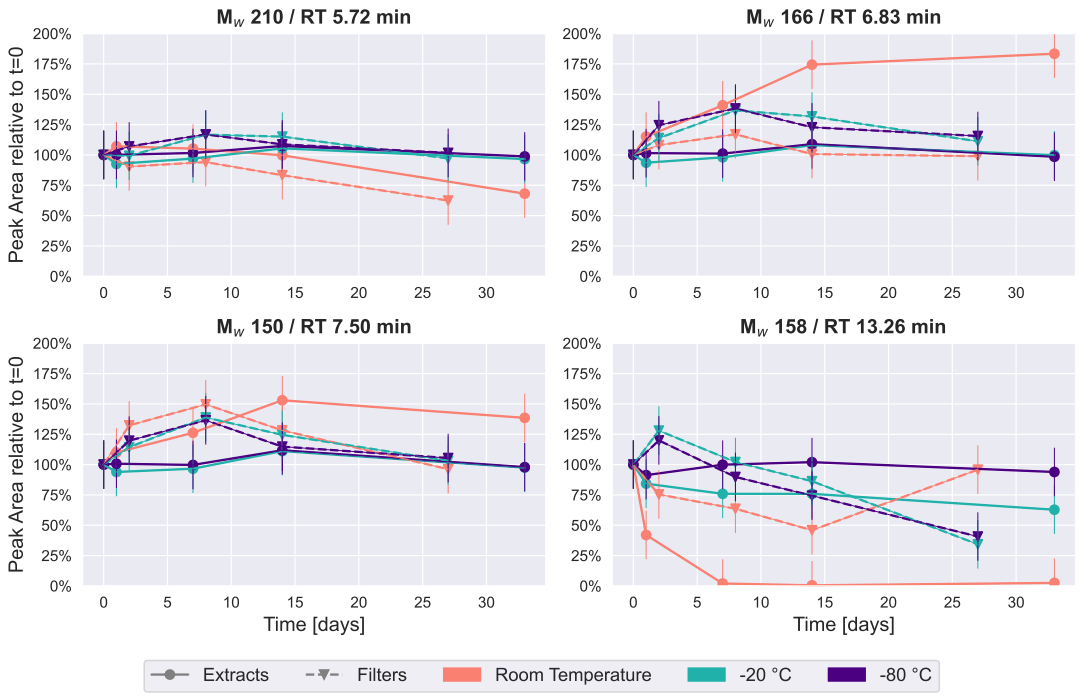

Figure 3.4: Time series plots of the four most intense peaks in the naphthalene SOA samples. Similar to β-pinene SOA (Figure 3.2), room temperature storage significantly affects the concentration of some compounds in naphthalene SOA.

These trends were also visible for the four most intense peaks in the base peak chromatogram of naphthalene SOA samples as presented in Fig. 4. Again, the most stable storage conditions were freezing of the samples, and extracted samples indicated a slightly improved temporal stability over the samples stored on filters in the freezers. The most noticeable changes occurred for samples kept at room temperature. The

most significant decay over time at room temperature was seen for M_w 158 (detected protonated anion of M_w 158: *m/z* 159.0451, $C_{10}H_7O_2$) at 13.26 min, which was identified as 1,2-naphthoquinone through comparison with an authentic standard. For extracts, the signal intensity dropped to less than half in the first 24 h, before disappearing completely in the samples analyzed after 1-4 weeks, and it appeared stable only when stored at -80 °C as the extract. 1,2-Naphthoquinone is of increasing interest in the literature, as oxidized polycyclic aromatic hydrocarbons (PAHs) are known to cause oxidative stress in human lung cells and are thus a direct contributor to particle toxicity from anthropogenic sources [180]. It is evident from this data that particle extraction and storage conditions need to be carefully described and considered when these compounds are used for source apportionment or to infer particle health effects from laboratory-generated samples.
M_w 166 (detected as *m/z* 165.0192, RT 6.83 min, $C_8H_5O_4$) has previously been found in naphthalene SOA samples and identified as phthalic acid [181]. The most stable conditions for this compound were again observed when samples were kept frozen, while in extracts stored at room temperature, this compound steadily increased to almost double the intensity after a month. A possible explanation for the increase in especially M_w 166 could again be the decay of oligomeric compounds, causing an increase in their monomeric counterparts.
The other isomers of M_w 210 (detected as *m/z* 209.0455, RT 5.72 min, $C_{10}H_9O_5$) and M_w 150 (detected as *m/z* 149.0243, RT 7.50 min, $C_8H_5O_3$) selected for Figure 3.4 showed moderate changes in comparison with the previously discussed compounds. Both exhibited relatively little change over time in samples which were kept in the freezers. The largest time-related effect can be seen for the samples kept at room temperature, where there is either a decrease (M_w 210) or an increase (M_w 150) of around 40 % after 4 weeks. These four most intense peaks contributed the most to the variance observed in the PCA score plots, thus driving the separation of samples by storage condition, and again reinforce the requirement to store organic aerosol samples in a freezer to best preserve their original composition.

3.3.3 Atmospheric Aerosol

To assess if the significant temporal trends and the differences in storage (i.e., filter vs. extracts) observed for laboratory-generated SOA samples were also visible in ambient samples, we collected five high-volume ambient aerosol samples in the city center of Basel and analyzed, extracted and stored them using the same methods as for the laboratory-generated SOA samples.

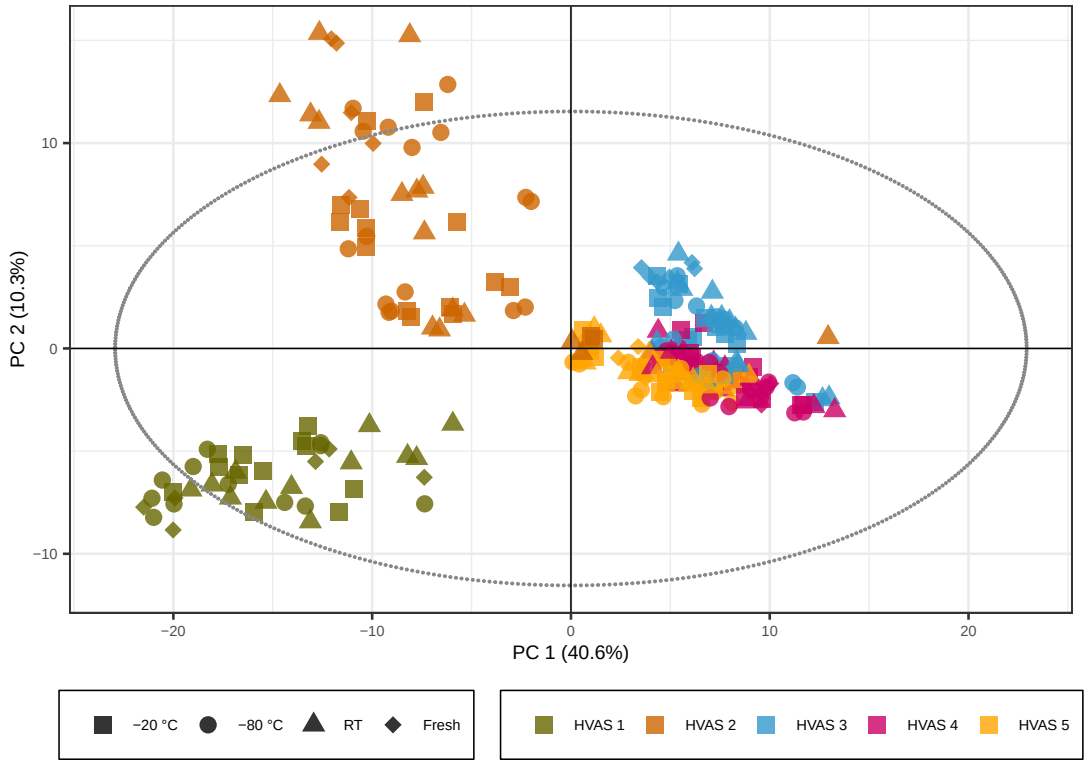

Figure 3.5: PCA score plot representing the HVAS filters with the exclusion of the batch effect due to different mobile phases. The colors represent the different HVAS filters and shapes the different storage temperatures. $R^2X[1]$ is 0.406, $R^2X[2]$ is 0.103, $Q^2[1]$ is 0.399, and $Q^2[2]$ is 0.157.

The PCA score plot with non-normalized peak intensities for the ambient samples is given in Figure 3.5 (the score plots with $\log_{10}(x)$ normalized peak intensities are given in Appendix B Figs. B.9 and B.11, showing the same trends). The colors represent the five different HVASs, and shapes correspond to storage temperatures. More detailed information on storage temperature and type is given in separate score plots in the Appendix B (Figs. B.8 and B.10). During LC–MS analysis of the ambient samples, a different batch of UHPLC-grade water from the supplier was needed for the samples stored for 3–4 weeks, causing higher background signals and a reduced overall signal intensity for peaks with lower intensities. This difference in signal intensity could be adjusted in the time series analysis of the compounds previously detected in SOA samples through the intensity of our standard mix but was difficult to account for in the PCA. In order to solve this problem, the peak intensity parameter was increased from 7 × 105 (as used for the SOA samples discussed above) to 4 × 106 (equivalent to 4 % of the highest peak intensity in the sample) to reduce the number of total compounds detected from 2800 to around 400 because the

higher intensity peaks were not significantly affected by this increased background. Additionally, a time series of the signal intensity of individual compounds was checked manually to exclude compounds which had a clear "step function", leaving roughly 240 compounds to be included in the PCA. The non-corrected version of the score plot is given in Appendix B Fig. B.12, where the same general trend is still visible as in Figure 3.5 and Appendix B Fig. B.8 and B.10.
In strong contrast to the laboratory-generated SOA samples, the PCA score plots for the ambient samples indicated little storage-dependent variation in the signals, as samples grouped together in the first two PCs independently of storage temperature or condition, indicating a much larger influence of individual samples on the variance than of the storage condition. The HVASs from days 3–5 showed similar scores, as they were all sampled in the same week or even on consecutive days. To ensure that there was no additional variation between the storage temperatures, we also looked at PCA score plots of the individual HVASs, which presented the same trends (data not shown).
We conclude that in ambient samples the concentration of organic components is overall more stable over time and is apparently less affected by storage conditions compared with laboratory-generated SOA samples. This could be due to several factors. Organic components in ambient particles originate not only from SOA sources but include many primary particle components from other sources such as biomass burning, fossil fuel combustion, industrial activities (e.g., solvents) and primary biological material [182]. Components from these sources might be more stable than SOA components. In addition, in ambient samples, a significant fraction of the total particle mass is inorganic components (mainly ions like sulfate, nitrate and ammonium), resulting in a more diluted concentration of individual organic components (compared with pure laboratory-generated SOA samples), which might limit the availability of organic reaction partners, and thus increasing the stability of some organic components.

For a compound-specific comparison between SOA and ambient samples, we analyzed four compounds which were detected in all HVASs, and which were also among the four highest peaks in the SOA samples (see Figure 3.2 and Figure 3.4). The time series for these compounds in the HVASs is given in Figure 3.6. HVAS 1 was excluded from this analysis because of the missing 2-week time point (Appendix B Table B.2). Overall, these compounds were more stable over time in the ambient samples compared with the pure SOA samples, as also indicated in the PCA analysis, supporting the hypothesis that the lower concentrations of individual organic compounds in

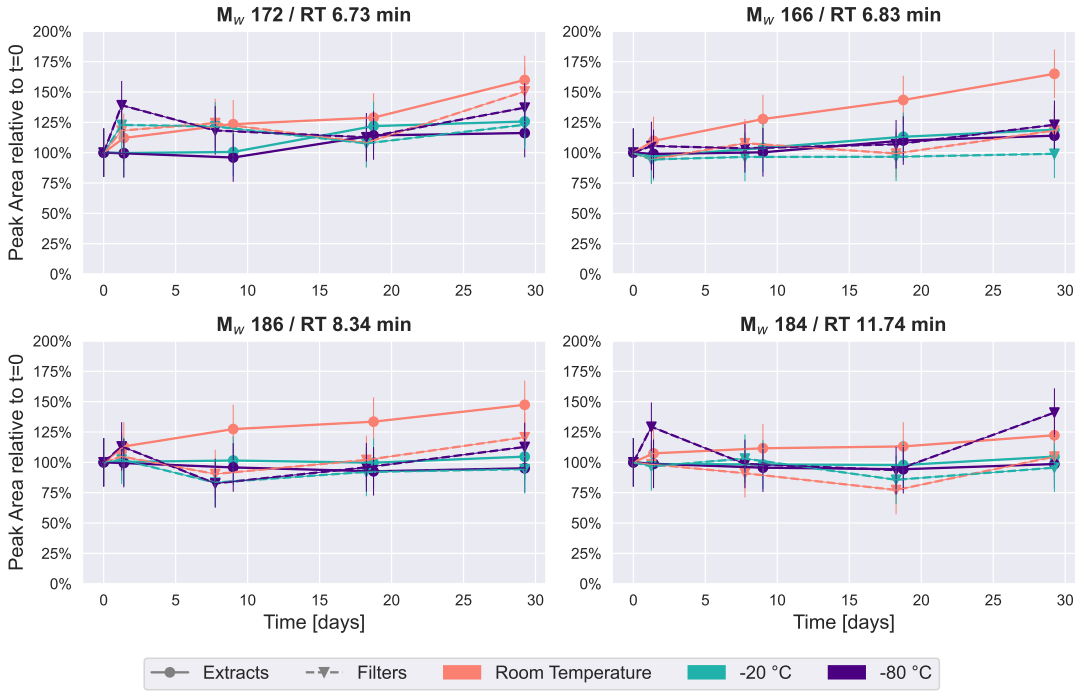

Figure 3.6: Time series of an average of 2-5 HVASs of four previously detected peaks in the SOA samples from β-pinene (*m/z* 171.0663, 185.0819 and 183.1027) and from naphthalene (*m/z* 165.0192).

ambient aerosol lead to less signal change over time. This increased stability might also be due to the lower oligomer content in ambient aerosol in comparison with laboratory-generated SOA [33]. Nevertheless, clear changes were observed for M_w 166 and 186 for samples stored at room temperature and as extracts, which showed similar patterns to ambient and pure SOA samples. Slight changes over time (especially after 4 weeks) were seen for the M_w 172 feature in the room temperature samples. The largest difference between ambient and laboratory SOA samples was observed for cis-pinonic acid (M_w 184), where there was no significant difference between filter and extract storage in the ambient samples, but a large decay occurred in the pure SOA samples stored on filters. Reasons for this very different behavior are unknown but could be related to the different filter material used for ambient and lab samples (quartz vs. PTFE). Another cause could be desorptive loss of cis-pinonic acid due to the large air masses in the HVAS as previously reported (Glasius et al., 2000) [54].

Overall, the storage of ambient samples on filters demonstrates very good stability of the signal intensity and provides confidence that the concentration of organic components may not change significantly in ambient urban samples which are collected weeks before analysis and which are stored on filters.

3.4 Conclusions and Recommendations

The results in this study represent a thorough investigation of the temporal changes in the detailed organic composition of offline aerosol samples collected on filters under different storage conditions and for different types of aerosol. Both SOA and ambient samples largely preserved their chemical profiles when stored at temperatures of -20 or -80 °C for up to 4-6 weeks. We could clearly demonstrate that there was no discernible difference in the particle composition when particles were stored at -20 or at -80 °C, with the exception of very few individual components such as cis-pinonic acid (Figure 3.2) and extracts stored for extended periods of time (i.e., ≥ 4 weeks) when the lower-intensity features are weighted more (as illustrated in Appendix B Fig. B.3).

However, for all investigated samples, but especially for laboratory-generated samples, storage of filters and of extracts at room temperature significantly affected the concentration of individual organic components, where compound formation as well as decomposition were observed. Many compounds with a high signal intensity in the chromatogram exhibited a significant increase in concentration over time when they were stored at room temperature. A possible explanation for this observation could be that some of these compounds are formed in the samples via decay of oligomers during storage, leading to an increase in their respective monomers. The different temporal behaviors of room temperature extracts and filters (as seen in Figure 3.1 and Figure 3.3) could be explained by the hydrolysis of components in the aqueous extracts versus continuing reactions of components in the organic matrix on the filters. Keeping the samples frozen between collection and analysis appeared to largely avoid such decomposition reactions.

In many previous studies, the time between sampling and analysis is at least a few days, potentially up to many years, and often storage conditions are only poorly described in publications. The study presented here evidently indicates that careful storage procedures should be adopted and described in detail in publications in order to assess potential distortions of the original particle composition, especially for laboratory or atmospheric simulation chamber samples, where significant changes can occur within a day after particle generation.

These compositional changes seemed to be less problematic for ambient particles at the urban site characterized here, but for some compounds the concentration changed by 50 % or more in ambient samples when analyzed several weeks after collection. Thus, when concentrations of individual organic particle components are studied in detail, a careful evaluation of their stability before analysis is demonstrably

important, especially when samples are kept for days or weeks at room temperature, for example during automated filter sampling. In samples from other locations, e.g., remote sites, with higher or even dominant SOA contributions, the stability could be less favorable than for the urban samples analyzed here and could resemble the laboratory-generated SOA samples analyzed in this study more.
Recommendations for future studies, when organic molecular-level composition analyses are performed, are that all samples should be kept frozen (-20 °C) as soon as possible after sampling, i.e., within a few hours, to avoid significant compositional changes. If this is not feasible, authors should mention in detail how the samples were stored and how much time passed between collection and analysis.

Supplement

The supplement related to this article is available online at: `https://doi.org/10.5194/acp-23-9161-2023-supplement`.

Author Contributions

JR, KW and MK designed the study. AB generated and collected the laboratory-generated SOA samples. JR collected the ambient aerosol samples and performed all other experimental and data analysis work. JR wrote the paper with contributions from all co-authors.

Financial Support

This research has been supported by the Schweizerischer Nationalfonds zur Förderung der Wissenschaftlichen Forschung (grant no. 200021_192192/1).

Chapter 4

Prolonged Dark Chemical Processes in Secondary Organic Aerosols on Filters and in Aqueous Solution

Julian Resch, Kangwei Li, and Markus Kalberer

Department of Environmental Sciences, Unversity of Basel, Klingelbergstrasse 27, 4056 Basel, Switzerland

Published in Environmental Science & Technology, **2024**, *58* (32), 14318-14328 [183]
DOI: 10.1021/acs.est.4c01647
`https://pubs.acs.org/doi/10.1021/acs.est.4c01647`

Keywords

SOA composition, dimer formation, esters, chemical analysis, LC-MS

TOC

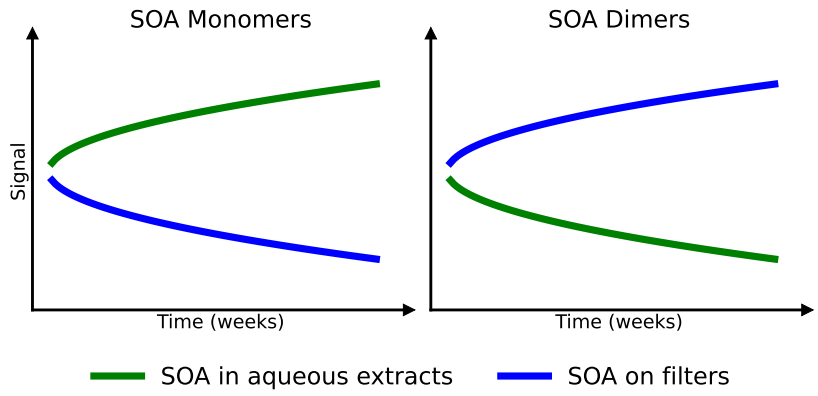

Abstract

Secondary organic aerosol (SOA) represents a large fraction of atmospheric aerosol particles that significantly affect both the Earth's climate and human health. Laboratory-generated SOA or ambient particles are routinely collected on filters for a detailed chemical analysis. Such filter sampling is prone to artifactual changes in composition during collection, storage, sample workup, and analysis. In this study, we investigate the chemical composition differences in SOA generated in the laboratory, kept at room temperature as aqueous extracts or on filters, and analyzed in detail after a storage time of a day and up to 4 weeks using liquid chromatography coupled to high-resolution mass spectrometry. We observe significantly different temporal concentration changes for monomers and oligomers in both extracts and on filters. In SOA aqueous extracts, many monomers increase in concentration over time, while many dimers decay at the same time. In contrast, on filters, we observe a strong and persistent concentration increase of many dimers and a decrease of many monomers. This study highlights artifacts arising from SOA chemistry occurring during storage, which should be considered when detailed organic aerosol compositions are studied. The particle-phase reactions can also serve as a model system for atmospheric particle aging processes.

4.1 Introduction

Atmospheric aerosols, especially secondary organic aerosol(SOA), have a large impact on climate and human health.[2, 3, 166] The detailed chemical composition of SOA is highly complex, typically containing thousands of compounds, and a molecular-level understanding of SOA composition and reactivity is important to evaluate sources and to characterize their health and climate effects in detail.[167] During the past decades, detailed chemical characterization of SOA has become a major research area,[2, 52] and a large number of compounds formed in particle-phase reactions were identified as major components of SOA.[40, 57, 184] Nevertheless, there is still large uncertainty regarding the formation of condensed-phase particle components (such as dimers and higher-order oligomers) to the total mass of SOA, sometimes being reported as high as 75% in freshly nucleated particles.[185, 186, 187, 188, 189, 190, 191, 192]

While direct online chemical characterization of aerosol composition (e.g., using aerosol mass spectrometry)[193, 194] has its advantages in fast acquisition time to provide near real-time data, collecting particles onto filters followed by extraction

and detailed offline chemical analysis, where particle collection and analysis (e.g., with liquid chromatography coupled to mass spectrometry (LC-MS)) are separated in time, is still the most often used method for both laboratory and ambient studies to characterize and quantify the detailed molecular-level composition of SOA.[52] A combination of the two is represented by Filter Inlet for Gases and AEROsols (FIGAERO) coupled to detectors such as chemical ionization mass spectrometers (CIMS), where particles are collected on filters for minutes to hours before being evaporated into the gas phase and measured after thermal desorption, which separates the compounds based on their volatility.[195] These systems have a higher time resolution than LC-MS measurements due to the absence of the filter extraction procedure. Nevertheless, we believe some of the chemical processes happening on the filters as discussed later might still have an effect on compounds collected on filters measured with these systems, especially when the filter collection times are in the time scale of hours or filters have been collected and stored for many days before being analyzed by FIGAERO-CIMS.[196, 197, 198]

One fundamental assumption of filter sample analysis is that the particle components are stable during storage and are not significantly affected by filter extraction and other workup procedures. This is likely true for most major inorganic components such as inorganic salts. However, organic compounds may undergo chemical reactions during filter storage or in extracts due to the complex nature of thousands of organic compounds present in aerosol particles. For example, Romonosky *et al.* [199] and Wong *et al.* [107] investigated the stability of organic aerosol components toward hydrolysis and hydration. The former study suggests that hydrolysis leads to a decomposition of compounds when filter samples are left in water in the dark, while the latter found little change in overall SOA composition during storage in water when focusing their analysis on several major carboxylic acids with direct infusion mass spectrometry for storage timescale of 1-2 days. Wong *et al.* [107] further observed changes between a factor of 0.05 and 4 when storing samples on foil substrates exposed to water vapor, which is in a similar range that we observed in the later discussion. Such partially contradictory results reflect the incomplete understanding of the stability of aerosol samples. Other aspects of offline filter processing such as filter extraction and storage of organic aerosol in solvents such as methanol were observed to alter the particle composition leading to methyl ester formation, while no such effects were observed for acetonitrile.[99, 200] More recently, a study from our group [113] illustrated that different filter storage conditions (i.e.,+20°C (room temperature) versus -20°C or -80°C or SOA stored on a filter versus

as extracts of a water/acetonitrile mixture) can lead to significantly different overall SOA chemical profiles, especially for samples kept at room temperature.
Here, we explore the chemical composition differences in β-pinene SOA when stored on filters and as extracts at room temperature over days and up to 4 weeks and characterized in detail using ultrahigh-performance liquid chromatography coupled to high-resolution mass spectrometry (UHPLC-HRMS). During aerosol filter sampling, for example, in automated high-volume samplers, filters are often kept at room temperature for many days or several weeks, and thus any compositional changes that might occur over such timescales need to be characterized. We observed significant composition changes in filter extracts as well as in SOA stored on filters, especially persistent concentration increases in many dimers of samples stored on filters. We further performed on-filter "spiking" experiments, where carboxylic acids were nebulized to the filters in excess to induce targeted esterification reactions on filters predeposited with β-pinene SOA, and the results support our observation of increased dimer formation on filters occurring over days. We highlight that these chemical processes after SOA filter collection and extraction are nonnegligible and deserve attention, especially when esters and other oligomers in SOA are characterized from offline particle samples.

4.2 Experimental Section

4.2.1 Filter Sample Collection and Extraction

SOA was generated via O_3 and OH oxidation of β-pinene (99%, Sigma-Aldrich, Switzerland) with a compact oxidation flow reactor, the "Organic Coating Unit" (OCU),[108] which produces stable and reproducible SOA mass concentrations. The setup used is given in Figure C.1. The average SOA concentrations in the OCU were around 6 mg/m^3, and around 300 µg SOA per filter quarter were collected (for details see Resch *et al.* [113]). Samples were collected on 47 mm PTFE membrane filters with 0.2 µm pore size (Whatman, Merck, Switzerland). The filters were cut into quarters and placed in 2 mL Eppendorf safe-lock tubes (Eppendorf, Switzerland) under laboratory conditions in approximately 40% RH and 20°C and either extracted and analyzed immediately or stored in a dark cupboard in the laboratory +20°C (room temperature) for approximately 2 days, 1, 2, or 4 weeks before analysis. Five filter samples were collected for each condition (i.e., stored as filter or extract and for different storage times) and injected in duplicates to assess reproducibility of the measurements and results.

The filter extraction procedure was as follows: each filter quarter was placed into 2 mL Eppendorf safe-lock tubes(Eppendorf, Switzerland) and either stored or extracted immediately. 1.5 mL of extraction solvent (1:5 water/acetonitrile (ACN) v/v) was added, and then the samples were vortexed at maximum speed (2400 rpm) for 2 min before being placed on a Fisherbrand Open Air Rocker (Fisher Scientific, Switzerland) for 30 min. The extract was then pipetted into an empty Eppendorf tube to remove the filter before being dried down in a benchtop rotary evaporator (Eppendorf Basic Concentrator Plus; Eppendorf, Switzerland)for 2 h at 45°C in vacuum concentrator alcohol (V-AL) mode until complete dryness. The samples were then reconstituted with 500 µL of reconstitution solvent (1:10 ACN/water v/v)and vortexed again for 90 s before being split into five aliquots of 100 µL in amber LC-MS vials with 150 µL glass inserts. Acetonitrile shows no evidence of reactions with the analyte molecules.[99] Samples were then either stored in the dark or placed in the autosampler of the LC instrument for immediate analysis. The extraction procedure was the same for the samples collected from additional "spiking" experiments as described below.

To isolate and accelerate an individual dimerization reaction among the complexity of many possible particle-phase reactions that occur in SOA deposited on filters, we performed "spiking" experiments to see if targeted reactions could be induced on the filters (see Figure C.1 for a visualization of the "spiking" process). We generated and collected two identical β-pinene SOA filters under similar conditions as for the experiments described above using the OCU shown in Figure C.1 (sampling flow rate: 10 L/min; sampling duration: 240 s; SOA mass concentration: ~500 mg/m^3. This results in a β-pinene SOA mass loading of 20 µg per filter. One filter was analyzed without further treatment, while the other filter was "spiked" with carboxylic acids. A solution containing three carboxylic acids (cis-pinic acid, cis-pinonic acid, and pimelic acid, each with a concentration of 0.2 mg/mL in water, all obtained from Sigma-Aldrich, Switzerland) was nebulized and dried with a silica gel dryer, generating dry aerosol particles containing these three carboxylic acids. These carboxylic acid particles were then deposited on the β-pinene SOA particles previously collected on a filter. This spiking process lasted for 70 min with an aerosol flow rate of 2.5 L/min passing through the β-pinene SOA filter, leading to deposition of a total of ca. 12.3 µg carboxylic acids and resulting in an even coating of the carboxylic acid as dry particles onto the β-pinene SOA particles. This procedure not only assures the even distribution of carboxylic acids on the entire filter but also that the spiked carboxylic acids are added to the SOA particles with no or only a minimal amount of liquid water and thus avoids aqueous-phase reaction conditions (as it might occur if

the carboxylic acid solutions would be added to the SOA particles through pipetting). The addition of carboxylic acid under these conditions aims to induce targeted particle-phase reactions of the carboxylic acid with alcohols present in SOA to form dimer esters.

4.2.2 UHPLC-HRMS Analysis

UHPLC-HRMS analysis of filter extracts was performed using a Thermo Vanquish Horizon UHPLC with binary pump and split sampler (Thermo Fisher Scientific, Reinach, Switzerland), equipped with a Waters HSS t3 UPLC column (100 mm × 2.1 mm, 1.8 µm, Waters AG, Baden, Switzerland), connected to an Orbitrap Q Exactive Plus (Thermo Fisher Scientific, Switzerland), which was used in negative polarity electrospray mode (all reported compounds are assumed to be the singly charged $[M\text{-}H]^-$ species). The scan parameters were set to full MS, a scan range of *m/z* 85-1000, an automated gain control target of 3 × 106, and a resolution of 70 000 with a maximum injection time of 25 ms. The mobile phases, where all solvents were Optima LC-MS grade, were obtained from Fisher Scientific (Switzerland). Water + 10 mM acetic acid (mobile phase A) and methanol (mobile phase B) were run at a flow rate of 400 µL/min in a 30 min method at the following gradient: 99.9% A from 0 to 2 min, a linear ramp up to 99.9%B from 2 to 26 min, 99.9% B was held until 28 min, and then switching to 99.9% A for column reequilibration from 28.1 to 30 min. To monitor system stability of the LC-MS over the course of measurements, daily calibrations were done using the Thermo Scientific Pierce Negative Ion Calibration Solution (Fisher scientific, Switzerland) along with injections of a HPLC gradient test mix (Sigma-Aldrich, Switzerland) and calibration curves in the range of 10 ng/mL to 10 µg/mL of a standards mixture of cis-pinonic acid, camphoric acid, 4-hydroxybenzoic acid, 1,2-naphthoquinone and pimelic acid (all obtained from Sigma-Aldrich, Merck, Switzerland). Filter blanks and solvent blanks were injected after every three sample injections to monitor the background intensity of the system and to check for carryover.

For the "spiking" experiments, the only difference in analysis was the use of an ACQUITY UPLC I-Class PLUS System with a Binary Solvent Manager (BSM) and a Sample Manager with a Flow-Through Needle (SM-FTN) (Waters AG, Switzerland) in front of the Orbitrap MS. Using the two LC instruments resulted in a slight retention time shift (which was accounted for using an HPLC Gradient System Diagnostics Mix from Sigma-Aldrich (Merck, Switzerland)). Additionally, the flow rate was reduced to 300 µL/min due to higher backpressure in this system. The mobile phases and

gradients remained the same. Untargeted LC-MS data analysis was performed in R4.2.1 (R Core Team, Austria) in RStudio 2022.07.01 (Boston,Massachusetts) using the XCMS package for untargeted peak detection.[121, 122, 123, 201]
In order to observe trends and variation in the data set, principal component analysis was used on the untargeted peaks identified. Multivariate statistical analysis was performed with SIMCA 17 (Sartorius, Germany); model performance was evaluated using R^2 values as a measure of the proportion of variance explained by the model. The Q^2 value estimates the predictive power of the model through 7-fold cross-validation using randomly selected test and train subsets taken from the data set. Hotelling's T^2 statistic was used to identify potential outliers in the data set. Hotelling's T^2 ellipse (95%) is represented by the gray dotted line in Figure 4.1. More details are given by Resch *et al.* [113].

4.3 Results and Discussion

The main focus of this study is to explore the temporal artifactual changes of β-pinene SOA composition that might occur during storage of sample extracts and filter samples at room temperature over days and up to several weeks, focusing specifically on dimer formation or decomposition. β-pinene was chosen as a representative biogenic SOA.[2] β-pinene is one of the main biogenic VOCs [27, 201, 202] and has been used for many previous laboratory SOA studies.[37, 178, 192] The compositional changes occurring on filters during storage over days also mimic particle-phase processes that might occur during the lifetime of SOA particles in the atmosphere.

4.3.1 Overall Characteristics

Figure 4.1 shows a principal component analysis (PCA) score plot for $\log_{10}(x)$ normalized peak intensities of 4735 peaks for all samples analyzed in this study and illustrates the significant differences in the temporal behaviour of chemical composition between SOA samples stored on filters (triangles) and as extracts (squares). The extract composition shows stronger changes over time in both principal component (PC) 1 and PC 2 compared to the samples stored on filters. The large distance between the composition of the directly extracted and analyzed samples (circles) and the samples stored for 2-3 days demonstrates that the most significant changes in particle composition occur over the first 2-3 days. After this initial change, the

filter samples show less variation over time, but for extracts, a continuous and strong change in composition is observed at least up to 4-5 weeks.

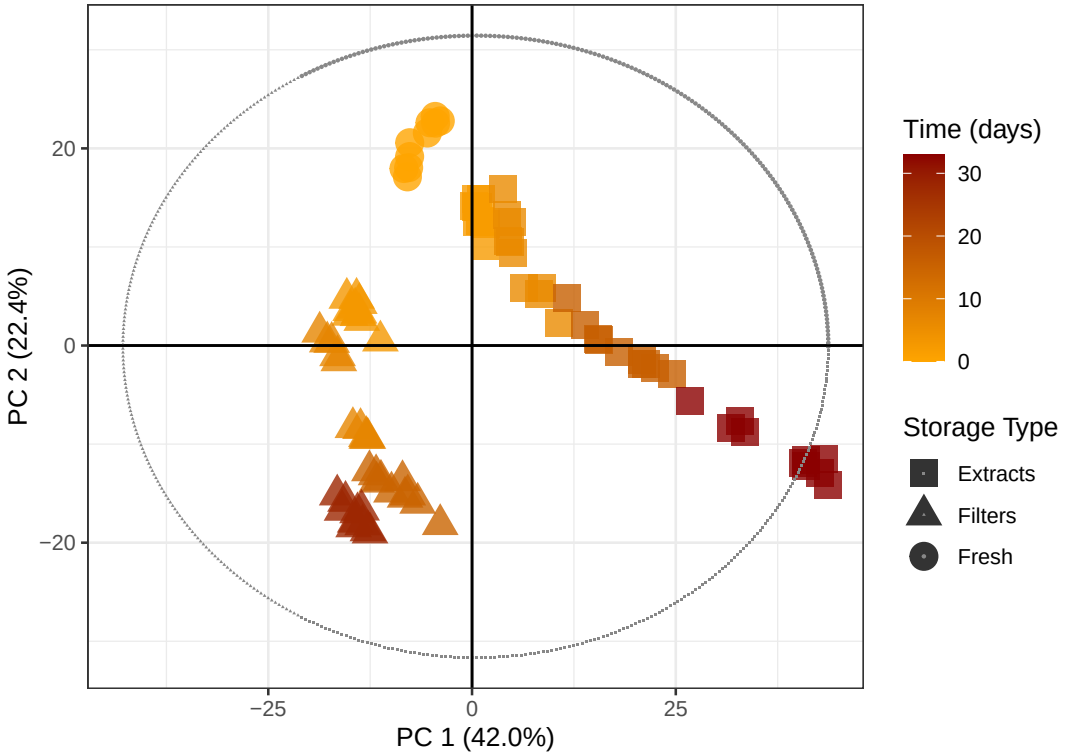

Figure 4.1: $Log_{10}(x)$ normalized PCA score plot of 4735 detected peaks in all samples. Shapes represent the storage type, and the colorbar represents the time between collection and analysis in days. The proportion of variance is displayed as PC 1 and 2, as well as $R^2X[1] = 0.420$ and $R^2X[2] = 0.224$. The predictive power of the model is given as $Q^2[1] = 0.405$ and $Q^2[2] = 0.370$.

One explanation for this observed difference between samples stored as extracts or on filters could be the hydrolysis of compounds, such as esters, decomposing into their monomeric components. It has been shown that esters form a large fraction of oligomers.[40, 57] Additionally, reactions of stabilized Criegee intermediates (SCI) with carboxylic acids have been shown to form dimer compounds containing hydroperoxide functional groups, which are known to decay quickly when stored in aqueous solutions.[144] These significant changes of particle composition over time, especially in SOA extracts, are also seen in the total ion chromatogram (TIC) shown in Figure 4.2A, including a fresh (immediately extracted and analyzed after collection), an extract stored for 33 days, and a filter stored for 28 days.
Monomers (*m/z* 100-280) and dimers (*m/z* 280-450) [33] generally elute at different retention times [178] and thus the chromatogram can be separated into two regions (Figure 4.2 B,C). In the earlier eluting monomer region (Figure 4.2 B), we observe an increase in the overall signal intensity for the stored extracts (green) compared

to that of the fresh samples (yellow). The filters (blue) on the other hand show an overall decreased signal in the chromatogram. The retention time range when most oligomers elute (>12 min, Figure 4.2 C) shows the opposite trend: for samples stored as extracts, the signal intensities stay relatively constant over 4 weeks or decreases lightly (especially peaks after 18 min retention time), while the signal intensity for samples stored on filters increases significantly over time. The same results are given as a base peak chromatogram (BPC) in Figure C.2.

These observations suggest that on filters oligomers are formed through particle-phase reactions even under conditions where no photochemistry occurs and in the absence of oxidants, continuously changing the composition of SOA particles and leading to a decrease in monomer concentrations. These reactions observed on filters during storage at room temperature are similar to particle composition changes seen for aging of SOA in other studies, where oligomer formation inthe particle phase has been reported for time scales of minutesto hours.[17, 41, 203, 204] An additional effect that could explain the temporal changes seen on filters for monomers could be the depletion of higher-volatility species through evaporative losses.[205, 206, 207, 208, 209] While this will certainly have an effect in the reduction of monomers over time, it would likely mainly explain part of the signal decrease we observe for monomers during the first day (as continuous evaporation over weeks is unlikely), and it would not explain the continuous concentration increase of dimers on filters due to their high molecular weight and thus low volatility. Hence, we assume that it is a combination of several effects taking place during the storage of filters.

Note that even though a majority of the changes observed are most prominent in room-temperature samples, there are still changes in the aerosol composition at storage temperatures at and below -20 °C. As discussed in our previous study,[113] storage temperatures of -20°C and -80°C significantly reduce these changes, but some chemical composition changes still occur.

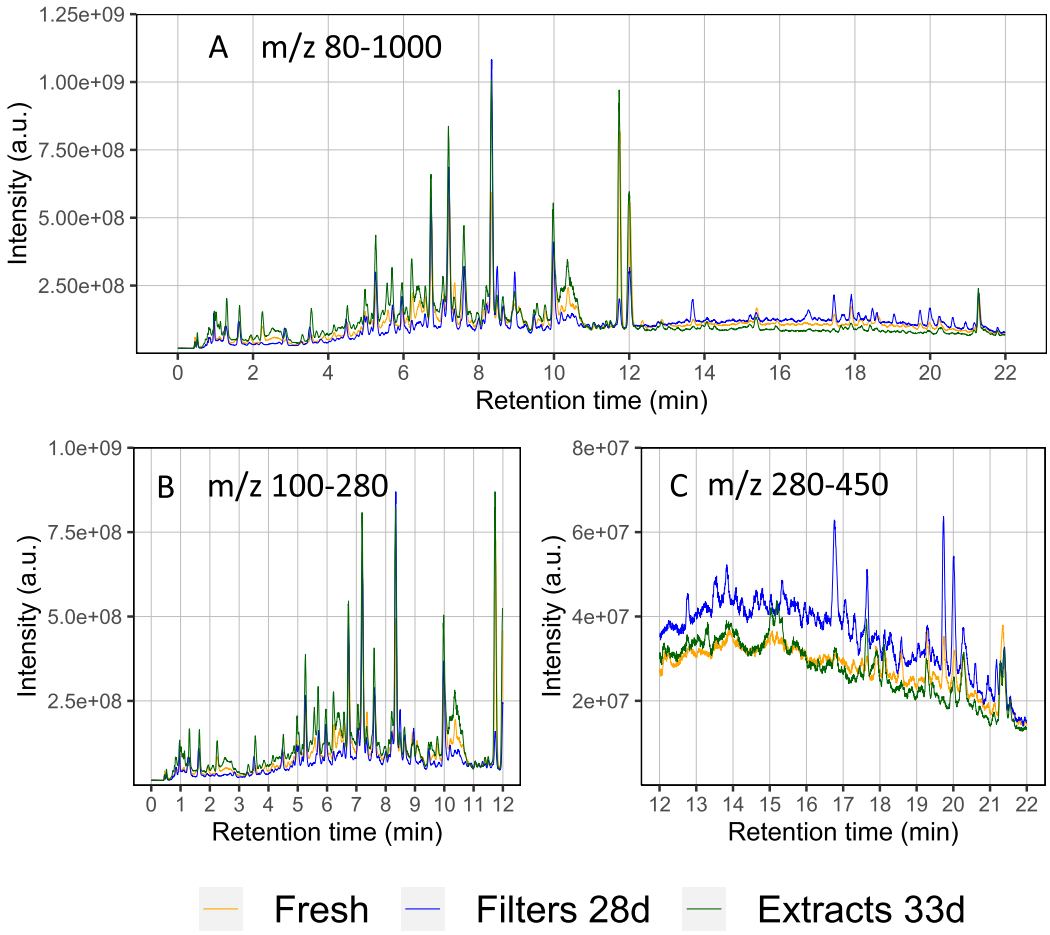

Figure 4.2: (A) TIC representing the fresh SOA extracts and SOA stored on a filter and as extract for 28 and 33 days, respectively. (B) TIC of the monomer region with *m/z* 100-280 and retention times between 0 and 12 min. (C) TIC of the dimer region with *m/z* 280-450 between 12 and 22 min. The stored filter and extract samples show inverse temporal effects in the monomer and dimer region.

4.3.2 Individual Compounds

We also characterized the temporal behavior of several individual compounds that have previously been tentatively identified in the literature as dimer esters in β-pinene SOA samples.[37, 40, 46, 57, 58, 178] A detailed list of the compounds (n = 33) investigated is given in Table C.1. From this list of previously identified ester dimers, we selected the 10 highest intensity peaks in the fresh samples and the 12 highest intensity peaks in the 4-week-old filter samples, resulting in 18 chromatographic peaks investigated in detail, which are given in Table C.2. These selection criteria avoid biased observations toward the previously discussed formation/decomposition processes in extracts/filters and enable a broad coverage of dimer esters. Extracted ion chromatograms and time series plots are given for each of the 18 *m/z* analyzed (see

Figures C.3-C.20). The individual compounds in our analysis show a wide range of temporal behaviours, depending on the specific reactions involved. All 18 *m/z* are identical to esters previously identified in the literature, but all *m/z* show several isomers in their extracted ion chromatogram (EIC) and there are likely numerous isomers without an ester functional group. A prominent trend among almost all EICs is the increase of several isomeric peaks on the filter samples stored over time. In Figure 4.3, we show the temporal behavior of representative examples of compounds in the monomer, dimer, and trimer mass range, respectively. Cis-pinonic acid (M_W 184, a monomer at *m/z* 183.1027, $C_{10}H_{16}O_3$, RT 11.73 min) is the peak with the highest intensity in fresh samples and shows a significant decrease by almost 75% in signal intensity in the 3 days after collection when samples are stored on filters and stays relatively stable in the following 3-4 weeks (this effect is even seen when the filters are stored at -20°C or -80°C).[113] In contrast, the signal intensity of the extracts seems to be stable within the measurement uncertainty over the course of a month. The significant decrease of cis-pinonic acid on filter samples could possibly be explained by the formation of oligomer compounds in the SOA formed through condensed-phase reactions [204] as well as through desorptive losses previously observed by Glasius *et al.* [54].

An EIC of the previously identified M_W 360 (*m/z* 359.1706, $C_{17}H_{28}O_8$, RT 17.57 min)[40] dimer is displayed in Figure 4.3 C. While the fresh samples show around eight distinguishable isomer peaks eluting between 13 and 18 min, the stored filter samples exhibit more than twice as many (at least 17 distinguishable isomer peaks). Several of these isomers are not detectable in the fresh or stored extract samples. The strongest increase in signal intensity is observed for the peak at 17.57 min, which shows an increase of around 500% over 4 weeks in comparison to the fresh samples (Figure 4.3 D). Possible explanations for the increase of dimers on filters are particle-phase esterification reactions of an alcohol and a carboxylic acid through Baeyer-Villiger reactions between ketones and organic peroxides.[204]

We additionally searched for trimers ($C_{20\text{-}30}$) in our samples and found several candidates that we could annotate with an according chemical formula using the XCalibur (Thermo Fisher Scientific, Switzerland) software. Figure 4.3 E displays the EIC of a trimer M_W 514 (*m/z* 513.1954, $C_{24}H_{34}O_{12}$, RT 17.72 min), which shows a strong signal intensity increase in the stored filter samples in comparison to the fresh samples for multiple isomers. The extracts show the opposite trend, with a significant decrease in peak height over time (Figure 4.3 F). This temporal behavior could indicate that some trimers listed in this work might also include an ester group, although this

could not be confirmed and the structural identification of these isomers was not the focus of this study. Several other trimers are presented in Figures C.21-C.25.

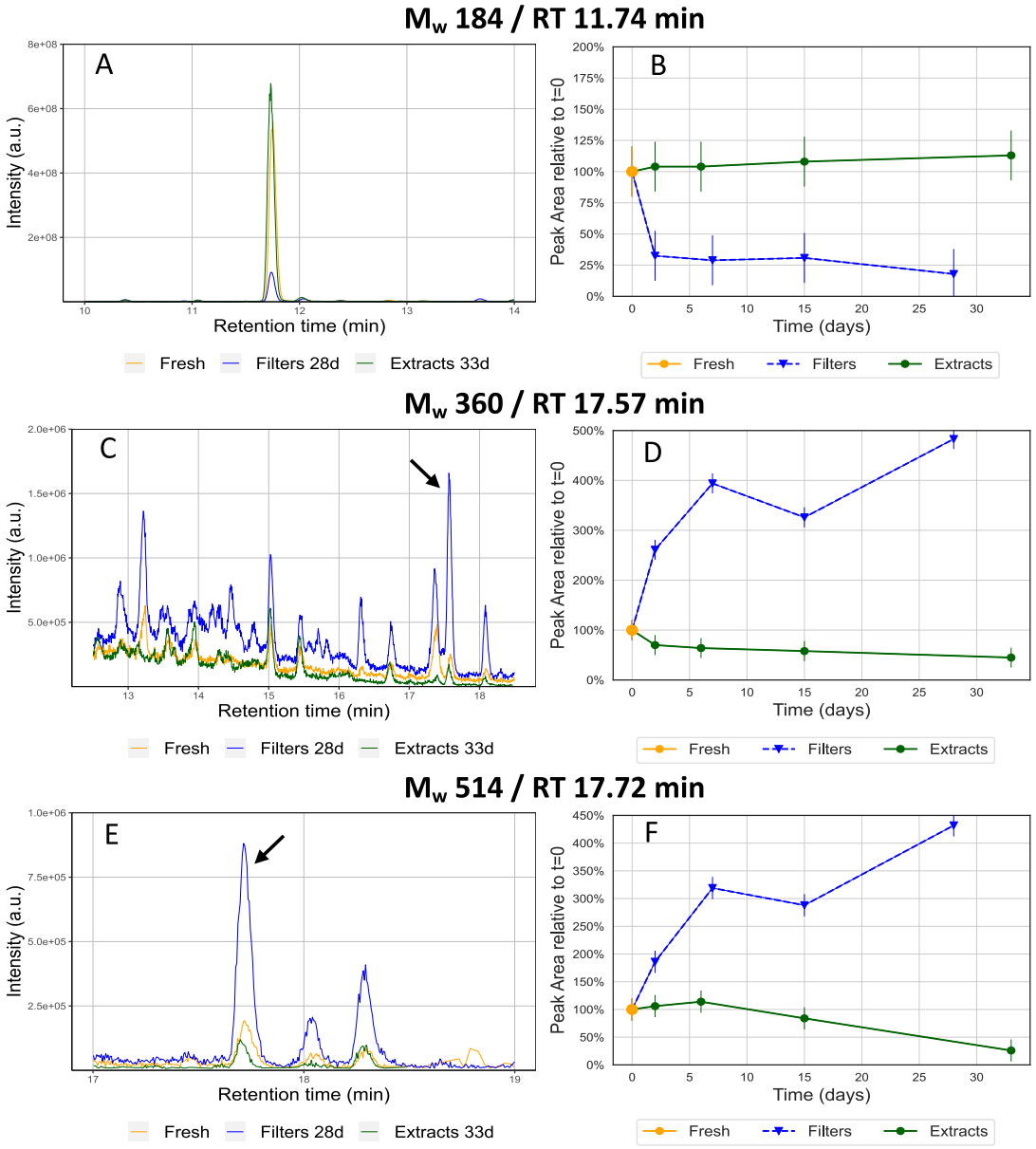

Figure 4.3: EICs and timer series plots of fresh and stored filters and extracts of (A,B) M_W 184 (*m/z* 183.1027) monomer, which shows a significant decrease after the first day when stored on filters and a slight increase in signal intensity when stored as extracts; (C,D) M_W 360 (*m/z* 359.1706) dimer, which shows a strong continuous increase in signal intensity when stored on filters and a decrease in extracts. Additionally, several new isomers are detectable in the EIC of the stored filter samples. (E,F) M_W 514 (*m/z* 513.1954) trimer, which shows a temporal behaviour similar to that of the dimer. Error bars represent the total relative uncertainty of ±20% as described in Resch *et al.* [113].

The selected *m/z* in Figure 4.3 and C.3-C.25 are only a few of the thousands of compounds present in these SOA samples. Therefore, we further examined the temporal

trends of all detected peaks in the monomer and dimer regions to determine the total amount of increasing and decreasing compounds (see Figure 4.4). Two statistical selection criteria were applied in order to categorize compounds with an increasing or decreasing trend: (a) for each of the five points analyzed (i.e., fresh, 2 days, 1 week, 2 weeks, and 4 weeks stored), the subsequent point in time must be higher (for increasing) or lower (for decreasing) than the previous one, and this condition must be true for $n \geq 3$ points with a maximum of $n = 4$. (b) a linear fit through the points must have a positive (for increasing) or negative (for decreasing) slope. Both conditions (a) and (b) must be fulfilled. 1514 peaks in the filter samples met these criteria for a clear temporal trend (1149 monomers and 365 dimers) and 1624 peaks in extract samples (1256 monomers and 368 dimers). In Figure 4.4 A, representing the monomers, almost twice as many peaks increase in the extracts over time compared with the number of decreasing peaks. Figure 4.4 B summarizes the temporal trend of dimeric compounds, illustrating that on filters almost three times more dimers increase over time than decrease in concentration. Figure 4.4 C,D shows the signal intensity fraction of all compounds that have increasing and decreasing temporal trends (relative to the sum of all monomers or dimers) on filters and extracts in the monomer and dimer regions, respectively. The number of peaks included in Figure 4.4 C,D is the same as displayed in panels A and B. These signal intensity fractions can be interpreted as a proxy of mass fractions. A large fraction (65-75% in the monomer and 45-65% in the dimer region) of the total signal intensity shows increasing and decreasing trends, suggesting that a large part of compounds in SOA shows such temporal changes.

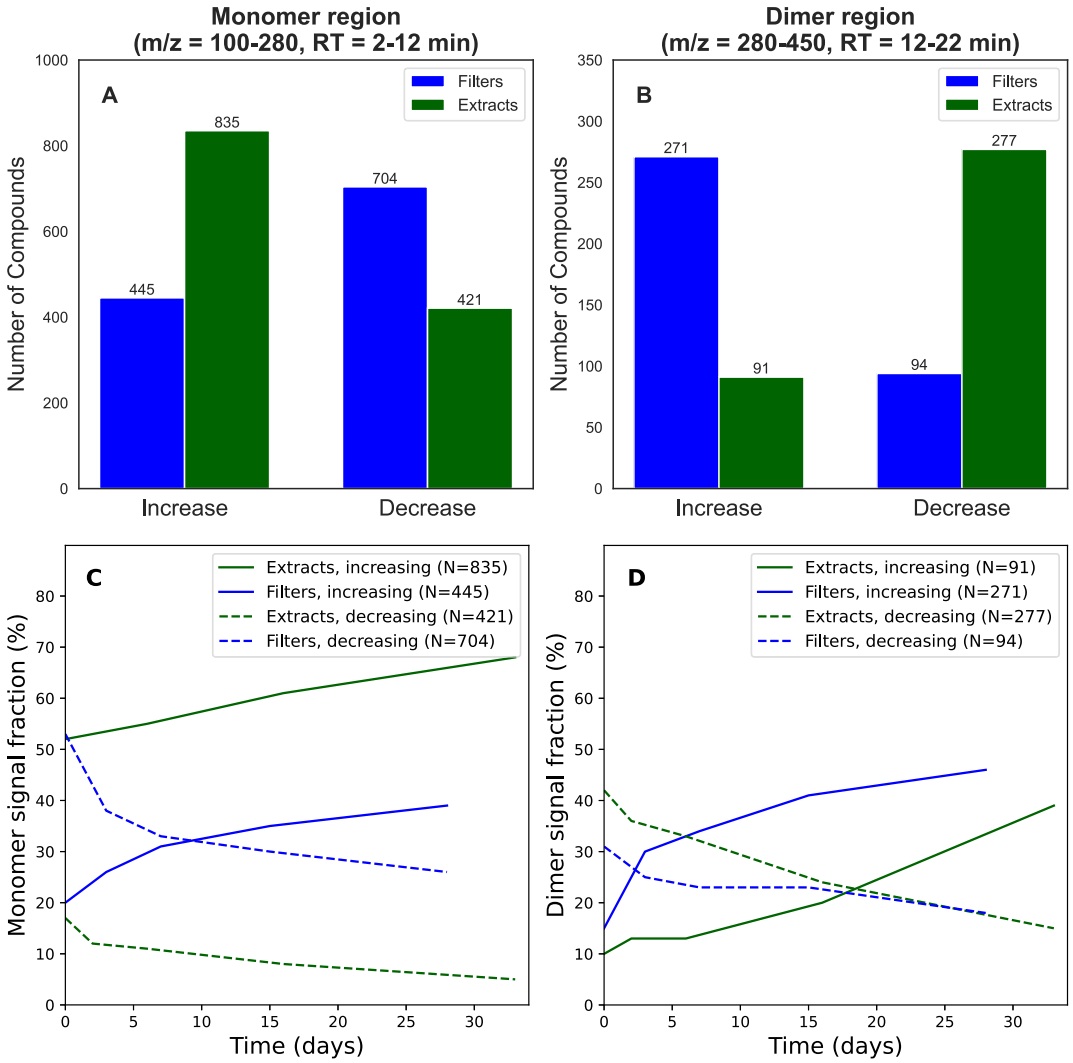

Figure 4.4: Overall number of compounds in the (A) monomer region and (B) dimer region that show an increasing or decreasing trend over 4 weeks when stored as extracts (green) or on filters (blue). The signal fraction of these categorized compounds compared to the total signal intensity of all monomers or dimers is given in panels (C,D), respectively. The remaining signal fraction shows no clear temporal trends and is not displayed here.

These results highlight that these temporal effects illustrated in Figure 4.3, and especially the persistent growth of dimers on filters, are observed for hundreds of compounds in complex SOA samples. Additionally, this overall trend reinforces the hypothesis that such temporal behaviors could be explained by a general mechanism, e.g., hydrolysis leading to decomposition of dimers and formation of monomers in SOA aqueous extracts, as also observed by Witkowski *et al.* [42]. In contrast, on filters, continuous SOA processing occurs and therefore results in a removal of monomers and formation of dimers. We acknowledge that with the high SOA concentrations used in this study, some constituents may have partitioned more from the gas phase into the particle phase compared to atmospheric conditions. We still believe the

observed composition changes on filters are not dominated by such concentration effects because we observe similar effects when the SOA concentrations in the OCU are reduced by an order of magnitude as in the “spiking” experiments discussed in the next section.

4.3.3 Accelerating Particle Phase Dimer Formation in β-Pinene SOA

In order to further test our hypothesis of continuous organic particle-phase reactions on filters over days, we nebulized a large excess of three carboxylic acid standards, pinic acid, pimelic acid, and cis-pinonic acid, onto filters (in order to evenly distribute dry carboxylic acid aerosol particles) preloaded with β-pinene SOA, which is expected to induce some targeted esterification reactions onto filters. We refer to this process as “spiking” (see Experimental Section 4.2 and Figure C.1 1) and compared their compositional evolution over time with β-pinene SOA filters without this addition, acting as controls, referred to as “filter-only”. We monitored the formation of a previously described dimer ester (M_W 358) from the esterification reaction of pinic acid (M_W 186, *m/z* 185.0819, $C_9H_{14}O_4$) and diaterpenylic acid (M_W 190, *m/z* 189.0768, $C_8H_{14}O_5$).[210] As diaterpenylic acid was previously identified as a major monomeric component in dimer formation processes through esterification.[58, 211, 212] We additionally investigated possible dimers being formed on the filters through reaction of diaterpenylic acid with the other two deposited carboxylic acids such as pimelic acid and cis-pinonic acid.

Figure 4.5 shows the EICs and the temporal behavior of both diaterpenylic acid (M_W, panel A and B) and the M_W 358 ester (panel C and D) for the "filter+spiking" and "filter-only" samples over a week. Through comparison of MS/MS measurements with the literature[210] (see Figure C.26), we tentatively assigned the peak eluting at 5.77 min (marked with an arrow in Figure 4.5 A) as diaterpenylic acid. The signal for both sample types is normalized to the fresh "filter-only", as it can be assumed that the initial concentration of diaterpenylic acid deposited onto the filters and the β-pinene SOA is the same for both "filter+spiking" and "filter-only". The signal intensity in both the “filter+spiking” and “filter-only” samples decreases by more than a half during the first day of storage. The fresh signal for the “filter+spiking” samples is significantly lower (at about 30%) than the “filter-only” signal, which can be explained by the high concentration of reaction partners (i.e., the three carboxylic acids) on the “filter+spiking” samples with which diaterpenylic acid reacts in the 2-3 h between spiking and prior to analysis.

We also observed a strong decrease in the two isomers of diaterpenylic acid eluting at 6.96 and 7.39 min for the "filter+spiking" samples (only a time series of the RT 6.96 min peak is presented, Figure C.27), while the "filter-only" samples remain stable over a week. It is likely these isomers are structurally similar and might therefore also react with different carboxylic acids to form oligomers, illustrating again the complexity of particle-phase reactions in SOA.

The M_W 358 dimer ester shows a stronger increase over time in the "filter+spiking" compared to the "filter-only" samples (Figure 4.5 C,D). This enhanced formation of the dimer in combination with the observed decrease in the precursor overtime on the treated filters provides further evidence that dimers are continuously formed in SOA over many days. As control experiments, we nebulized the three carboxylic acids onto filters in the absence of β-pinene SOA and no dimer formation was observed (see Figures C.27-C.30), suggesting that the observed dimer is indeed a reaction product of the nebulized acid and a SOA component. M_W 332 and 356 dimers, corresponding to diaterpenylic acid and pimelic or cis-pinonic acid dimer esters are given in Figures C.28 and C.29, both of which also show a stronger increase in signal intensity overtime on the "filter+spiking" samples. Note that the pathways presented here are only one of many complex and often still poorly understood dimer formation pathways in secondary organic aerosol,[39, 40, 128, 177, 178, 210, 213, 214] such as the recently described formation of the M_W 358 dimer ester through particle-phase reactions of alcohols with acylperoxyhemiacetal by Kenseth *et al.* [38], similar to oligomer formation reactions reported by Claflin *et al.* [204].

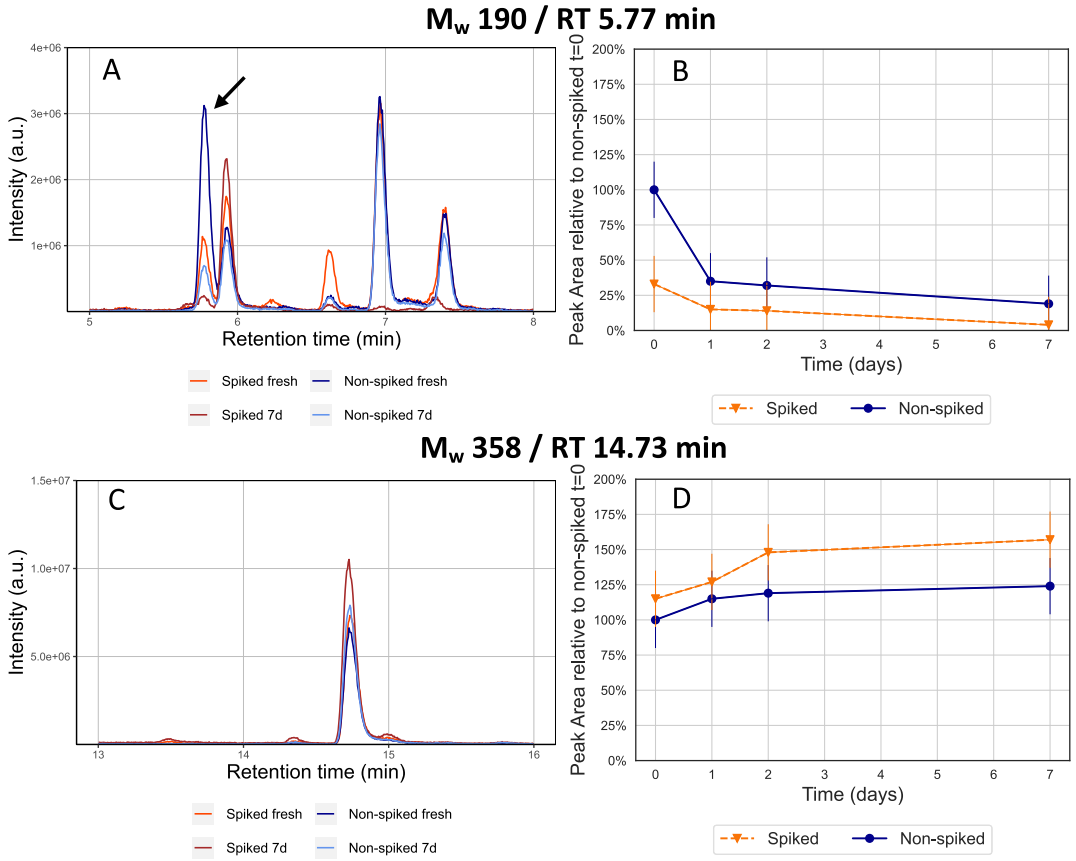

Figure 4.5: (A,B) EIC and time series plot of the "filter+spiking" and "filter-only" fresh and 7-day old filter samples for diaterpenylic acid (M_W 190, *m/z* 189.0776). A clear decrease in signal intensity is observed over time for both the "filter+spiking" and "filter-only" samples, suggesting particle-phase reaction of diaterpenylic acid over days in the SOA samples, although a much stronger decrease is observed within hours for the "filter+spiking" samples. The signal intensities in panels (B,D) are normalized to the fresh "filter-only" samples. (C,D) EIC and time series plot of the "filter+spiking" and "filter-only" fresh and 7-day old filter samples for the M_W 358 (*m/z* 357.1550) assigned to a dimer ester of pinic acid and diaterpenylic acid. There is a stronger increase in the "filter+spiking" samples over time compared to the "filter-only" samples, indicating that an excess of pinic acid in the spiked samples promotes dimer ester formation.

4.3.4 Atmospheric Implications

The results of this study show significant changes of the SOA molecular composition over several weeks after particle collection, when laboratory-generated β-pinene SOA particles are stored either on filters or as extracts in aqueous solution. We suggest two dominant processes explaining this observation: (a) continuous particle-phase chemical reactions on filters and (b) hydrolysis of dimers and higher oligomers in aqueous solution. In particular, we propose SOA condensed-phase reactions occurring on filters as important but overlooked SOA processes in previous studies, which lead to the formation of dimers and thus alter particle dimer composition

compared to the time of sampling. As illustrated in Figure 4.3 C, not only relative concentration changes of SOA components are observed over time but also new compounds are formed for some *m/z*. The total number of peaks in the samples, however, stays constant within 5%.
Our study raises concerns for filter-based offline chemical analyses, especially for detailed molecular-level organic analyses, where such stability issues need to be considered. We demonstrated in a recent study that storing samples at -20°C or below can significantly reduce compositional changes over time although not completely prevent these changes.[113] This strongly suggests that filter samples should be immediately stored in a freezer and not kept at room temperature over days before the analysis of organic components.
Continuous reactions of SOA components over days and weeks on filters might also mimic dark aging particle-phase processes of SOA in particles with low water content in the ambient atmosphere, causing an increase in dimer formation and compositional complexity over the entire lifetime of SOA particles in the atmosphere. Such long processing times are usually not accessible with existing experimental methods, e.g., atmospheric simulation chamber or flow tube studies. While the findings presented in this study focus on dimer esters, the processes described above are likely not limited to this compound class but might affect the overall chemical composition of SOA.

Supporting Information

The Supporting Information is available free of charge at `https://pubs.acs.org/doi/10.1021/acs.est.4c01647`.

> Tables including the compounds discussed in this study; as well as EICs and time series plots of those compounds; and additional illustration of the experimental setup and methods used. See Appendix C.

Acknowledgement

The authors acknowledge the funding from the Schweizerischer Nationalfonds zur Förderung der Wissenschaftlichen Forschung (SNF, Grant No. 200021_192192/1)

Chapter 5

Quantification of Peroxides in Aerosols through Chemiluminescence using HPLC In-Column Derivatization with Luminol

Julian Resch[1], Julia Bechter[1], Kangwei Li[1], Arianne Soliven[2], and Markus Kalberer[1]

[1]*Department of Environmental Sciences, University of Basel, Klingelbergstrasse 27, 4056 Basel, Switzerland*

[2]*Avantor, 1 The Markham Centre, Station Road, Theale, Reading, RG7 4PE, UK*

Manuscript in preparation

Abstract

Secondary organic aerosols (SOA) compose a large fraction of atmospheric particulate matter which affect both the Earth's climate and damage human health. One major class of SOA components are organic peroxides, which might be relevant for aerosol toxicity and health effects due to their high reactivity and oxidation potential. Despite their importance, there are large uncertainties about their concentration in SOA, which can partially be attributed to differences in detection methods. One of these methods is iodometric titration, which is used to determine the total peroxide concentration in aerosol samples. A major drawback of such methods is the inability to identify and quantify individual peroxide concentrations in organic aerosol. In this study a novel high-performance liquid-chromatography (HPLC) in-column derivatization method is presented to separate and quantify individual organic peroxides in SOA through chemiluminescence of luminol catalyzed by cytochrome c. Three different sample types were measured: several commercially available peroxide standards, samples with a complex mixture of peroxides generated through liquid-phase ozonolysis of α-pinene and 3-carene, and laboratory generated SOA from α-pinene, 3-carene, naphthalene, and a 3-carene and naphthalene mix also containing complex mixtures of peroxides. The results presented highlight the method's capability of identifying clear differences in the peroxide profile of different organic aerosol samples. All samples are additionally analyzed by traditional iodometry with UV-Vis to obtain a total peroxide concentration without any chromatographic separation. A clear linear correlation can be made between the total luminol chemiluminescence from the HPLC in-column derivatization method and total peroxide concentration quantified by iodometry with UV-Vis. This allows for identification and quantification of individual peaks, such as a unique cross-product peroxide peak in the 3-carene/naphthalene mix SOA. This peak was found to contribute 5.5% of the total peroxide concentration.

5.1 Introduction

Organic peroxides, which are organic molecules with one or more peroxide (-O-O-) functional group, have been identified as important reactive intermediates in atmospheric oxidation of organic compounds and have been associated as significant contributors to health effects of aerosols and aerosol formation in the atmosphere.[28, 29, 73, 126, 127, 130, 187] Organic peroxides are usually denoted as ROOR', where R is an organic group, and R' can either be a hydrogen atom in hydroperoxides (ROOH)

and peroxy acids (RC(O)OOH), or another organic group.[71, 215] They account for 10-70% of ambient fine particulate matter and can contribute significantly to the mass of secondary organic aerosol (SOA), ranging from ≤ 1% to ≥ 80%.[2, 3, 55, 71, 128] The large uncertainty in organic peroxide quantification can be attributed to different SOA systems and differences in detection methods and therefore reflects the uncertainty of our knowledge of organic peroxides in SOA.

Most methods were developed for bulk phase quantification measurements, which are not developed/optimized for identifying and quantifying individual peroxide concentrations in organic aerosols.[71] Several methods have been used to quantify peroxides in aerosols. These methods include electrochemical reduction [131], fluorescent detection of a derivatized fluorescing dimer produced through the derivatization of peroxides [82, 132, 133, 134], and the most common method of iodometric titration (also called iodometry).[71, 135, 136, 137]

Iodometry with UV-Vis detection is a well established method for total peroxide quantification in all sort of samples, as it is easily applicable and has the benefit of being able to quantify the sum of all peroxides in a sample. The disadvantage being the long reaction time of 3 h+ between peroxides and potassium iodide (KI) and studies have even shown that longer reaction times may be necessary until all peroxides have reacted.[136, 216] A recent study by Alba-Elena *et al.* [137] presents a summary of previous work in which iodometric titration has been applied to quantify peroxides in SOA samples. In this work iodometry was used to quantify the total peroxide concentration in samples after 24 h reaction time.

A possibility of individual peroxide quantification and ability to capture the peroxide profile of complex aerosol samples, is the use of chromatography-based methods such as liquid- or gas-chromatography (LC or GC), which are capable of identifying different types of organic peroxides in complex samples through separation within a column. A combination of chromatographic separation and derivatization is possible through either pre- or post-column LC derivatization methods. While pre-column derivatization allows for identification, quantification is only possible if standards of the compounds are available. One application of such pre-column peroxide identification is a recently presented method by Zhao *et al.* [144], where 2 aliquots of the same sample are prepared and one sample is stored as is, while the other has KI added to convert the peroxides present in the samples. Both samples are then injected into an LC-MS and comparison of these allows for identification of peroxides, as the peaks that decrease in intensity in the KI prepared sample are identified as peroxides.

Post-column derivatization has the advantage over other (pre-column) derivatization methods of being non-destructive (i.e. the sample is not mixed with a reagent until after injection, hence the same sample can be used for multiple injections of different analysis techniques) and allowing for quantification of individual compounds in the whole sample due to the chromatographic separation, which is not the case in pre-column derivatization methods. In this study we present the implementation and application of a novel high-performance liquid-chromatography (HPLC) in-column derivatization method to separate and quantify organic peroxides in aerosol samples using chemiluminescent detection of luminol catalyzed by cytochrome c. Post-column derivatization methods using luminol for peroxide detection have been used in other areas of research where complex matrices are often encountered, examples include forensic sciences and the fragrance industry, but no one has applied it to organic aerosol samples.[83, 217, 218, 219, 220, 221]
Three different types of samples were measured and quantified, commercially available standards, samples generated through liquid-phase ozonolysis of relevant monoterpenes, and laboratory generated SOA samples from different anthropogenic (naphthalene) and biogenic (α-pinene and 3-carene) precursors using an oxidation flow reactor. We highlight the methods capability of identifying the differences and similarities in chemical profiles between LPO and SOA samples. Generation of SOA using a mixture of naphthalene and 3-carene show that we are able to identify a unique cross-product peroxide. The organic peroxide quantification capability of the method is established as a clear linear correlation between HPLC-Chemiluminescence (HPLC-CL) and iodometry using UV-Vis. We quantify the individual peroxide concentration of this cross-product peroxide peak. Additionally, the peroxide mass fraction and moles of peroxide functional group per mass of particle are reported for all SOA samples.

5.2 Materials and Methods

5.2.1 Chemicals

All chemicals were purchased from Sigma Aldrich (Merck, Switzerland) unless stated otherwise and were used as purchased. Abbreviations and suppliers are given in parentheses. α-pinene (a-pin, 98%), 3-carene (3-car, 95%), 3-chloroperbenzoic acid (mCPBA, ≥77%), acetic acid (Optima LC-MS grade, Fisher Scientific), acetonitrile (MeCN, Optima LC-MS grade, Fisher Scientific), benzoyl peroxide (b-per,75%), boric acid (≥99.5%), cumene hydroperoxide (Cu-HP, 80%), cytochrome c from equine

heart (cyt c, C2506, ≥95%), dimethyl sulfoxide (DMSO, ≥99.9%), hydrogen peroxide solution (HP, 30wt.% in H_2O), luminol (≥97%), methanol (MeOH, Optima LC-MS grade, Fisher Scientific), naphthalene (nap, ≥99.7% analytical standard), potassium chloride (99.0-100.5%), potassium hydroxide (≥85%), potassium iodide (KI, ≥99.0%), sodium carbonate (≥99.5%), tert-butyl hydroperoxide (tB-HP, 70% solution in water), water (Optima LC-MS grade, Fisher Scientific).

5.2.2 Sample Generation

Standards

HP, tB-HP, mCPBA, Cu-HP, and b-per standards samples were generated by preparing 1 M stock solutions. Hydrogen peroxide and tert-butyl hydroperoxide were diluted with water, mCPBA and cumene hydroperoxide were dissolved in MeCN and benzoyl peroxide was dissolved in MeCN with minimal amounts of DMSO added to increase solubility. All sample dilution series were made using MeCN.

Liquid-Phase Ozonolysis

Liquid-phase ozonolysis (LPO) experiments were done according to Li *et al.* [222] and Zhao *et al.* [144] without addition of carboxylic acid standards to generate samples in a simple experimental protocol, which contain highly complex peroxides mixtures that resemble organic peroxides present in SOA. Stock solutions of α-pinene and 3-carene were prepared in acetonitrile to prevent decomposition of peroxides in solution after bubbling. They were then diluted to 1 mM each and topped up with MeCN until a total volume of 10 mL was reached in an impinger. A 100 mL/min flow of clean air was irradiated with an UV lamp (Pen-Ray photochemical quartz lamp, λ= 185 nm) to generate high concentrations of O_3 (~ 500 ppm). This flow of O_3 enriched air was bubbled through the impinger. Aliquots were taken at 0, 1, 3, 5, and 7 min of bubbling (i.e. reaction time). All samples were stored at 4°C and analyzed immediately on the day of collection to prevent storage effects changing the chemical profile of the samples.[113] No samples were stored for longer than 3 h prior to analysis.

Secondary Organic Aerosol

SOA was generated using a combination of the organic coating unit (OCU)[108] and a 2.4 L flow tube. A schematic illustration of the setup is given in Figure D.1, a list of the samples collected and detailed collection parameters are given in Table

D.1. The SOA was produced by mixing dry or humidified air (3% or 50% relative humidity) with a flow of O_3 enriched air, which was generated by passing clean air through an UV lamp (Pen-Ray photochemical quartz lamp, λ= 185 nm). This flow was guided into the inlet of the OCU. To ensure stable and constant levels of SOA-precursor vapor, the OCU has two VOC dosing systems to regulate the flow of gas through the bottles containing the liquid precursor. The gas-phase VOC is then added to the main flow where it is mixed with O_3. For the generation of naphthalene containing SOA, the UV-lamps (spotlight type GPH212T5L/4, doped quartz glass, wavelength λ= 254 nm, WISAG, Switzerland) of the oxidation flow reactor inside the OCU were turned on to generate additional OH, as OH is the primary reaction partner of naphthalene in the atmosphere.[223, 224] SOA was generated under different reaction conditions by changing the relative humidity (3% or 50%), the number of used lamps (1 or 2 ozone generating UV lamps and 0 or 4 UV-lamps in the OCU) and the VOC flow through the bottles containing the liquid precursors (70 to 100 mL/min). During these experiments α-pinene, 3-carene, naphthalene and a mixture of 3-carene and naphthalene VOCs were used to generate SOA in the OCU. To investigate possible cross-product reactions of 3-carene and naphthalene SOA (referred to as nap & 3-car SOA), the two VOCs were placed in individual dosing vials of the OCU and introduced into the reaction chamber where they were oxidized as a mixture of VOCs. In addition to generating SOA through a mixture of naphthalene and 3-carene, two individual previously in acetonitrile extracted SOA samples of naphthalene and 3-carene were mixed in a vial as a control (referred to as nap & 3-car mix).

The outlet flow of the OCU is then led to the flow tube and it is diluted after exiting the flow tube. Subsequently, the oxidants and any gaseous VOC residuals are removed by two charcoal denuders. The mass of the SOA is then measured with a scanning mobility particle sizer (SMPS 3938, TSI, USA), and simultaneously collected onto 47 mm PTFE membrane filters (0.2 µm pore size, Whatman, Merck, Switzerland) at a flow of 10 L/min.

Prior to collection the filters were washed with methanol and air-dried in the fume hood, to ensure they were clean. After collection the extraction procedure was as followed: each filter was immediately cut into 4 equal pieces and placed in 2 mL Eppendorf safe-lock tubes (Eppendorf, Switzerland) with 1 mL MeCN. The quarters were vortexed at maximum speed (2400 rpm) for 90 s and subsequently the extract solution was transferred into empty tubes. The extracts were concentrated to complete dryness in an Eppendorf Concentrator plus (Eppendorf, Switzerland) during 55 min at 30°C in vacuum concentrator V-AL mode. The quarter samples

were then reconstituted in 50 µL MeCN and two quarter extracts of each filter were combined into one amber LC-MS vial (Waters, Switzerland) with 200 µL inserts. The vials were then placed in the autosampler of the LC at 4°C and analyzed immediately on the day of collection to prevent changes of the chemical profile due to extended storage periods of the samples.[113, 183]

5.2.3 Iodometric Titration

Iodometric determination of peroxide concentration was done by adding 5-15 µL (depending on injection volume of the sample in the HPLC-Chemiluminescence system) of sample, 18 µL acetic acid (1 M in MeCN), and 90 µL KI (1 M in H_2O) to a dark amber vial and MeCN was added until a total volume of 1.5 mL was reached, according to Gautam *et al.* [225]. After addition of KI, the samples were closed and left in the dark at room temperature (20°C) to react for either 3 or 24 h. After reaction, the samples were then diluted by a factor of 100-300, depending on the total peroxide concentration in each sample. Absorbance measurements were conducted using an UV-VIS spectrophotometer (Lambda 365 Spectrophotometer UV express, Perkin Elmer, Switzerland). Blanks were prepared for each set of measurements to account for self-oxidation of the solution. Blanks consisted of 18 µL acetic acid (1 M in MeCN), 90 µL KI (1 M in H_2O), and 1392 µL MeCN. Absorbance values of the blanks were subtracted from samples, and all results shown are blank subtracted. Peroxide concentration was calculated using the Beer-Lambert law

$$A = \varepsilon \cdot c \cdot l \tag{5.1}$$

where A = absorbance, c = peroxide concentration, ε= molar extinction coefficient and l = optical path length. Absorbance was measured at 361 nm, and calculations were done using l = 1 cm, with ε= 22 200 M^{-1} cm^{-1}.[148]

5.2.4 HPLC-Chemiluminescence

Setup

Liquid chromatography was performed using a Thermo Vanquish Horizon UHPLC with a binary pump and split sampler (Thermo Fisher Scientific, Reinach, Switzerland). The column (P/N EXL-1111-2546U, 250 mmx4.6 mm, 3 µm particle size, 90 Å pore size) with ICD-fitting is a prototype provided by Avantor (England, UK).[78, 164, 165] The derivatization reagent was supplied using an auxiliary pump (Dionex AXP Auxiliary Pump, Thermo Fisher Scientific, Reinach, Switzerland). Chemilumi-

nescence was captured using a 12.4 µL flow-through cuvette (CUV) (Hellma, Merck, Switzerland) and connecting it to the window of a photo-multiplier tube (PMT, PMM01 - Bialkali Amplified PMT, 280 - 630 nm, Thorlabs GmbH, Germany) operated with a supply voltage of 1.05 V, which was connected to a PicoLog 1216 (Pico Technology). The PMT and cuvette were placed in a self-built cuvette holder to reduce incoming light, which was additionally wrapped in tin foil to ensure no outside light interfered with the measurements. The HPLC-CL setup used for peroxide detection is illustrated in Figure 5.1. Several conditions were tested until optimal operating parameters were found. The HPLC flow rate was varied between 0.5 - 1.25 mL/min, the auxiliary pump flowrate was set between 0.1 - 0.5 mL/min, and the column temperature was set at 30, 40, and 50°C. Optimal operating conditions were found to be at 1 mL/min HPLC flow, 0.25 mL/min auxiliary pump flow, and 40°C column temperature. The final gradient used in the 59 min method with water (mobile phase A) and a 50:50 mixture of methanol (MeOH) and acetonitrile (MeCN) (mobile phase B) was as follows: 99.9% A from 0-3 min, a linear ramp-up to 90% B from 3-50 min; 90% B was held constant until 53 min and was then switched to 99.9% A for column re-equilibration from 53.1 until 59 min.

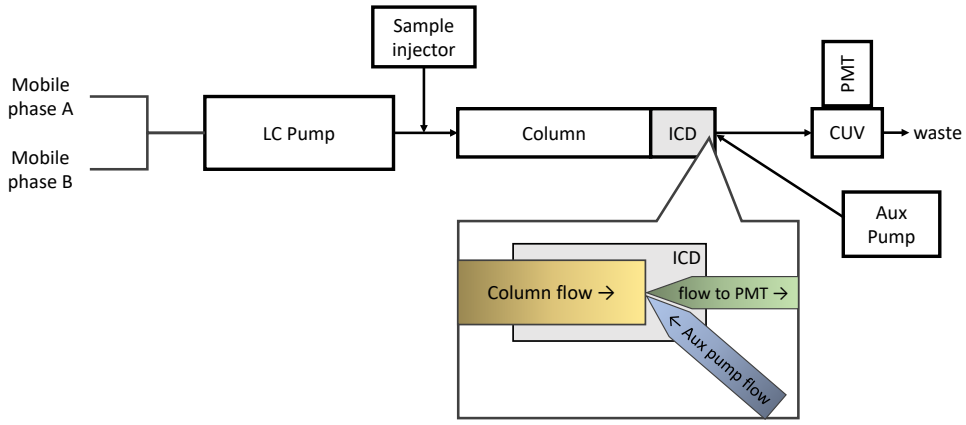

Figure 5.1: Schematic of the LC in-column derivatization (ICD) setup used to detect individual peroxides through luminol chemiluminescence. The LC pump delivers the sample flow to the column and the ICD frit, where it is mixed with the derivatization reagent (luminol/cytochrome c solution) supplied by the auxiliary (Aux) pump. The resulting chemiluminescence signal is then detected by a Photomultiplier Tube (PMT) connected to a 12 µL flow-through cell cuvette (CUV).

Derivatization Reagent

The derivatization reagent was prepared according to Calandra *et al.* [83], except the luminol and cytochrome c concentrations were increased by a factor of 20 and 10, respectively. These conditions were found to increase sensitivity. For the preparation of the buffer solution, 500 mL of 2.0 M stock solution of sodium carbonate and potassium chloride was prepared. Sodium carbonate (1.0 mol, 74.6 g) and potassium chloride (105.6 g) were dissolved in 500 mL HPLC-grade water and stirred until dissolved. Boric acid (0.1 mol, 6.2 g) was added to a tared 2000 mL beaker and 1700 mL of water was added. The sodium carbonate/potassium chloride solution was added until pH 10 was reached, after potassium hydroxide pellets were added until a pH of 10.5 was reached. Water was added until a total weight of 2000 g was reached, the solution was then transferred to glass bottles and stored tightly sealed at room temperature until used. New buffer solution was made every month.
To prepare the luminol solution, 25 mg of luminol were added to 20 mL borate buffer solution and shortly sonicated until completely dissolved. This luminol stock solution was stored at 4°C for up to 1.5 months. The final derivatization reagent consisted of 564 µM luminol, 8.10 µM cytochrome c (which was added to the solution under stirring) dissolved in a pH 10.5 borate buffer solution. The solution was degassed by sonication under vacuum for 2 min, followed by sparging with helium for 8 min. The luminol/cytochrome c solution was only kept at room temperature during measurements and was stored at 4°C otherwise. Different amounts of derivatizatîon reagent were prepared, depending on how many measurements were conducted in the following days. Any remaining solution was discarded after a maximum of 1 week.

5.2.5 Data Analysis

Chemiluminescence was recorded using the PicoLog software with continuous recording of data points every 25 ms. Raw data was smoothed using adjacent averaging with a window of 20 points. Peak areas of the chromatogram were determined using the integration tool provided in OriginPro 2022b (OriginiLab, USA). The peak areas were used to quantify peroxides in the samples. Blank measurements were used as the baseline for integration to account for baseline signal increase due to temperature fluctuations of the system. To determine the lower limit of detection (LLOD), the standard deviation of the un-smoothed baseline was calculated from data points recorder over a 5 minute time frame. This standard deviation was multiplied by 3, which resulted in a LLOD of 18 mV + the baseline intensity. Hence, only

peaks which had an intensity of at least 18 mV above the baseline intensity were considered for individual quantification.
Several sources of uncertainty were determined including the variability of the HPLC from multiple injections, the variability of the absorbance measurements, the variability in SOA mass concentration, and the variability of filter collection and extraction. To assess variability of multiple injections, two different samples were injected in triplicates and the peak areas were averaged, which led to a variability of 1%. The variability of absorbance measurements was determined for each sample by measuring the absorbance three times in 1 s intervals, and was 0.3%. The variability in mass concentrations was determined by calculating the standard deviation of the mass concentrations during SOA collection using the SMPS data. The variability of filter collection and extraction was obtained by collecting three filters for each condition in the OCU and comparing their reproducibility. The variability in peak area from these triplicate filter samples was less than 2%, therefore the error bars are excluded in Figures as they are smaller than the icon size.

5.3 Results and Discussion

The main focus of this study was to develop and apply a novel HPLC in-column derivatization method for the detection and quantification of peroxides in aerosol samples. Three different types of samples were measured to optimize the different measurement parameters and to test the method: commercially available peroxide standards, samples obtained through liquid-phase ozonolysis, and SOA samples. The HPLC-CL results are presented as chromatograms and quantification is done through determination of peak areas, referred to as peroxide concentration measured through luminol chemiluminescence in the following text. The results are compared to total peroxide concentrations of the samples obtained through iodometric titration experiments with UV-Vis, which is a well-established method for peroxide quantification in SOA samples.[137] Quantification is done through comparison of chemiluminescence to peroxide concentrations of the standards and the peroxide concentrations measured with iodometry.

5.3.1 HPLC-CL Testing with Peroxide Standards and Optimization for SOA

In order to test the feasibility and performance of the proposed HPLC-CL method, a range of different commercially available peroxide standards at different concentra-

tions were measured. The standards used were hydrogen peroxide (HP), tert-butyl hydroperoxide (tB-HP), cumene hydroperoxide (Cu-HP), 3-chloroperbenzoic acid (mCPBA), and benzoyl peroxide (b-per), their individual chromatograms are overlapped and displayed in Figure 5.2. Cu-HP, mCPBA, and b-per were measured at 100 µM and show very similar chemiluminescent signals which allows for quantification of peroxides even in the absence of exact standards. Both HP and tB-HP needed to be measured at higher concentrations (1000 and 5000 µM, respectively) to have similar intensities in the chromatogram. This lower sensitivity for these two standards can also be seen in SI Figure D.2, comparing the obtained luminol chemiluminescence of the standards versus their respective theoretical peroxide concentration. The lower limit of detection (LLOD) of the method for Cu-HP, mCPBA, and b-per is below 10 µM. All peak area values are calculated as the area under the curve and are always blank subtracted. The elevated blank signal after about 22 min is due to the increase in organic solvent in the mobile phase. An example to visualize the peak area above a blank is given in SI Figure D.3.

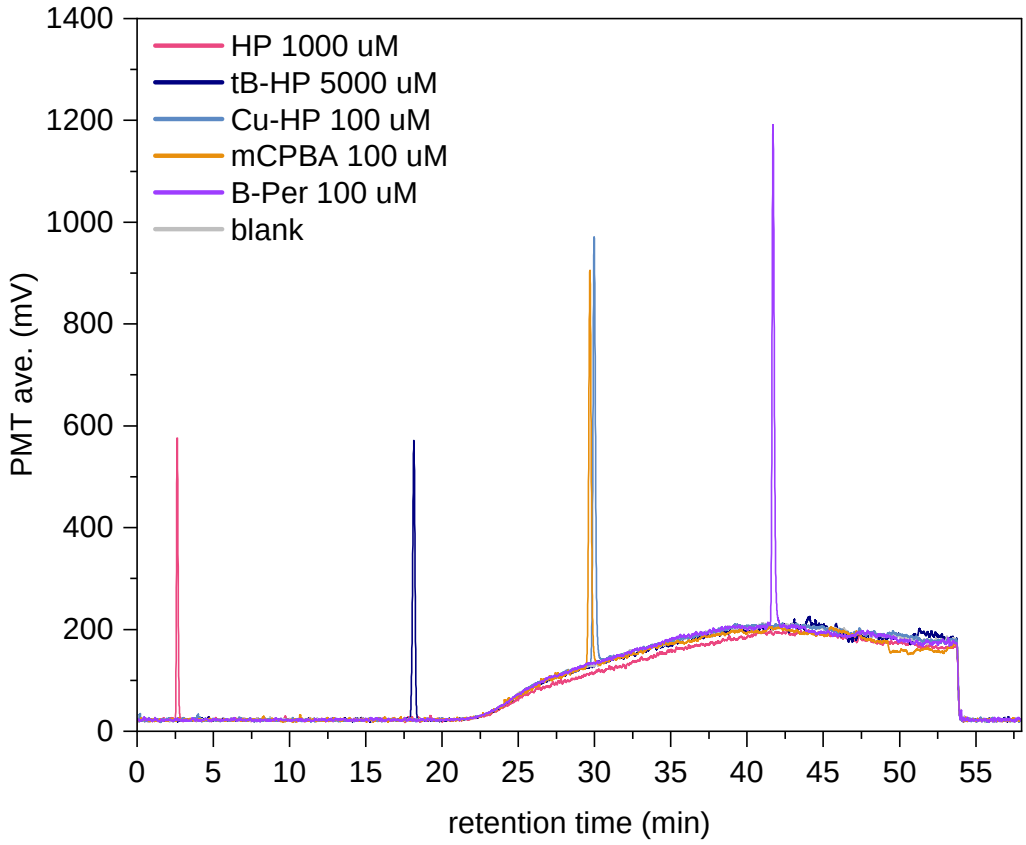

Figure 5.2: Chromatogram of the different standards used. Cu-HP, mCPBA, and b-per are all at a concentration of 100 µM, this similar response enables quantification of peroxides even if no exact standards are available. Due to the lower sensitivity, both HP and tB-HP are displayed at higher concentrations of 1000 and 5000 µM, respectively.

Having confirmed that the method successfully enables detection of peroxide standards, different parameters (i.e. pH of the buffer solution, column temperature, mobile phase, the luminol and cytochrome c concentrations, and the flow rates and ratios of the LC and auxiliary pump) were tested to optimize the method towards peroxide detection in different samples. An example of a parameter that was varied can be seen in Figure 5.3, which shows the behavior of a LPO/SOA mix sample (more details on these samples in Chapter 5.3.2) chromatogram when the pH of of the luminol/cytochrome c buffer solution is varied between 9 and 11. The initial condition used in Calandra *et al.* [83] was pH 10. The reaction mechanism is complex and needs alkaline pH to provide the luminol monoanoin (LH^-). Lower pH resulted in a significantly decreased signal intensity. The best results are achieved when a buffer solution with pH 10.5 is used. When the pH is increased to 11, the chromatogram loses intensity and peak resolution, no explanation can be given for such behavior, but identical pH dependency of luminol chemiluminescence

catalyzed by cytochrome c has been seen by Plieth [160]. Further parameters that were investigated are the column temperature, the mobile phase, the luminol and cytochrome c concentrations, and the flow rates and ratios of the LC and auxiliary pump, as seen in Figures SI D.4, D.5, D.6, D.7, and D.8. The final conditions that were used for further experiments are 1 mL/min HPLC flow, 0.25 mL/min auxiliary pump flow, 40°C column temperature, pH of the buffer solution of 10.5, a 1:1 mixture of methanol:acetonitrile as mobile phase B, and a luminol/cytochrome c concentration of L20/C10. More details on the final conditions are given in Chapter 5.2.4. Note that the luminol and cytochrome c concentrations selected were not the ones which gave the highest signal intensity, but further increase of cytochrome c was not feasible due to its high cost. The results presented in Figure 5.2 were obtained after testing for optimal conditions. It is worth mentioning that some conditions changed the sensitivity of HP and enabled lower limits of detection for this standard, but came at the cost of lower sensitivity and signal intensity at later stages of the chromatogram. As the most relevant compounds in aerosol samples usually elute with higher organic content in the mobile phase, a condition was chosen where the signal intensity for these compounds was higher. If the focus of experiments is on quantification of HP, then other conditions may enable better results and higher sensitivity.

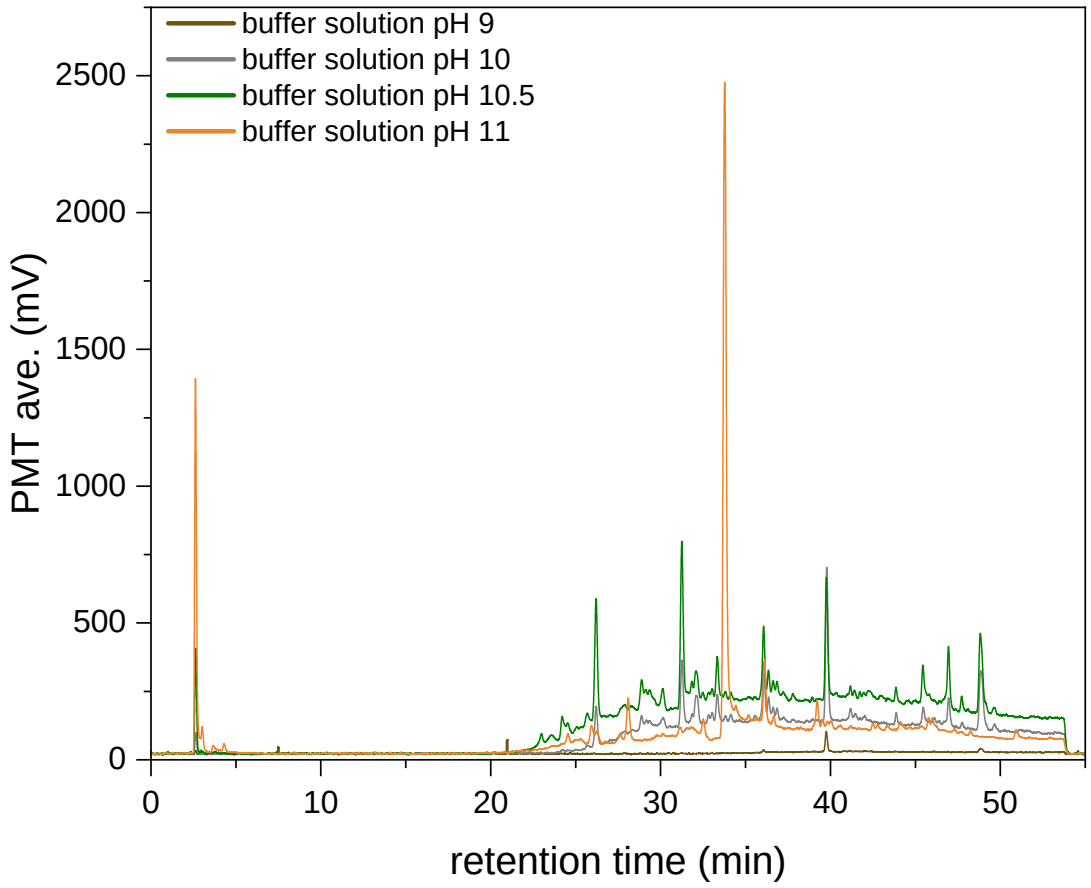

Figure 5.3: Chromatogram of a LPO/SOA mix sample measured with different luminol solutions where the pH of the buffer solution used was changed. An increase in signal intensity and peak resolution can be seen between pH 9 to 10.5. At pH 11 the chromatogram loses intensity and peak resolution. Based on these results using a buffer solution with pH 10.5 was chosen as the best condition for further experiments.

5.3.2 Liquid-Phase Ozonolysis and Secondary Organic Aerosol

Using the optimized HPLC-CL method, two major categories of samples were investigated. Samples obtained through liquid-phase ozonolysis and SOA samples generated in oxidation flow reactor experiments. The LPO experiments represent a simplified system of the complex peroxides mixtures expected in real atmospheric samples, generated by bubbling ozone through a solution containing a monoterpene in an impinger. This system was investigated first to see if the O_3 + monoterpene reaction would produce detectable peroxides. Furthermore, the experiments are straightforward and efficient to perform and some of the products detected are expected to match with peaks observed in the chromatograms of the SOA samples. Figure 5.4 shows the chromatograms for (A) α-pinene and (B) 3-carene SOA and LPO samples. (A) presents a SOA sample in purple, the LPO sample before bubbling at t = 0 min in light blue, the LPO sample at the end of bubbling with O_3 at t = 7 min in dark

blue, and a blank in grey. (B) presents a SOA sample in brown, the LPO sample before bubbling at t = 0 min in light green, the LPO sample at the end of bubbling with O_3 at t = 7 min in dark green, and a blank in grey. Peaks eluting at certain retention times, that are mentioned in the text, are highlighted with arrows.

α-Pinene and 3-Carene LPO

It can be seen that in the chromatogram at 0 min of bubbling three peaks were detected at around rt = 36 min in both monoterpenes. As these peaks are detectable without the addition of O_3 (i.e. in a dilution of the original commercially available chemical standard, see Figures D.13 and D.14), it is assumed they are auto-oxidation products of the monoterpenes stored in their commercial vials through reaction with oxygen in the headspace during storage, as previously seen in Calandra *et al.* [83] for limonene in citrus oils. Iodometry of these samples confirmed that the peroxide concentration in the 1 mM samples was 10 or 15 µM for α-pinene or 3-carene, respectively (see Table D.2). These auto-oxidation products gradually decay during ozonolysis, and are only present in the 0 min and 1 min samples.
Upon bubbling with O_3, there is an increase in detectable organic peroxide peaks (only the last time point is presented in Figure 5.4). The LPO 7 min sample for α-pinene has three major peaks eluting at retention times of ~24, 32, and 33 min, with the most intense peak being the one at ~32 min. The LPO 7 min sample for 3-carene has five major peaks eluting at retention times of ~26, 33, and 40 min, with three peaks closely eluting next to each other at ~33 min. With this method it can be shown that the reaction of O_3 with α-pinene and 3-carene leads to different organic peroxides formed. As previously seen in Li *et al.* [222], the peroxides formed from α-pinene elute at retention times slightly earlier than the isomeric ones from 3-carene.
At rt ~2 min in the chromatogram a small signal for H_2O_2 can be detected in both 7 min LPO samples, which allows for quantification of the H_2O_2 content in these samples, through comparison of the calibration curve for H_2O_2 standards. Figures 5.5 and 5.6 compare the peroxide concentration obtained through iodometry (black lines) with the luminol chemiluminescence of the samples taken at different reaction times of bubbling with O_3. Both, the peroxide concentration measured with iodometry and luminol chemiluminescence, show a similar temporal evolution with a strong increase in the first three minutes of reaction followed by a flattening of the curve. It can be quantified that from the initial 1 mM α-pinene and 3-carene present in the solution, upon bubbling around 600 µM total peroxides are formed in this system. The H_2O_2 subtracted peroxide concentration in both samples is around

25-30% of the total α-pinene and 3-carene concentrations (due to the low sensitivity of H_2O_2 such a small peak still represents such high intensities, see Figure 5.2).

α-Pinene and 3-Carene SOA

The chromatograms of the SOA samples display their higher complexity compared to the simplified liquid-phase ozonolysis experiments. The baseline is strongly increased for both monoterpenes. This strong baseline increase for SOA samples can be attributed to the high complexity of the sample and multiple peroxides eluting at overlapping retention times. Further optimization of the chromatographic parameters need to be done to separate the peaks further. Nevertheless, it is possible to detect several individual peaks in both SOA chromatograms. In Figure 5.4 almost all peaks in the LPO samples match retention times with a peak in the SOA sample. For example, in: (A) the first two peaks at ~23 and 24 min, and the 3 peaks detected in the α-pinene standard prior to bubbling at ~36 min and (B) the first peak at ~26 min and the 2 peaks detected in the 3-carene standard prior to bubbling at ~37 min are detected in both types of samples. Varying the conditions such as the initial VOC concentration or RH content during SOA generation of the same precursor (see Table D.1 and Figures D.10 and D.11) do not significantly change the HPLC-CL chromatogram.
Without further identification of peaks eluting at these retention times, it is difficult to say if the compounds are indeed the same compound, or if they just have the same retention time. In a next step, it would be ideal to combine this HPLC-CL method with MS or NMR detection to be able to not only quantify, but also identify these unknown peroxide compounds in different samples.
No H_2O_2 signal was detected in the SOA samples. A small increase of H_2O_2 signal was observed when re-running a sample for testing purposes after several days. As the storage effects of samples were not the focus of this study, and all samples were analyzed immediately on the day of collection, this effect was ignored but should be investigated in a future study. As an increase in H_2O_2 over time may lead to an increase in total peroxide concentration in aerosol samples, which would lead to a misinterpretation of data.

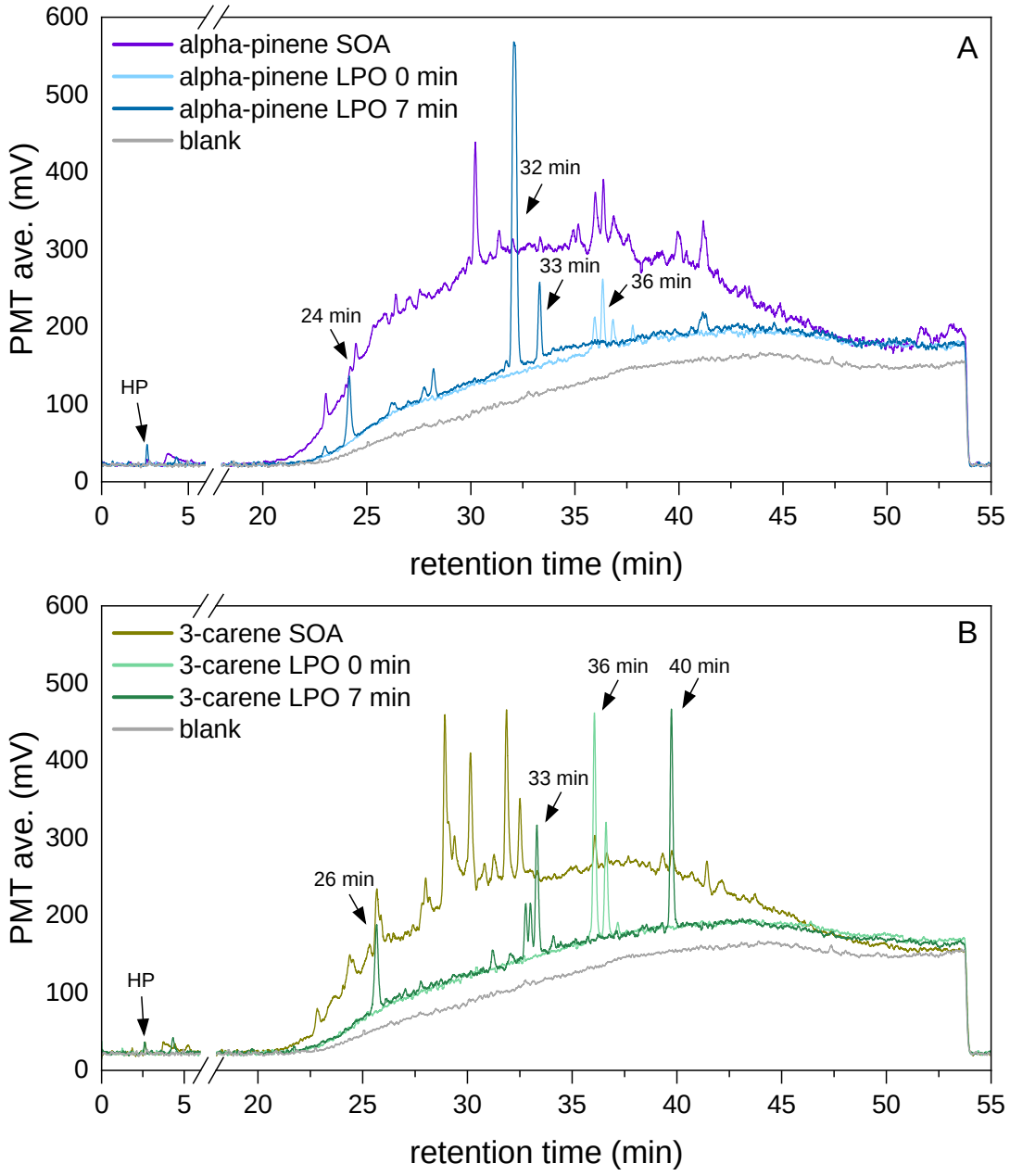

Figure 5.4: Chromatograms of SOA and LPO samples at 0 min and 7 min reaction time for (A) α-pinene and (B) 3-carene. The smoothed signal of the PMT is displayed on the y-axis and the retention time on the x-axis. (A) α-pinene SOA is given in purple, LPO 0 min before bubbling in light blue, LPO after 7 min of bubbling in dark blue, and a blank in grey. (B) 3-carene SOA is given in brown, LPO 0 min before bubbling in light green, LPO after 7 min of bubbling in dark green, and a blank in grey. No peaks are detected between rt = 5 and 20 min.

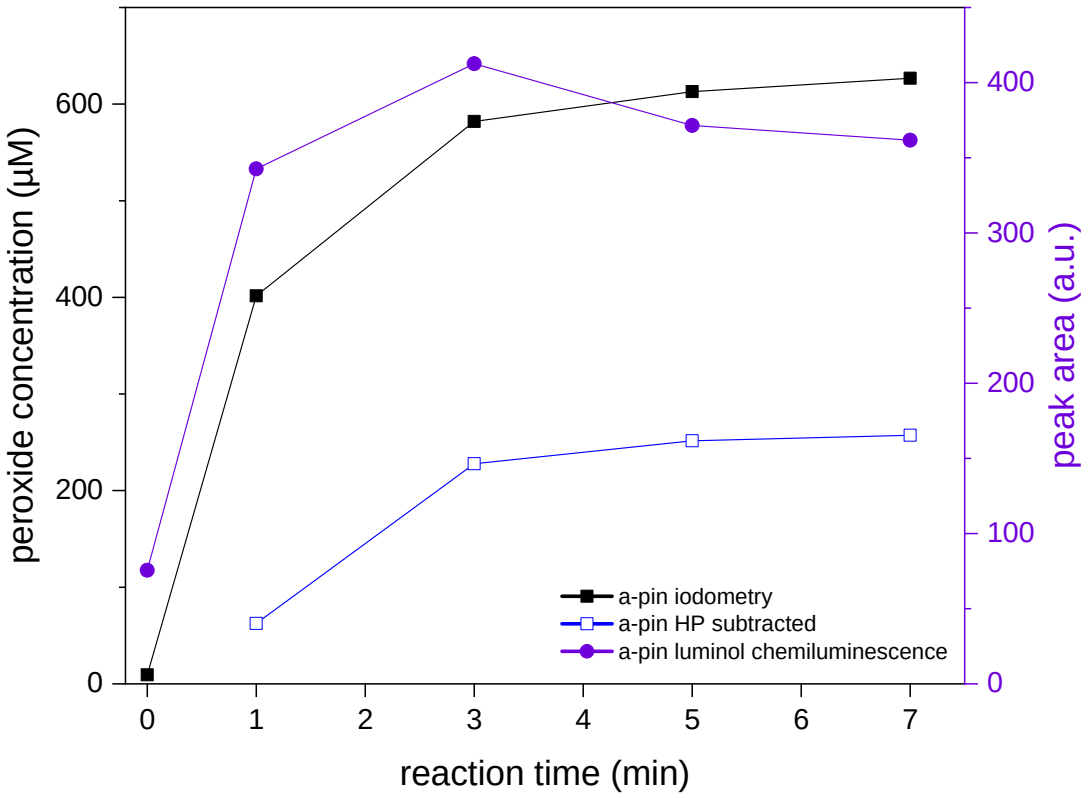

Figure 5.5: The temporal evolution of peroxide concentration measured through iodometry and luminol chemiluminescence and HP subtracted peroxide concentration for α-pinene LPO samples. After bubbling with O_3 for 7 min, 1 mM α-pinene forms around 600 µM peroxides. The HP subtracted peroxide concentration is around 25% of the initial 1 mM α-pinene.

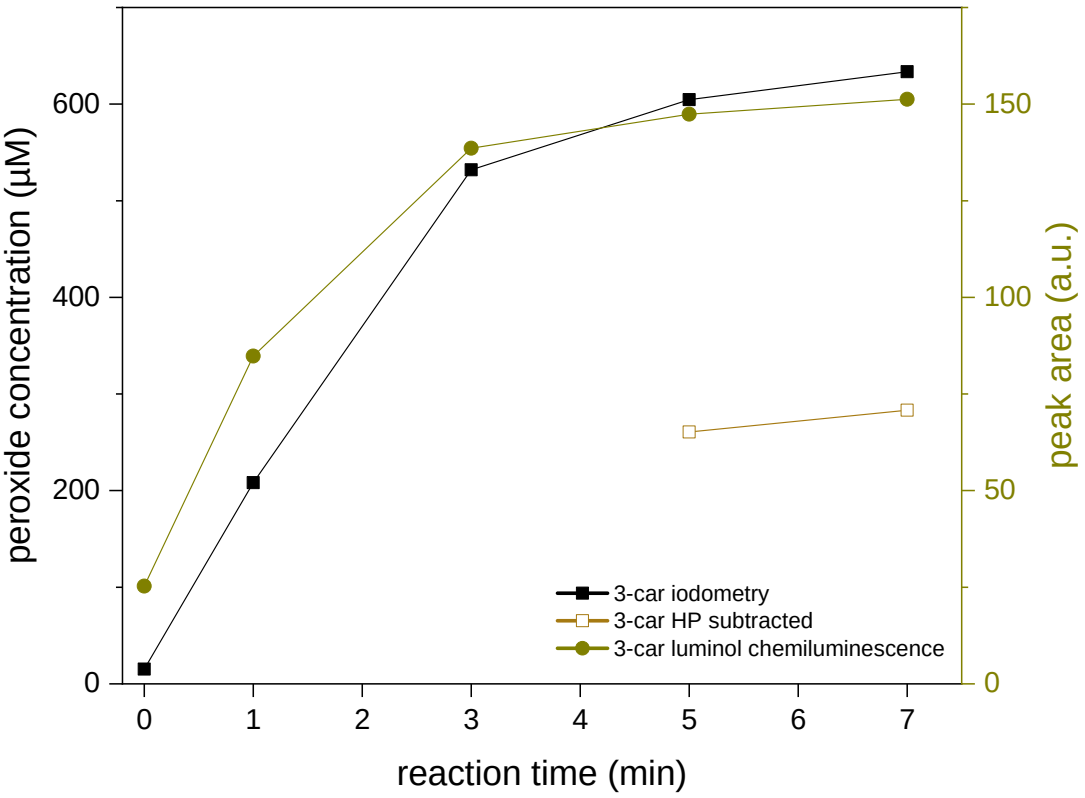

Figure 5.6: The temporal evolution of peroxide concentration measured through iodometry and luminol chemiluminescence and HP subtracted peroxide concentration for 3-carene LPO samples. After bubbling with O_3 for 7 min, 1 mM 3-carene forms around 600 µM peroxides. The HP subtracted peroxide concentration is around 25% of the initial 1 mM 3-carene. No quantification of HP subtracted peroxide concentration can be made for 1 and 3 min samples, as the HP concentration was below the limit of detection.

3-Carene and Naphthalene SOA

SOA samples were generated under different conditions and using different VOC precursors to increase the number of available samples used for method validation, and to see if differences between these SOA samples from different precursors could be identified. As discussed above, a clear distinction can be made between SOA generated from the two monoterpenes α-pinene and 3-carene. In order to further test the applicability of the HPLC-CL method beyond biogenic SOA precursors, naphthalene SOA was additionally used as a representative anthropogenic aerosol.[179]
Figure 5.7 displays the chromatograms of a biogenic (3-carene, brown) and anthropogenic (naphthalene, blue) SOA, as well as SOA generated in the presence of both VOCs in the OCU (nap & 3-car SOA, turquoise). As a control experiment, individual SOA samples were mixed in a vial and are presented as the dark green chromatogram (nap & 3-car mix). A blank is given in grey. In these experiments, the additional OH generating UV-lamps inside the OCU were turned on during 3-carene

SOA generation to ensure identical conditions between naphthalene and 3-carene SOA generation.

Differences in the HPLC-CL chromatograms for 3-carene SOA generated with and without the UV-lamps inside the OCU are given in Figure D.12. These chromatograms show different peak profiles, which can be explained by the different reaction pathways leading to peroxide formation through O_3 or OH. These detectable differences further show the capability of the method to characterize peroxide profiles of SOA from the same precursor generated under different conditions.

The naphthalene SOA samples have a significantly lower signal intensity in the chromatogram and only a small number of peaks is detectable between rt = 20 and 30 min. This is likely due to the different reaction mechanisms of aromatics and alkenes and the fact that SOA generation from naphthalene leads to lower mass concentrations and therefore some of the detectable peroxides may be below the detection limit. Also there is almost no baseline increase in comparison to the other SOA samples, which highlights the methods capability to successfully separate the organic peroxides in naphthalene SOA samples. Furthermore, the peroxide mass fraction in the naphthalene SOA (~ 15%) is lower compared to the α-pinene SOA (~ 23%) and 3-carene SOA (~ 20%). Similar trends and values have been reported in other studies.[130, 216, 226]

A recently presented study by Thomsen *et al.* [227] investigated possible cross-product dimers when mixtures of VOCs are oxidized rather than oxidation of individual compounds. Hence, the hypothesis was tested that new cross-product peroxides are formed when two individual VOCs are mixed during ozonolysis to generate mixed SOA samples. All peaks in the nap & 3-car mix (dark green) sample are present in either the naphthalene or the 3-carene individual SOA samples, suggesting that the additional peaks observed in the nap & 3-car SOA (light green) sample are not formed in the sample extracts but indeed are formed during SOA particle formation. Analyzing the nap & 3-car SOA chromatogram shows a peak with significantly enhanced intensity at rt ~25.5 min, and additionally there is a peak at rt ~36 min which appears to be a newly formed compound, these peaks are highlighted by arrows in the chromatogram. This further strengthens the assumption that when two precursors are present in the gas phase, they do not entirely react independently of each other, but rather some cross-product peroxides are formed, similar to the cross-product dimers observed by Thomsen *et al.* [227].

This highlights that the post-column derivatization method allows for comparison of different SOA samples and that identification of different peroxide profiles is possible, rather than obtaining a total peroxide concentration of the sample through

iodometry or other bulk analysis methods. Differences can be seen between SOA samples from different biogenic and anthropogenic precursors, SOA generation under different conditions, and between SOA mixtures and oxidation products of mixed precursors.

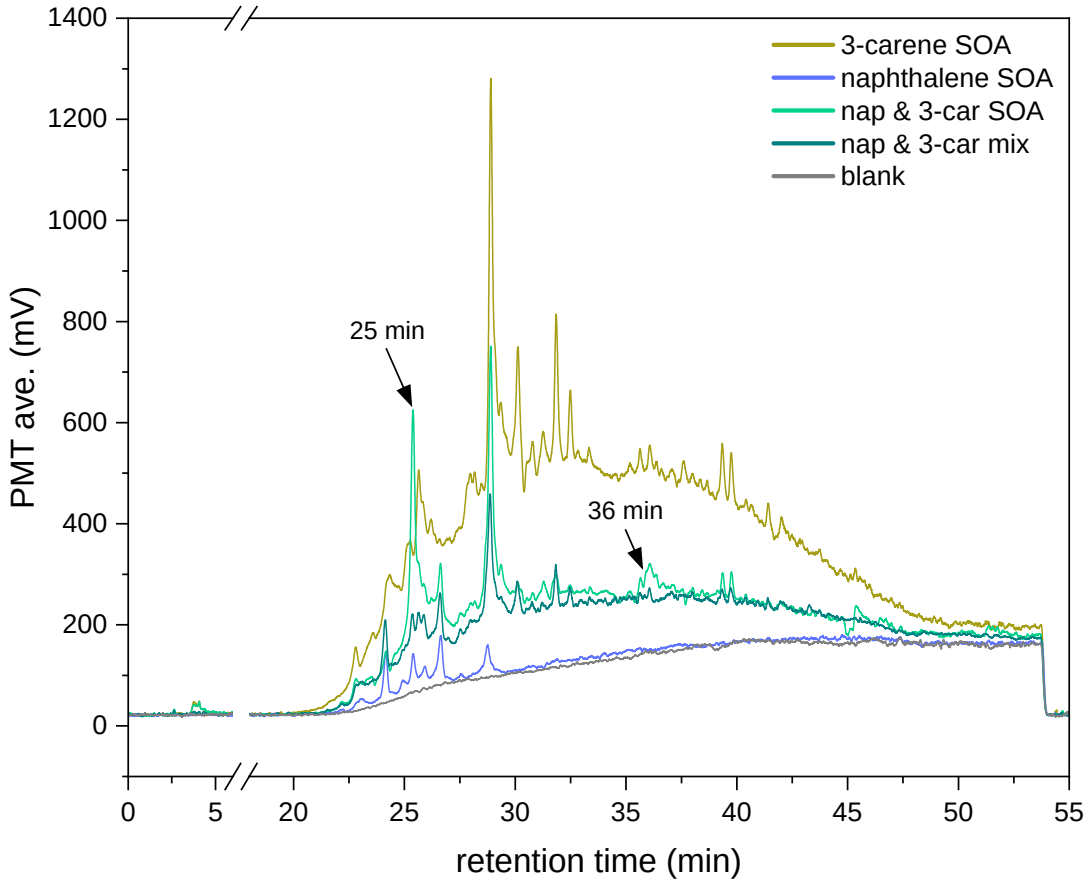

Figure 5.7: 3-carene (brown) and naphthalene (blue) SOA generated individually and SOA generated through a mixture of both VOCs (turquoise). Individual naphthalene and 3-carene SOA samples were mixed (green) to compare if additional cross-reaction products are formed. No peaks are detected between rt = 5 and 20 min.

Additionally, using the total peroxide concentration obtained through iodometry and the aerosol mass deposited on each filter, the peroxide mass fraction, and moles of peroxide functional group per mass of particle for all SOA samples were calculated. These values are given in Table D.3. The mass fractions (assuming a MW of 200) are between 10 to 25% in the SOA samples generated and analyzed for the different precursors and conditions used in this study. This is in accordance to previously reported peroxide mass fractions in literature using iodometry, which report values for α-pinene, 3-carene, and naphthalene of 5-65%, 24-43%, and 3-26%, respectively.[71]

5.3.3 Correlation between HPLC-CL and Iodometric Titration

Iodometry measurements were conducted after 24 h reaction time in order to assure complete reaction of the peroxides, see Figure D.15. Two different samples were measured continuously over 24h by monitoring the absorbance at 361 nm every 15 s, a mixture of standards (HP, tB-HP, mCPBA, and Cu-HP) and a mixture of LPO and SOA (AP-LPO, 3C-LPO, AP-SOA, and 3C-SOA) samples. The LPO and SOA mix reaches a plateau after 12 h+, while the standards mix continuously increases. This increase is due to the slow reactivity of the tB-HP, as also previously observed by Mertes *et al.* [136], which is most likely due to the steric hindrance and stabilization of the peroxide bond in this compound. The reactivity of different kinds of peroxides has also been investigated by Baj and Krawczyk [156] and the results of the iodometry measurements conducted in this study are coherent. Iodometry measurements were done for all samples analyzed in this study as control measurements so the results of the HPLC-CL method can be compared.

To be able to use the HPLC-CL method for peroxide quantification a correlation between peak area and peroxide concentration must be made. This was done for the peroxide standards and a clear linear correlation was observed (see Figure D.2). An upper limit of detection for the standards was reached when peak intensities were at 2500 mV for individual peaks. To extend the dynamic range of the method, additional peroxide quantification was done for all samples collected in this study. This was done by comparing the measured peroxide concentration of each sample using iodometry to the blank subtracted peak area of the chromatogram, as presented by the shaded area in Figure D.3. The samples covered a wide range of total peroxide concentrations from 10 µM to 16 mM and a total peak area from 10 to 13000 a.u., allowing for quantification of individual peaks in the chromatogram. The peak areas of individual compounds are calculated as the area under the curve until the blank, even though there are likely several co-eluting compounds. The peroxide concentration measured with iodometry and luminol chemiluminescence are presented for all samples in Figure 5.8 and 5.9, and additionally given as exact values in Table D.2. Excellent linear correlation (linear fit with $R^2 = 0.998$) can be observed for all samples, covering a concentration range of 3 orders of magnitude, with the exception of the HP and tB-HP samples, as also observed in Figure D.2 displaying the lower sensitivity of the method towards these peroxides. In Figure 5.9, the other standards (Cu-HP, mCPBA, and b-per) are all on the linear fit, which shows that peroxide quantification could be done by only comparing the signal response of the luminol chemiluminescence and the peroxide concentration.

To show the total peroxide concentration quantification capabilities of the method through correlation of iodometry and luminol chemiluminescence, the cross-product peroxide peak detected at rt = 25.5 min in the nap-3-car SOA sample (as seen in Figure 5.7) was analyzed further. The blank subtracted peak area of this compound accounts for 5.5% of the total peak area in this sample. The total peroxide concentration measured with iodometry of this sample (NA-3C-F1c in Table D.2) is ~4500 µM, hence ~250 µM (5.5%) of the total peroxide concentration can be attributed to the cross-product peroxide peak. To the best of the authors knowledge, this is the first quantification of an individual but unknown peroxide compound in an aerosol sample. This single peak quantification is possible for all other peaks in the samples discussed in this study, but only one peak was selected to show the applicability of the method. This sort of quantification is possible with many further aerosol samples and combination with MS identification or fraction collection and NMR identification will enable more precise quantification of individual peroxides.

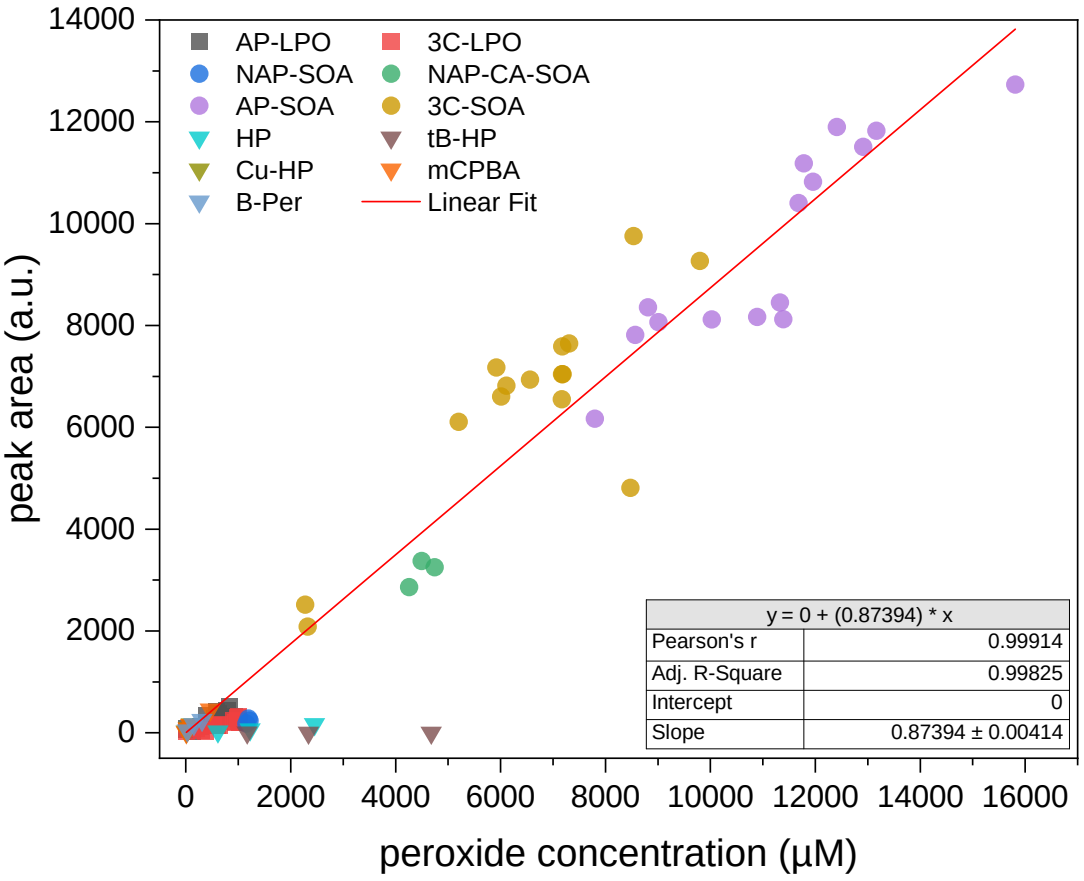

Figure 5.8: Total peak area of the HPLC-CL chromatograms plotted against the total peroxide concentration measured with iodometry for all samples and their linear fit. All samples except the tB-HP and HP show good correlation. Squares represent the LPO samples, circles are the SOA samples and triangles are standards.

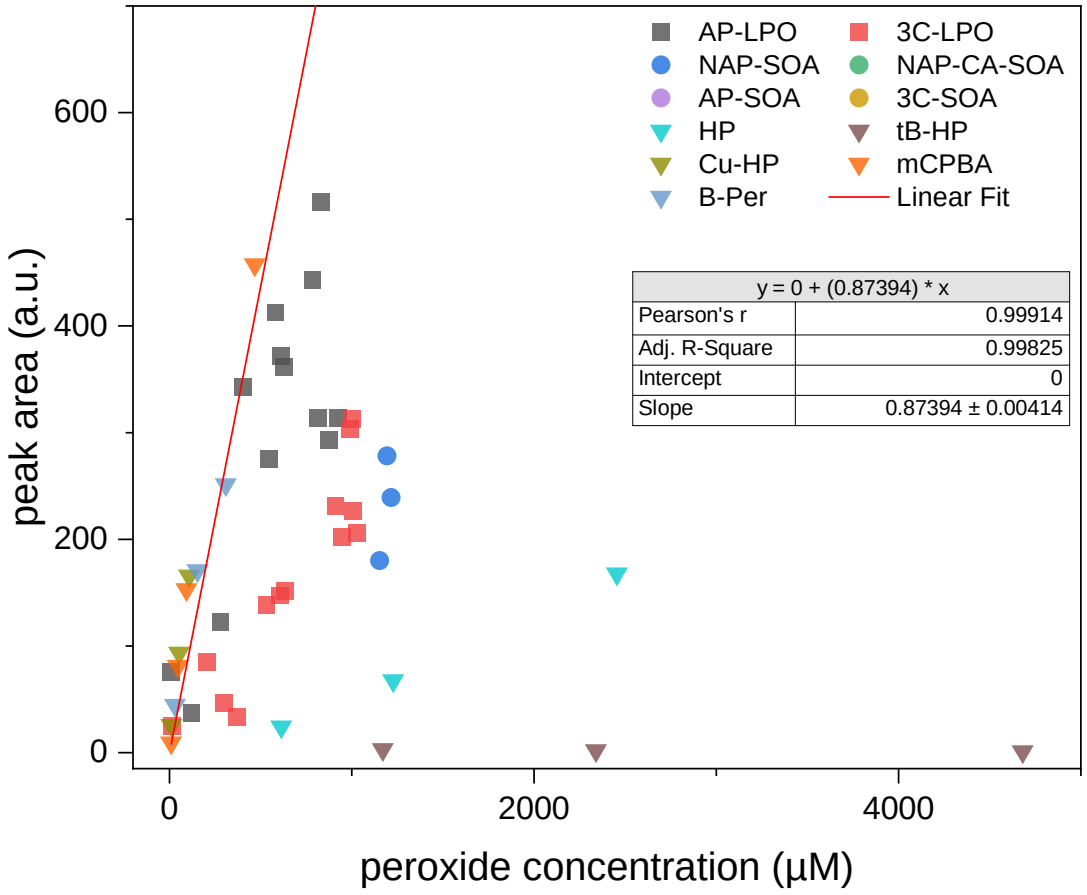

Figure 5.9: Close up of Figure 5.8 displaying lower concentrations. Total peak area of the HPLC-CL chromatograms plotted against the total peroxide concentration measured with iodometry for all samples and their linear fit. All samples except the tB-HP and HP show good correlation. Squares represent the LPO samples, circles are the SOA samples and triangles are the commercially available peroxide standards.

5.4 Conclusions and Outlook

The HPLC in-column derivatization method for the detection of peroxides through luminol chemiluminescence introduced in this study presents a novel technique to unambiguously separate peroxides from the complex organic mixture in organic aerosol and allows to quantify individual peroxides, even if their structure is unknown. Chromatographic parameters such as pH of the buffer solution, column temperature, flow rates, and different luminol and cytochrome c concentrations

were tested at different conditions and optimized for detection of peroxides in relevant aerosol samples.
Identification of differences in the SOA chromatograms between the two monoterpenes was possible, such as a different peak profile, and a shift in retention time for some of the major peaks, similar to results seen in a previous study.[222] Additionally, naphthalene SOA was generated as a representative anthropogenic SOA. To further test the possibilities of this method, SOA was generated through oxidation of a mixture of both VOCs present at the same time in the OCU and unique cross-product peroxides were identified in this sample.
The total peroxide concentration in all samples was determined using iodometric titration and a clear linear correlation could be made between iodometry and luminol chemiluminescence. This allows for quantification of individual peroxide peaks in a chromatogram. A first application of this is done for the unique cross-product peroxide peak in the naphthalene and 3-carene SOA. This compound was quantified to be 5.5% of the total peroxide concentration. In a next step, combination of this method with chemical characterization through either MS or NMR would significantly enhance the capabilities of measuring peroxides in aerosol samples.
The samples analyzed in this study are all generated at concentrations and masses orders of magnitude higher than atmospherically relevant concentrations below 50 µg, which is due to the relatively high limit of detection in the low µM range. Further optimization needs to be done to increase the sensitivity of the method to be able to quantify peroxides in samples generated at more atmospherically relevant concentrations or in ambient atmospheric samples. Additionally, further improvements of the chromatographic separation conditions need to be made. The complexity of SOA composition lead to many peaks eluting at similar retention times or even overlapping, which makes unambiguous identification challenging.

Chapter 6

Summary, Conclusion and Outlook

Organic aerosols have been identified as important components of atmospheric particulate matter. Extensive amounts of research in the last decades have been dedicated to characterizing the chemical composition of aerosols to better understand their formation processes in the atmosphere, their contributions to climate, and their effects on human health. Despite these efforts and the improvement of analytical tools available, there are still large uncertainties regarding these topics. The research conducted in this thesis was motivated by two main topics; addressing a large uncertainty of molecular-level compositional analysis of aerosols which arises from storage of filter samples between collection and analysis used in offline measurements and understanding the processes occurring during storage, and developing a novel method to quantify individual peroxides in aerosol after chromatographic separation through in-column derivatization with luminol.
In Chapter 3 the uncertainty of storage effects in offline chemical analysis of aerosol filters is addressed. β-Pinene SOA, naphthalene SOA and atmospheric aerosol samples were collected and stored for 4 weeks. The samples were either stored as filters or as aqueous extracts at +20°C, -20°C, or -80°C and analyzed by UHPLC-HRMS after 24 h, 1 week, 2 weeks and 4 weeks. Principal component analysis of untargeted LC-MS data and time series of selected compounds shows that samples stored during low-temperature conditions retain their chemical composition compared to the fresh samples. Significant compositional changes are observed for samples stored at room temperature, even at short storage times of only 1 day. Based on these results the recommendations to avoid significant compositional changes for future studies, when organic molecular-level composition analyses are performed, are that all samples should be kept frozen (i.e. -20°C or -80°C) as soon as possible after sampling, ideally within a few hours. If this is not possible, for example in field campaigns or automated sampling at remote sites, the authors should mention in

detail how the samples were stored and how much time passed between collection and analysis.

Another factor which is not mentioned in this study, but is worth consideration is the solution in which the extracts are stored. In this study the extracts were stored in aqueous solution, which promotes unwanted hydrolysis in samples. An alternative could be the storage in pure organic solvents such as acetonitrile to prevent such effects. A promising alternative to filter collection for aerosol sampling could be the use of particle into liquid samplers (PILS) with subsequent frozen storage. This would reduce the uncertainties in compositional analysis arising from differences in extraction methods and extraction artifacts.

The significant compositional change observed during storage for SOA samples at room temperature motivated the study presented in Chapter 4. Further analysis of the β-Pinene SOA filter and extract samples highlighted significantly different temporal concentration changes for monomers and oligomers. In SOA aqueous extracts a significant increase in concentration is observed for monomers, while many dimers decay at the same time. On filters the inverse can be seen, a strong and persistent concentration increase for dimers, while many of the monomers decrease. Two main effects to explain the observed trends are proposed, the hydrolysis of dimers in aqueous extracts, and the formation of oligomers formed through reactions of monomers in the SOA particles deposited on the filter. To test this hypothesis, additional experiments were conducted where carboxylic acid standards were nebulized onto filters containing SOA. The additional carboxylic acids present on the filters promote specific known esterification pathways which increase certain dimers. Such on-filter reaction artifacts need to be considered when detailed organic aerosol compositions are studied. The continuous reactions of SOA components on filters over days and weeks may also mimic dark aging processes in the particle phase of SOA with low water content. These reactions could resemble the processes occurring in ambient atmospheric particles over their entire lifetime of up to several days. The findings in this study focus on dimer esters, but the processes are likely not limited to this compound class and may therefore affect the overall chemical composition of SOA. Future studies need to further investigate the extent of such effects and how they contribute to uncertainties and variations in results presented in different studies. Another possible consequence of such dimer formations on filters could be related to the volatility of monomers and dimers. As dimers are less volatile than the monomers, it could mean that SOA samples are more volatile than previously suggested.

The second major topic of this thesis is presented in Chapter 5. In order to address the high uncertainty regarding peroxide content of SOA and the inability of current methods to separate and quantify individual organic peroxides, a novel HPLC in-column derivatization method was presented. The method utilizes chemiluminescent detection of chromatography separated peroxides through reaction with luminol and cytochrome c. Three different classes of samples were measured: commercially available peroxides, samples generated through liquid-phase ozonolysis of the two monoterpenes α-Pinene and 3-Carene, and SOA from α-Pinene, 3-Carene, naphthalene, and a mixture of 3-Carene and naphthalene. The standards were used to test and validate the method and identify optimal operating conditions, such as pH of the buffer solution, flow rates, luminol and cytochrome c concentrations, and column temperature, to increase signal response. After optimal conditions were found different LPO and SOA samples were compared to determine differences and similarities. Many of the peaks of the simplified LPO sample can be aligned with peaks found in the SOA samples. The retention times of the compounds between the two monoterpenes also shows a shift, where 3-Carene isomeric peaks elute later, this is consistent with the results seen in Li *et al.* [222]. Additionally, 3-Carene and naphthalene, chosen as representative biogenic and anthropogenic precursors, show differences in peroxide profile. To test the identification capabilities of the method, additional experiments were done where a mixture of the two precursors is oxidized, rather than individually. Unique cross-product peroxide peaks were identified in this 3-Carene/naphthalene SOA mix.

Furthermore, all samples were also analyzed using iodometry to determine the total peroxide concentration. These values are compared to the blank subtracted peak area of the chromatograms and excellent linear correlation between the two can be observed. Hence the method is capable of quantifying peroxide concentrations in aerosol samples. This is demonstrated on the example of the previously identified cross-product peroxide peak, which is quantified to be 5.5% of the total peroxide concentration.

In a next step, combination of this method with chemical characterization through either MS or NMR would significantly enhance the organic peroxide detection capabilities. Additionally, further optimization steps would need to be done in order to reduce the lower limit of detection, so peroxides can be quantified in samples which are generated at more atmospherically relevant concentrations. Examples of such optimization steps could be further increase of the luminol/cytochrome c concentrations, the use of a shorter column or lengthening of the HPLC method to enable better peak separation, or an improved PMT to enhance the sensitivity.

Chapter 7

References

[1] W. C. Hinds, *Aerosol Technology: Properties, Behavior, and Measurement of Airborne Particles*, 2nd. John Wiley & Sons, Inc., 1999, p. 504, ISBN: 978-0-471-19410-1. [Online]. Available: https://www.wiley.com/en-us/Aerosol+Technology%3A+Properties%2C+Behavior%2C+and+Measurement+of+Airborne+Particles%2C+2nd+Edition-p-9780471194101 (cit. on pp. 1–3).

[2] M. Hallquist *et al.*, „The formation, properties and impact of secondary organic aerosol: Current and emerging issues“, *Atmospheric Chemistry and Physics*, vol. 9, no. 14, pp. 5155–5236, 2009, ISSN: 16807324. DOI: 10.5194/acp-9-5155-2009 (cit. on pp. 1, 4, 5, 15, 32, 38, 52, 57, 71).

[3] J. L. Jimenez *et al.*, „Evolution of organic aerosols in the atmosphere“, *Science*, vol. 326, no. 5959, pp. 1525–1529, 2009, ISSN: 00368075. DOI: 10.1126/science.1180353 (cit. on pp. 1, 5, 32, 52, 71).

[4] D. V. Spracklen *et al.*, „Contribution of particle formation to global cloud condensation nuclei concentrations“, *Geophysical Research Letters*, vol. 35, no. 6, pp. 1–5, 2008, ISSN: 00948276. DOI: 10.1029/2007GL033038 (cit. on p. 1).

[5] I. Colbeck and M. Lazaridis, „Aerosols and environmental pollution“, *Naturwissenschaften*, vol. 97, no. 2, pp. 117–131, Feb. 2010, ISSN: 0028-1042. DOI: 10.1007/s00114-009-0594-x. [Online]. Available: http://link.springer.com/10.1007/s00114-009-0594-x (cit. on p. 1).

[6] „IPCC, 2023: Climate Change 2023: Synthesis Report. Contribution of Working Groups I, II and III to the Sixth Assessment Report of the Intergovernmental Panel on Climate Change [Core Writing Team, H. Lee and J. Romero (eds.)]. IPCC, Geneva, Switzerland.“, Intergovernmental Panel on Climate Change, Tech. Rep., Jul. 2023, pp. 35–115. DOI: 10.59327/IPCC/AR6-9789291691647. [Online]. Available: https://www.ipcc.ch/report/ar6/syr/ (cit. on p. 1).

[7] G. Hoek *et al.*, „Long-term air pollution exposure and cardio-respiratory mortality: A review“, *Environmental Health: A Global Access Science Source*, vol. 12, no. 1, 2013, ISSN: 1476069X. DOI: 10.1186/1476-069X-12-43 (cit. on p. 1).

[8] R. D. Brook *et al.*, „Particulate matter air pollution and cardiovascular disease: An update to the scientific statement from the american heart association“, *Circulation*, vol. 121, no. 21, pp. 2331–2378, 2010, ISSN: 00097322. DOI: 10.1161/CIR.0b013e3181dbece1 (cit. on p. 1).

[9] D. W. Dockery *et al.*, „An Association between Air Pollution and Mortality in Six U.S. Cities“, *New England Journal of Medicine*, vol. 329, no. 24, pp. 1753–1759, Dec. 1993, ISSN: 0028-4793. DOI: 10.1056/NEJM199312093292401. [Online]. Available: http://www.nejm.org/doi/10.1056/NEJM199312093292401 (cit. on p. 2).

[10] F. Laden, J. Schwartz, F. E. Speizer, and D. W. Dockery, „Reduction in fine particulate air pollution and mortality: Extended follow-up of the Harvard Six Cities Study“, *American Journal of Respiratory and Critical Care Medicine*, vol. 173, no. 6, pp. 667–672, 2006, ISSN: 1073449X. DOI: 10.1164/rccm.200503-443OC (cit. on p. 2).

[11] J. Lepeule, F. Laden, D. Dockery, and J. Schwartz, „Chronic exposure to fine particles and mortality: An extended follow-up of the Harvard six cities study from 1974 to 2009“, *Environmental Health Perspectives*, vol. 120, no. 7, pp. 965–970, 2012, ISSN: 00916765. DOI: 10.1289/ehp.1104660 (cit. on p. 2).

[12] M. L. Bell and D. L. Davis, „Reassessment of the lethal London fog of 1952: Novel indicators of acute and chronic consequences of acute exposure to air pollution“, *Environmental Health Perspectives*, vol. 109, no. SUPPL. 3, pp. 389–394, 2001, ISSN: 00916765. DOI: 10.1289/ehp.01109s3389 (cit. on p. 2).

[13] P. R. Buseck and K. Adachi, „Nanoparticles in the Atmosphere“, *Elements*, vol. 4, no. 6, pp. 389–394, Dec. 2008, ISSN: 1811-5209. DOI: 10.2113/gselements.4.6.389. [Online]. Available: https://pubs.geoscienceworld.org/elements/article/4/6/389-394/137793 (cit. on pp. 2, 3).

[14] P. McMurry, „AEROSOLS | Observations and Measurements“, in *Encyclopedia of Atmospheric Sciences*, 1923, Elsevier, 2003, pp. 20–34. DOI: 10.1016/B0-12-227090-8/00048-8. [Online]. Available: https://linkinghub.elsevier.com/retrieve/pii/B0122270908000488 (cit. on p. 2).

[15] J. H. Seinfeld and S. N. Pandis, *Atmospheric chemistry and physics : from air pollution to climate change*, eng, Third edit. Hoboken, New Jersey SE - xxvi, 1120 pages : illustrations ; 29 cm: John Wiley & Sons, Inc. Hoboken, New Jersey, 2016, ISBN: 9781118947401. DOI: LK-https://worldcat.org/title/929985301 (cit. on pp. 2–5, 16).

[16] T. Wu and B. E. Boor, „Urban aerosol size distributions: A global perspective“, *Atmospheric Chemistry and Physics*, vol. 21, no. 11, pp. 8883–8914, 2021, ISSN: 16807324. DOI: 10.5194/acp-21-8883-2021 (cit. on p. 2).

[17] H. K. Maben and P. J. Ziemann, „Kinetics of oligomer-forming reactions involving the major functional groups present in atmospheric secondary organic aerosol particles“, *Environmental Science: Processes and Impacts*, vol. 25, pp. 214–228, 2022, ISSN: 20507895. DOI: 10.1039/d2em00124a. [Online]. Available: http://dx.doi.org/10.1039/D2EM00124A (cit. on pp. 2, 5, 59).

[18] B. R. Bzdek and M. V. Johnston, „New Particle Formation and Growth in the Troposphere“, *Analytical Chemistry*, vol. 82, no. 19, pp. 7871–7878, Oct. 2010, ISSN: 0003-2700. DOI: 10.1021/ac100856j. [Online]. Available: https://pubs.acs.org/doi/10.1021/ac100856j (cit. on pp. 3, 5).

[19] U. Pöschl, „Atmospheric Aerosols: Composition, Transformation, Climate and Health Effects“, *Angewandte Chemie International Edition*, vol. 44, no. 46, pp. 7520–7540, Nov. 2005, ISSN: 1433-7851. DOI: 10.1002/anie.200501122. [Online]. Available: https://onlinelibrary.wiley.com/doi/10.1002/anie.200501122 (cit. on p. 3).

[20] M. Kanakidou *et al.*, „Organic aerosol and global climate modelling: A review“, *Atmospheric Chemistry and Physics*, vol. 5, no. 4, pp. 1053–1123, 2005, ISSN: 16807316. DOI: 10.5194/acp-5-1053-2005 (cit. on p. 4).

[21] Q. Zhang *et al.*, „Ubiquity and dominance of oxygenated species in organic aerosols in anthropogenically-influenced Northern Hemisphere midlatitudes“, *Geophysical Research Letters*, vol. 34, no. 13, pp. 1–6, 2007, ISSN: 00948276. DOI: 10.1029/2007GL029979 (cit. on p. 4).

[22] A. H. Goldstein and I. E. Galbally, „Known and Unexplored Organic Constituents in the Earth's Atmosphere“, *Environmental Science & Technology*, vol. 41, no. 5, pp. 1514–1521, Mar. 2007, ISSN: 0013-936X. DOI: 10.1021/es072476p. [Online]. Available: https://pubs.acs.org/doi/10.1021/es072476p (cit. on pp. 4, 5).

[23] M. Shrivastava *et al.*, „Recent advances in understanding secondary organic aerosol: Implications for global climate forcing“, *Reviews of Geophysics*, vol. 55, no. 2, pp. 509–559, 2017, ISSN: 19449208. DOI: 10.1002/2016RG000540 (cit. on p. 4).

[24] C. E. Scott *et al.*, „The direct and indirect radiative effects of biogenic secondary organic aerosol“, *Atmospheric Chemistry and Physics*, vol. 14, no. 1, pp. 447–470, 2014, ISSN: 16807316. DOI: 10.5194/acp-14-447-2014 (cit. on p. 4).

[25] J. H. Kroll and J. H. Seinfeld, „Chemistry of secondary organic aerosol: Formation and evolution of low-volatility organics in the atmosphere“, *Atmospheric Environment*, vol. 42, no. 16, pp. 3593–3624, 2008, ISSN: 13522310. DOI: 10.1016/j.atmosenv.2008.01.003 (cit. on p. 5).

[26] S. Han and M. Jang, „Modeling daytime and nighttime secondary organic aerosol formation via multiphase reactions of biogenic hydrocarbons“, *Atmospheric Chemistry and Physics*, vol. 23, no. 2, pp. 1209–1226, 2023, ISSN: 16807324. DOI: 10.5194/acp-23-1209-2023 (cit. on p. 5).

[27] A. B. Guenther *et al.*, „The model of emissions of gases and aerosols from nature version 2.1 (MEGAN2.1): An extended and updated framework for modeling biogenic emissions“, *Geoscientific Model Development*, vol. 5, no. 6, pp. 1471–1492, 2012, ISSN: 1991959X. DOI: 10.5194/gmd-5-1471-2012 (cit. on pp. 5, 57).

[28] R. Atkinson and J. Arey, „Atmospheric Degradation of Volatile Organic Compounds“, *Chemical Reviews*, vol. 103, no. 12, pp. 4605–4638, 2003, ISSN: 00092665. DOI: 10.1021/cr0206420 (cit. on pp. 5, 70).

[29] J. Tröstl *et al.*, „The role of low-volatility organic compounds in initial particle growth in the atmosphere“, *Nature*, vol. 533, no. 7604, pp. 527–531, 2016, ISSN: 14764687. DOI: 10.1038/nature18271 (cit. on pp. 5, 70).

[30] H. Gordon *et al.*, „Causes and importance of new particle formation in the present-day and preindustrial atmospheres“, *Journal of Geophysical Research: Atmospheres*, vol. 122, no. 16, pp. 8739–8760, 2017, ISSN: 21698996. DOI: 10.1002/2017JD026844 (cit. on p. 5).

[31] P. M. Winkler *et al.*, „Identification of the biogenic compounds responsible for size-dependent nanoparticle growth“, *Geophysical Research Letters*, vol. 39, no. 20, pp. 1–6, 2012, ISSN: 00948276. DOI: 10.1029/2012GL053253 (cit. on p. 5).

[32] T. Hoffmann, R. Bandur, U. Marggraf, and M. Linscheid, „Molecular composition of organic aerosols formed in the α-pinene/O 3 reaction: Implications for new particle formation processes“, *Journal of Geophysical Research: Atmospheres*, vol. 103, no. D19, pp. 25 569–25 578, Oct. 1998, ISSN: 0148-0227. DOI: 10.1029/98JD01816. [Online]. Available: http://doi.wiley.com/10.1029/98JD01816%20https://agupubs.onlinelibrary.wiley.com/doi/10.1029/98JD01816 (cit. on pp. 5, 6).

[33] I. Kourtchev *et al.*, „Enhanced volatile organic compounds emissions and organic aerosol mass increase the oligomer content of atmospheric aerosols“, *Scientific Reports*, vol. 6, no. July, pp. 1–9, 2016, ISSN: 20452322. DOI: 10.1038/srep35038. [Online]. Available: http://dx.doi.org/10.1038/srep35038 (cit. on pp. 5, 47, 58).

[34] R. G. W. Norrish and C. H. Bamford, „Photodecomposition of Aldehydes and Ketones“, *Nature*, vol. 138, no. 3502, pp. 1016–1016, Dec. 1936, ISSN: 0028-0836. DOI: 10.1038/1381016a0. [Online]. Available: https://www.nature.com/articles/1381016a0 (cit. on p. 5).

[35] R. G. W. Norrish and C. H. Bamford, „Photo-decomposition of Aldehydes and Ketones“, *Nature*, vol. 140, no. 3535, pp. 195–196, Jul. 1937, ISSN: 0028-0836. DOI: 10.1038/140195b0. [Online]. Available: https://www.nature.com/articles/140195b0 (cit. on p. 5).

[36] H. J. Chacon-Madrid and N. M. Donahue, „Fragmentation vs. functionalization: Chemical aging and organic aerosol formation“, *Atmospheric Chemistry and Physics*, vol. 11, no. 20, pp. 10 553–10 563, 2011, ISSN: 16807316. DOI: 10.5194/acp-11-10553-2011 (cit. on p. 5).

[37] K. Sato, T. Jia, K. Tanabe, Y. Morino, Y. Kajii, and T. Imamura, „Terpenylic acid and nine-carbon multifunctional compounds formed during the aging of β-pinene ozonolysis secondary organic aerosol“, *Atmospheric Environment*, vol. 130, pp. 127–135, 2016, ISSN: 18732844. DOI: 10.1016/j.atmosenv.2015.08.047. [Online]. Available: http://dx.doi.org/10.1016/j.atmosenv.2015.08.047 (cit. on pp. 5, 40, 57, 60, 145).

[38] C. M. Kenseth *et al.*, „Particle-phase accretion forms dimer esters in pinene secondary organic aerosol“, *Science*, vol. 382, no. 6672, pp. 787–792, Nov. 2023, ISSN: 0036-8075. DOI: 10.1126/science.adi0857. [Online]. Available: https://www.science.org/doi/10.1126/science.adi0857 (cit. on pp. 5, 66).

[39] K. Kristensen *et al.*, „Formation and occurrence of dimer esters of pinene oxidation products in atmospheric aerosols“, *Atmospheric Chemistry and Physics*, vol. 13, no. 7, pp. 3763–3776, 2013. DOI: 10.5194/acp-13-3763-2013 (cit. on pp. 5, 66).

[40] K. Kristensen *et al.*, „High-Molecular Weight Dimer Esters Are Major Products in Aerosols from α-Pinene Ozonolysis and the Boreal Forest“, *Environmental Science and Technology Letters*, vol. 3, no. 8, pp. 280–285, 2016, ISSN: 23288930. DOI: 10.1021/acs.estlett.6b00152 (cit. on pp. 5, 41, 52, 58, 60, 61, 66, 144, 145).

[41] V. Pospisilova *et al.*, „On the fate of oxygenated organic molecules in atmospheric aerosol particles“, *Science Advances*, vol. 6, no. 11, pp. 1–12, 2020, ISSN: 23752548. DOI: 10.1126/sciadv.aax8922 (cit. on pp. 5, 59).

[42] B. Witkowski, M. al-Sharafi, K. Błaziak, and T. Gierczak, „Aging of α-Pinene Secondary Organic Aerosol by Hydroxyl Radicals in the Aqueous Phase: Kinetics and Products“, *Environmental Science and Technology*, vol. 57, no. 15, pp. 6040–6051, 2023, ISSN: 15205851. DOI: 10.1021/acs.est.2c07630 (cit. on pp. 5, 64).

[43] S. Offer *et al.*, „Effect of Atmospheric Aging on Soot Particle Toxicity in Lung Cell Models at the Air–Liquid Interface: Differential Toxicological Impacts of Biogenic and Anthropogenic Secondary Organic Aerosols (SOAs)“, *Environmental Health Perspectives*, vol. 130, no. 2, pp. 1–19, Feb. 2022, ISSN: 0091-6765. DOI: 10.1289/EHP9413. [Online]. Available: https://ehp.niehs.nih.gov/doi/10.1289/EHP9413 (cit. on p. 5).

[44] W. A. Hall, M. R. Pennington, and M. V. Johnston, „Molecular Transformations Accompanying the Aging of Laboratory Secondary Organic Aerosol“, *Environmental Science & Technology*, vol. 47, no. 5, pp. 2230–2237, Mar. 2013, ISSN: 0013-936X. DOI: 10.1021/es303891q. [Online]. Available: https://pubs.acs.org/doi/10.1021/es303891q (cit. on p. 5).

[45] P. Tu, W. A. Hall, and M. V. Johnston, „Characterization of Highly Oxidized Molecules in Fresh and Aged Biogenic Secondary Organic Aerosol“, *Analytical Chemistry*, vol. 88, no. 8, pp. 4495–4501, 2016, ISSN: 15206882. DOI: 10.1021/acs.analchem.6b00378 (cit. on p. 5).

[46] I. Kourtchev *et al.*, „Molecular composition of fresh and aged secondary organic aerosol from a mixture of biogenic volatile compounds: A high-resolution mass spectrometry study“, *Atmospheric Chemistry and Physics*, vol. 15, no. 10, pp. 5683–5695, 2015, ISSN: 16807324. DOI: 10.5194/acp-15-5683-2015 (cit. on pp. 5, 60, 145).

[47] A. Tiusanen, J. Ruiz-Jimenez, K. Hartonen, and S. K. Wiedmer, „Analytical methodologies for oxidized organic compounds in the atmosphere“, *Environmental Science: Processes and Impacts*, vol. 25, no. 8, pp. 1263–1287, 2023, ISSN: 20507895. DOI: 10.1039/d3em00163f (cit. on pp. 5–7).

[48] G. B. Ellison, A. F. Tuck, and V. Vaida, „Atmospheric processing of organic aerosols“, *Journal of Geophysical Research Atmospheres*, vol. 104, no. D9, pp. 11 633–11 641, 1999, ISSN: 01480227. DOI: 10.1029/1999JD900073 (cit. on p. 6).

[49] Y. Rudich, N. M. Donahue, and T. F. Mentel, „Aging of organic aerosol: Bridging the gap between laboratory and field studies“, *Annual Review of Physical Chemistry*, vol. 58, pp. 321–352, 2007, ISSN: 0066426X. DOI: 10.1146/annurev.physchem.58.032806.104432 (cit. on p. 6).

[50] M. Jaoui, T. E. Kleindienst, M. Lewandowski, J. H. Offenberg, and E. O. Edney, „Identification and Quantification of Aerosol Polar Oxygenated Compounds Bearing Carboxylic or Hydroxyl Groups. 2. Organic Tracer Compounds from Monoterpenes“, *Environmental Science & Technology*, vol. 39, no. 15, pp. 5661–5673, Aug. 2005, ISSN: 0013-936X. DOI: 10.1021/es048111b. [Online]. Available: https://pubs.acs.org/doi/10.1021/es048111b (cit. on p. 6).

[51] M. Claeys *et al.*, „Hydroxydicarboxylic acids: Markers for secondary organic aerosol from the photooxidation of α-pinene“, *Environmental Science and Technology*, vol. 41, no. 5, pp. 1628–1634, 2007, ISSN: 0013936X. DOI: 10.1021/es0620181 (cit. on p. 6).

[52] B. Nozière *et al.*, „The Molecular Identification of Organic Compounds in the Atmosphere: State of the Art and Challenges“, *Chemical Reviews*, vol. 115, no. 10, pp. 3919–3983, 2015, ISSN: 15206890. DOI: 10.1021/cr5003485 (cit. on pp. 6–12, 18, 33, 52, 53).

[53] T. S. Christoffersen *et al.*, „Cis-pinic acid, a possible precursor for organic aerosol formation from ozonolysis of α-pinene“, *Atmospheric Environment*, vol. 32, no. 10, pp. 1657–1661, 1998, ISSN: 13522310. DOI: 10.1016/S1352-2310(97)00448-2 (cit. on p. 6).

[54] M. Glasius *et al.*, „Carboxylic acids in secondary aerosols from oxidation of cyclic monoterpenes by ozone“, *Environmental Science and Technology*, vol. 34, no. 6, pp. 1001–1010, 2000, ISSN: 0013936X. DOI: 10.1021/es990445r (cit. on pp. 6, 40, 41, 47, 61).

[55] J. D. Surratt *et al.*, „Chemical composition of secondary organic aerosol formed from the photooxidation of isoprene“, *Journal of Physical Chemistry A*, vol. 110, no. 31, pp. 9665–9690, 2006, ISSN: 10895639. DOI: 10.1021/jp061734m (cit. on pp. 6, 23, 24, 71).

[56] M. Claeys *et al.*, „Formation of Secondary Organic Aerosols Through Photooxidation of Isoprene“, *Science*, vol. 303, no. 5661, pp. 1173–1176, 2004, ISSN: 00368075. DOI: 10.1126/science.1092805 (cit. on p. 6).

[57] L. Müller, M. C. Reinnig, J. Warnke, and T. Hoffmann, „Unambiguous identification of esters as oligomers in secondary organic aerosol formed from cyclohexene and cyclohexene/α-pinene ozonolysis“, *Atmospheric Chemistry and Physics*, vol. 8, no. 5, pp. 1423–1433, 2008, ISSN: 16807324. DOI: 10.5194/acp-8-1423-2008 (cit. on pp. 6, 52, 58, 60, 145).

[58] F. Yasmeen *et al.*, „Terpenylic acid and related compounds: precursors for dimers in secondary organic aerosol from the ozonolysis of α- and β-pinene“, *Atmospheric Chemistry and Physics*, vol. 10, no. 19, pp. 9383–9392, Oct. 2010, ISSN: 1680-7324. DOI: 10.5194/acp-10-9383-2010. [Online]. Available: https://acp.copernicus.org/articles/10/9383/2010/ (cit. on pp. 6, 40, 60, 65, 145).

[59] R. Szmigielski *et al.*, „3-methyl-1,2,3-butanetricarboxylic acid: An atmospheric tracer for terpene secondary organic aerosol“, *Geophysical Research Letters*, vol. 34, no. 24, pp. 2–7, 2007, ISSN: 00948276. DOI: 10.1029/2007GL031338 (cit. on p. 6).

[60] J. P. Abbatt, K. Broekhuizen, and P. Pradeep Kumar, „Cloud condensation nucleus activity of internally mixed ammonium sulfate/organic acid aerosol particles“, *Atmospheric Environment*, vol. 39, no. 26, pp. 4767–4778, 2005, ISSN: 13522310. DOI: 10.1016/j.atmosenv.2005.04.029 (cit. on p. 6).

[61] U. Dusek *et al.*, „Size matters more than chemistry for cloud-nucleating ability of aerosol particles“, *Science*, vol. 312, no. 5778, pp. 1375–1378, 2006, ISSN: 00368075. DOI: 10.1126/science.1125261 (cit. on p. 6).

[62] M. D. Petters and S. M. Kreidenweis, „A single parameter representation of hygroscopic growth and cloud condensation nucleus activity-Part 3: Including surfactant partitioning“, *Atmospheric Chemistry and Physics*, vol. 13, no. 2, pp. 1081–1091, 2013, ISSN: 16807316. DOI: 10.5194/acp-13-1081-2013 (cit. on p. 6).

[63] T. C. Bond and R. W. Bergstrom, „Light absorption by carbonaceous particles: An investigative review“, *Aerosol Science and Technology*, vol. 40, no. 1, pp. 27–67, 2006, ISSN: 02786826. DOI: 10.1080/02786820500421521 (cit. on p. 6).

[64] I. N. Sokolik *et al.*, „Introduction to special section: Outstanding problems in quantifying the radiative impacts of mineral dust“, *Journal of Geophysical Research Atmospheres*, vol. 106, no. 16, pp. 18 015–18 027, 2001, ISSN: 01480227. DOI: 10.1029/2000jd900498 (cit. on p. 6).

[65] M. Xie *et al.*, „Light Absorption of Secondary Organic Aerosol: Composition and Contribution of Nitroaromatic Compounds“, *Environmental Science and Technology*, vol. 51, no. 20, pp. 11 607–11 616, 2017, ISSN: 15205851. DOI: 10.1021/acs.est.7b03263 (cit. on p. 6).

[66] C. E. Chung, V. Ramanathan, and D. Decremer, „Observationally constrained estimates of carbonaceous aerosol radiative forcing“, *Proceedings of the National Academy of Sciences of the United States of America*, vol. 109, no. 29, pp. 11 624–11 629, 2012, ISSN: 00278424. DOI: 10.1073/pnas.1203707109 (cit. on p. 6).

[67] R. Saleh *et al.*, „Absorptivity of brown carbon in fresh and photo-chemically aged biomass-burning emissions“, *Atmospheric Chemistry and Physics*, vol. 13, no. 15, pp. 7683–7693, 2013, ISSN: 16807316. DOI: 10.5194/acp-13-7683-2013 (cit. on p. 6).

[68] J. Liu *et al.*, „Optical properties and aging of light-absorbing secondary organic aerosol“, *Atmospheric Chemistry and Physics*, vol. 16, no. 19, pp. 12 815–12 827, 2016, ISSN: 16807324. DOI: 10.5194/acp-16-12815-2016 (cit. on p. 6).

[69] N. K. Kumar *et al.*, „Production of particulate brown carbon during atmospheric aging of residential wood-burning emissions“, *Atmospheric Chemistry and Physics*, vol. 18, no. 24, pp. 17 843–17 861, 2018, ISSN: 16807324. DOI: 10.5194/acp-18-17843-2018 (cit. on p. 6).

[70] J. T. Bates *et al.*, „Review of Acellular Assays of Ambient Particulate Matter Oxidative Potential: Methods and Relationships with Composition, Sources, and Health Effects“, *Environmental Science and Technology*, vol. 53, no. 8, pp. 4003–4019, 2019, ISSN: 15205851. DOI: 10.1021/acs.est.8b03430 (cit. on p. 7).

[71] S. Wang, Y. Zhao, A. W. H. Chan, M. Yao, Z. Chen, and J. P. D. Abbatt, „Organic Peroxides in Aerosol: Key Reactive Intermediates for Multiphase Processes in the Atmosphere“, *Chemical Reviews*, vol. 123, no. 4, pp. 1635–1679, Feb. 2023, ISSN: 0009-2665. DOI: 10.1021/acs.chemrev.2c00430. [Online]. Available: https://pubs.acs.org/doi/10.1021/acs.chemrev.2c00430 (cit. on pp. 7, 24, 25, 71, 89, 181).

[72] T. Hoffmann, R. J. Huang, and M. Kalberer, „Atmospheric analytical chemistry“, *Analytical Chemistry*, vol. 83, no. 12, pp. 4649–4664, 2011, ISSN: 00032700. DOI: 10.1021/ac2010718 (cit. on pp. 9–12).

[73] J. T. Bates *et al.*, „Review of Acellular Assays of Ambient Particulate Matter Oxidative Potential: Methods and Relationships with Composition, Sources, and Health Effects“, *Environmental Science and Technology*, vol. 53, no. 8, pp. 4003–4019, Apr. 2019, ISSN: 15205851. DOI: 10.1021/acs.est.8b03430. [Online]. Available: https://pubs.acs.org/doi/10.1021/acs.est.8b03430 (cit. on pp. 9, 23, 70).

[74] M. Kalberer, J. Yu, D. R. Cocker, R. C. Flagan, and J. H. Seinfeld, „Aerosol formation in the cyclohexene-ozone system“, *Environmental Science and Technology*, vol. 34, no. 23, pp. 4894–4901, 2000, ISSN: 0013936X. DOI: 10.1021/es001180f (cit. on pp. 9, 11).

[75] V. Pashynska, R. Vermeylen, G. Vas, W. Maenhaut, and M. Claeys, „Development of a gas chromatographic/ion trap mass spectrometric metod for the determination of levoglucosan and saccharidic compounds in atmospheric aerosols. Application to urban aerosols“, *Journal of Mass Spectrometry*, vol. 37, no. 12, pp. 1249–1257, 2002, ISSN: 10765174. DOI: 10.1002/jms.391 (cit. on p. 9).

[76] I. Kourtchev, T. Ruuskanen, W. Maenhaut, M. Kulmala, and M. Claeys, „Observation of 2-methyltetrols and related photo-oxidation products of isoprene in boreal forest aerosols from Hyytiälä, Finland“, *Atmospheric Chemistry and Physics*, vol. 5, no. 10, pp. 2761–2770, 2005, ISSN: 16807324. DOI: 10.5194/acp-5-2761-2005 (cit. on p. 9).

[77] R. M. Flores and P. V. Doskey, „Evaluation of multistep derivatization methods for identification and quantification of oxygenated species in organic aerosol“, *Journal of Chromatography A*, vol. 1418, pp. 1–11, 2015, ISSN: 18733778. DOI: 10.1016/j.chroma.2015.09.041. [Online]. Available: http://dx.doi.org/10.1016/j.chroma.2015.09.041 (cit. on p. 9).

[78] A. Jones, S. Pravadali-Cekic, A. Soliven, and R. A. Shalliker, „A Review on Post-Column Derivatisation (PCD) using Active Flow Technology (AFT) in Reaction Flow (RF) Mode“, *Chromatography Today*, no. December, pp. 54–59, 2015 (cit. on pp. 9, 27, 75).

[79] A. Jones, S. Pravadali-Cekic, G. R. Dennis, and R. A. Shalliker, „Post column derivatisation analyses review. Is post-column derivatisation incompatible with modern HPLC columns?“, *Analytica Chimica Acta*, vol. 889, pp. 58–70, 2015, ISSN: 18734324. DOI: 10.1016/j.aca.2015.07.003. [Online]. Available: http://dx.doi.org/10.1016/j.aca.2015.07.003 (cit. on p. 9).

[80] G. Gałβzowska, J. Ratajczyk, and L. Wolska, „Determination of amino acids in human biological fluids by high-performance liquid chromatography: critical review“, *Amino Acids*, vol. 53, no. 7, pp. 993–1009, 2021, ISSN: 14382199. DOI: 10.1007/s00726-021-03002-x. [Online]. Available: https://doi.org/10.1007/s00726-021-03002-x (cit. on p. 9).

[81] H. Miyano and A. Nakayama, „Development of Precolumn Derivatization–LC/MS for Amino-Acid-Focused Metabolomics“, *Chromatography*, vol. 42, no. 1, pp. 17–27, 2021, ISSN: 1342-8284. DOI: 10.15583/jpchrom.2020.023 (cit. on p. 9).

[82] K. Wang and W. H. Glaze, „High-performance liquid chromatography with postcolumn derivatization for simultaneous determination of organic peroxides and hydrogen peroxide“, *Journal of Chromatography A*, vol. 822, no. 2, pp. 207–213, 1998, ISSN: 00219673. DOI: 10.1016/S0021-9673(98)00598-6 (cit. on pp. 9, 24, 71).

[83] M. J. Calandra, J. Impellizzeri, and Y. Wang, „An HPLC method for hydroperoxides derived from limonene and linalool in citrus oils, using post-column luminol-mediated chemiluminescence detection“, *Flavour and Fragrance Journal*, vol. 30, no. 2, pp. 121–130, 2015, ISSN: 10991026. DOI: 10.1002/ffj.3232 (cit. on pp. 9, 26, 72, 77, 80, 83).

[84] T. Y. Zhang, S. Li, Q. F. Zhu, Q. Wang, D. Hussain, and Y. Q. Feng, „Derivatization for liquid chromatography-electrospray ionization-mass spectrometry analysis of small-molecular weight compounds“, *TrAC - Trends in Analytical Chemistry*, vol. 119, p. 115 608, 2019, ISSN: 18793142. DOI: 10.1016/j.trac.2019.07.019. [Online]. Available: https://doi.org/10.1016/j.trac.2019.07.019 (cit. on p. 9).

[85] K. A. Pratt and K. A. Prather, „Mass spectrometry of atmospheric aerosols—Recent developments and applications. Part I: Off-line mass spectrometry techniques“, *Mass Spectrometry Reviews*, vol. 31, no. 1, pp. 1–16, Jan. 2012. DOI: 10.1002/mas.20322. [Online]. Available: https://apps.who.int/iris/bitstream/handle/10665/254610/WHO-MSD-MER-2017.2-eng.pdf?sequence=1%0Ahttp://apps.who.int/iris/bitstream/handle/10665/254610/WHO-MSD-MER-2017.2-eng.pdf;jsessionid=F9A3B620D10ECFAF8498AC0E08EFCBC8?sequence=1%0Ahttp://apps.who.int/ (cit. on pp. 10, 12).

[86] K. A. Pratt and K. A. Prather, „Mass spectrometry of atmospheric aerosols—Recent developments and applications. Part II: On-line mass spectrometry techniques“, *Mass Spectrometry Reviews*, vol. 31, no. 1, pp. 17–48, Jan. 2012, ISSN: 0277-7037. DOI: 10.1002/mas.20330. [Online]. Available: https://apps.who.int/iris/bitstream/handle/10665/254610/WHO-MSD-MER-2017.2-eng.pdf?sequence=1%0Ahttp://apps.who.int/iris/bitstream/handle/10665/254610/WHO-MSD-MER-2017.2-eng.pdf;jsessionid=F9A3B620D10ECFAF8498AC0E08EFCBC8?sequence=1%0Ahttp://apps.who.int/ (cit. on pp. 10, 12).

[87] A. Laskin, J. Laskin, and S. A. Nizkorodov, „Mass spectrometric approaches for chemical characterisation of atmospheric aerosols: critical review of the most recent advances“, *Environmental Chemistry*, vol. 9, no. 3, p. 163, 2012. DOI: 10.1071/EN12052. [Online]. Available: http://www.publish.csiro.au/?paper=EN12052 (cit. on pp. 10, 12).

[88] J. Laskin, A. Laskin, and S. A. Nizkorodov, „Mass Spectrometry Analysis in Atmospheric Chemistry“, *Analytical Chemistry*, vol. 90, no. 1, pp. 166–189, Jan. 2018, ISSN: 0003-2700. DOI: 10.1021/acs.analchem.7b04249. [Online]. Available: https://pubs.acs.org/doi/10.1021/acs.analchem.7b04249 (cit. on pp. 10–12, 18).

[89] W. Zhang, L. Xu, and H. Zhang, „Recent advances in mass spectrometry techniques for atmospheric chemistry research on molecular-level“, *Mass Spectrometry Reviews*, no. June, pp. 1–44, 2023, ISSN: 10982787. DOI: 10.1002/mas.21857 (cit. on pp. 10, 12).

[90] J. Parshintsev and T. Hyötyläinen, „Methods for characterization of organic compounds in atmospheric aerosol particles Aerosols and Health“, *Analytical and Bioanalytical Chemistry*, vol. 407, no. 20, pp. 5877–5897, 2015, ISSN: 16182650. DOI: 10.1007/s00216-014-8394-3 (cit. on p. 10).

[91] J. T. Watson and O. D. Sparkman, *Introduction to Mass Spectrometry*. Chichester, UK: John Wiley & Sons, Ltd, Oct. 2007, p. 854, ISBN: 9780470516898. DOI: 10.1002/9780470516898. [Online]. Available: http://link.springer.com/10.1385/0-89603-215-9:191%20http://doi.wiley.com/10.1002/9780470516898 (cit. on pp. 10, 20, 21).

[92] Z. Liu and J. B. Phillips, „Comprehensive two-dimensional gas chromatography using an on-column thermal modulator interface“, *Journal of Chromatographic Science*, vol. 29, no. 5, pp. 227–231, 1991, ISSN: 1945239X. DOI: 10.1093/chromsci/29.6.227 (cit. on p. 11).

[93] A. C. Lewis *et al.*, „A larger pool of ozone-forming carbon compounds in urban atmospheres“, *Nature*, vol. 405, no. 6788, pp. 778–781, 2000, ISSN: 00280836. DOI: 10.1038/35015540 (cit. on p. 11).

[94] J. F. Hamilton, P. J. Webb, A. C. Lewis, J. R. Hopkins, S. Smith, and P. Davy, „Partially oxidised organic components in urban aerosol using GCXGC-TOF/MS“, *Atmospheric Chemistry and Physics*, vol. 4, no. 5, pp. 1279–1290, 2004, ISSN: 16807316. DOI: 10.5194/acp-4-1279-2004 (cit. on p. 11).

[95] A. H. Falkovich and Y. Rudich, „Analysis of semivolatile organic compounds in atmospheric aerosols by direct sample introduction thermal desorption GC/MS“, *Environmental Science and Technology*, vol. 35, no. 11, pp. 2326–2333, 2001, ISSN: 0013936X. DOI: 10.1021/es000280i (cit. on p. 11).

[96] Z. An, X. Li, Z. Shi, B. J. Williams, R. M. Harrison, and J. Jiang, „Frontier review on comprehensive two-dimensional gas chromatography for measuring organic aerosol“, *Journal of Hazardous Materials Letters*, vol. 2, no. December 2020, p. 100 013, 2021, ISSN: 26669110. DOI: 10.1016/j.hazl.2021.100013. [Online]. Available: https://doi.org/10.1016/j.hazl.2021.100013 (cit. on p. 11).

[97] P. F. DeCarlo *et al.*, „Field-deployable, high-resolution, time-of-flight aerosol mass spectrometer“, *Analytical Chemistry*, vol. 78, no. 24, pp. 8281–8289, 2006, ISSN: 00032700. DOI: 10.1021/ac061249n (cit. on p. 11).

[98] C. P. Lee *et al.*, „Online Aerosol Chemical Characterization by Extractive Electrospray Ionization-Ultrahigh-Resolution Mass Spectrometry (EESI-Orbitrap)“, *Environmental Science and Technology*, vol. 54, no. 7, pp. 3871–3880, 2020, ISSN: 15205851. DOI: 10.1021/acs.est.9b07090 (cit. on p. 12).

[99] A. P. Bateman, M. L. Walser, Y. Desyaterik, J. Laskin, A. Laskin, and S. A. Nizkorodov, „The effect of solvent on the analysis of secondary organic aerosol using electrospray ionization mass spectrometry“, *Environmental Science and Technology*, vol. 42, no. 19, pp. 7341–7346, 2008, ISSN: 0013936X. DOI: 10.1021/es801226w (cit. on pp. 12, 53, 55).

[100] B. J. Turpin, P. Saxena, and E. Andrews, „Measuring and simulating particulate organics in the atmosphere: Problems and prospects“, *Atmospheric Environment*, vol. 34, no. 18, pp. 2983–3013, 2000, ISSN: 13522310. DOI: 10.1016/S1352-2310(99)00501-4 (cit. on p. 12).

[101] Y. Cheng, K. B. He, F. K. Duan, M. Zheng, Y. L. Ma, and J. H. Tan, „Measurement of semivolatile carbonaceous aerosols and its implications: A review“, *Environment International*, vol. 35, no. 3, pp. 674–681, 2009, ISSN: 18736750. DOI: 10.1016/j.envint.2008.11.007. [Online]. Available: http://dx.doi.org/10.1016/j.envint.2008.11.007 (cit. on p. 12).

[102] G. Mark *et al.*, „OH-radical formation by ultrasound in aqueous solution - Part II: Terephthalate and Fricke dosimetry and the influence of various conditions on the sonolytic yield“, *Ultrasonics Sonochemistry*, vol. 5, no. 2, pp. 41–52, 1998, ISSN: 13504177. DOI: 10.1016/S1350-4177(98)00012-1 (cit. on pp. 12, 33).

[103] S. J. Fuller, F. P. Wragg, J. Nutter, and M. Kalberer, „Comparison of on-line and off-line methods to quantify reactive oxygen species (ROS) in atmospheric aerosols“, *Atmospheric Environment*, vol. 92, pp. 97–103, 2014, ISSN: 18732844. DOI: 10.1016/j.atmosenv.2014.04.006. [Online]. Available: http://dx.doi.org/10.1016/j.atmosenv.2014.04.006 (cit. on pp. 12, 33).

[104] J. Parshintsev, J. Ruiz-Jimenez, T. Petäjä, K. Hartonen, M. Kulmala, and M. L. Riekkola, „Comparison of quartz and Teflon filters for simultaneous collection of size-separated ultrafine aerosol particles and gas-phase zero samples“, *Analytical and Bioanalytical Chemistry*, vol. 400, no. 10, pp. 3527–3535, 2011, ISSN: 16182642. DOI: 10.1007/s00216-011-5041-0 (cit. on pp. 12, 33).

[105] C. Perrino, S. Canepari, and M. Catrambone, „Comparing the performance of Teflon and quartz membrane filters collecting atmospheric PM: Influence of atmospheric water“, *Aerosol and Air Quality Research*, vol. 13, no. 1, pp. 137–147, 2013, ISSN: 16808584. DOI: 10.4209/aaqr.2012.07.0167 (cit. on pp. 12, 33).

[106] C. Roper, L. S. Delgado, D. Barrett, S. L. Massey Simonich, and R. L. Tanguay, „PM 2.5 Filter Extraction Methods: Implications for Chemical and Toxicological Analyses“, *Environmental Science and Technology*, vol. 53, no. 1, pp. 434–442, 2019, ISSN: 15205851. DOI: 10.1021/acs.est.8b04308 (cit. on pp. 12, 33).

[107] C. Wong, D. Vite, and S. A. Nizkorodov, „Stability of α-Pinene and d - Limonene Ozonolysis Secondary Organic Aerosol Compounds Toward Hydrolysis and Hydration“, *ACS Earth and Space Chemistry*, vol. 5, no. 10, pp. 2555–2564, 2021, ISSN: 24723452. DOI: 10.1021/acsearthspacechem.1c00171 (cit. on pp. 12, 33, 41, 53).

[108] A. Keller *et al.*, „The organic coating unit, an all-in-one system for reproducible generation of secondary organic matter aerosol“, *Aerosol Science and Technology*, vol. 56, no. 10, pp. 947–958, 2022, ISSN: 15217388. DOI: 10.1080/02786826.2022.2110448. [Online]. Available: https://doi.org/10.1080/02786826.2022.2110448 (cit. on pp. 15, 16, 35, 54, 73, 127).

[109] E. Kang, M. J. Root, D. W. Toohey, and W. H. Brune, „Introducing the concept of Potential Aerosol Mass (PAM)“, *Atmospheric Chemistry and Physics*, vol. 7, no. 22, pp. 5727–5744, 2007, ISSN: 16807324. DOI: 10.5194/acp-7-5727-2007 (cit. on p. 15).

[110] A. T. Lambe *et al.*, „Characterization of aerosol photooxidation flow reactors: Heterogeneous oxidation, secondary organic aerosol formation and cloud condensation nuclei activity measurements“, *Atmospheric Measurement Techniques*, vol. 4, no. 3, pp. 445–461, 2011, ISSN: 18671381. DOI: 10.5194/amt-4-445-2011 (cit. on p. 15).

[111] E. A. Bruns *et al.*, „Inter-comparison of laboratory smog chamber and flow reactor systems on organic aerosol yield and composition“, *Atmospheric Measurement Techniques*, vol. 8, no. 6, pp. 2315–2332, 2015, ISSN: 18678548. DOI: 10.5194/amt-8-2315-2015 (cit. on p. 15).

[112] Z. Zhang, W. Xu, A. T. Lambe, W. Hu, T. Liu, and Y. Sun, „Insights Into Formation and Aging of Secondary Organic Aerosol From Oxidation Flow Reactors: A Review“, *Current Pollution Reports*, no. 3, 2024, ISSN: 21986592. DOI: 10.1007/s40726-024-00309-7. [Online]. Available: https://doi.org/10.1007/s40726-024-00309-7 (cit. on pp. 15, 16).

[113] J. Resch, K. Wolfer, A. Barth, and M. Kalberer, „Effects of storage conditions on the molecular-level composition of organic aerosol particles“, *Atmospheric Chemistry and Physics*, vol. 23, no. 16, pp. 9161–9171, Aug. 2023, ISSN: 1680-7324. DOI: 10.5194/acp-23-9161-2023. [Online]. Available: https://acp.copernicus.org/articles/23/9161/2023/ (cit. on pp. 16, 31, 53, 54, 57, 59, 61, 62, 68, 73, 75, 144, 193, 197).

[114] T. D. Lee, *Introduction to Modern Liquid Chromatography, Third Edition*. 2011, vol. 22, pp. 196–196, ISBN: 9780470167540. DOI: 10.1007/s13361-010-0021-8 (cit. on pp. 18, 19).

[115] W. H. Pirkle and J. E. McCune, „An improved chiral stationary phase for the facile separation of enantiomers“, *Journal of Chromatography A*, vol. 441, no. 2, pp. 311–322, 1988, ISSN: 00219673. DOI: 10.1016/S0021-9673(01)83874-7 (cit. on p. 18).

[116] T. Hanai, „Fundamental properties of packing materials for liquid chromatography“, *Separations*, vol. 6, no. 1, 2019, ISSN: 22978739. DOI: 10.3390/separations6010002 (cit. on p. 19).

[117] J. R. Mazzeo, U. D. Neue, M. Kele, and R. S. Plumb, „Advancing LC performance with smaller particles and higher pressure“, *Analytical Chemistry*, vol. 77, no. 23, pp. 460–467, 2005, ISSN: 00032700. DOI: 10.1021/ac053516f (cit. on p. 19).

[118] S. Eliuk and A. Makarov, „Evolution of Orbitrap Mass Spectrometry Instrumentation“, *Annual Review of Analytical Chemistry*, vol. 8, pp. 61–80, 2015, ISSN: 19361335. DOI: 10.1146/annurev-anchem-071114-040325 (cit. on p. 19).

[119] D. Norena-Caro, *Example of a 3D LC-MS spectrum of each resolved peak*. 2017. [Online]. Available: https://en.wikipedia.org/wiki/File:Liquid_chromatography_MS_spectrum_3D_analysis.png (cit. on p. 22).

[120] A. M. Wolfer *et al.*, „peakPantheR, an R package for large-scale targeted extraction and integration of annotated metabolic features in LC–MS profiling datasets“, *Bioinformatics*, no. June, pp. 1–3, 2021, ISSN: 1367-4803. DOI: 10.1093/bioinformatics/btab433 (cit. on pp. 22, 37).

[121] C. A. Smith, E. J. Want, G. O'Maille, R. Abagyan, and G. Siuzdak, „XCMS: Processing mass spectrometry data for metabolite profiling using nonlinear peak alignment, matching, and identification“, *Analytical Chemistry*, vol. 78, no. 3, pp. 779–787, 2006, ISSN: 00032700. DOI: 10.1021/ac051437y (cit. on pp. 22, 37, 57).

[122] R. Tautenhahn, C. Bottcher, and S. Neumann, „Highly sensitive feature detection for high resolution LC/MS“, *BMC Bioinformatics*, vol. 9, pp. 1–16, 2008, ISSN: 14712105. DOI: 10.1186/1471-2105-9-504 (cit. on pp. 22, 37, 57).

[123] H. P. Benton, E. J. Want, and T. M. Ebbels, „Correction of mass calibration gaps in liquid chromatography-mass spectrometry metabolomics data“, *Bioinformatics*, vol. 26, no. 19, pp. 2488–2489, 2010, ISSN: 13674803. DOI: 10.1093/bioinformatics/btq441 (cit. on pp. 22, 37, 57).

[124] M. C. Chambers *et al.*, „A cross-platform toolkit for mass spectrometry and proteomics“, *Nature Biotechnology*, vol. 30, no. 10, pp. 918–920, 2012, ISSN: 10870156. DOI: 10.1038/nbt.2377 (cit. on pp. 23, 37).

[125] G. Van Rossum and F. L. Drake, *Python 3 Reference Manual*. Scotts Valley, CA: CreateSpace, 2009, ISBN: 1441412697 (cit. on pp. 23, 37).

[126] L. A. Morio *et al.*, „Tissue injury following inhalation of fine particulate matter and hydrogen peroxide is associated with altered production of inflammatory mediators and antioxidants by alveolar macrophages“, *Toxicology and Applied Pharmacology*, vol. 177, no. 3, pp. 188–199, 2001, ISSN: 0041008X. DOI: 10.1006/taap.2001.9316 (cit. on pp. 23, 70).

[127] L. He and J. Zhang, „Particulate matter (PM) oxidative potential: Measurement methods and links to PM physicochemical characteristics and health effects“, *Critical Reviews in Environmental Science and Technology*, vol. 53, no. 2, pp. 177–197, 2023, ISSN: 15476537. DOI: 10.1080/10643389.2022.2050148. [Online]. Available: https://doi.org/10.1080/10643389.2022.2050148 (cit. on pp. 23, 70).

[128] A. Kahnt, R. Vermeylen, Y. Iinuma, M. Safi Shalamzari, W. Maenhaut, and M. Claeys, „High-molecular-weight esters in α-pinene ozonolysis secondary organic aerosol: Structural characterization and mechanistic proposal for their formation from highly oxygenated molecules“, *Atmospheric Chemistry and Physics*, vol. 18, no. 11, pp. 8453–8467, 2018, ISSN: 16807324. DOI: 10.5194/acp-18-8453-2018 (cit. on pp. 23, 66, 71).

[129] S. H. Lee *et al.*, „New Particle Formation in the Atmosphere: From Molecular Clusters to Global Climate“, *Journal of Geophysical Research: Atmospheres*, vol. 124, no. 13, pp. 7098–7146, 2019, ISSN: 21698996. DOI: 10.1029/2018JD029356 (cit. on p. 23).

[130] K. S. Docherty, W. Wu, Y. B. Lim, and P. J. Ziemann, „Contributions of organic peroxides to secondary aerosol formed from reactions of monoterpenes with O 3“, *Environmental Science and Technology*, vol. 39, no. 11, pp. 4049–4059, 2005, ISSN: 0013936X. DOI: 10.1021/es050228s (cit. on pp. 23–25, 70, 88).

[131] X. Qi and R. P. Baldwin, „Liquid chromatography and electrochemical detection of organic peroxides by reduction at an iron phthalocyanine chemically modified electrode“, *Electroanalysis*, vol. 5, no. 7, pp. 547–554, 1993, ISSN: 15214109. DOI: 10.1002/elan.1140050704 (cit. on pp. 24, 71).

[132] A. L. Lazrus, G. L. Kok, J. A. Lind, S. N. Gitlin, B. G. Heikes, and R. E. Shetter, „Automated Fluorometric Method for Hydrogen Peroxide in Air“, *Analytical Chemistry*, vol. 58, no. 3, pp. 594–597, 1986, ISSN: 15206882. DOI: 10.1021/ac00294a024 (cit. on pp. 24, 71).

[133] G. L. Kok, K. Thompson, A. L. Lazrus, and S. E. McLaren, „Derivatization Technique for the Determination of Peroxides in Precipitation“, *Analytical Chemistry*, vol. 58, no. 6, pp. 1192–1194, 1986, ISSN: 15206882. DOI: 10.1021/ac00297a047 (cit. on pp. 24, 71).

[134] F. P. Wragg, S. J. Fuller, R. Freshwater, D. C. Green, F. J. Kelly, and M. Kalberer, „An automated online instrument to quantify aerosol-bound reactive oxygen species (ROS) for ambient measurement and health-relevant aerosol studies“, *Atmospheric Measurement Techniques*, vol. 9, no. 10, pp. 4891–4900, 2016, ISSN: 18678548. DOI: 10.5194/amt-9-4891-2016 (cit. on pp. 24, 71).

[135] D. K. Banerjee and C. C. Budke, „Spectrophotometric Determination of Traces of Peroxides in Organic Solvents“, *Analytical Chemistry*, vol. 36, no. 4, pp. 792–796, 1964, ISSN: 15206882. DOI: 10.1021/ac60210a027 (cit. on pp. 24, 71).

[136] P. Mertes, L. Pfaffenberger, J. Dommen, M. Kalberer, and U. Baltensperger, „Development of a sensitive long path absorption photometer to quantify peroxides in aerosol particles (Peroxide-LOPAP)“, *Atmospheric Measurement Techniques*, vol. 5, no. 10, pp. 2339–2348, 2012, ISSN: 18671381. DOI: 10.5194/amt-5-2339-2012 (cit. on pp. 24, 25, 71, 90).

[137] D. Alba-Elena, M. T. Baeza-Romero, M. Antiñolo, E. M. Espildora-García, and E. Valero, „A new iodometric microwave-assisted method for peroxide determination in Secondary Organic Aerosols“, *Atmospheric Environment*, vol. 310, no. July, 2023, ISSN: 18732844. DOI: 10.1016/j.atmosenv.2023.119960 (cit. on pp. 24, 25, 71, 78).

[138] M. S. Bloomfield, „The spectrophotometric determination of hydroperoxide and peroxide in a lipid pharmaceutical product by flow injection analysis“, *Analyst*, vol. 124, no. 12, pp. 1865–1871, 1999, ISSN: 00032654. DOI: 10.1039/a906243b (cit. on p. 24).

[139] P. J. Ziemann, „Aerosol products, mechanisms, and kinetics of heterogeneous reactions of ozone with oleic acid in pure and mixed particles“, *Faraday Discussions*, vol. 130, pp. 469–490, 2005, ISSN: 13596640. DOI: 10.1039/b417502f (cit. on p. 24).

[140] S. Wang, T. Liu, J. Jang, J. P. Abbatt, and A. W. Chan, „Heterogeneous interactions between SO2and organic peroxides in submicron aerosol“, *Atmospheric Chemistry and Physics*, vol. 21, no. 9, pp. 6647–6661, 2021, ISSN: 16807324. DOI: 10.5194/acp-21-6647-2021 (cit. on p. 24).

[141] Z. Zhao *et al.*, „Diverse Reactions in Highly Functionalized Organic Aerosols during Thermal Desorption“, *ACS Earth and Space Chemistry*, vol. 4, no. 2, pp. 283–296, 2020, ISSN: 24723452. DOI: 10.1021/acsearthspacechem.9b00312 (cit. on p. 24).

[142] A. D. Awtrey and R. E. Connick, „The Absorption Spectra of I2, I3-, I-, IO3-, S4O6- and S2O3-. Heat of the Reaction I3- = I2 + I-“, *Journal of the American Chemical Society*, vol. 73, no. 4, pp. 1842–1843, Apr. 1951, ISSN: 15205126. DOI: 10.1021/ja01148a504. [Online]. Available: https://pubs.acs.org/doi/abs/10.1021/ja01148a504 (cit. on p. 24).

[143] S. A. Epstein, S. L. Blair, and S. A. Nizkorodov, „Direct photolysis of α-pinene ozonolysis secondary organic aerosol: Effect on particle mass and peroxide content“, *Environmental Science and Technology*, vol. 48, no. 19, pp. 11 251–11 258, 2014, ISSN: 15205851. DOI: 10.1021/es502350u (cit. on p. 24).

[144] R. Zhao, C. M. Kenseth, Y. Huang, N. F. Dalleska, and J. H. Seinfeld, „Iodometry-Assisted Liquid Chromatography Electrospray Ionization Mass Spectrometry for Analysis of Organic Peroxides: An Application to Atmospheric Secondary Organic Aerosol“, *Environmental Science and Technology*, vol. 52, no. 4, pp. 2108–2117, 2018, ISSN: 15205851. DOI: 10.1021/acs.est.7b04863 (cit. on pp. 24, 25, 41, 58, 71, 73).

[145] A. Mutzel, M. Rodigast, Y. Iinuma, O. Böge, and H. Herrmann, „An improved method for the quantification of SOA bound peroxides“, *Atmospheric Environment*, vol. 67, pp. 365–369, 2013, ISSN: 13522310. DOI: 10.1016/j.atmosenv.2012.11.012 (cit. on p. 24).

[146] M. Krapf *et al.*, „Labile Peroxides in Secondary Organic Aerosol“, *Chem*, vol. 1, no. 4, pp. 603–616, 2016, ISSN: 24519294. DOI: 10.1016/j.chempr.2016.09.007 (cit. on p. 24).

[147] H. Li, Z. Chen, L. Huang, and D. Huang, „Organic peroxides' gas-particle partitioning and rapid heterogeneous decomposition on secondary organic aerosol“, *Atmospheric Chemistry and Physics*, vol. 16, no. 3, pp. 1837–1848, 2016, ISSN: 16807324. DOI: 10.5194/acp-16-1837-2016 (cit. on pp. 24, 25).

[148] J. M. Gardner, M. Abrahamsson, B. H. Farnum, and G. J. Meyer, „Visible light generation of iodine atoms and I-I bonds: Sensitized I - oxidation and I3- photodissociation“, *Journal of the American Chemical Society*, vol. 131, no. 44, pp. 16 206–16 214, 2009, ISSN: 00027863. DOI: 10.1021/ja905021c (cit. on pp. 25, 75).

[149] S. Deepa, R. Venkatesan, S. Jayalakshmi, M. Priya, and S. C. Kim, „Recent advances in catalyst-enhanced luminol chemiluminescence system and its environmental and chemical applications“, *Journal of Environmental Chemical Engineering*, vol. 11, no. 3, p. 109 853, 2023, ISSN: 22133437. DOI: 10.1016/j.jece.2023.109853. [Online]. Available: https://doi.org/10.1016/j.jece.2023.109853 (cit. on p. 26).

[150] S. Baj, „Quantitative determination of organic peroxides“, *Fresenius' Journal of Analytical Chemistry*, vol. 350, no. 3, pp. 159–161, 1994, ISSN: 09370633. DOI: 10.1007/BF00323180 (cit. on p. 26).

[151] S. Ashida, S. Okazaki, W. Tsuzuki, and T. Suzuki, „Chemiluminescent Method for the Evaluation of Antioxidant Activity Using Lipid Hydroperoxide-Luminol“, *Analytical Sciences*, vol. 7, no. 1, pp. 93–96, 1991, ISSN: 13482246. DOI: 10.2116/analsci.7.93 (cit. on p. 26).

[152] O. A. Fedyaeva and E. G. Poshelyuzhnaya, „Luminescent Technique for Determining Hydrogen Peroxide Concentrations“, *Russian Journal of Physical Chemistry A*, vol. 92, no. 8, pp. 1636–1637, 2018, ISSN: 00360244. DOI: 10.1134/S0036024418080125 (cit. on p. 26).

[153] P. Khan *et al.*, „Luminol-based chemiluminescent signals: Clinical and non-clinical application and future uses“, *Applied Biochemistry and Biotechnology*, vol. 173, no. 2, pp. 333–355, 2014, ISSN: 15590291. DOI: 10.1007/s12010-014-0850-1 (cit. on p. 26).

[154] P. Morozzi *et al.*, „Chemiluminescent fingerprints from airborne particulate matter: A luminol-based assay for the characterization of oxidative potential with kinetical implications“, *Science of the Total Environment*, vol. 789, 2021, ISSN: 18791026. DOI: 10.1016/j.scitotenv.2021.148005 (cit. on p. 26).

[155] A. L. Rose and T. D. Waite, „Chemiluminescence of luminol in the presence of iron(II) and oxygen: Oxidation mechanism and implications for its analytical use“, *Analytical Chemistry*, vol. 73, no. 24, pp. 5909–5920, 2001, ISSN: 00032700. DOI: 10.1021/ac015547q (cit. on p. 26).

[156] S. Baj and T. Krawczyk, „An investigation into the reaction of hemin-catalysed luminol oxidation by peroxy compounds“, *Journal of Photochemistry and Photobiology A: Chemistry*, vol. 183, no. 1-2, pp. 111–120, 2006, ISSN: 10106030. DOI: 10.1016/j.jphotochem.2006.03.002 (cit. on pp. 26, 90).

[157] S. Uchida, Y. Satoh, N. Yamashiro, and T. Satoh, „Determination of hydrogen peroxide in water by chemiluminescence detection, (II) theoretical analysis of luminol chemiluminescence processes“, *Journal of Nuclear Science and Technology*, vol. 41, no. 9, pp. 898–906, 2004, ISSN: 00223131. DOI: 10.1080/18811248.2004.9715562 (cit. on p. 26).

[158] G. Merényi, J. Lind, and T. E. Eriksen, „Luminol chemiluminescence: Chemistry, excitation, emitter“, *Journal of Bioluminescence and Chemiluminescence*, vol. 5, no. 1, pp. 53–56, Jan. 1990, ISSN: 0884-3996. DOI: 10.1002/bio.1170050111. [Online]. Available: https://onlinelibrary.wiley.com/doi/10.1002/bio.1170050111 (cit. on p. 26).

[159] C. Plieth, „Redox Modulators Determine Luminol Luminescence Generated by Porphyrin-Coordinated Iron and May Repress "suicide Inactivation"“, *ACS Omega*, vol. 3, no. 9, pp. 12 295–12 303, 2018, ISSN: 24701343. DOI: 10.1021/acsomega.8b01261 (cit. on p. 26).

[160] C. Plieth, „Peroxide-Induced Liberation of Iron from Heme Switches Catalysis during Luminol Reaction and Causes Loss of Light and Heterodyning of Luminescence Kinetics“, *ACS Omega*, vol. 4, no. 2, pp. 3268–3279, 2019, ISSN: 24701343. DOI: 10.1021/acsomega.8b03564 (cit. on pp. 26, 81).

[161] K. Shimojo, T. Oshima, H. Naganawa, and M. Goto, „Calixarene-assisted protein refolding via liquid-liquid extraction“, *Biomacromolecules*, vol. 8, no. 10, pp. 3061–3066, 2007, ISSN: 15257797. DOI: 10.1021/bm070418q (cit. on p. 26).

[162] R. Vazquez-Duhalt, D. W. Westlake, and P. M. Fedorak, „Cytochrome c as a biocatalyst for the oxidation of thiophenes and organosulfides“, *Enzyme and Microbial Technology*, vol. 15, no. 6, pp. 494–499, 1993, ISSN: 01410229. DOI: 10.1016/0141-0229(93)90082-D (cit. on p. 26).

[163] S. Baj, A. Chrobok, M. Cieślik, and T. Krawczyk, „Application of chemiluminescence for the detection of peroxy compounds in high-performance liquid chromatography“, *Analytical and Bioanalytical Chemistry*, vol. 375, no. 2, pp. 327–330, 2003, ISSN: 16182642. DOI: 10.1007/s00216-002-1678-z (cit. on p. 27).

[164] C. W. Manwaring *et al.*, „Using HPLC with In-Column Derivatization to Authenticate Coffee Samples“, *Molecules*, vol. 28, no. 4, 2023, ISSN: 14203049. DOI: 10.3390/molecules28041651 (cit. on pp. 27, 28, 75).

[165] A. Soliven *et al.*, „Improving HPLC post-column derivatisation assays via In-Column Derivatisation“, *Microchemical Journal*, p. 111 252, Jul. 2024, ISSN: 0026265X. DOI: 10.1016/j.microc.2024.111252. [Online]. Available: https://doi.org/10.1016/j.microc.2024.111252%20https://linkinghub.elsevier.com/retrieve/pii/S0026265X2401364X (cit. on pp. 27, 75).

[166] U. Pöschl and M. Shiraiwa, „Multiphase Chemistry at the Atmosphere-Biosphere Interface Influencing Climate and Public Health in the Anthropocene“, *Chemical Reviews*, vol. 115, no. 10, pp. 4440–4475, 2015, ISSN: 15206890. DOI: 10.1021/cr500487s (cit. on pp. 32, 52).

[167] M. V. Johnston and D. E. Kerecman, „Molecular Characterization of Atmospheric Organic Aerosol by Mass Spectrometry“, *Annual Review of Analytical Chemistry*, vol. 12, pp. 247–274, 2019, ISSN: 19361335. DOI: 10.1146/annurev-anchem-061516-045135 (cit. on pp. 33, 52).

[168] H. Stark *et al.*, „Methods to extract molecular and bulk chemical information from series of complex mass spectra with limited mass resolution“, *International Journal of Mass Spectrometry*, vol. 389, pp. 26–38, 2015, ISSN: 13873806. DOI: 10.1016/j.ijms.2015.08.011. [Online]. Available: http://dx.doi.org/10.1016/j.ijms.2015.08.011 (cit. on p. 33).

[169] A. M. Dillner, C. H. Phuah, and J. R. Turner, „Effects of post-sampling conditions on ambient carbon aerosol filter measurements“, *Atmospheric Environment*, vol. 43, no. 37, pp. 5937–5943, 2009, ISSN: 13522310. DOI: 10.1016/j.atmosenv.2009.08.009. [Online]. Available: http://dx.doi.org/10.1016/j.atmosenv.2009.08.009 (cit. on p. 34).

[170] E. C. f. S. (CEN), *EN 12341:2014 Ambient air - Standard gravimetric measurement method for the determination of the PM10 or PM2,5 mass concentration of suspended particulate matter*. 2014 (cit. on p. 34).

[171] NABEL, „Technischer Bericht zum Nationalen Beobachtungsnetz für Luftfremdstoffe (NABEL), 2023“, Tech. Rep., 2023, p. 209 (cit. on p. 34).

[172] H. Wickham, *ggplot2: Elegant Graphics for Data Analysis. Springer-Verlag New York*. 2016, vol. 35, p. 211, ISBN: 978-3-319-24277-4. [Online]. Available: http://link.springer.com/10.1007/978-0-387-98141-3 (cit. on p. 37).

[173] P. Raybaut, „Spyder-documentation“, *Available online at: pythonhosted. org*, 2009 (cit. on p. 37).

[174] J. D. Hunter, „Matplotlib: A 2D Graphics Environment“, *Computing in Science & Engineering*, vol. 9, no. 3, pp. 90–95, 2007, ISSN: 1521-9615. DOI: 10.1109/MCSE.2007.55. [Online]. Available: http://ieeexplore.ieee.org/document/4160265/ (cit. on p. 37).

[175] C. R. Harris *et al.*, „Array programming with NumPy“, *Nature*, vol. 585, no. 7825, pp. 357–362, 2020, ISSN: 14764687. DOI: 10.1038/s41586-020-2649-2. [Online]. Available: http://dx.doi.org/10.1038/s41586-020-2649-2 (cit. on p. 37).

[176] K. L. Pereira *et al.*, „An Automated Methodology for Non-targeted Compositional Analysis of Small Molecules in High Complexity Environmental Matrices Using Coupled Ultra Performance Liquid Chromatography Orbitrap Mass Spectrometry“, *Environmental Science and Technology*, vol. 55, no. 11, pp. 7365–7375, 2021, ISSN: 15205851. DOI: 10.1021/acs.est.0c08208 (cit. on p. 38).

[177] W. A. Hall and M. V. Johnston, „Oligomer formation pathways in secondary organic aerosol from MS and MS/MS measurements with high mass accuracy and resolving power“, *Journal of the American Society for Mass Spectrometry*, vol. 23, no. 6, pp. 1097–1108, 2012, ISSN: 18791123. DOI: 10.1007/s13361-012-0362-6 (cit. on pp. 41, 66).

[178] C. M. Kenseth *et al.*, „Synergistic O 3 + OH oxidation pathway to extremely low-volatility dimers revealed in β-pinene secondary organic aerosol“, *Proceedings of the National Academy of Sciences of the United States of America*, vol. 115, no. 33, pp. 8301–8306, 2018, ISSN: 10916490. DOI: 10.1073/pnas.1804671115 (cit. on pp. 41, 57, 58, 60, 66, 145).

[179] A. Eiguren-Fernandez, A. H. Miguel, J. R. Froines, S. Thurairatnam, and E. L. Avol, „Seasonal and spatial variation of polycyclic aromatic hydrocarbons in vapor-phase and PM2.5 in Southern California urban and rural communities“, *Aerosol Science and Technology*, vol. 38, no. 5, pp. 447–455, 2004, ISSN: 02786826. DOI: 10.1080/02786820490449511 (cit. on pp. 42, 87).

[180] F. J. Kelly, „Oxidative stress: Its role in air pollution and adverse health effects“, *Occupational and Environmental Medicine*, vol. 60, no. 8, pp. 612–616, 2003, ISSN: 13510711. DOI: 10.1136/oem.60.8.612 (cit. on p. 44).

[181] T. E. Kleindienst, M. Jaoui, M. Lewandowski, J. H. Offenberg, and K. S. Docherty, „The formation of SOA and chemical tracer compounds from the photooxidation of naphthalene and its methyl analogs in the presence and absence of nitrogen oxides“, *Atmospheric Chemistry and Physics*, vol. 12, no. 18, pp. 8711–8726, 2012, ISSN: 16807316. DOI: 10.5194/acp-12-8711-2012 (cit. on p. 44).

[182] J. H. Seinfeld and J. F. Pankow, „Organic Atmospheric Particulate Material“, *Annual Review of Physical Chemistry*, vol. 54, pp. 121–140, 2003, ISSN: 0066426X. DOI: 10.1146/annurev.physchem.54.011002.103756 (cit. on p. 46).

[183] J. Resch, K. Li, and M. Kalberer, „Prolonged Dark Chemical Processes in Secondary Organic Aerosols on Filters and in Aqueous Solution“, *Environmental Science & Technology*, vol. 58, no. 32, pp. 14 318–14 328, Aug. 2024, ISSN: 0013-936X. DOI: 10.1021/acs.est.4c01647. [Online]. Available: https://pubs.acs.org/doi/10.1021/acs.est.4c01647 (cit. on pp. 51, 75).

[184] M. P. Tolocka, M. Jang, J. M. Ginter, F. J. Cox, R. M. Kamens, and M. V. Johnston, „Formation of Oligomers in Secondary Organic Aerosol“, *Environmental Science and Technology*, vol. 38, no. 5, pp. 1428–1434, 2004, ISSN: 0013936X. DOI: 10.1021/es035030r (cit. on p. 52).

[185] A. Bellcross, A. G. Bé, F. M. Geiger, and R. J. Thomson, „Molecular Chirality and Cloud Activation Potentials of Dimeric α-Pinene Oxidation Products“, *Journal of the American Chemical Society*, vol. 143, no. 40, pp. 16 653–16 662, 2021, ISSN: 15205126. DOI: 10.1021/jacs.1c07509 (cit. on p. 52).

[186] F. Couvidat, M. G. Vivanco, and B. Bessagnet, „Simulating secondary organic aerosol from anthropogenic and biogenic precursors: Comparison to outdoor chamber experiments, effect of oligomerization on SOA formation and reactive uptake of aldehydes“, *Atmospheric Chemistry and Physics*, vol. 18, no. 21, pp. 15 743–15 766, 2018, ISSN: 16807324. DOI: 10.5194/acp-18-15743-2018 (cit. on p. 52).

[187] M. Ehn *et al.*, „A large source of low-volatility secondary organic aerosol“, *Nature*, vol. 506, no. 7489, pp. 476–479, 2014, ISSN: 00280836. DOI: 10.1038/nature13032 (cit. on pp. 52, 70).

[188] W. A. Hall IV and M. V. Johnston, „Oligomer content of α-pinene secondary organic aerosol“, *Aerosol Science and Technology*, vol. 45, no. 1, pp. 37–45, 2011, ISSN: 02786826. DOI: 10.1080/02786826.2010.517580 (cit. on p. 52).

[189] Y. Gao, W. A. Hall, and M. V. Johnston, „Molecular composition of monoterpene secondary organic aerosol at low mass loading“, *Environmental Science and Technology*, vol. 44, no. 20, pp. 7897–7902, 2010, ISSN: 0013936X. DOI: 10.1021/es101861k (cit. on p. 52).

[190] I. Kourtchev *et al.*, „Molecular composition of biogenic secondary organic aerosols using ultrahigh-resolution mass spectrometry: Comparing laboratory and field studies“, *Atmospheric Chemistry and Physics*, vol. 14, no. 4, pp. 2155–2167, 2014, ISSN: 16807316. DOI: 10.5194/acp-14-2155-2014 (cit. on p. 52).

[191] M. Kalberer *et al.*, „Identification of Polymers as Major Components of Atmospheric Organic Aerosols“, *Science*, vol. 303, no. 5664, pp. 1659–1662, 2004, ISSN: 00368075. DOI: 10.1126/science.1092185 (cit. on p. 52).

[192] C. M. Kenseth, N. J. Hafeman, Y. Huang, N. F. Dalleska, B. M. Stoltz, and J. H. Seinfeld, „Synthesis of Carboxylic Acid and Dimer Ester Surrogates to Constrain the Abundance and Distribution of Molecular Products in α-Pinene and β-Pinene Secondary Organic Aerosol“, *Environmental Science and Technology*, vol. 54, no. 20, pp. 12 829–12 839, 2020, ISSN: 15205851. DOI: 10.1021/acs.est.0c01566 (cit. on pp. 52, 57).

[193] J. T. Jayne *et al.*, „Development of an Aerosol Mass Spectrometer for Size and Composition Analysis of Submicron Particles“, *Aerosol Science and Technology*, vol. 33, no. 1-2, pp. 49–70, Jul. 2000, ISSN: 0278-6826. DOI: 10.1080/027868200410840. [Online]. Available: http://www.tandfonline.com/doi/abs/10.1080/027868200410840 (cit. on p. 52).

[194] D. G. Nash, T. Baer, and M. V. Johnston, „Aerosol mass spectrometry: An introductory review“, *International Journal of Mass Spectrometry*, vol. 258, no. 1-3, pp. 2–12, 2006, ISSN: 13873806. DOI: 10.1016/j.ijms.2006.09.017 (cit. on p. 52).

[195] F. D. Lopez-Hilfiker *et al.*, „A novel method for online analysis of gas and particle composition: Description and evaluation of a filter inlet for gases and AEROsols (FIGAERO)“, *Atmospheric Measurement Techniques*, vol. 7, no. 4, pp. 983–1001, 2014, ISSN: 18678548. DOI: 10.5194/amt-7-983-2014 (cit. on p. 53).

[196] J. Cai *et al.*, „Characterization of offline analysis of particulate matter with FIGAERO-CIMS“, *Atmospheric Measurement Techniques*, vol. 16, no. 5, pp. 1147–1165, 2023, ISSN: 18678548. DOI: 10.5194/amt-16-1147-2023 (cit. on p. 53).

[197] J. A. Thornton, C. Mohr, S. Schobesberger, E. L. D'Ambro, B. H. Lee, and F. D. Lopez-Hilfiker, „Evaluating Organic Aerosol Sources and Evolution with a Combined Molecular Composition and Volatility Framework Using the Filter Inlet for Gases and Aerosols (FIGAERO)“, *Accounts of Chemical Research*, vol. 53, no. 8, pp. 1415–1426, 2020, ISSN: 15204898. DOI: 10.1021/acs.accounts.0c00259 (cit. on p. 53).

[198] M. Du *et al.*, „Combined application of online FIGAERO-CIMS and offline LC-Orbitrap mass spectrometry (MS) to characterize the chemical composition of secondary organic aerosol (SOA) in smog chamber studies“, *Atmospheric Measurement Techniques*, vol. 15, no. 14, pp. 4385–4406, 2022, ISSN: 18678548. DOI: 10.5194/amt-15-4385-2022 (cit. on p. 53).

[199] D. E. Romonosky, Y. Li, M. Shiraiwa, A. Laskin, J. Laskin, and S. A. Nizkorodov, „Aqueous Photochemistry of Secondary Organic Aerosol of α-Pinene and α-Humulene Oxidized with Ozone, Hydroxyl Radical, and Nitrate Radical“, *Journal of Physical Chemistry A*, vol. 121, no. 6, pp. 1298–1309, 2017, ISSN: 15205215. DOI: 10.1021/acs.jpca.6b10900 (cit. on p. 53).

[200] K. Chen *et al.*, „Solvent effects on chemical composition and optical properties of extracted secondary brown carbon constituents“, *Aerosol Science and Technology*, vol. 56, no. 10, pp. 917–930, 2022, ISSN: 15217388. DOI: 10.1080/02786826.2022.2100734. [Online]. Available: https://doi.org/10.1080/02786826.2022.2100734 (cit. on p. 53).

[201] H. Hakola, H. Hellén, V. Tarvainen, J. Bäck, J. Patokoski, and J. Rinne, „Annual variations of atmospheric VOC concentrations in a boreal forest“, *Boreal Environment Research*, vol. 14, no. 4, pp. 722–730, 2009, ISSN: 12396095 (cit. on p. 57).

[202] J. Bäck, J. Aalto, M. Henriksson, H. Hakola, Q. He, and M. Boy, „Chemodiversity of a Scots pine stand and implications for terpene air concentrations“, *Biogeosciences*, vol. 9, no. 2, pp. 689–702, 2012, ISSN: 17264170. DOI: 10.5194/bg-9-689-2012 (cit. on p. 57).

[203] X. Zhang *et al.*, „Formation and evolution of molecular products in α-pinene secondary organic aerosol“, *Proceedings of the National Academy of Sciences of the United States of America*, vol. 112, no. 46, pp. 14 168–14 173, 2015, ISSN: 10916490. DOI: 10.1073/pnas.1517742112 (cit. on p. 59).

[204] M. S. Claflin, J. E. Krechmer, W. Hu, J. L. Jimenez, and P. J. Ziemann, „Functional Group Composition of Secondary Organic Aerosol Formed from Ozonolysis of α-Pinene under High VOC and Autoxidation Conditions“, *ACS Earth and Space Chemistry*, vol. 2, no. 11, pp. 1196–1210, 2018, ISSN: 24723452. DOI: 10.1021/acsearthspacechem.8b00117 (cit. on pp. 59, 61, 66).

[205] T. D. Vaden, D. Imre, J. Beránek, M. Shrivastava, and A. Zelenyuk, „Evaporation kinetics and phase of laboratory and ambient secondary organic aerosol“, *Proceedings of the National Academy of Sciences of the United States of America*, vol. 108, no. 6, pp. 2190–2195, 2011, ISSN: 00278424. DOI: 10.1073/pnas.1013391108 (cit. on p. 59).

[206] J. Wilson, D. Imre, J. Beránek, M. Shrivastava, and A. Zelenyuk, „Evaporation kinetics of laboratory-generated secondary organic aerosols at elevated relative humidity“, *Environmental Science and Technology*, vol. 49, no. 1, pp. 243–249, 2015, ISSN: 15205851. DOI: 10.1021/es505331d (cit. on p. 59).

[207] Z. Li *et al.*, „Effect of Decreased Temperature on the Evaporation of α-Pinene Secondary Organic Aerosol Particles“, *ACS Earth and Space Chemistry*, vol. 3, no. 12, pp. 2775–2785, 2019, ISSN: 24723452. DOI: 10.1021/acsearthspacechem.9b00240 (cit. on p. 59).

[208] Z. Li *et al.*, „Isothermal evaporation of α-pinene secondary organic aerosol particles formed under low NOx and high NOx conditions“, *Atmospheric Chemistry and Physics*, vol. 23, no. 1, pp. 203–220, 2023, ISSN: 16807324. DOI: 10.5194/acp-23-203-2023 (cit. on p. 59).

[209] A. Ylisirniö *et al.*, „Composition and volatility of secondary organic aerosol (SOA) formed from oxidation of real tree emissions compared to simplified volatile organic compound (VOC) systems“, *Atmospheric Chemistry and Physics*, vol. 20, no. 9, pp. 5629–5644, 2020, ISSN: 16807324. DOI: 10.5194/acp-20-5629-2020 (cit. on p. 59).

[210] F. Yasmeen, R. Vermeylen, N. Maurin, E. Perraudin, J. F. Doussin, and M. Claeys, „Characterisation of tracers for aging of $$\alpha$$-pinene secondary organic aerosol using liquid chromatography/negative ion electrospray ionisation mass spectrometry“, *Environmental Chemistry*, vol. 9, no. 3, pp. 236–246, 2012, ISSN: 14482517. DOI: 10.1071/EN11148 (cit. on pp. 65, 66, 158, 199).

[211] F. Yasmeen *et al.*, „Mass spectrometric characterization of isomeric terpenoic acids from the oxidation of $$\alpha$$-pinene, $$\beta$$-pinene, d-limonene, and Î" 3-carene in fine forest aerosol“, *Journal of Mass Spectrometry*, vol. 46, no. 4, pp. 425–442, 2011, ISSN: 10765174. DOI: 10.1002/jms.1911 (cit. on p. 65).

[212] M. Claeys *et al.*, „Terpenylic acid and related compounds from the oxidation of α-pinene: Implications for new particle formation and growth above forests“, *Environmental Science and Technology*, vol. 43, no. 18, pp. 6976–6982, 2009, ISSN: 0013936X. DOI: 10.1021/es9007596 (cit. on p. 65).

[213] M. Beck and T. Hoffmann, „A detailed MSn study for the molecular identification of a dimer formed from oxidation of pinene“, *Atmospheric Environment*, vol. 130, pp. 120–126, 2016, ISSN: 18732844. DOI: 10.1016/j.atmosenv.2015.09.012. [Online]. Available: http://dx.doi.org/10.1016/j.atmosenv.2015.09.012 (cit. on p. 66).

[214] M. S. Claflin, J. Liu, L. M. Russell, and P. J. Ziemann, „Comparison of methods of functional group analysis using results from laboratory and field aerosol measurements“, *Aerosol Science and Technology*, vol. 55, no. 9, pp. 1042–1058, 2021, ISSN: 15217388. DOI: 10.1080/02786826.2021.1918325. [Online]. Available: https://doi.org/10.1080/02786826.2021.1918325 (cit. on p. 66).

[215] A. V. Jackson and C. N. Hewitt, „Atmosphere hydrogen peroxide and organic hydroperoxides: A review“, *Critical Reviews in Environmental Science and Technology*, vol. 29, no. 2, pp. 175–228, 1999, ISSN: 10643389. DOI: 10.1080/10643389991259209 (cit. on p. 71).

[216] S. Wang *et al.*, „Relationship between chemical composition and oxidative potential of secondary organic aerosol from polycyclic aromatic hydrocarbons“, *Atmospheric Chemistry and Physics*, vol. 18, no. 6, pp. 3987–4003, 2018, ISSN: 16807324. DOI: 10.5194/acp-18-3987-2018 (cit. on pp. 71, 88).

[217] M. J. Calandra and Y. Wang, „An HPLC method for the detection of hydro peroxides derived from linalyl acetate in citrus oils, using post-column luminol-mediated chemiluminescence detection“, *Flavour and Fragrance Journal*, vol. 32, no. 3, pp. 178–183, 2017, ISSN: 10991026. DOI: 10.1002/ffj.3372 (cit. on p. 72).

[218] T. Miyazawa, K. Yasuda, and K. Fujimoto, „Chemiluminescence-high performance liquid chromatography of phosphatidylcholine hydroperoxide“, *Analytical Letters*, vol. 20, no. 6, pp. 915–925, 1987, ISSN: 1532236X. DOI: 10.1080/00032718708062941 (cit. on p. 72).

[219] T. Miyazawa, „Determination of phospholipid hydroperoxides in human blood plasma by a chemiluminescence-HPLC assay“, *Free Radical Biology and Medicine*, vol. 7, no. 2, pp. 209–218, 1989, ISSN: 08915849. DOI: 10.1016/0891-5849(89)90017-8 (cit. on p. 72).

[220] T. Miyazawa, T. Suzuki, K. Fujimoto, and K. Yasuda, „Chemiluminescent simultaneous determination of phosphatidylcholine hydroperoxide and phosphatidylethanolamine hydroperoxide in the liver and brain of the rat“, *Journal of Lipid Research*, vol. 33, no. 7, pp. 1051–1058, 1992, ISSN: 00222275. DOI: 10.1016/s0022-2275(20)41420-8. [Online]. Available: http://dx.doi.org/10.1016/S0022-2275(20)41420-8 (cit. on p. 72).

[221] M. Yamaguchi, H. Yoshida, and H. Nohta, „Luminol-type chemiluminescence derivatization reagents for liquid chromatography and capillary electrophoresis“, *Journal of Chromatography A*, vol. 950, no. 1-2, pp. 1–19, 2002, ISSN: 00219673. DOI: 10.1016/S0021-9673(02)00004-3 (cit. on p. 72).

[222] K. Li, J. Resch, and M. Kalberer, „Synthesis and Characterization of Organic Peroxides from Monoterpene-Derived Criegee Intermediates in Secondary Organic Aerosol“, *Environmental Science & Technology*, Feb. 2024, ISSN: 0013-936X. DOI: 10.1021/acs.est.3c07048. [Online]. Available: https://pubs.acs.org/doi/10.1021/acs.est.3c07048 (cit. on pp. 73, 83, 93, 97, 127).

[223] Z. Zhang, L. Lin, and L. Wang, „Atmospheric oxidation mechanism of naphthalene initiated by OH radical. A theoretical study“, *Physical Chemistry Chemical Physics*, vol. 14, no. 8, pp. 2645–2650, 2012, ISSN: 14639076. DOI: 10.1039/c2cp23271e (cit. on p. 74).

[224] N. J. Bunce, L. Liu, J. Zhu, and D. A. Lane, „Reaction of naphthalene and its derivatives with hydroxyl radicals in the gas phase“, *Environmental Science and Technology*, vol. 31, no. 8, pp. 2252–2259, 1997, ISSN: 0013936X. DOI: 10.1021/es960813g (cit. on p. 74).

[225] T. Gautam, S. Wu, J. Ma, and R. Zhao, „Potential Matrix Effects in Iodometry Determination of Peroxides Induced by Olefins“, *Journal of Physical Chemistry A*, vol. 126, no. 17, pp. 2632–2644, 2022, ISSN: 15205215. DOI: 10.1021/acs.jpca.1c10717 (cit. on p. 75).

[226] K. E. Kautzman *et al.*, „Chemical composition of gas- and aerosol-phase products from the photooxidation of naphthalene“, *Journal of Physical Chemistry A*, vol. 114, no. 2, pp. 913–934, 2010, ISSN: 10895639. DOI: 10.1021/jp908530s (cit. on p. 88).

[227] D. Thomsen *et al.*, „ Ozonolysis of α-Pinene and Δ 3 -Carene Mixtures: Formation of Dimers with Two Precursors “, *Environmental Science & Technology*, 2022, ISSN: 0013-936X. DOI: 10.1021/acs.est.2c04786 (cit. on p. 88).

[228] P. A. Dominutti, J.-l. Jaffrezo, A. Marsal, T. Mhadhbi, and R. Elazzouzi, „An interlaboratory comparison to quantify oxidative potential measurement in aerosol particles : challenges and recommendations for harmonisation“, *Atmospheric Measurement Techniques Discussions*, pp. 1–32, 2024. DOI: https://doi.org/10.5194/amt-2024-107. [Online]. Available: https://amt.copernicus.org/preprints/amt-2024-107/ (cit. on p. 127).

[229] K. Kristensen, T. Cui, H. Zhang, A. Gold, M. Glasius, and J. D. Surratt, „Dimers in α-pinene secondary organic aerosol: Effect of hydroxyl radical, ozone, relative humidity and aerosol acidity“, *Atmospheric Chemistry and Physics*, vol. 14, no. 8, pp. 4201–4218, 2014, ISSN: 16807324. DOI: 10.5194/acp-14-4201-2014 (cit. on p. 145).

Appendices

Appendix A

Further Contributions

In addition to the work presented in the main text, I contributed to further projects and publications as listed below:

- For the publication of Keller *et al.* [108], I did all of the LC-MS related laboratory work, including extraction of all filter samples and conducting the LC-MS measurements.
- For the publication of Li *et al.* [222], I helped in experiment conceptualization and data analysis as well as interpretation. I introduced Dr. Li to the LC-MS and helped with measurements. I also contributed to the writing of the manuscript.
- In a currently submitted manuscript by Campbell *et al.*, on online vs. offline OP measurements, I helped during the measurements and planning of NO_x experiments for the cell campaign held at the University of Basel in cooperation with the University of Bern. I also did principal component analysis of the results, and helped with further data analysis and interpretation.
- In a manuscript currently in review by Dominutti *et al.* [228], of an intercomparison study of different oxidative potential measurements, I helped with all of the sample analysis done in our lab, as well as the data analysis. Our lab further helped in correcting several mistakes in the calculations of results presented by the authors. As only two authors per group were allowed to be listed as authors on this paper (because it was a very large intercomparison with more than 15 labs participating), I am not mentioned as an author but only in the Acknowledgements.
- In a currently submitted manuscript by Jones *et al.*, which updates the 2.26 Analytical Derivatization Techniques chapter in the book "Comprehensive

Sampling and Sample Preparation" (ISBN: 9780123813749), I contributed to the subchapter "Derivatization of Analytes from Air Samples or Aerosols".

Appendix B

Supplementary Material to "Effects of Storage Conditions on the Molecular-Level Composition of Organic Aerosol Particles"

Supplement of Atmospheric Chemistry and Physics, 23, 9161-9171, 2023.
https://doi.org/10.5194/acp-23-9161-2023-supplement

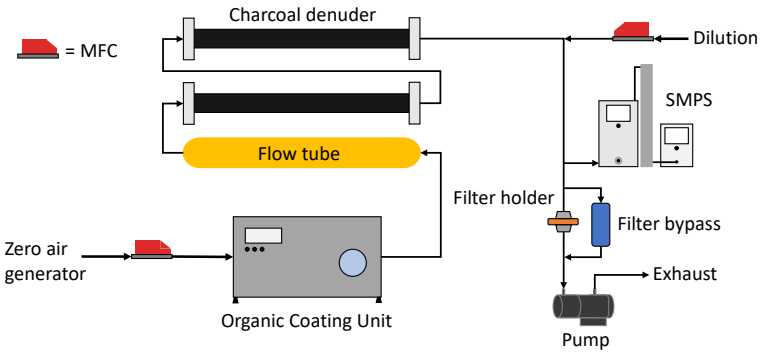

Figure B.1: Setup used for the collection of laboratory-generated secondary organic aerosol samples.

Table B.1: Table of all SOA filters collected displaying the collection time for each filter, the sum of collected mass per filter quarter and the average SOA mass concentration in the OCU measured by the SMPS.

SOA sample	Filter number	Collection time (hh:mm:ss)	Sum of collected mass per filter quarter (µg)	Average concentration in OCU/SMPS (µg m^{-3})
β-pinene	Filter 1	0:30:41	319.9	6582.8
β-pinene	Filter 2	0:30:36	315.5	6511.8
β-pinene	Filter 3	0:30:43	313.7	6445.8
β-pinene	Filter 4	0:30:44	315.8	6490.8
β-pinene	Filter 5	0:30:40	311.6	6418.4
β-pinene	Filter 6	0:30:37	314.4	6485.4
β-pinene	Filter 7	0:30:40	317.3	6536.1
β-pinene	Filter 8	0:28:59	304.3	6604.4
β-pinene	Filter 9	0:30:41	309.9	6379
β-pinene	Filter 10	0:30:44	312	6410.6
β-pinene	Filter 11	0:30:42	310.9	6396.4
β-pinene	Filter 12	0:30:41	319.8	6583.4
β-pinene	Filter 13	0:30:44	318.4	6543.5
β-pinene	Filter 14	0:30:39	315.7	6506.9
β-pinene	Filter 15	0:30:36	315	6502.4
β-pinene	Filter 16	0:34:05	303.7	5658.5

Table B.1 continued from previous page

β-pinene	Filter 17	0:34:07	291.3	5421.6
β-pinene	Filter 18	0:29:02	256.6	5565.5
β-pinene	Filter 19	0:34:05	299.7	5583.3
β-pinene	Filter 20	0:34:11	301.3	5597.3
β-pinene	Filter 21	0:34:02	291.7	5443
β-pinene	Filter 22	0:34:13	288.4	5352.9
β-pinene	Filter 23	0:34:05	302.6	5641.2
β-pinene	Filter 24	0:34:01	299.2	5587.2
β-pinene	Filter 25	0:34:14	303.5	5630.8
Naphthalene	Filter 1	0:42:37	306	4605.4
Naphthalene	Filter 2	0:39:10	306.9	5004.4
Naphthalene	Filter 3	0:39:16	309.8	5042.3
Naphthalene	Filter 4	0:39:35	309.6	4990.5
Naphthalene	Filter 5	0:42:39	299.3	4528.3
Naphthalene	Filter 6	0:34:12	288.5	5360
Naphthalene	Filter 7	0:34:10	296.5	5511.5
Naphthalene	Filter 8	0:37:30	306.7	5216.3
Naphthalene	Filter 9	0:34:07	292.4	5439.2
Naphthalene	Filter 10	0:37:30	310.6	5283.5
Naphthalene	Filter 11	0:41:14	293.2	4553.3
Naphthalene	Filter 12	0:42:50	304.9	4563.8
Naphthalene	Filter 13	0:37:37	297	5034.3
Naphthalene	Filter 14	0:37:40	309	5230.3
Naphthalene	Filter 15	0:37:40	300.5	5087.1
Naphthalene	Filter 16	0:46:04	334	4659.3
Naphthalene	Filter 17	0:37:30	338.8	5763.2
Naphthalene	Filter 18	0:37:34	298	5055
Naphthalene	Filter 19	0:37:26	297.9	5075.4
Naphthalene	Filter 20	0:37:26	302	5144.8
Naphthalene	Filter 21	0:39:08	315.3	5147.3
Naphthalene	Filter 22	0:37:27	290.1	4939.3
Naphthalene	Filter 23	0:39:07	308.9	5044.9
Naphthalene	Filter 24	0:37:35	311.3	5282.9
Naphthalene	Filter 25	0:37:31	304.1	5169.8

Table B.2: List of all samples analyzed and exact days between collection and analysis. Each condition was analyzed for samples stored at +20°C, -20°C and -80°C. *Due to technical problems during the filter extraction for these samples they were excluded from the analysis.

Sample	Immediately		24 hours		1 week		2 weeks		4 weeks	
	Extract [days]	Filter [days]	Extract [days]	Filter [days]	Extract [days]	Filter [days]	Extract [days]	Filter [days]	Extract [days]	Filter [days]
β-pinene-SOA	0		2	2	6	7	16	15	33	28
Naphth-alene-SOA	0		1	2	7	8	14	14	27	33
HVAS 1 11.-12.05.2022	0		2	1	7	7	/*	/*	44	44
HVAS 2 17.-18.05.2022	0		1	1	10	7	19	18	33	32
HVAS 3 25.-26.05.2022	0		1	1	10	9	20	19	28	29
HVAS 4 29.-30.05.2022	0		2	1	8	7	18	18	28	28
HVAS 5 30.-31.05.2022	0		2	2	8	8	18	18	28	28

Preparation of standards used for calibration

Stock solutions of 1 $mgmL^{-1}$ were prepared for each chemical. Cis-pinonic acid and 4-hydroxy benzoic acid were dissolved in the standard diluent (SD) of 1:10 ACN:H_2O, pimelic acid and camphoric acid in a 1:10 mixture of Dimethyl Sulfoxide (DMSO):SD and 1,2-naphthoquinone in 1:5 DMSO:SD. The addition of DMSO was necessary to completely dissolve the standards in the mixture. The concentrations used are given in Table B.3. Dilution (Dil) 1 was made up of 100 µL of each of the 5 standards used and 500 µL SD in order to have 1 mL total volume. The standards dilution series 1-4 were then run twice in the LC-MS in reversed order starting with the least concentrated. Peak area was obtained for each compound in the chromatogram

Table B.3: Concentration, mixture, solution and diluent of the standards used for calibration

Standard Dilution	Concentration (mg)	Mixture	Solution (ul)	Standard Diluent (uL)
Stock 1	1			
Stock 2	0.1	1:10; stock 1:SD	100	900
Dil 1	0.01	1:10; stock 2:SD	5*100	500
Dil 2	0.001	1:10; dilution 1:SD	100	900
Dil 3	0.0001	1:10; dilution 2:SD	100	900
Dil 4	0.00001	1:10; dilution 3:SD	100	900

and then averaged between the two runs and then used for comparison between different measurement days.

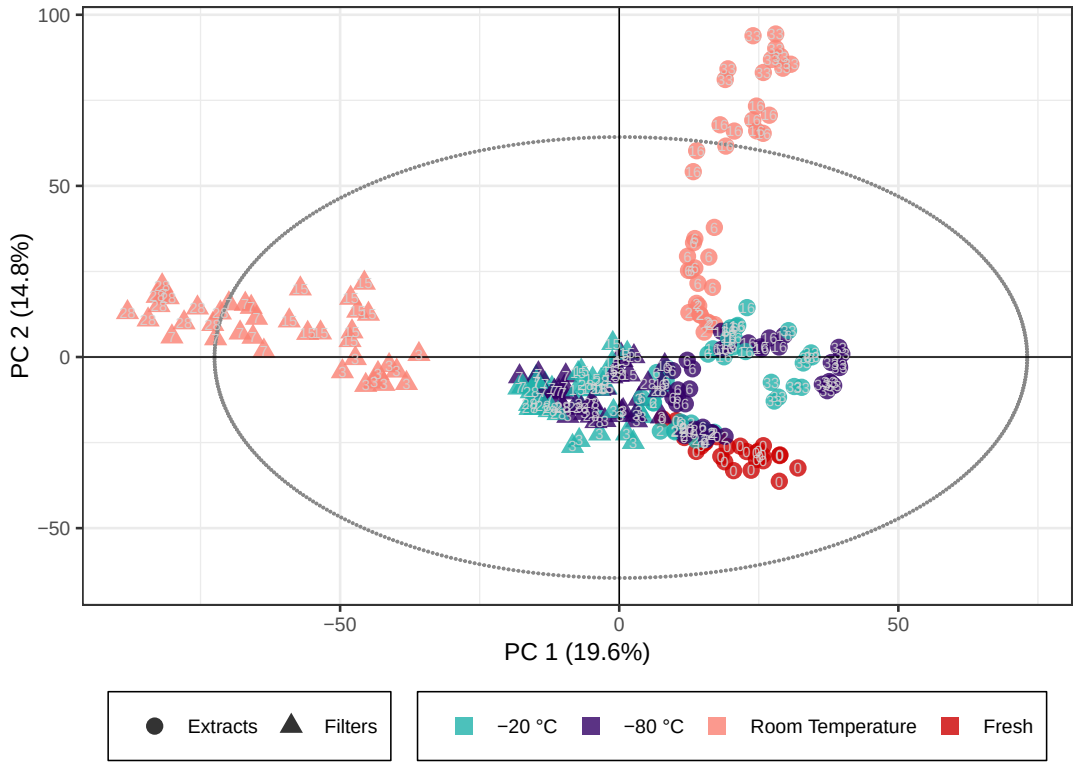

Figure B.2: Same PCA scores plot as shown in Figure 3.1 but with the storage time [days] of each sample represented by the numbers inside the icons.

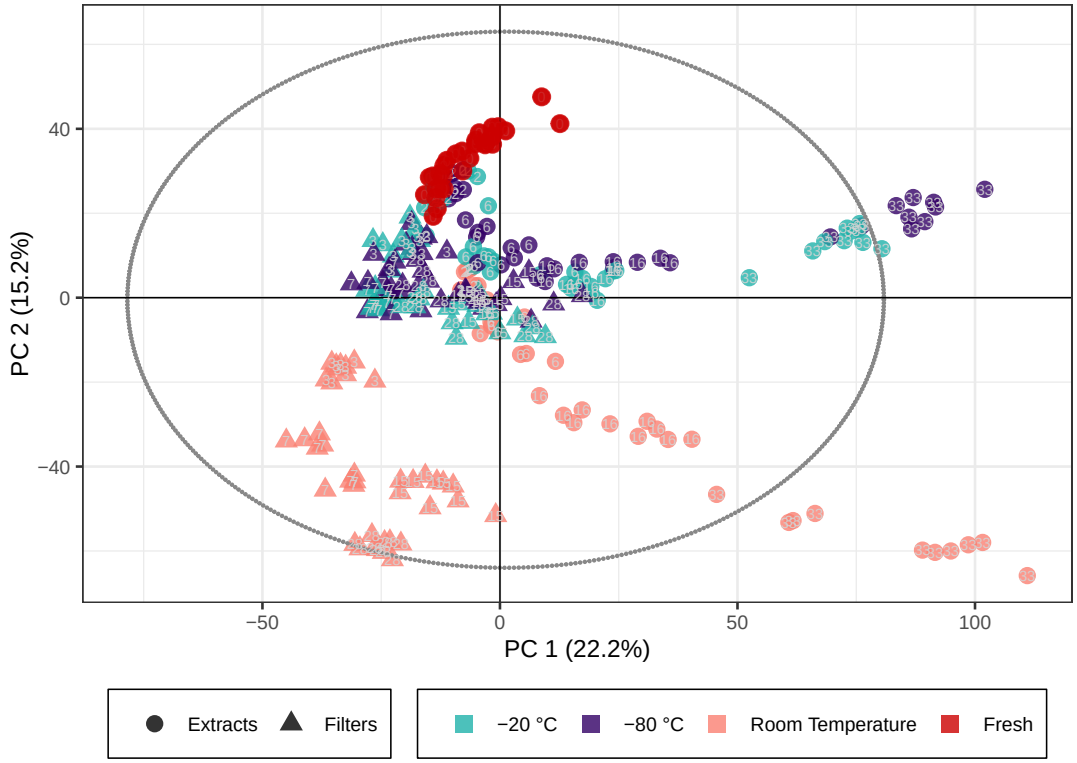

Figure B.3: $Log_{10}(x)$ normalized PCA scores plot of the β-pinene SOA samples with the storage time [days] of each sample represented by the numbers inside the icons.

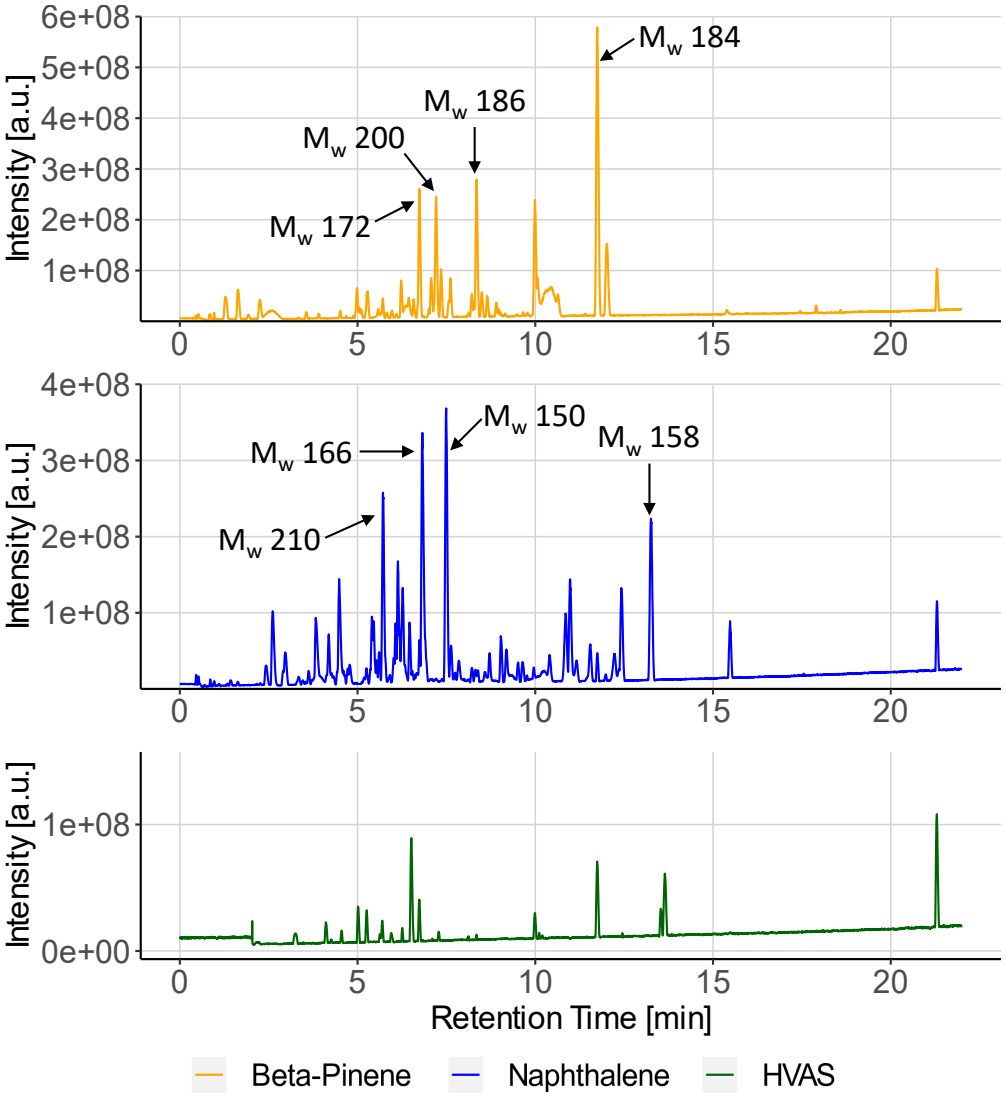

Figure B.4: Base peak chromatogram of the different immediately extracted aerosol samples in this study.

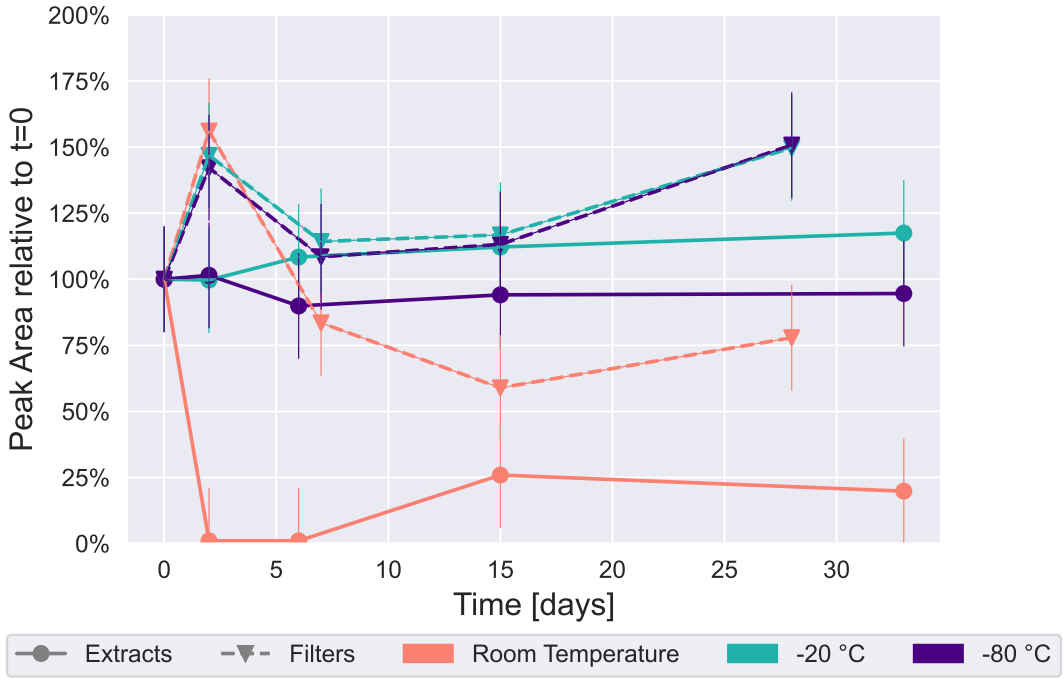

Figure B.5: Time series of the M_W 338 (m/z 387.1659, $C_{18}H_{28}O_9$) compound detected at 18.59 min in β-Pinene SOA.

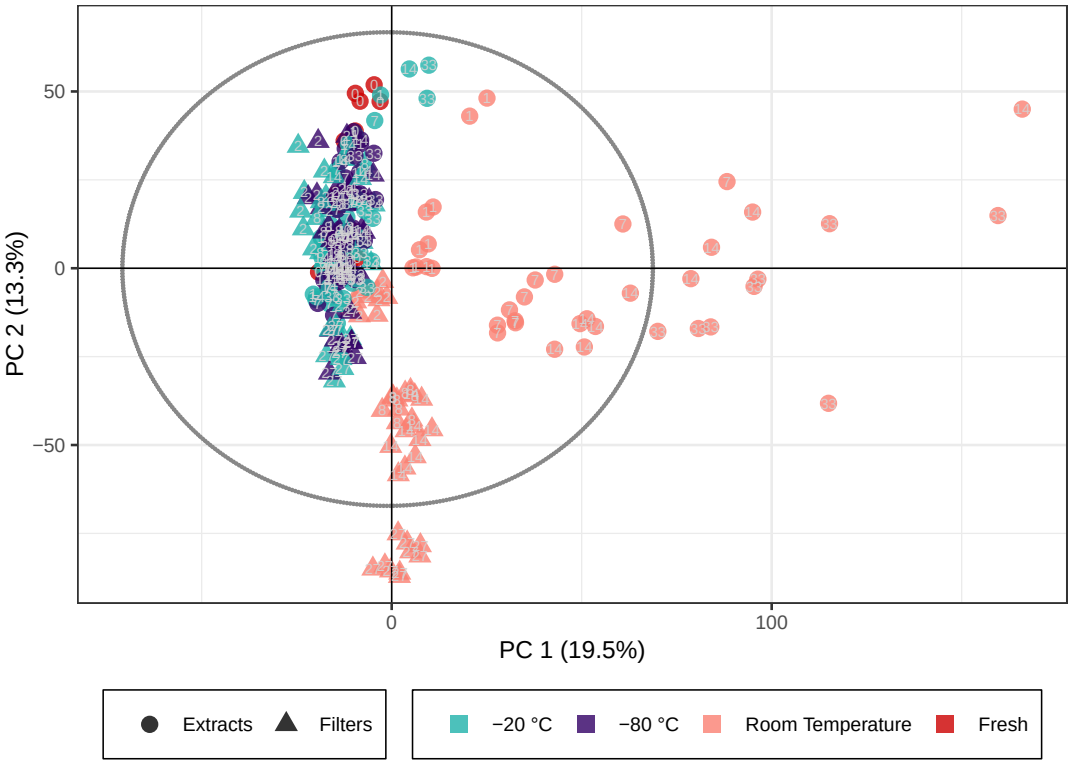

Figure B.6: Same PCA scores plot as shown in Figure 3.3, but with storage time [days] of each sample represented by the numbers inside the icons.

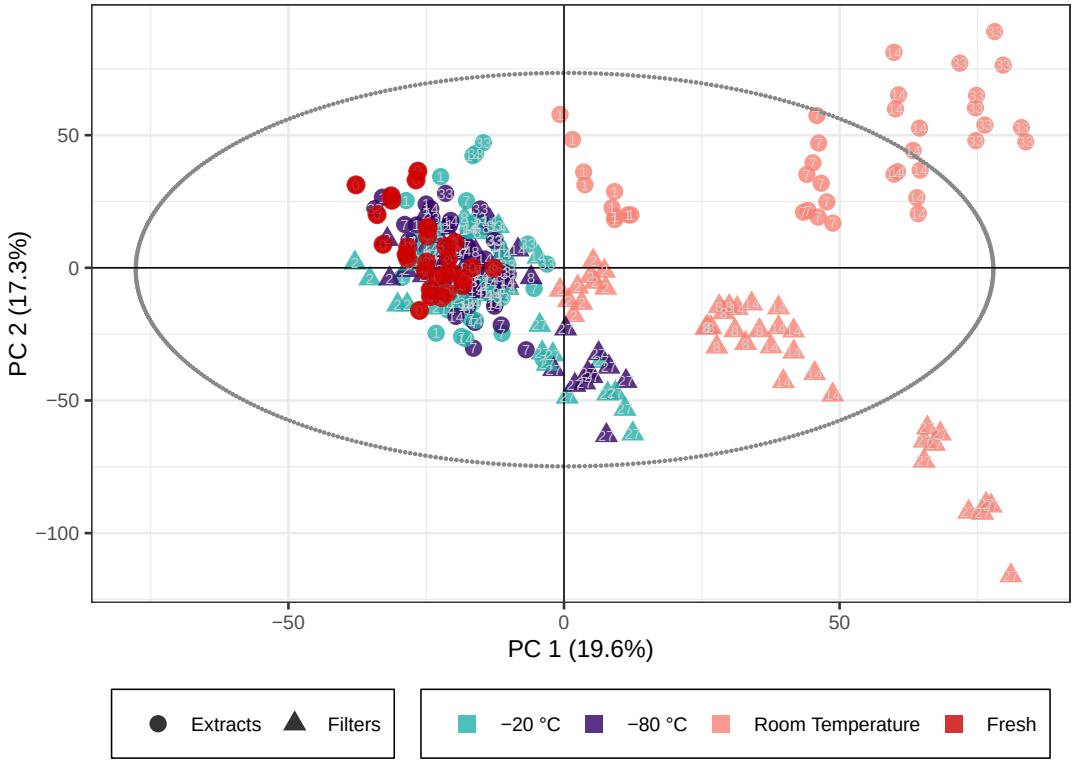

Figure B.7: $Log_{10}(x)$ normalized PCA scores plot of the naphthalene SOA samples with the storage time [days] of each sample represented by the numbers inside the icons.

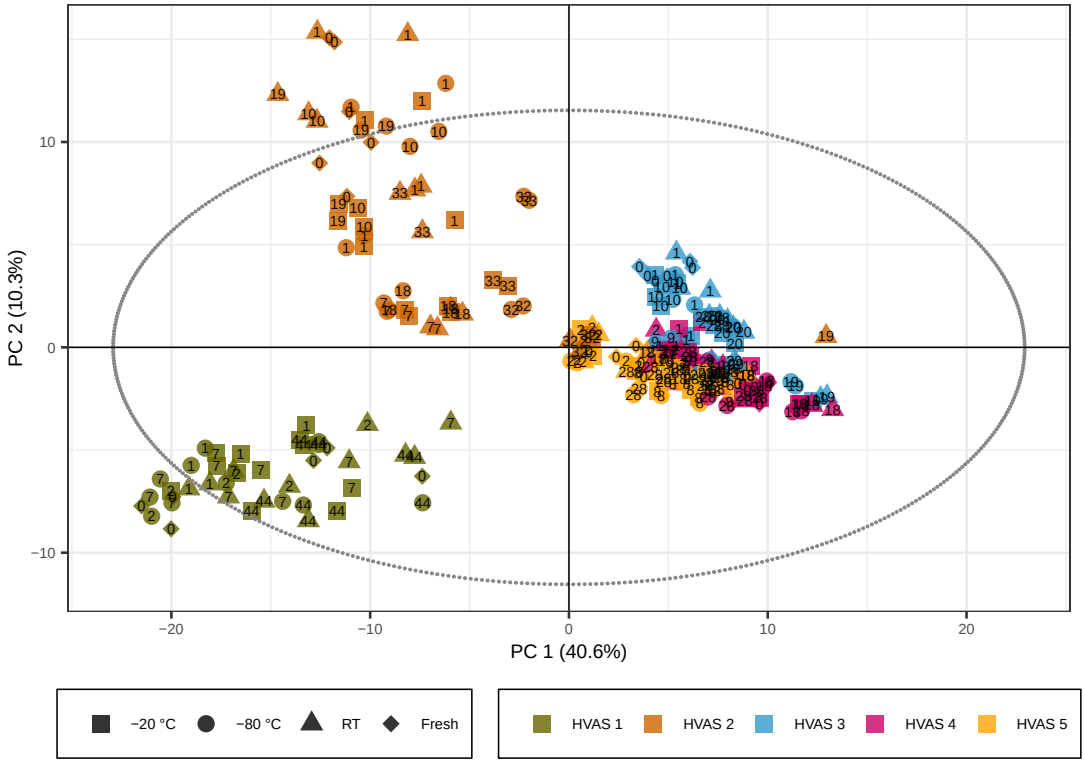

Figure B.8: Corrected PCA scores plots of all ambient samples and storage times [days] given as the numbers inside the icons.

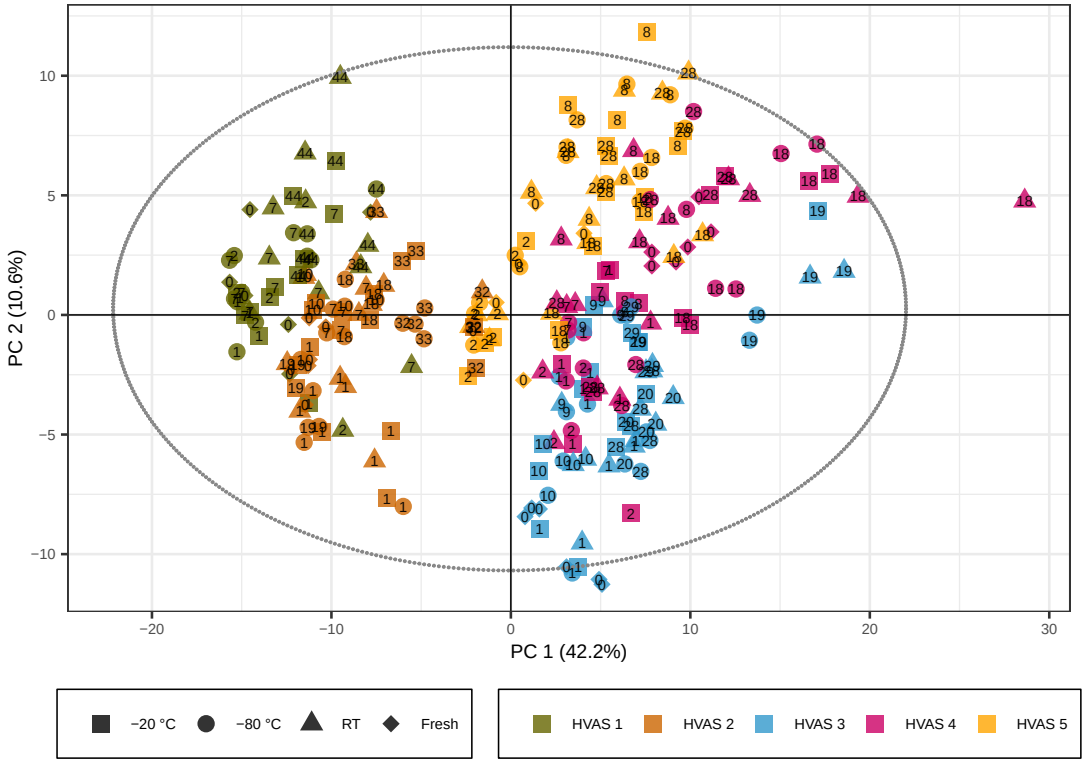

Figure B.9: $Log_{10}(x)$ normalized PCA scores plot of the corrected ambient samples with the storage time [days] of each sample represented by the numbers inside the icons.

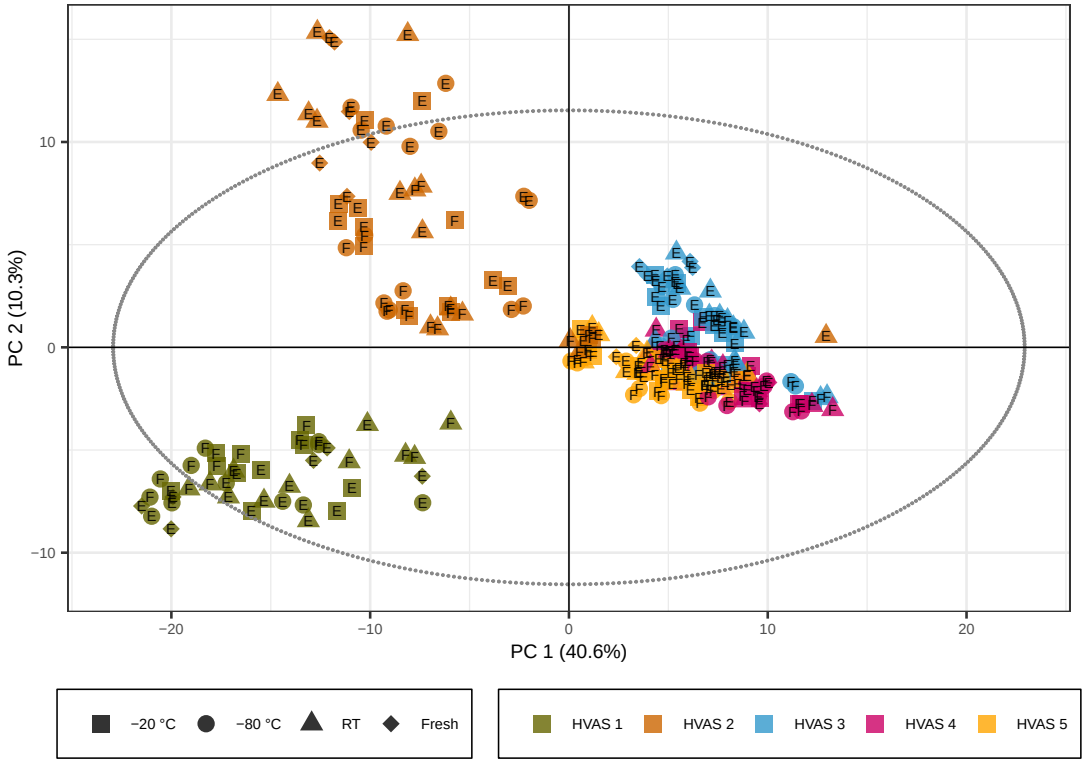

Figure B.10: Corrected PCA scores plots of all ambient samples and the storage type given as labels inside the icons (E=Extracts and F=Filters).

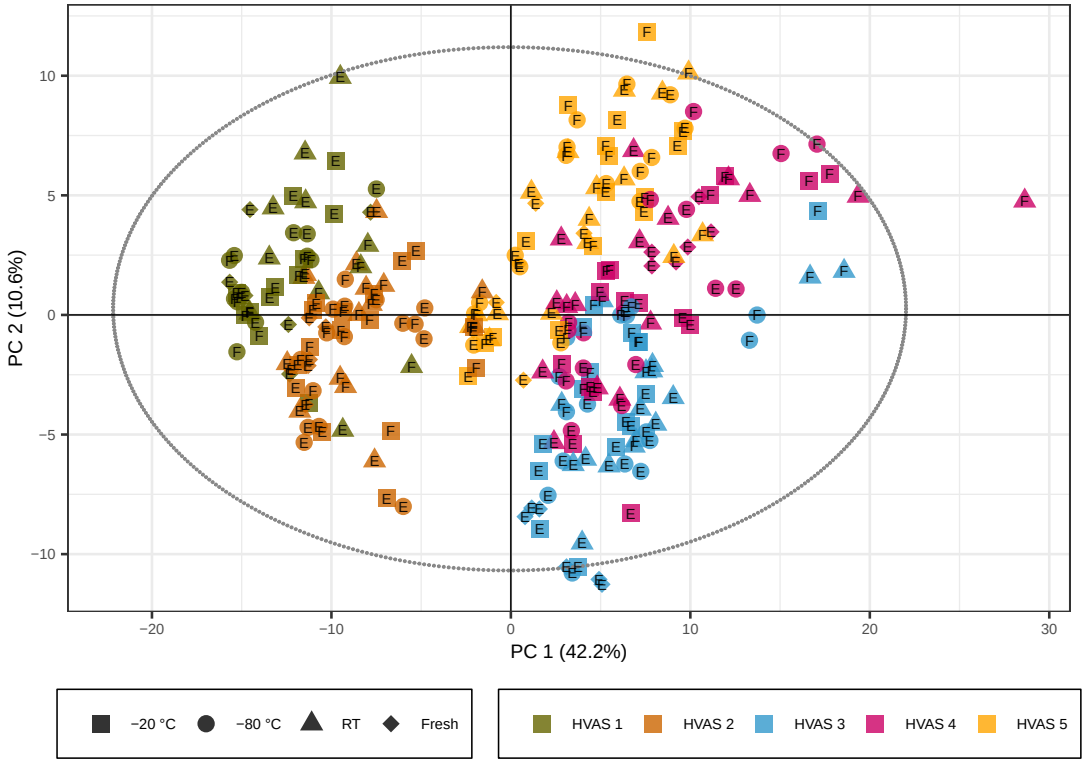

Figure B.11: $Log_{10}(x)$ normalized PCA scores plot of the corrected ambient samples and the storage type given as labels inside the icons (E=Extracts and F=Filters).

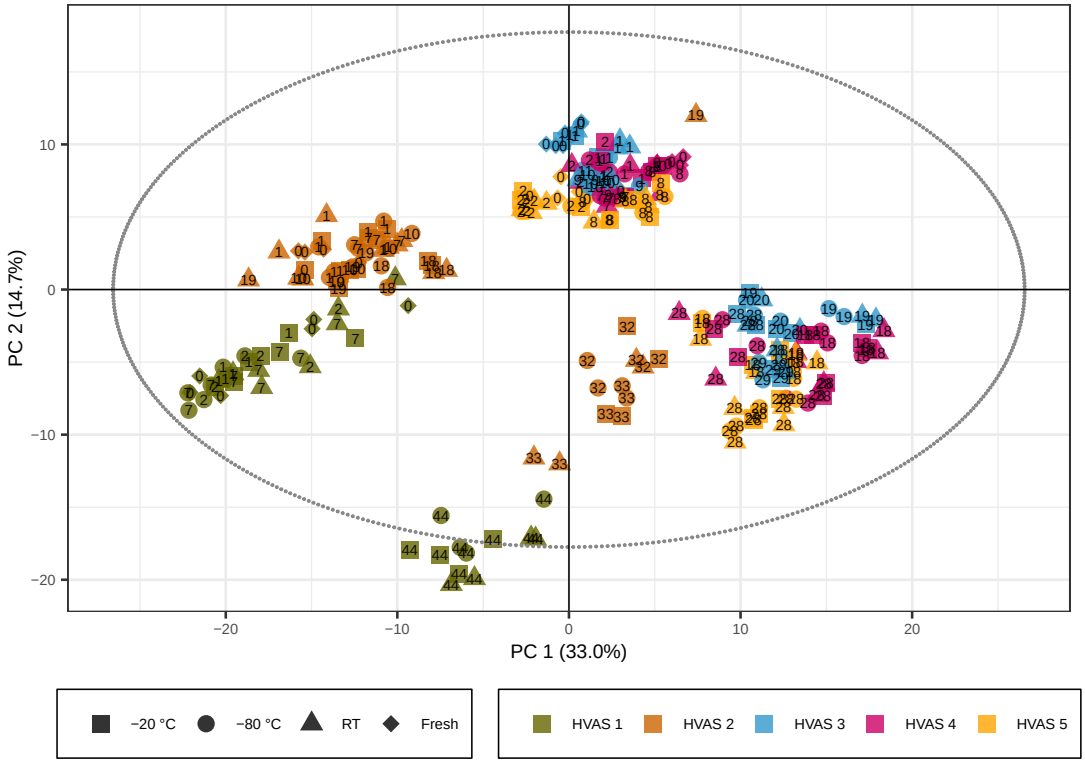

Figure B.12: Non-corrected PCA scores plot of all ambient samples with storage time [days] given as numbers in the icons. A clear batch effect can be seen between samples which were analyzed before (top left) and after (bottom right) the switch of water as mobile phase A.

Appendix C

Supplementary Material to "Prolonged Dark Chemical Processes in Secondary Organic Aerosols on Filters and in Aqueous Solution"

The Supporting Information is available free of charge at https://pubs.acs.org/doi/10.1021/acs.est.4c01647.

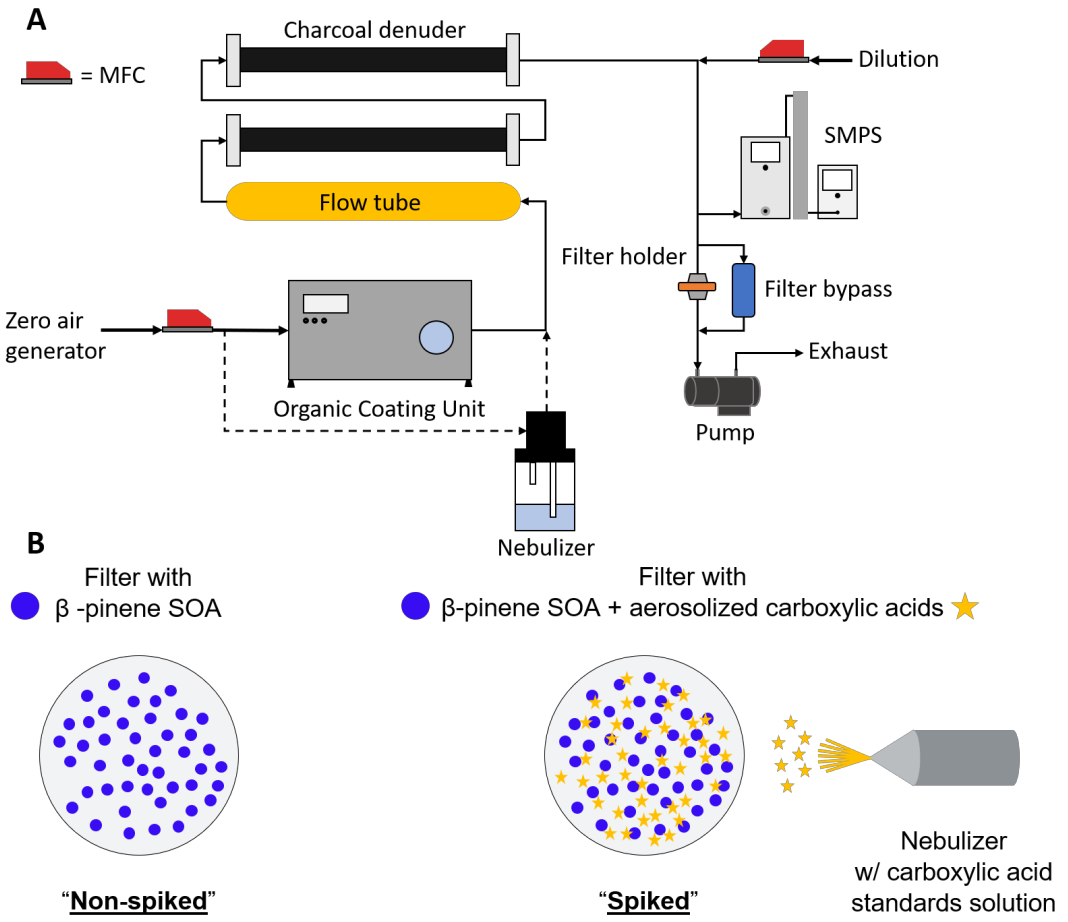

Figure C.1: (A) Setup used for the collection of laboratory-generated β-pinene secondary organic aerosol samples as described in Resch *et al.* [113]. (B) For "spiking" experiments a nebulized was additionally used instead of the OCU to deposit carboxylic acid standards onto the previously collected β-pinene filters. Nebulizing a mixture of carboxylic acid standards onto the SOA filter assures that the carboxylic acids are deposited on the filters without a solvent, which could interfere with the SOA particle phase reaction studied.

Table C.1: Complete list containing Compound ID, observed *m/z* in negative polarity mode, Molecular Formula and literature references for all dimer esters investigated.

Compound ID[reference]	Observed *m/z* (-)	Molecular Formula
M_W 302[40]	301.1651	$C_{15}H_{26}O_6$
M_W 312[40]	311.1504	$C_{16}H_{24}O_6$
M_W 314[40]	313.1651	$C_{16}H_{26}O_6$
M_W 316[40]	315.1443	$C_{15}H_{24}O_7$
M_W 324	323.1860	$C_{18}H_{28}O_5$
M_W 328[40]	327.1444	$C_{16}H_{24}O_7$
M_W 330[40]	329.1600	$C_{16}H_{26}O_7$
M_W 332[40]	331.1393	$C_{15}H_{24}O_8$

Table C.1 continued from previous page

M_W 336[40]	335.1859	$C_{19}H_{28}O_5$
M_W 338[40, 46, 178]	337.2015	$C_{19}H_{30}O_5$
M_W 340[40]	339.1808	$C_{18}H_{28}O_6$
M_W 342[40]	341.1600	$C_{17}H_{26}O_7$
M_W 344a[37, 40, 46, 58, 229]	343.1393	$C_{16}H_{24}O_8$
M_W 344b[40]	343.1756	$C_{17}H_{28}O_7$
M_W 352[40, 178]	351.1828	$C_{19}H_{28}O_6$
M_W 354[40]	353.1964	$C_{19}H_{30}O_6$
M_W 356[40, 178]	355.1766	$C_{18}H_{28}O_7$
M_W 358[37, 40, 46, 58, 229]	357.1558	$C_{17}H_{26}O_8$
M_W 360[40]	359.1715	$C_{17}H_{28}O_8$
M_W 362[40]	361.1508	$C_{16}H_{26}O_9$
M_W 368[40, 46, 57, 58, 229]	367.1764	$C_{19}H_{28}O_7$
M_W 370[40, 46, 178]	369.1921	$C_{19}H_{30}O_7$
M_W 372[40]	371.1714	$C_{18}H_{28}O_8$
M_W 374a[40]	373.1499	$C_{17}H_{26}O_9$
M_W 374b[178]	373.1851	$C_{18}H_{30}O_8$
M_W 378[40]	377.1432	$C_{16}H_{26}O_{10}$
M_W 384[40]	383.1715	$C_{19}H_{28}O_8$
M_W 386[40]	385.1872	$C_{19}H_{30}O_8$
M_W 388a[40]	387.1665	$C_{18}H_{28}O_9$
M_W 388b[46, 229]	387.2022	$C_{19}H_{32}O_8$
M_W 400[40]	399.1663	$C_{19}H_{28}O_9$
M_W 406[40, 178]	405.1770	$C_{18}H_{30}O_{10}$
M_W 420[178]	419.1525	$C_{18}H_{28}O_{11}$

Table C.2: List of oligomers analyzed. Molecular weight, tentative chemical formula, retention time and sample type of highest observed peak are given.

Compound ID	Observed *m/z* (-)	Molecular formula	Retention time (min)	Sample type of highest observed peak
M_W 338	337.2015	$C_{19}H_{30}O_5$	20.03	Both
M_W 340	339.1808	$C_{18}H_{28}O_6$	16.77	Aged
			18.54	Fresh
M_W 344a	343.1393	$C_{16}H_{24}O_8$	13.51	Aged
M_W 344b	343.1757	$C_{17}H_{28}O_7$	16.74	Aged
			16.34	Fresh
			16.58	Fresh
M_W 354	353.1964	$C_{19}H_{30}O_6$	21.17	Aged
			22.23	Fresh
M_W 356	355.1757	$C_{18}H_{28}O_7$	17.48	Aged
			15.72	Fresh
M_W 360	359.1706	$C_{17}H_{28}O_8$	17.57	Aged
M_W 362	361.1499	$C_{16}H_{26}O_9$	14.68	Both
M_W 368	367.1757	$C_{19}H_{28}O_7$	13.83	Aged
M_W 370	369.1913	$C_{19}H_{30}O_7$	17.66	Aged
			18.54	Fresh
M_W 372	371.1706	$C_{18}H_{28}O_8$	14.87	Aged
			15.64	Fresh
M_W 386	385.1862	$C_{19}H_{30}O_8$	15.05	Both
M_W 465	464.2585	$C_{29}H_{36}O_5$	18.42	/
M_W 471	470.2095	$C_{30}H_{30}O_8$	18.47	/
M_W 479	478.2355	$C_{29}H_{34}O_6$	15.67	/
M_W 494	493.2294	$C_{22}H_{37}O_{12}$	18.53	/
M_W 514	513.1954	$C_{24}H_{33}O_{12}$	17.72	/
M_W 572	571.3123	$C_{29}H_{47}O_{11}$	17.9	/

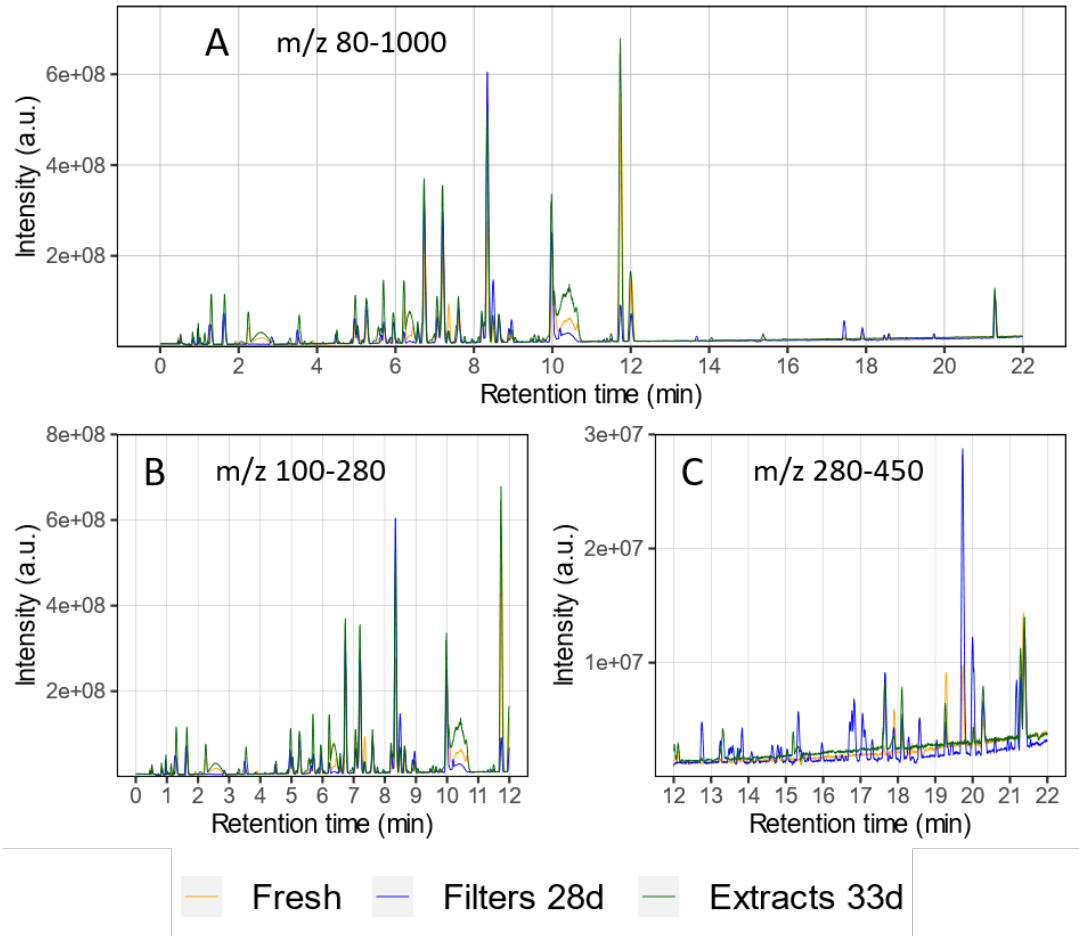

Figure C.2: (A) BPC representing fresh and aged filter and extract samples with *m/z* 80-1000. (B) BPC of the monomer region with *m/z* 100-280 between 0 and 12 min. The signal intensity is increased for almost all peaks in the 33-day old extracts compared to the fresh samples and stored filters. (C) BPC of the dimer region with *m/z* 280-450 between 12 and 22 min. The 28-day old filter samples show a significant increase in both intensity and number of peaks compared to the fresh samples and aged extracts. A higher background (assigned to an unknown compound detected at *m/z* 305.0230, which is a constant background signal in our system) between peaks is observed for the stored extract samples. This increase in the base peak background leads to an increase of TIC signal in the stored extracts in Figure 2 (C), hence the signal intensity minus the background signal would be lower than the fresh samples.

Highest Intensity Dimers in the 28-day Old Filters

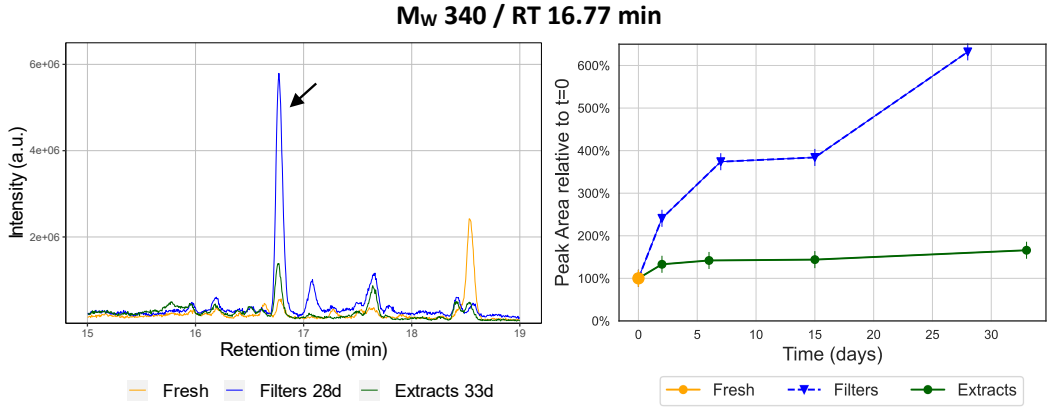

Figure C.3: EIC of the *m/z* 339.1808 dimer ester with highest intensity in the 28-day old filter samples. The corresponding time series for this isomer is given on the right.

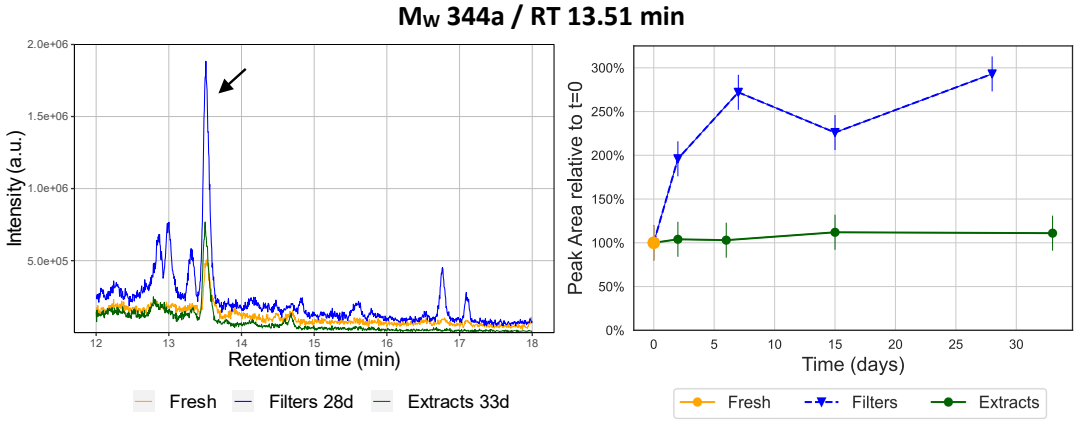

Figure C.4: EIC of the *m/z* 343.1393 dimer ester with highest intensity in the 28-day old filter samples. The corresponding time series for this isomer is given on the right.

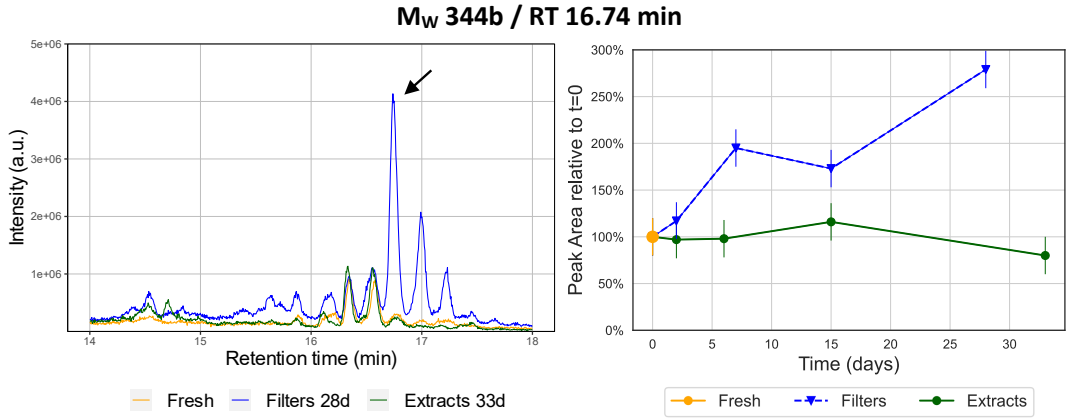

Figure C.5: EIC of the *m/z* 343.1757 dimer ester with highest intensity in the 28-day old filter samples. The corresponding time series for this isomer is given on the right.

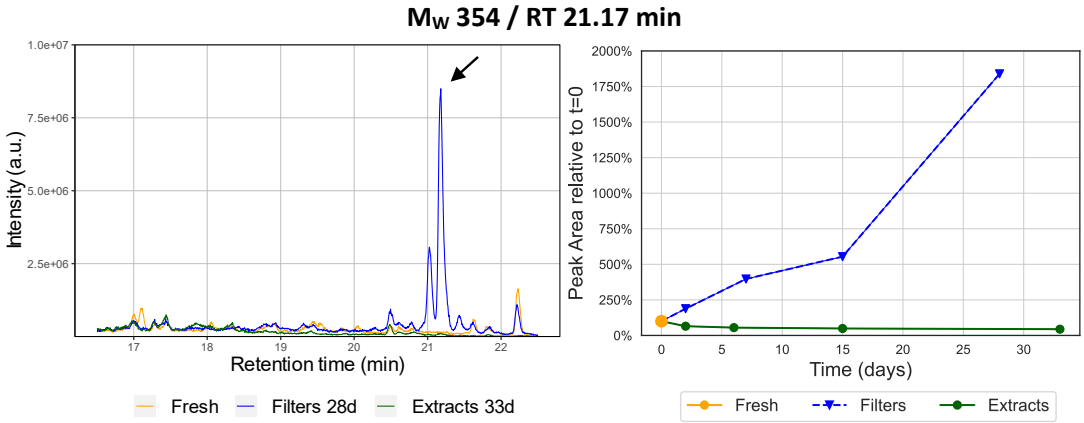

Figure C.6: EIC of the *m/z* 353.1964 dimer ester with highest intensity in the 28-day old filter samples. The corresponding time series for this isomer is given on the right.

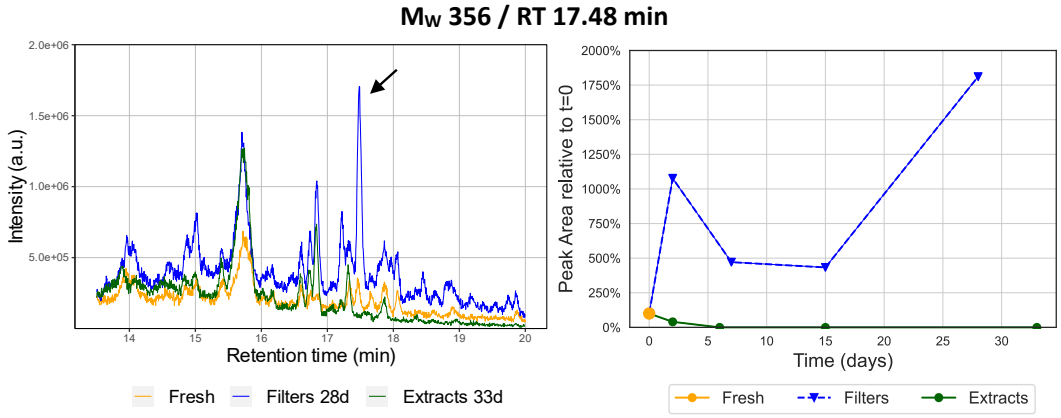

Figure C.7: EIC of the *m/z* 355.1757 dimer ester with highest intensity in the 28-day old filter samples. The corresponding time series for this isomer is given on the right.

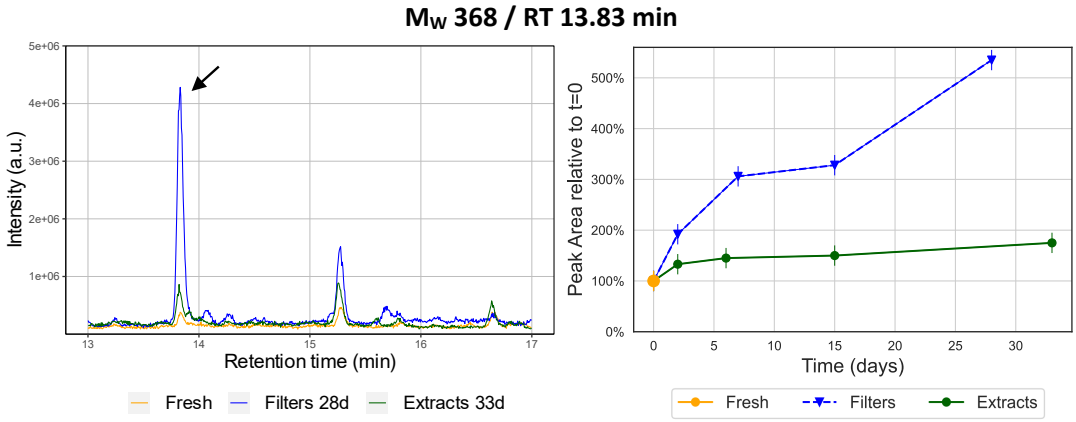

Figure C.8: EIC of the *m/z* 367.1757 dimer ester with highest intensity in the 28-day old filter samples. The corresponding time series for this isomer is given on the right.

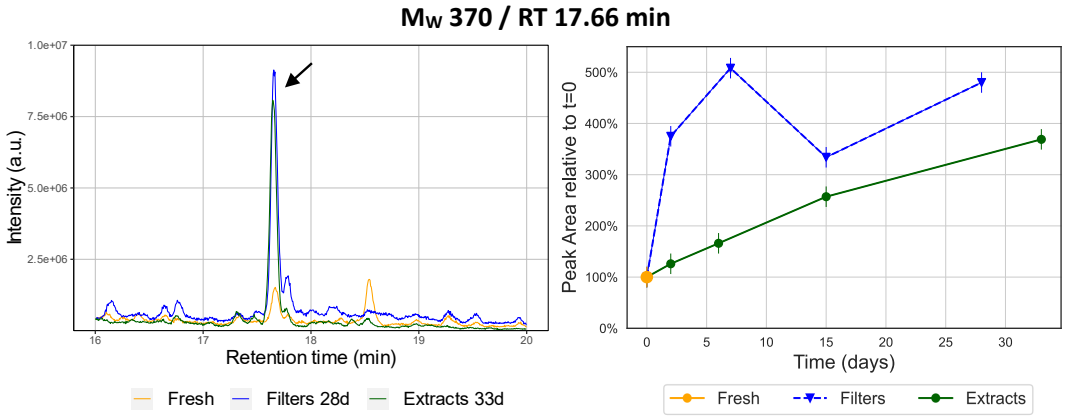

Figure C.9: EIC of the *m/z* 369.1913 dimer ester with highest intensity in the 28-day old filter samples. The corresponding time series for this isomer is given on the right.

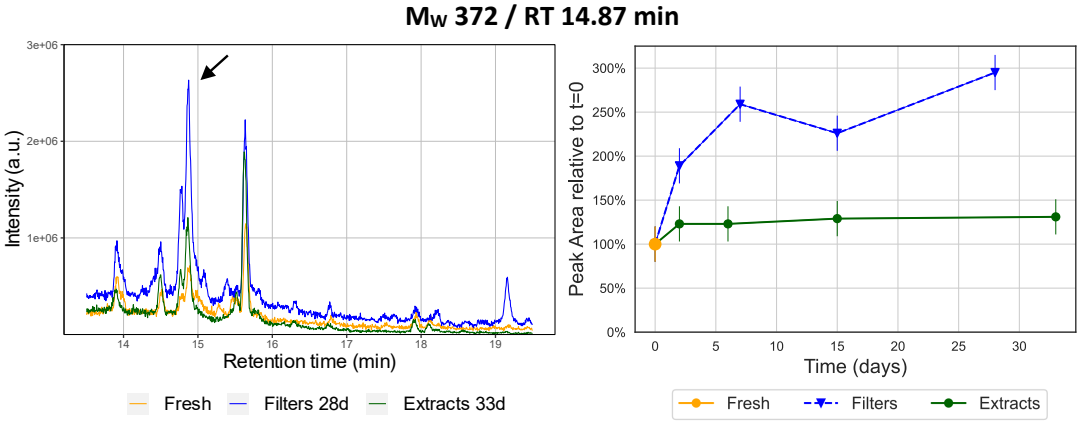

Figure C.10: EIC of the *m/z* 371.1706 dimer ester with highest intensity in the 28-day old filter samples. The corresponding time series for this isomer is given on the right.

Highest Intensity Dimers in Fresh Samples

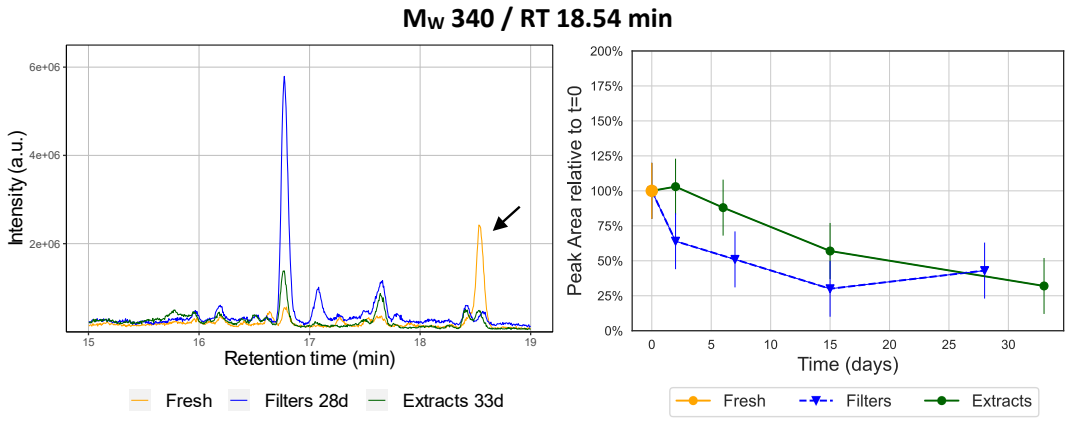

Figure C.11: EIC of the *m/z* 339.1808 dimer ester with highest intensity in the fresh samples. The corresponding time series for this isomer is given on the right.

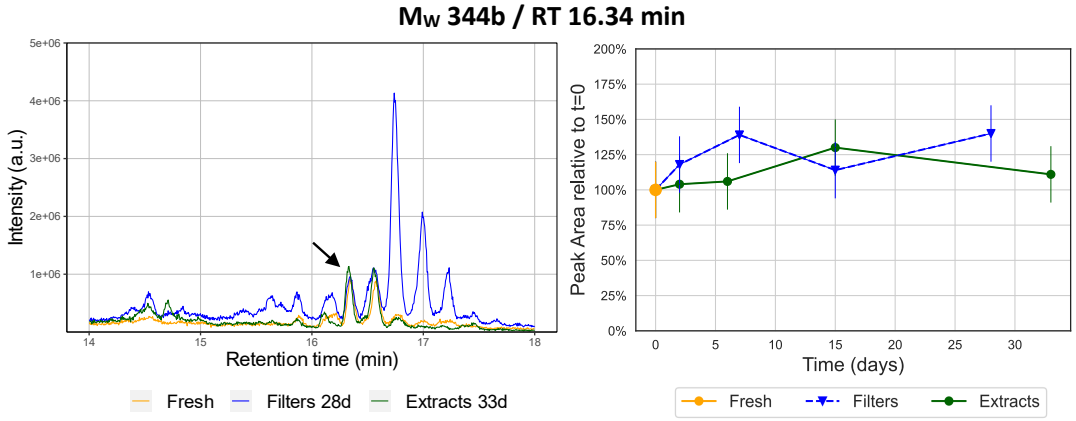

Figure C.12: EIC of the *m/z* 343.1757 dimer ester with highest intensity in the fresh samples. The corresponding time series for this isomer is given on the right.

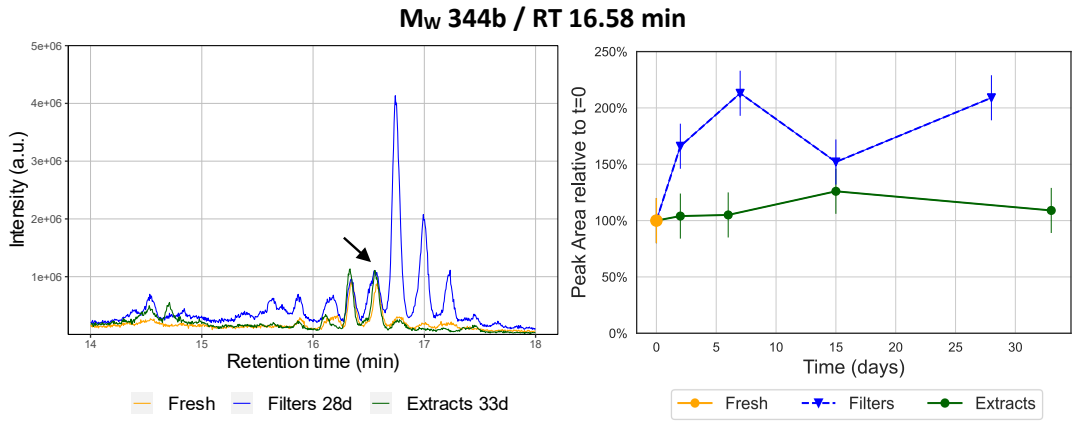

Figure C.13: EIC of the *m/z* 343.1757 dimer ester with highest intensity in the fresh samples. The corresponding time series for this isomer is given on the right.

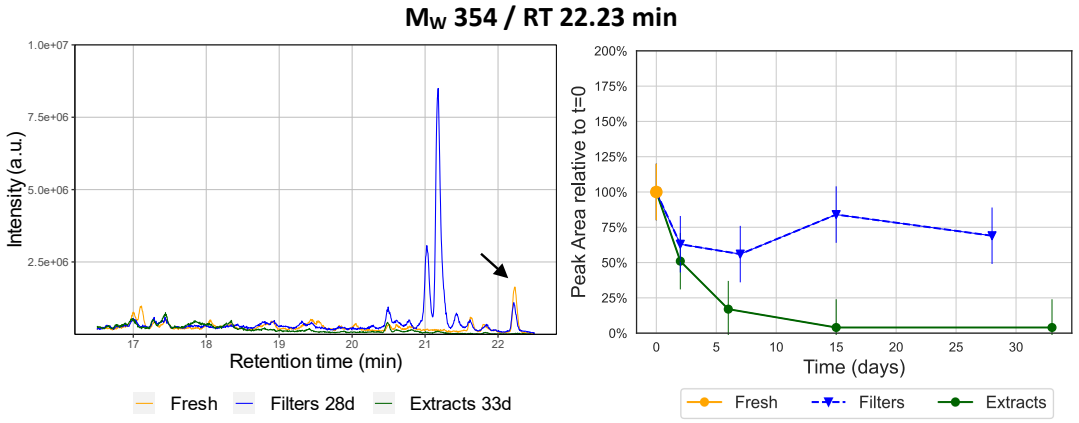

Figure C.14: EIC of the *m/z* 353.1964 dimer ester with highest intensity in the fresh samples. The corresponding time series for this isomer is given on the right.

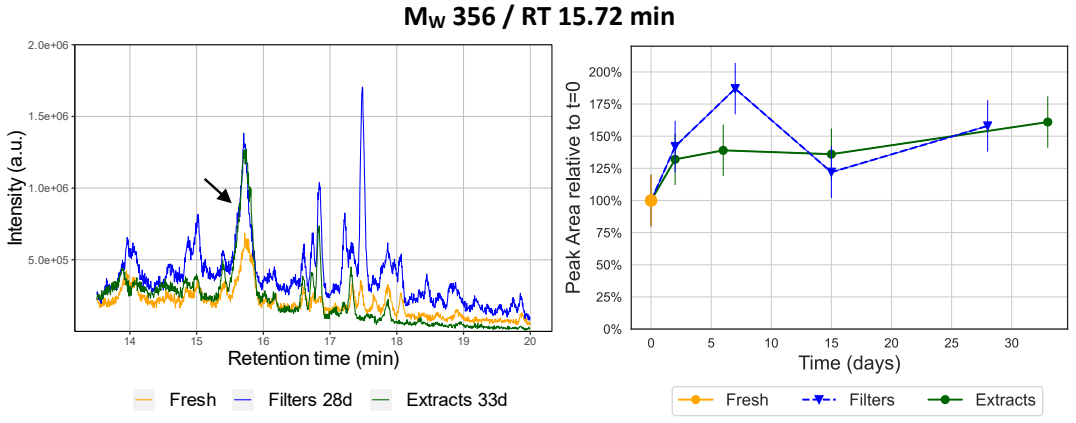

Figure C.15: EIC of the *m/z* 355.1757 dimer ester with highest intensity in the fresh samples. The corresponding time series for this isomer is given on the right.

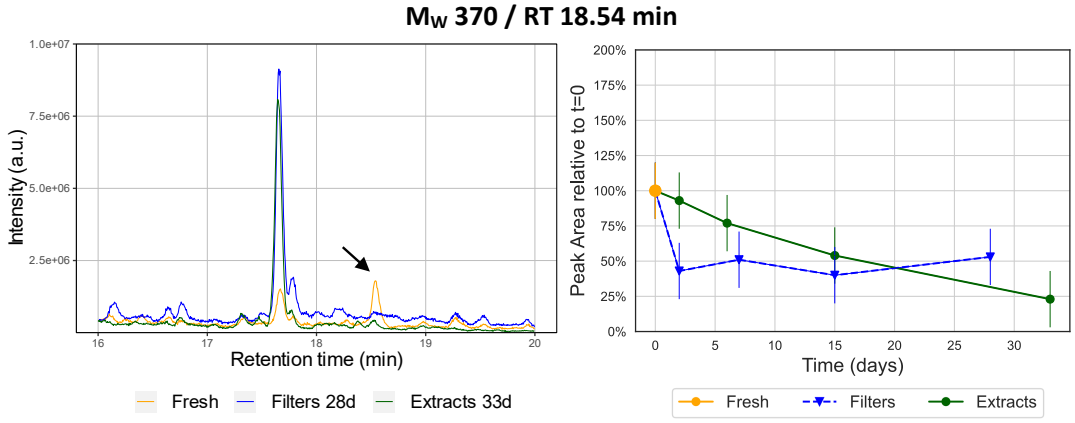

Figure C.16: EIC of the *m/z* 369.1913 dimer ester with highest intensity in the fresh samples. The corresponding time series for this isomer is given on the right.

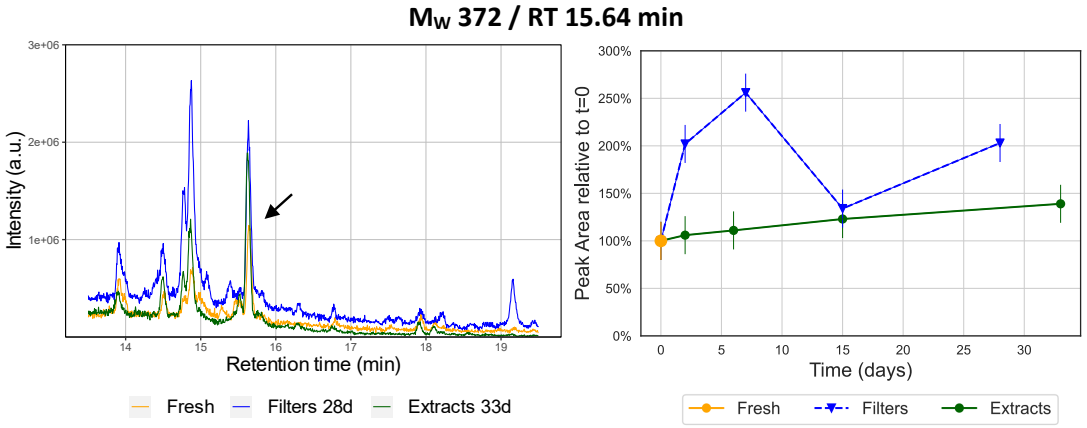

Figure C.17: EIC of the *m/z* 371.1706 dimer ester with highest intensity in the fresh samples. The corresponding time series for this isomer is given on the right.

Highest Intensity Dimers in Both Fresh Samples and 28-Day Old Filter Samples

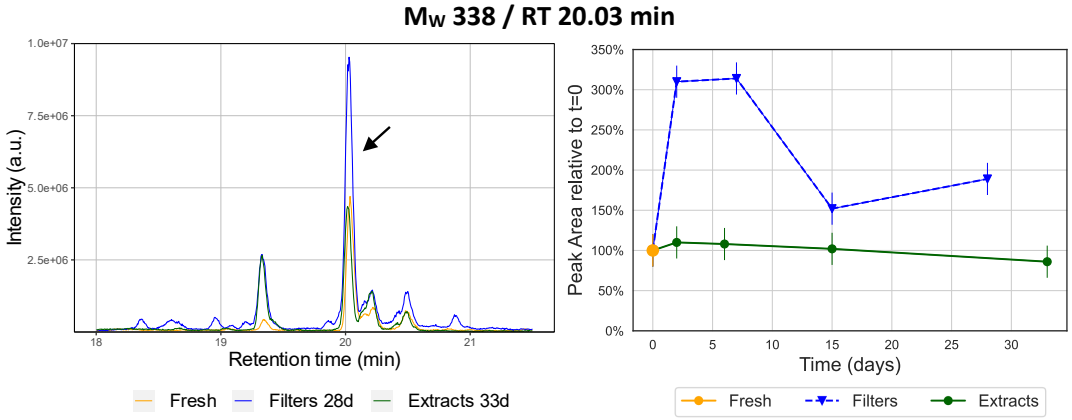

Figure C.18: EIC of the *m/z* 337.2015 dimer ester with highest intensity in both the fresh and 28-day old filter samples. The corresponding time series for this isomer is given on the right.

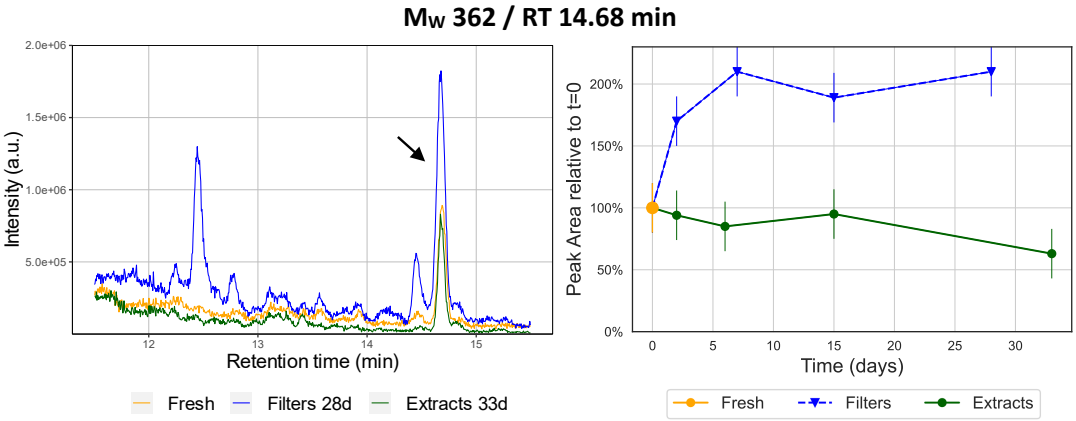

Figure C.19: EIC of the *m/z* 361.1499 dimer ester with highest intensity in both the fresh and 28-day old filter samples. The corresponding time series for this isomer is given on the right.

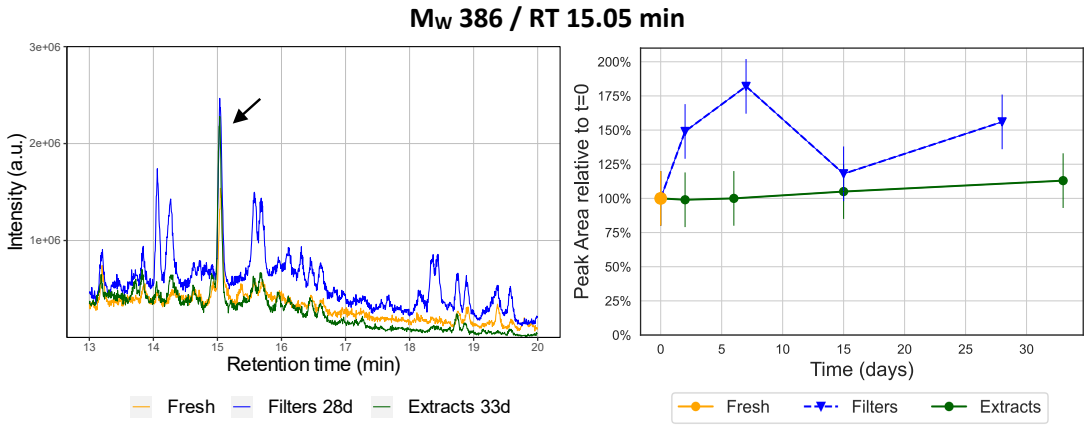

Figure C.20: EIC of the *m/z* 385.1862 dimer ester with highest intensity in both the fresh and 28-day old filter samples. The corresponding time series for this isomer is given on the right.

Trimer Compounds Investigated in this Study

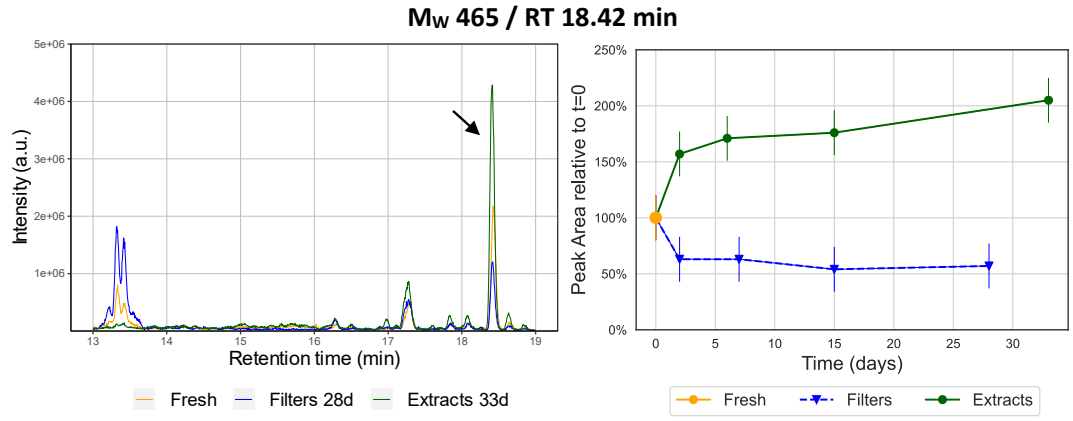

Figure C.21: EIC of the *m/z* 464.2585 compound tentatively assigned as a trimer. The corresponding time series for this isomer is given on the right.

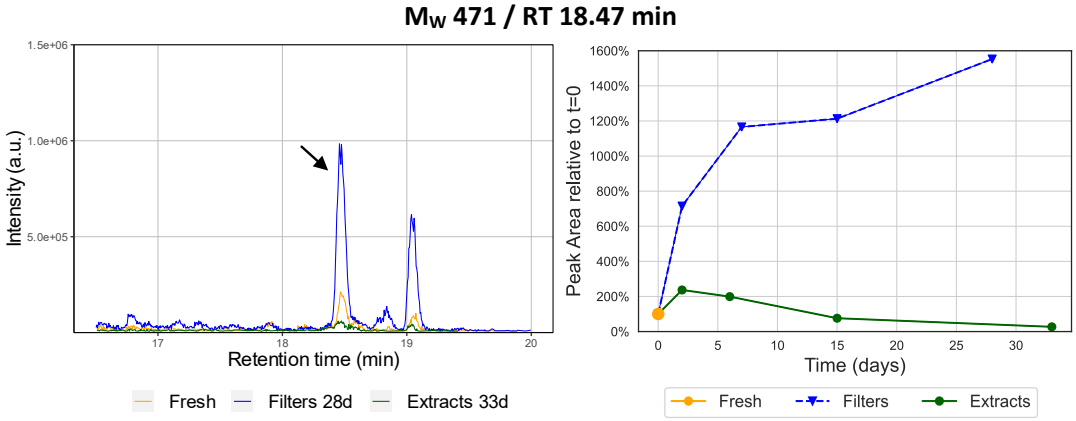

Figure C.22: EIC of the *m/z* 470.2095 compound tentatively assigned as a trimer. The corresponding time series for this isomer is given on the right.

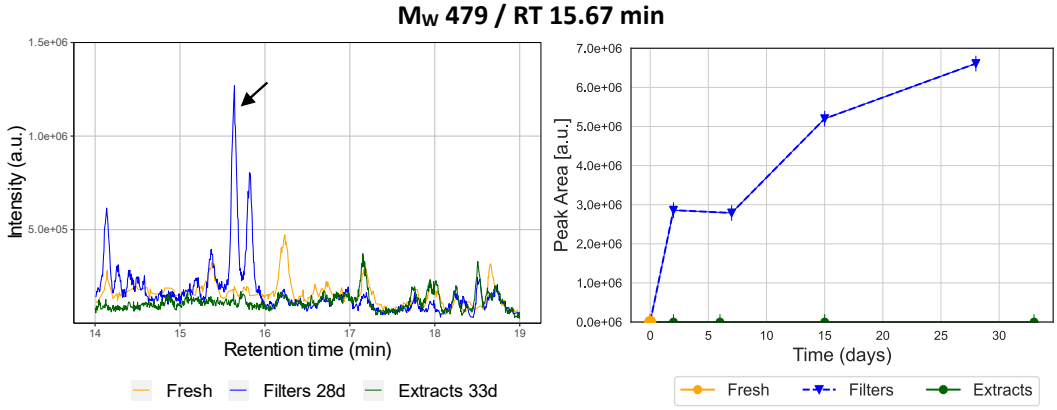

Figure C.23: EIC of the *m/z* 478.2331 compound tentatively assigned as a trimer. The corresponding time series for this isomer is given on the right.

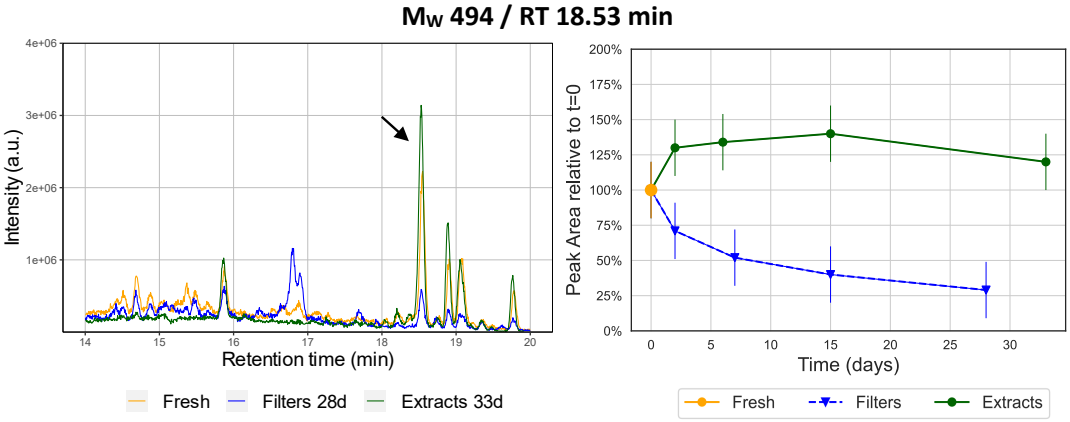

Figure C.24: EIC of the *m/z* 493.2294 compound tentatively assigned as a trimer. The corresponding time series for this isomer is given on the right.

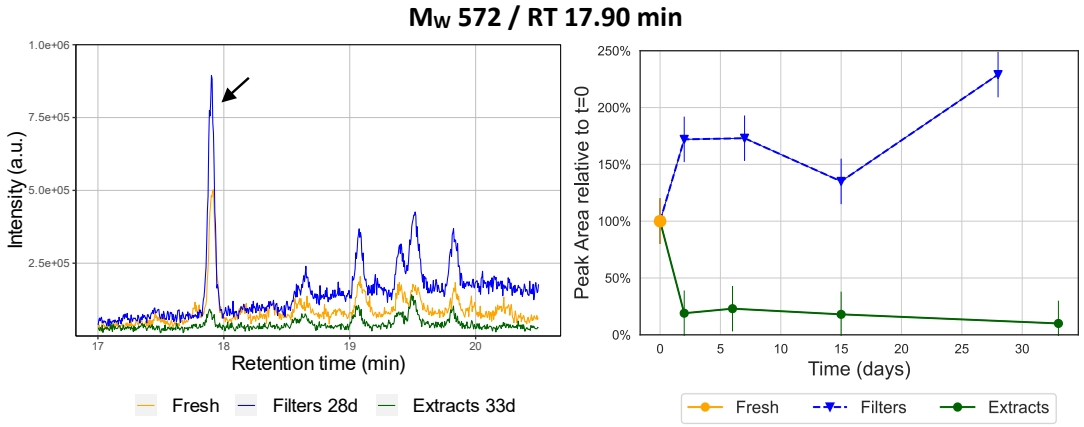

Figure C.25: EIC of the *m/z* 571.3123 compound tentatively assigned as a trimer. The corresponding time series for this isomer is given on the right.

"Spiking" Experiments

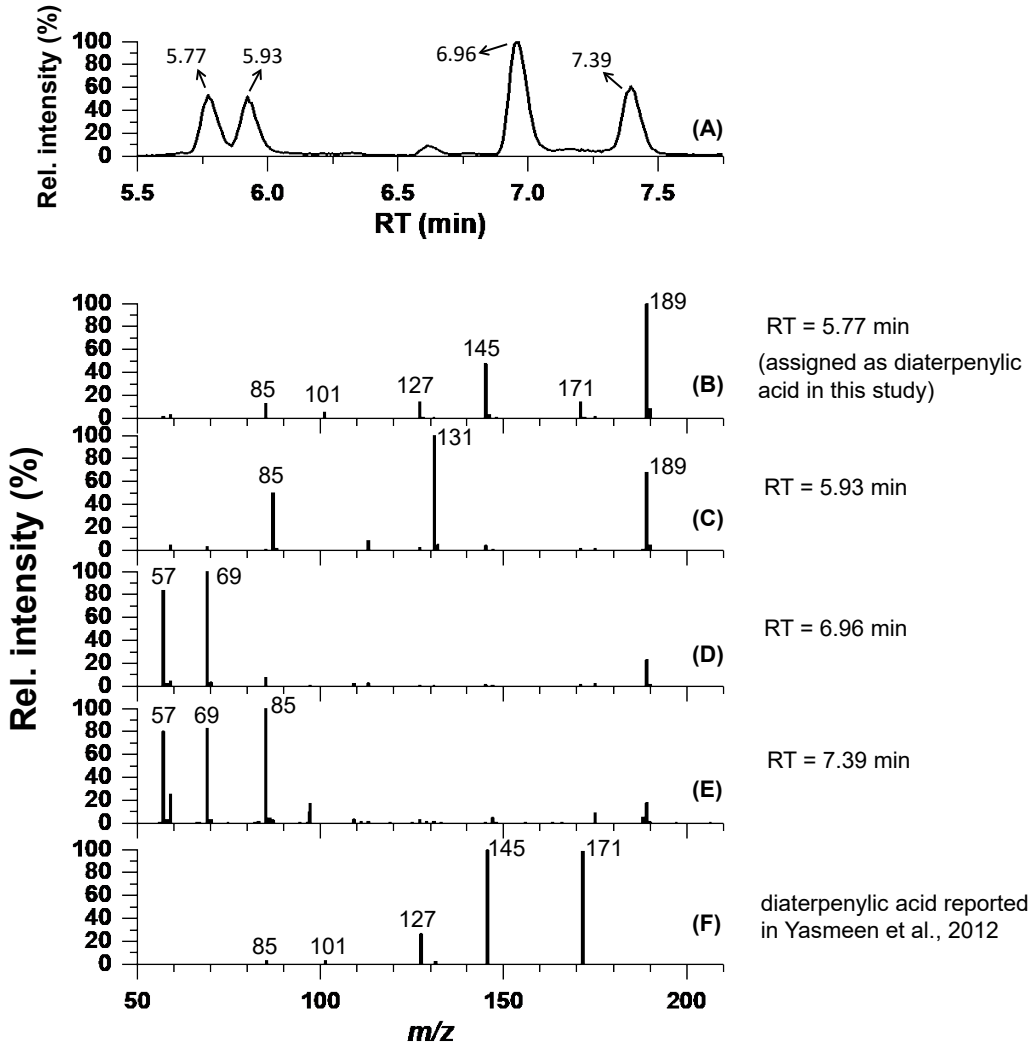

Figure C.26: EIC of *m/z* 189.0768 and the corresponding MS/MS results for each of the eluting isomer peaks at a set higher-energy collisional dissociation (HCD) of 10. The isomer eluting at 5.77 min shows the same fragmentation pattern as diaterpenylic acid in Yasmeen *et al.* [210]. (F) reconstructed from data in Yasmeen *et al.* [210].

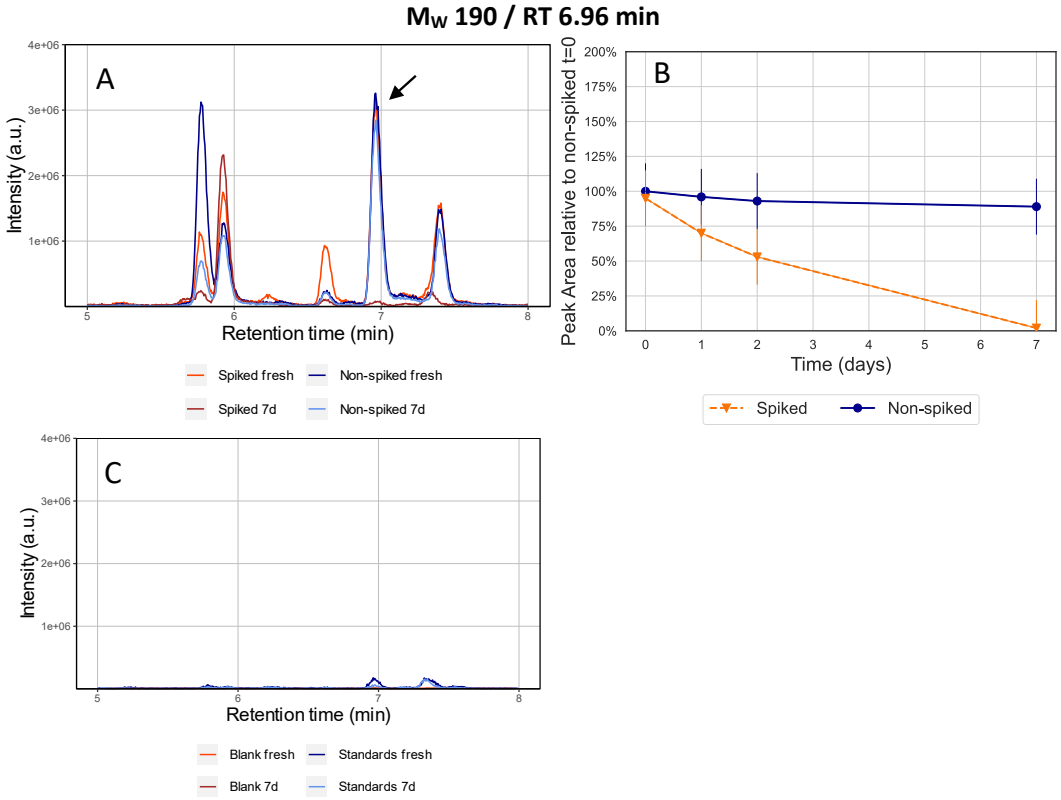

Figure C.27: (A) EIC of an isomer of diaterpenylic acid with *m/z* 189.0768 eluting at 6.96 min in the "non-spiked" and "spiked" fresh and 7-day old filter samples. (B) The time series of this isomer is given on the right. (C) EICs of fresh and stored blank and "standards only" samples of *m/z* 189.0776.

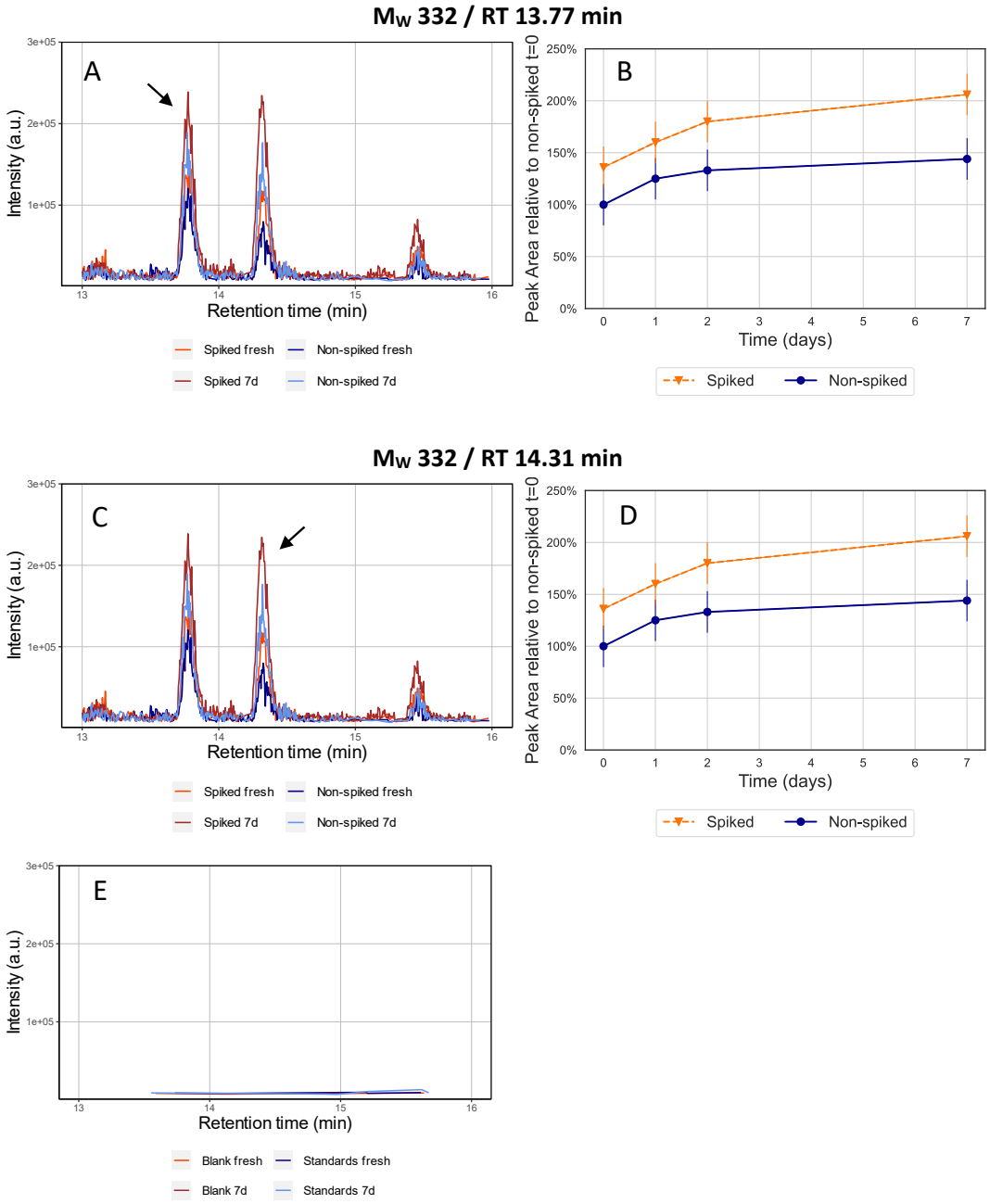

Figure C.28: (A,C) EICs of isomers of the *m/z* 331.1393 proposed to be an ester of diaterpenylic acid and pimelic acid eluting at 13.77 and 14.31 min in the "non-spiked" and "spiked" fresh and 7-day old filter samples. (B,D) The time series of these isomers are given on the right. (E) EICs of fresh and stored blanks and "standards only" samples of *m/z* 331.1393.

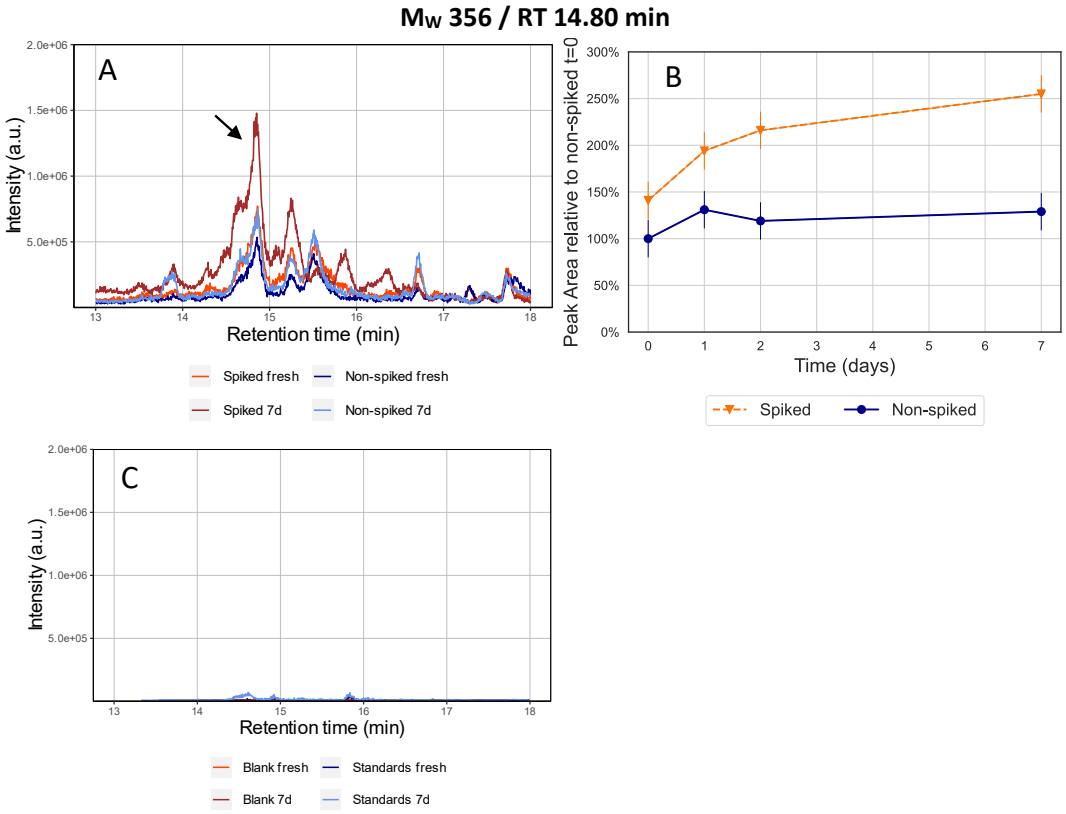

Figure C.29: (A) EIC of an isomer of the *m/z* 355.1757 proposed to be an ester of diaterpenylic acid and cis-pinonic acid eluting at 14.80 min in the "non-spiked" and "spiked" fresh and 7-day old filter samples. (B) The time series of this isomer is given on the right. (C) EIC of fresh and stored blank and "standards only" samples of *m/z* 355.1757.

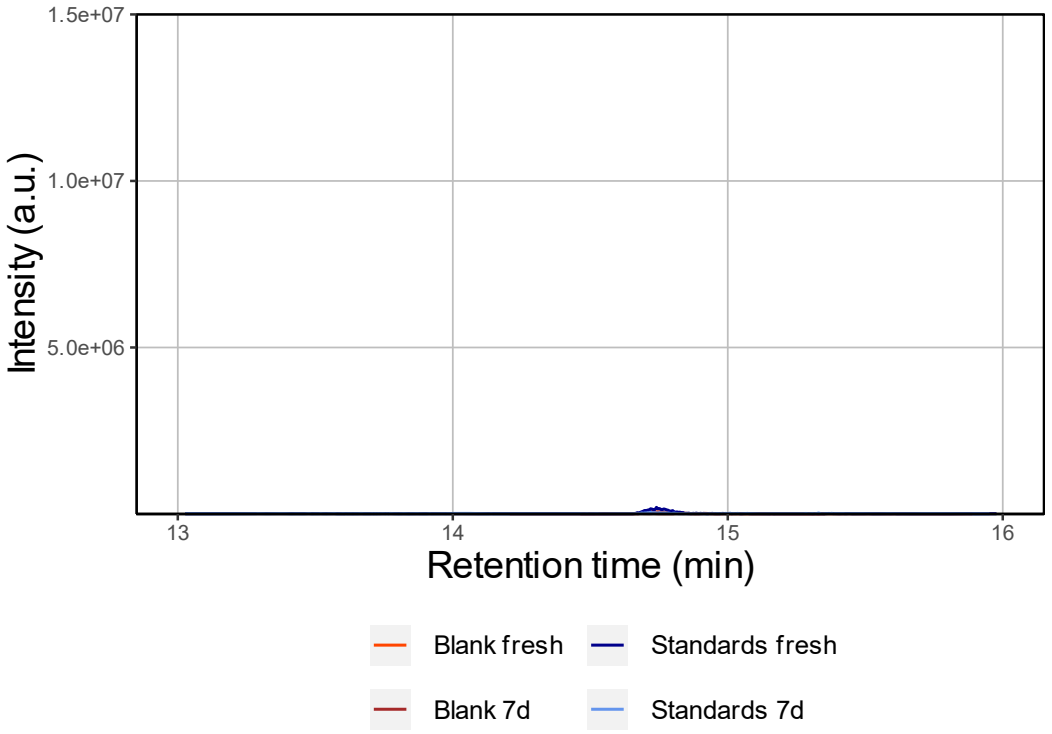

Figure C.30: EIC of fresh and aged blank and "standards only" samples of *m/z* 357.1550. The corresponding EICs are given in the main text Figure 4.5.

Appendix D

Quantification of Peroxides in Aerosols through Chemiluminescence using HPLC In-Column Derivatization with Luminol

SOA Generation

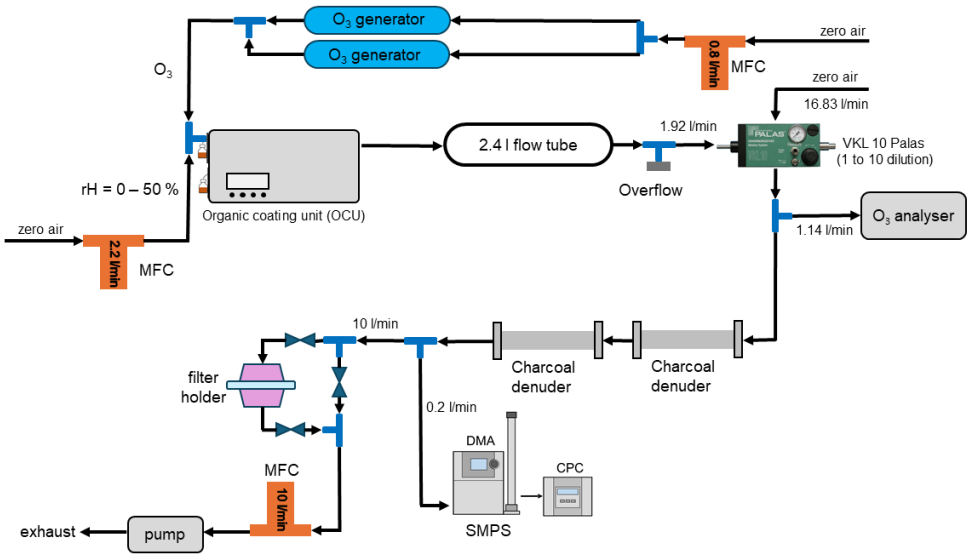

Figure D.1: Flowtube setup for the generation of SOA filter samples. In dark experiments, the OCU was only used to generate controlled and constant VOC vapor before mixing with O_3. For naphthalene and parts of the 3-carene SOA generation, the UV-lamps inside the OCU were turned on.

Table D.1: Collection parameters for the SOA samples generated using the OCU and the setup described in D.1, including collection duration, number of O_3 and OH lamps turned on, VOC flow, rH and collected mass per filter.

sample	collection duration (min)	# of O_3 lamps	# of OH lamps	VOC1 (mL/min)	VOC2 (mL/min)	RH (%)	mass/filter (µg)
AP-F27b	10	1	-	-	70	3	2113 ± 17
AP-F27c	10	1	-	-	70	3	1942 ± 9
AP-F28a	7	1	-	-	90	3	2002 ± 20
AP-F28b	7	1	-	-	90	3	1966 ± 82
AP-F28c	7	1	-	-	90	3	1979 ± 64
AP-F29a	10	1	-	-	70	50	1821 ± 63
AP-F29b	10	1	-	-	70	50	1782 ± 65
AP-F29c	10	1	-	-	70	50	1739 ± 44
AP-F30a	7	1	-	-	90	50	1822 ± 55
AP-F30b	7	1	-	-	90	50	1812 ± 60
AP-F30c	7	1	-	-	90	50	1843 ± 60
AP-F31	5	1	-	-	100	3	1457 ± 10
AP-F32	7	1	-	-	90	3	2106 ± 111
AP-F33	5	1	-	-	100	50	1324 ± 36
3C-F1a	20	1	-	-	70	3	1620 ± 27
3C-F1b	20	1	-	-	70	3	1474 ± 54
3C-F1c	20	1	-	-	70	3	1429 ± 9
3C-F2a	12	1	-	-	90	3	1705 ± 43
3C-F2b	12	1	-	-	90	3	1710 ± 39
3C-F2c	12	1	-	-	90	3	1697 ± 25
3C-F3a	20	1	-	-	70	50	1287 ± 58
3C-F3b	20	1	-	-	70	50	1215 ± 21
3C-F3c	20	1	-	-	70	50	1205 ± 29
3C-F4a	12	1	-	-	90	50	1391 ± 35
3C-F4b	12	1	-	-	90	50	1399 ± 43
3C-F4c	12	1	-	-	90	50	1369 ± 36
3C-F5a	20	2	4.5	-	100	50	1153 ± 59
3C-F5b	20	2	4.5	-	100	50	1097 ± 17
3C-F5c	20	2	4.5	-	100	50	1076 ± 34
NA-F1a	30	2	4.5	100	100	50	360 ± 21
NA-F1b	30	2	4.5	100	100	50	309 ± 12
NA-F1c	30	2	4.5	100	100	50	285 ± 5
NA-3C-F1	20	2	4.5	100	100	50	857 ± 25
NA-3C-F2	20	2	4.5	100	100	50	835 ± 9
NA-3C-F3	20	2	4.5	100	100	50	805 ± 17

HPLC-CL Standards

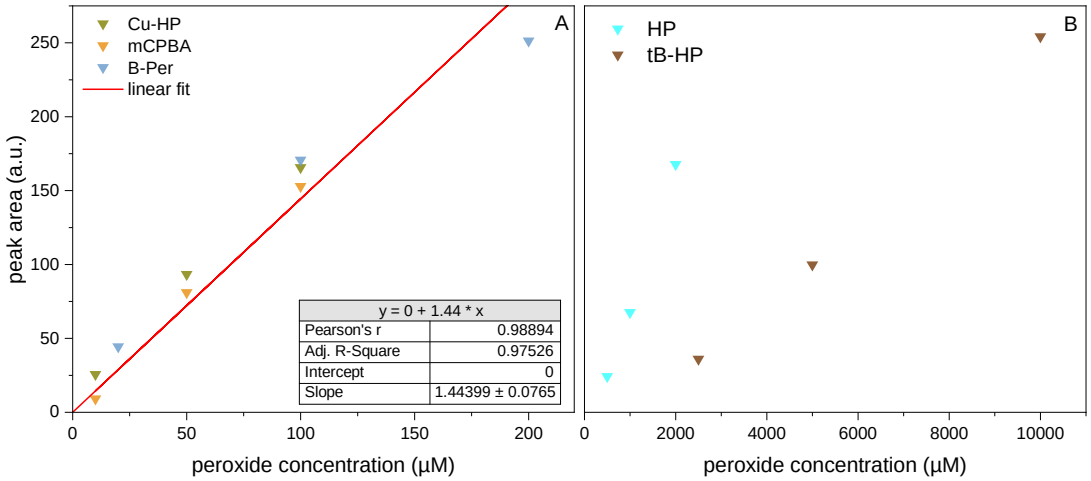

Figure D.2: Peak area of the HPLC-CL chromatograms for the different standards used at different concentrations near the LLOD. (A) shows the linear response for Cu-HP, mCPBA, and B-Per, which have a LLOD around 10 µM. (B) shows the linear response for HP and tB-HP, where the LLOD is much higher in comparison to the other standards. This can also be seen in Figure 5.2 above, where these standards are also detected with much lower sensitivity. The x-axis displays the theoretical peroxide concentration as calculated from diluting down the available standards.

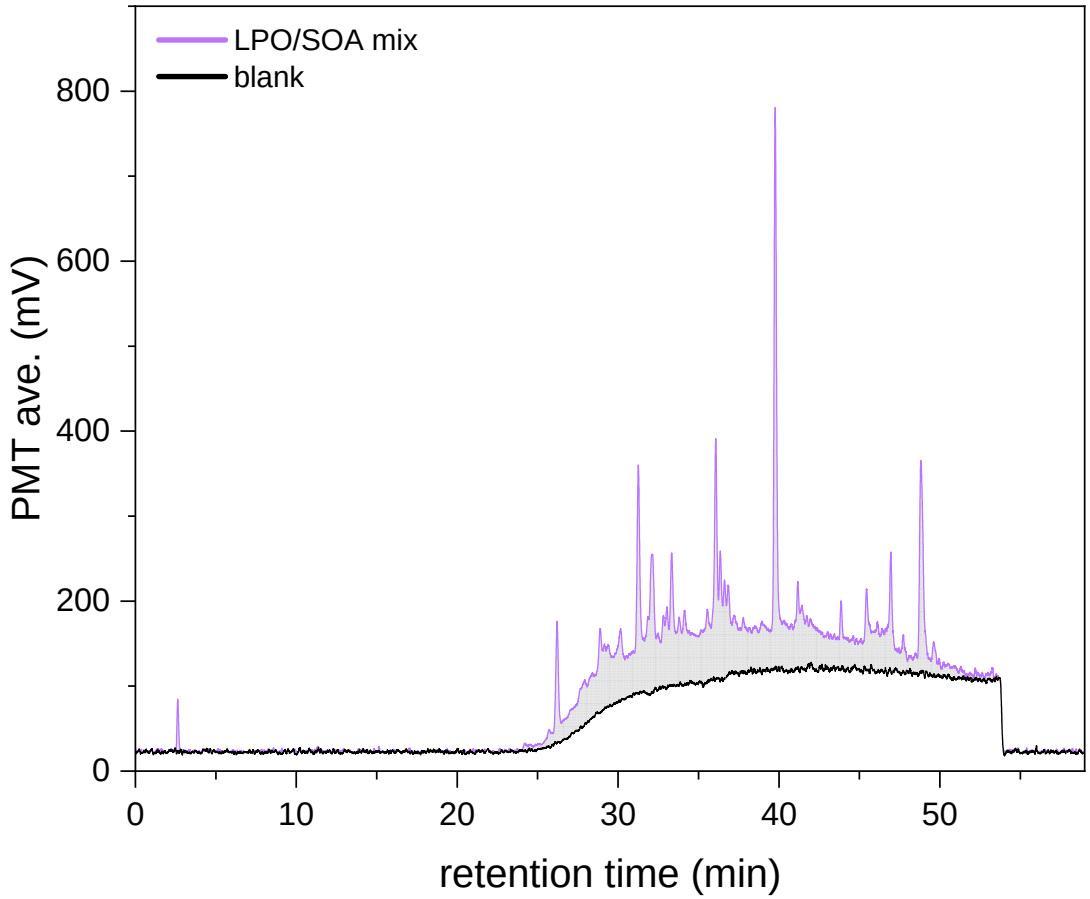

Figure D.3: HPLC-CL chromatogram of the LPO/SOA mix. Peak areas are calculated as the area under the curve and are always blank subtracted. The peak area is given as the grey shaded area and is used for the quantification of peroxides.

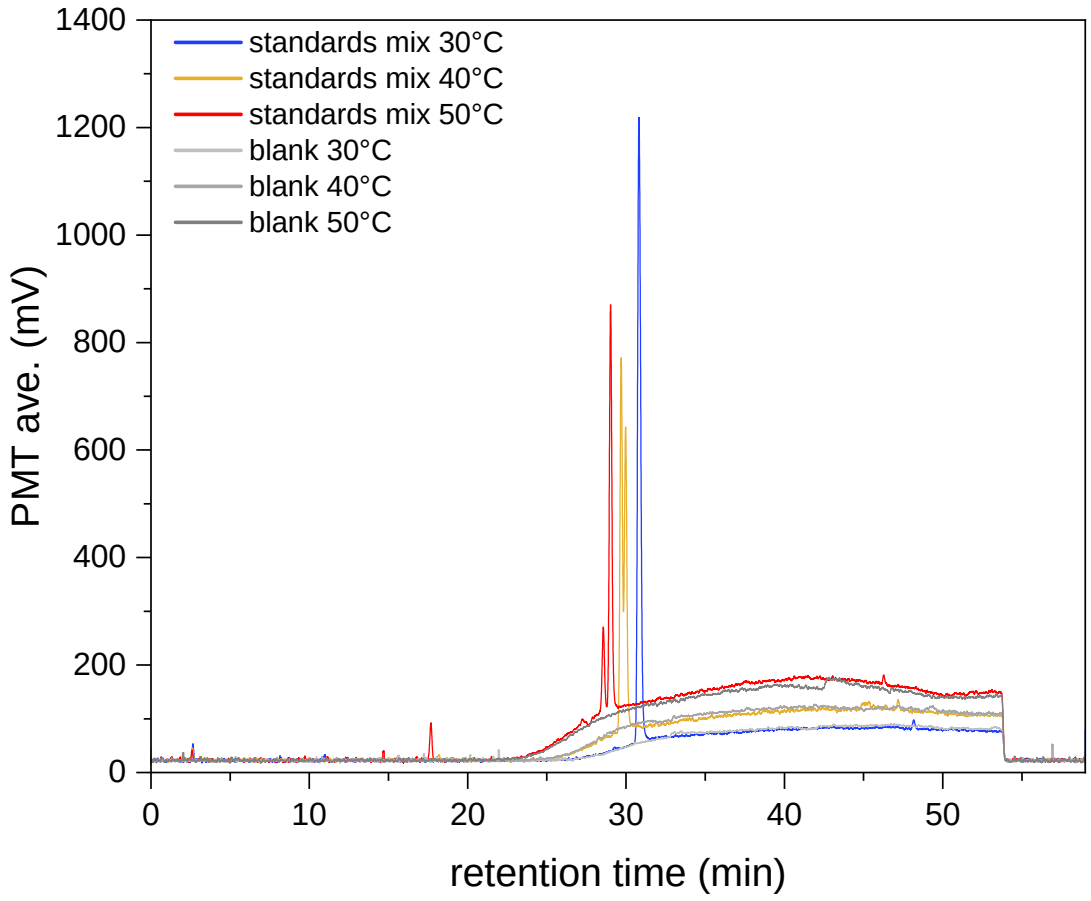

Figure D.4: HPLC-CL chromatogram of the standards mix for different column temperatures. Blanks are given in different shades of grey.

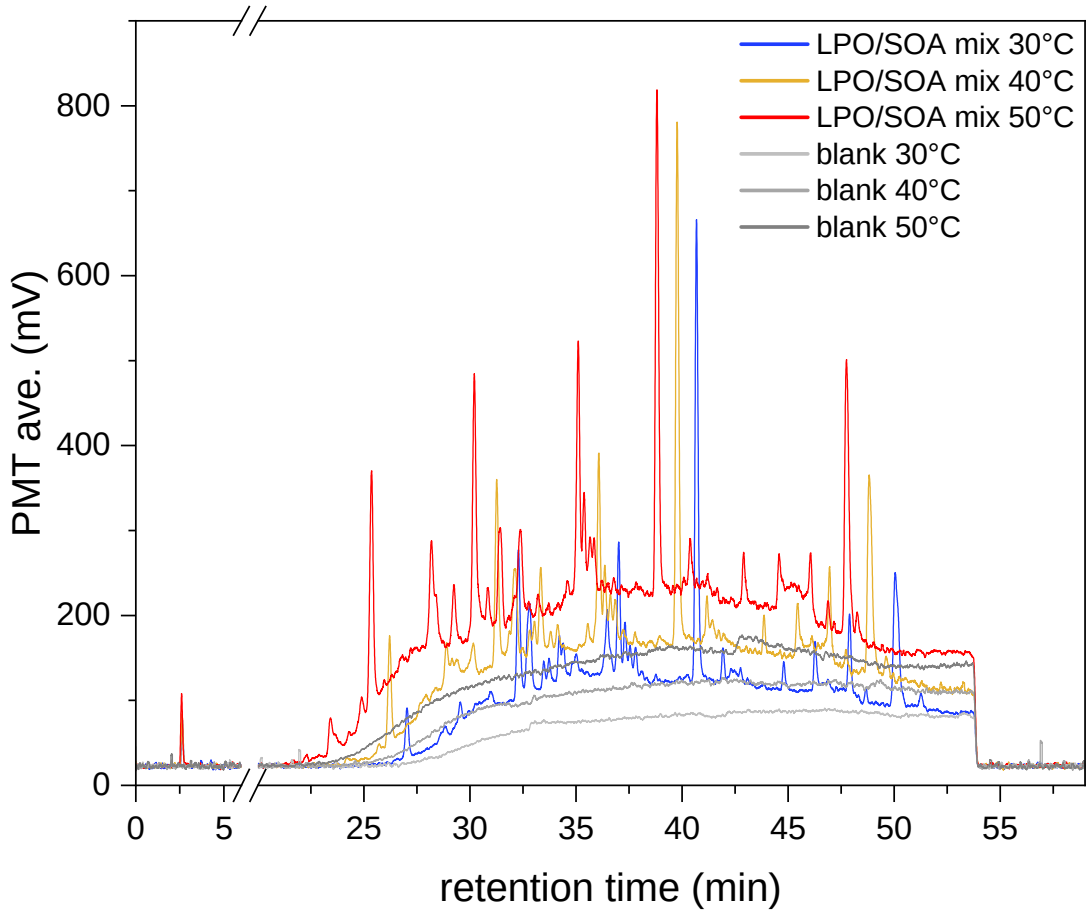

Figure D.5: HPLC-CL chromatogram of the LPO/SOA mix sample for different column temperatures. Blanks are given in different shades of grey. No peaks are detected between rt = 5 and 20 min.

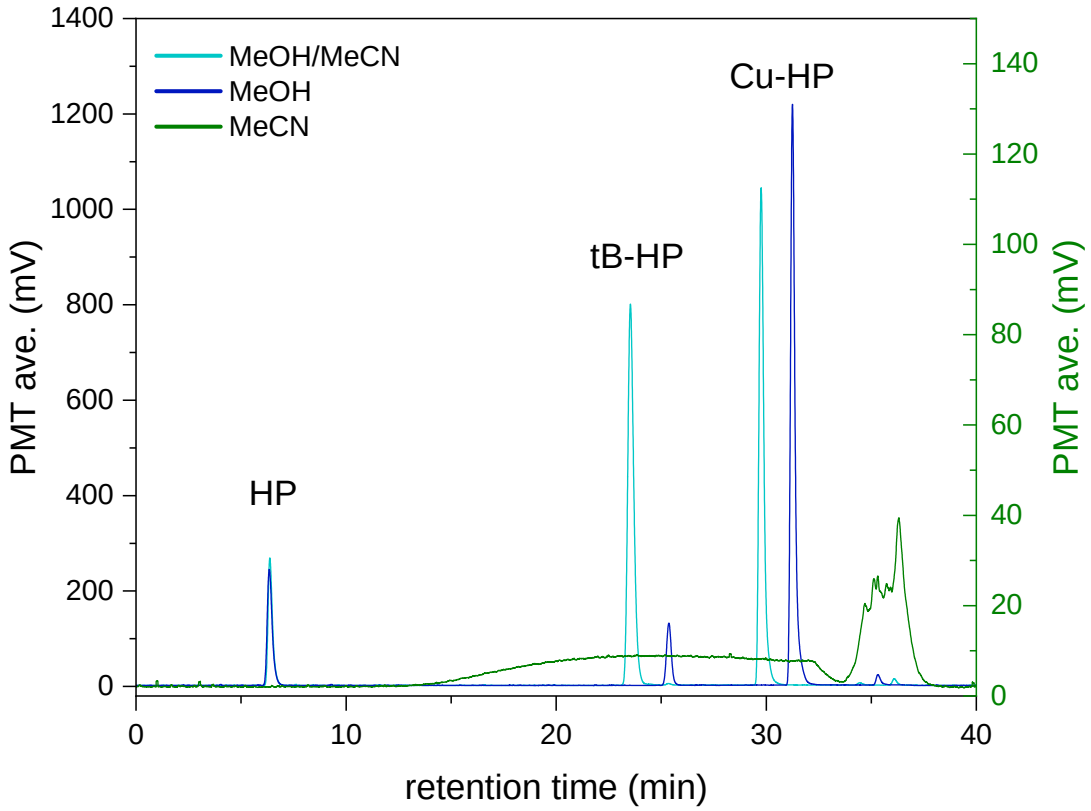

Figure D.6: HPLC-CL chromatogram of a HP, tB-HP, and Cu-HP standards mix for different mobile phases.

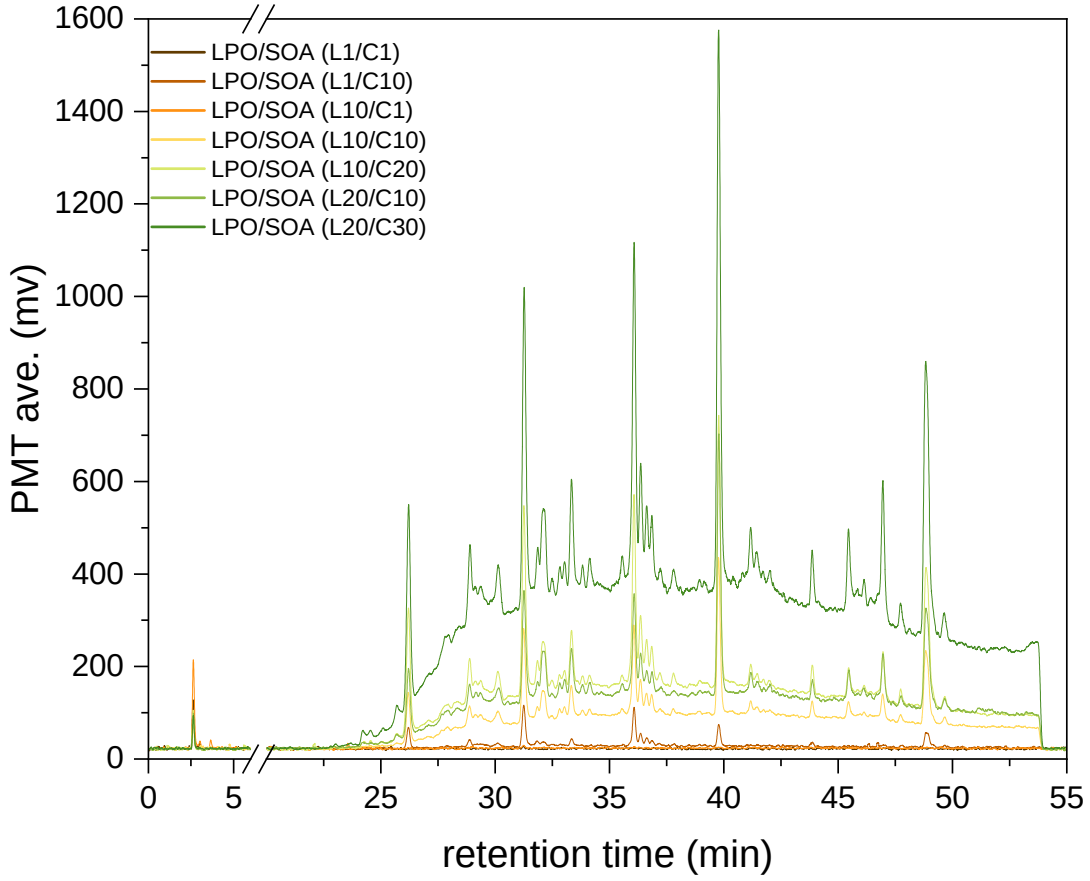

Figure D.7: HPLC-CL chromatogram of the LPO/SOA mix sample for different mobile phases. No peaks are detected between rt = 5 and 20 min.

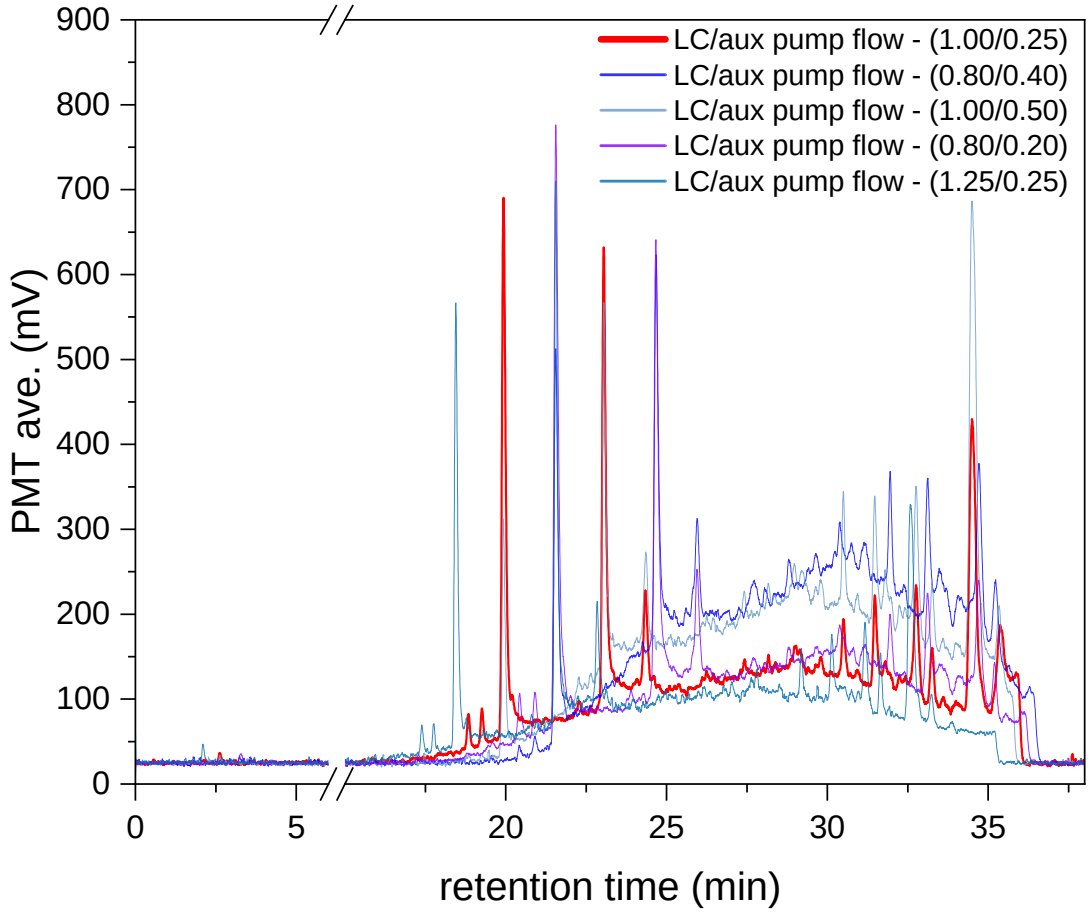

Figure D.8: HPLC-CL chromatogram for the LPO/SOA mix sample for different LC and auxiliary pump flows. At this stage of method development, a shorter 40 min method was used. No peaks are detected between rt = 5 and 15 min.

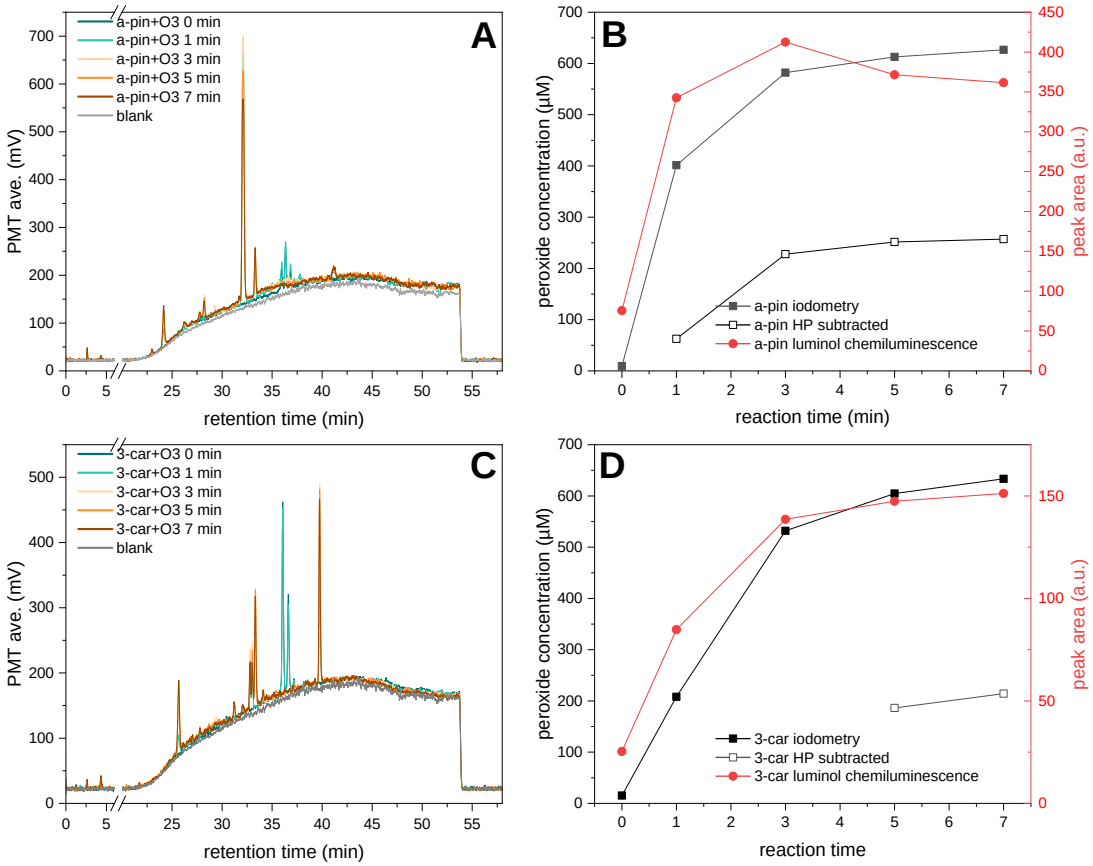

Figure D.9: Liquid-phase ozonolysis experiments of both α-pinene and 3-carene with O_3. (A,C) show the different chromatograms for different durations of bubbling with O_3, for α-pinene and 3-carene, respectively. (B,D) show the peroxide concentration obtained through offline iodometry (black) and through luminol chemiluminescence (red). The HP subtracted peroxide concentration is given in black with empty squares. HP subtraction was only performed on samples where HP could be quantified.

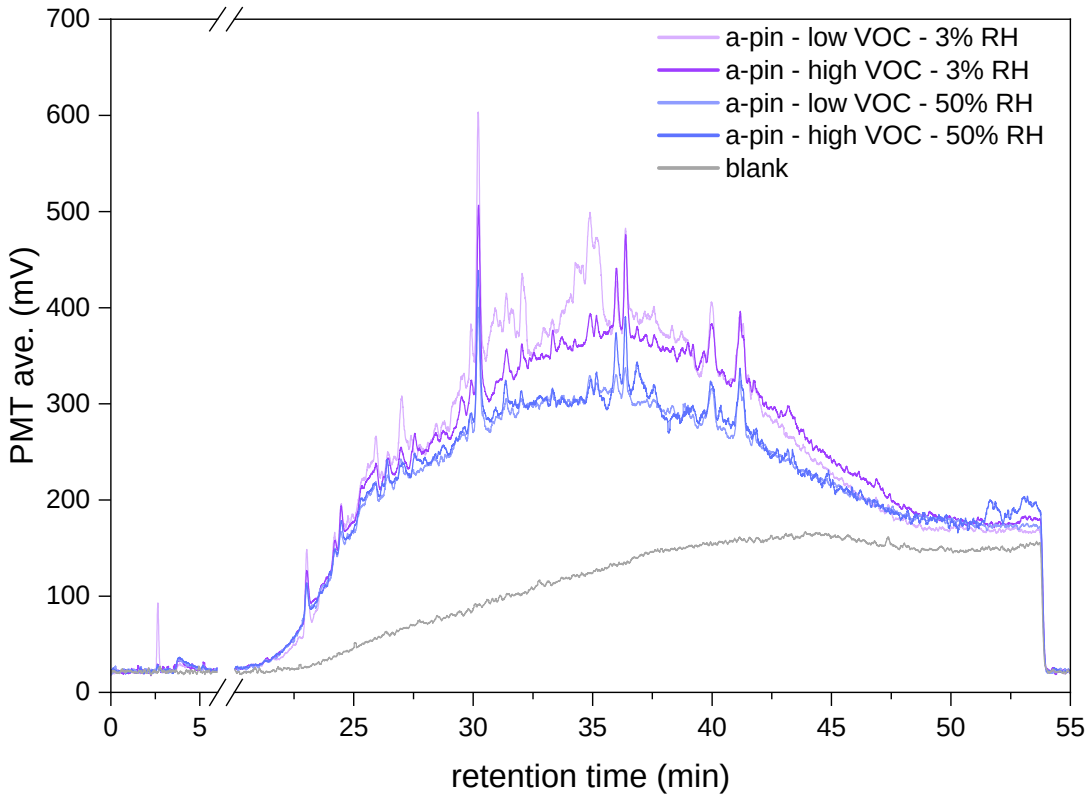

Figure D.10: HPLC-CL chromatogram for the α-pinene SOA samples generated at different conditions as seen in Table D.1. No peaks are detected between rt = 5 and 20 min.

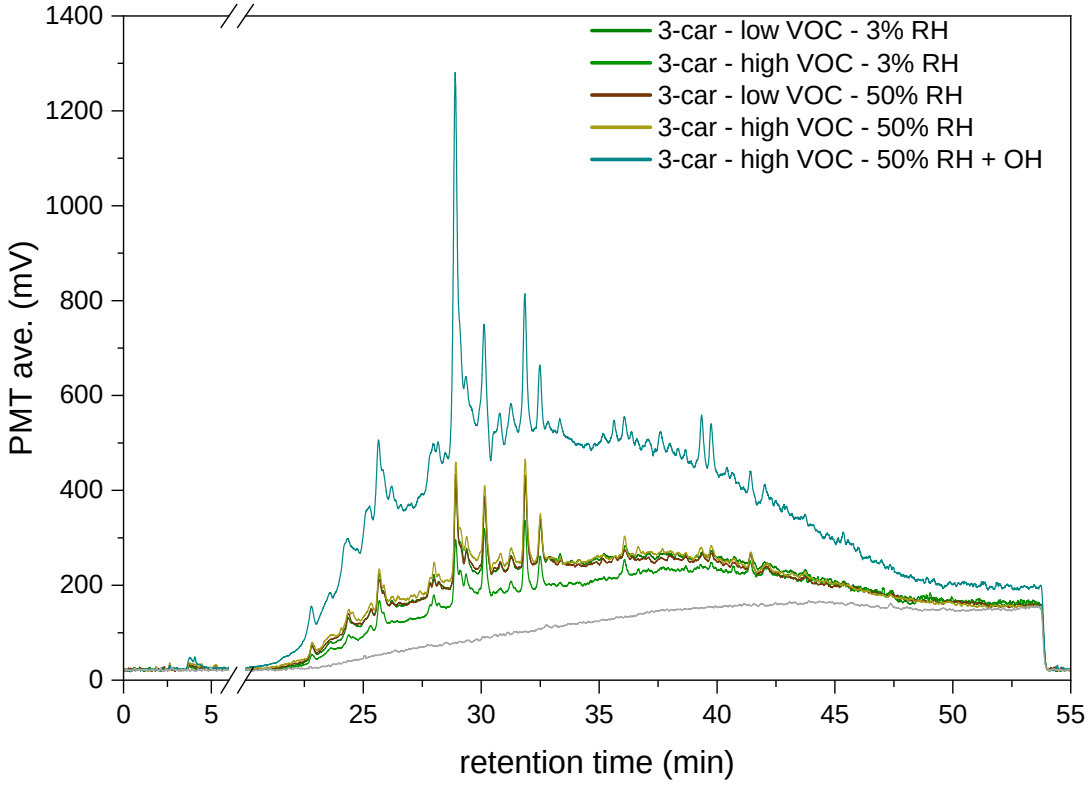

Figure D.11: HPLC-CL chromatogram for the 3-carene SOA samples generated at different conditions as seen in Table D.1. No peaks are detected between rt = 5 and 20 min.

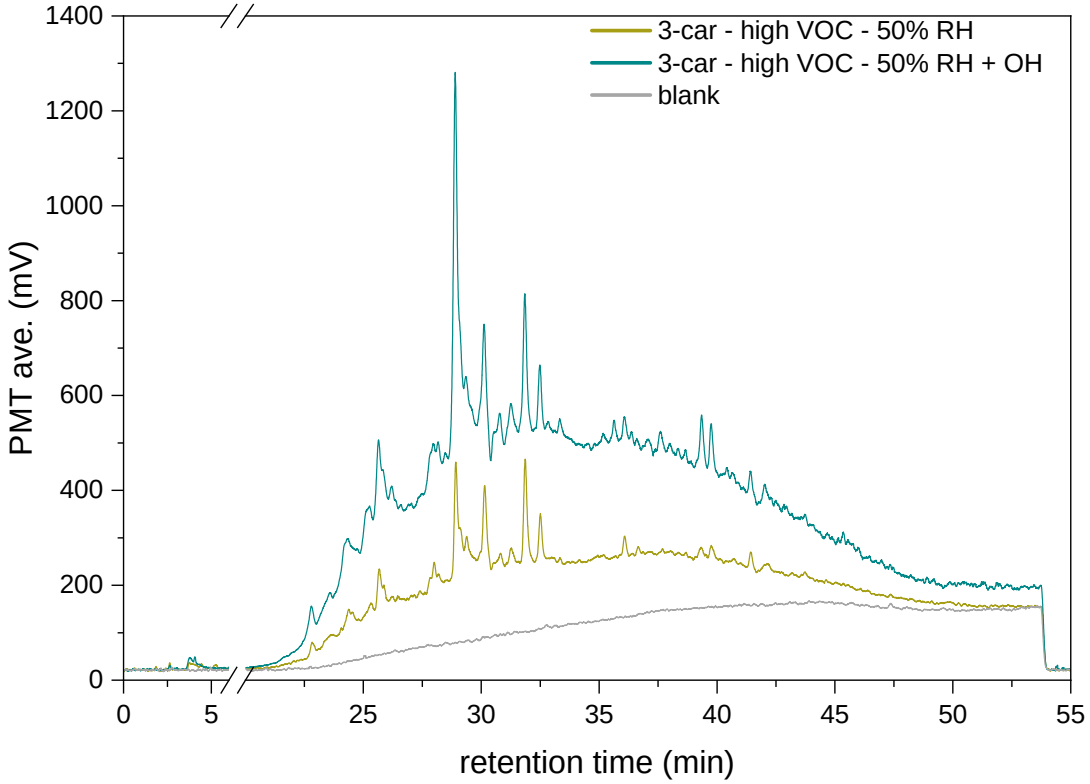

Figure D.12: HPLC-CL chromatogram for the 3-carene SOA samples generated with and without the OH generating UV-lamps inside the OCU. No peaks are detected between rt = 5 and 20 min.

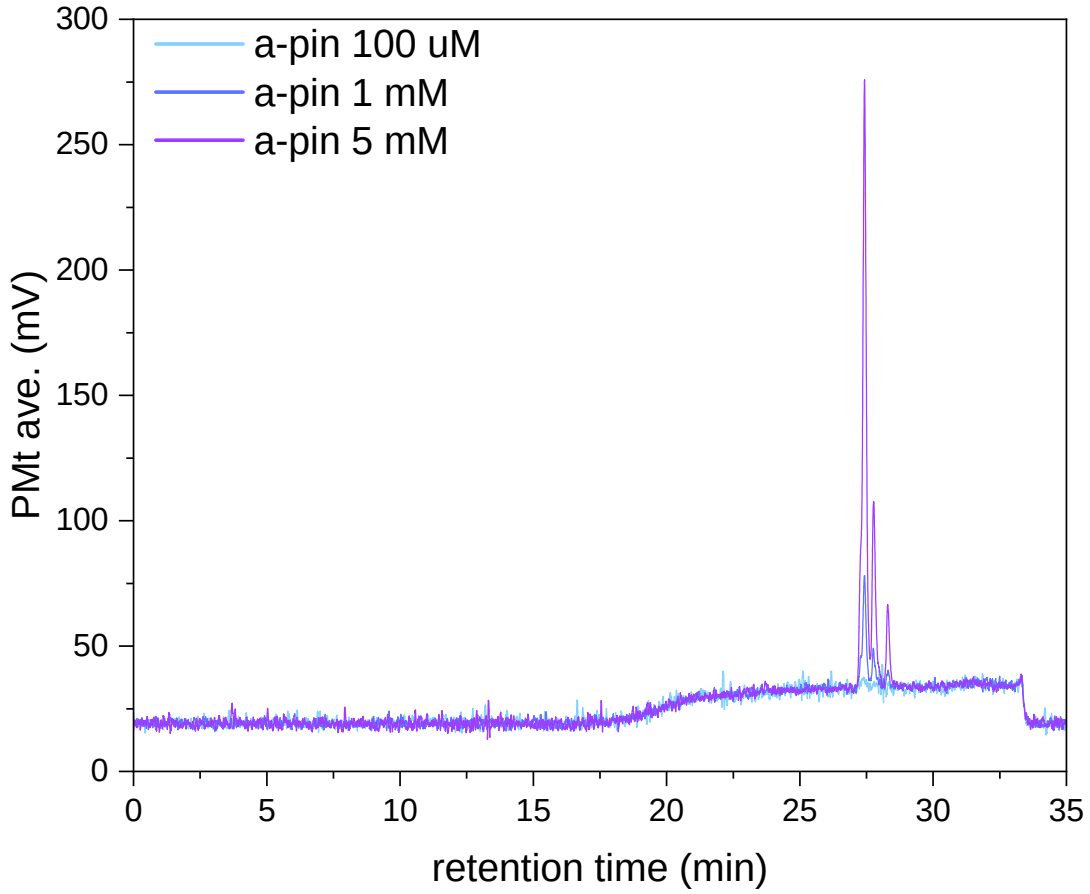

Figure D.13: Different concentrations of α-pinene Standards and the corresponding auto-oxidation products.

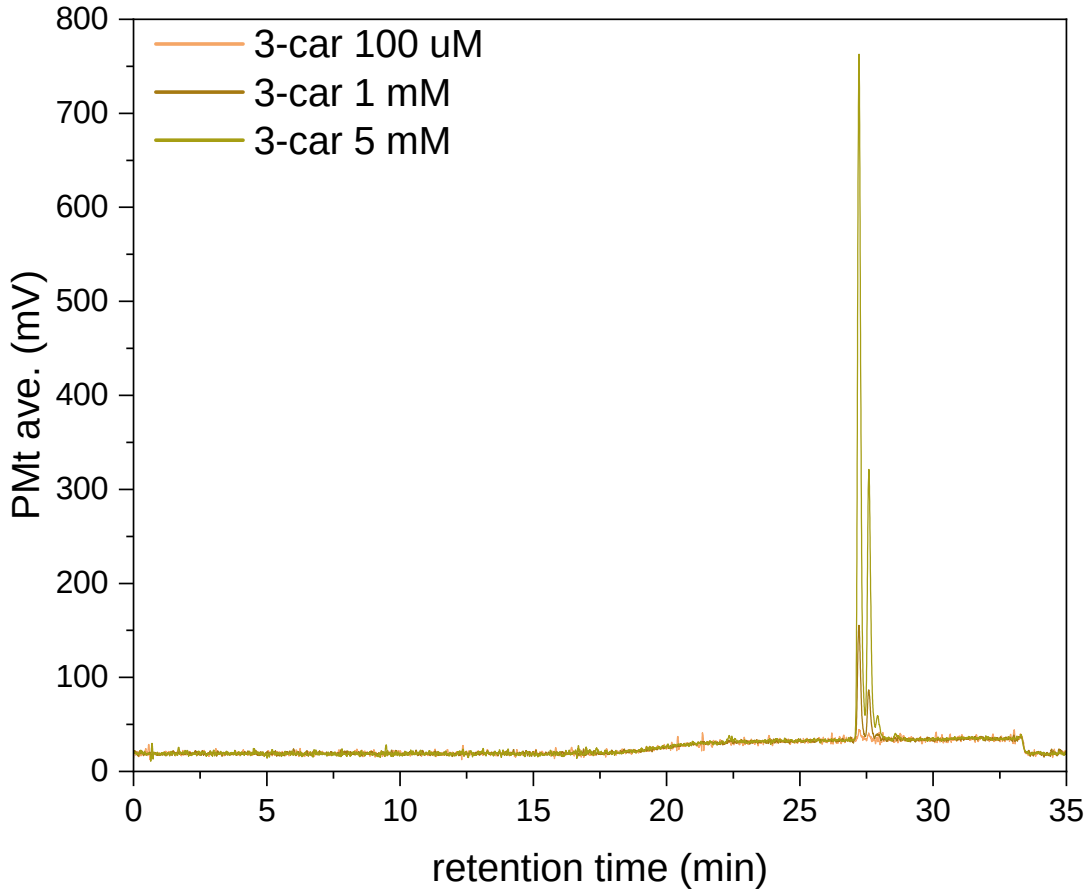

Figure D.14: Different concentrations of 3-carene Standards and the corresponding auto-oxidation products.

Comparison of HPLC-CL and Iodometry

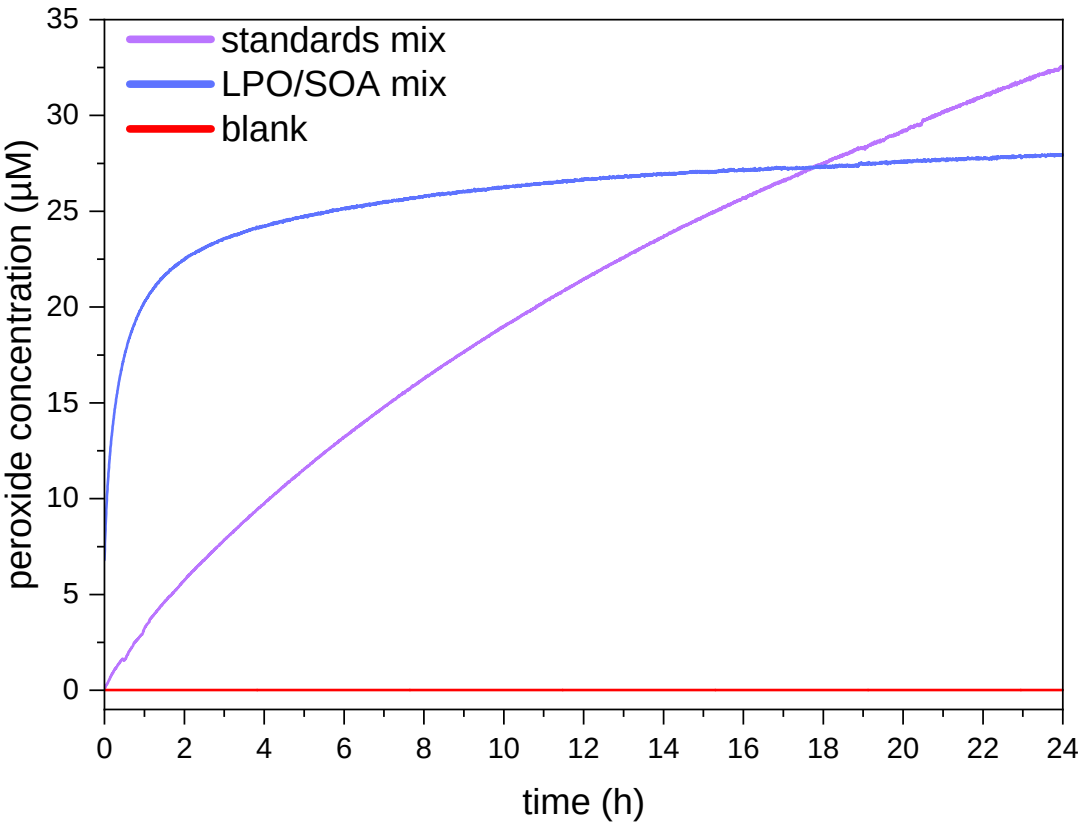

Figure D.15: Continuous UV absorbance measurements over 24 h. Standards mix (HP, tB-HP, mCPBA, and Cu-HP) and LPO/SOA mix (equal parts of α-pinene and 3-carene LPO and SOA samples mixed in one vial) were used. The LPO/SOA sample reaches a maximum after around 12 h, while the standards mix shows continuous increase, which is due to the tB-HP and its slow reactivity.

Table D.2: Peroxide concentration, determined through iodometry, and luminol chemiluminescence peak area of the different samples measured.

sample name	peroxide concentration (µM)	peak area
HP 2000 uM	2455.4 ± 0.1	167.8 ± 1.7
HP 1000 uM	1227.7 ± 0.1	67.6 ± 0.7
HP 500 uM	613.9 ± 0.1	24.3 ± 0.2
tB-HP 10000 uM	4680.8 ± 13.3	254.2 ± 2.5
tB-HP 5000 uM	2340.4 ± 13.3	99.8 ± 1
tB-HP 2500 uM	1170.2 ± 13.3	36 ± 0.4
Cu-HP 100 uM	107.9 ± 1.4	165.7 ± 1.7
Cu-HP 50 uM	54 ± 1.4	93.4 ± 0.9
Cu-HP 10 uM	10.8 ± 1.4	25.7 ± 0.3

Table D.2 continued from previous page

mCPBA 500 uM	468.4 ± 8.5	457.5 ± 4.6
mCPBA 100 uM	93.7 ± 8.5	152.9 ± 1.5
mCPBA 50 uM	46.8 ± 8.5	81.1 ± 0.8
mCPBA 10 uM	9.4 ± 8.5	9.2 ± 0.1
B-Per 200 uM	309.1 ± 3.4	251.4 ± 2.5
B-Per 100 uM	154.5 ± 3.4	170.7 ± 1.7
B-Per 20 uM	30.9 ± 3.4	44.4 ± 0.4
AP-NA 0 min	9.3 ± 0.7	75.6 ± 0.8
AP-NA 1 min	401.5 ± 0.5	342.7 ± 3.4
AP-NA 3 min	582.1 ± 1.2	412.6 ± 4.1
AP-NA 5 min	612.9 ± 1.1	371.6 ± 3.7
AP-NA 7 min	626.7 ± 0.8	361.7 ± 3.6
3CAR-NA 0 min	15.2 ± 0.6	25.3 ± 0.3
3CAR-NA 1 min	208.1 ± 0.7	84.8 ± 0.8
3CAR-NA 3 min	532 ± 1.1	138.6 ± 1.4
3CAR-NA 5 min	604.7 ± 0.8	147.4 ± 1.5
3CAR-NA 7 min	633.5 ± 0.3	151.2 ± 1.5
AP-F27a	15810.8 ± 2.3	12732 ± 127
AP-F27b	12409 ± 19.6	11897 ± 119
AP-F27c	13162.6 ± 22	11826 ± 118
AP-F28a	11958.1 ± 17.8	10825 ± 108
AP-F28b	11779.7 ± 2.3	11185 ± 112
AP-F28c	12914.9 ± 2.3	11507 ± 115
AP-F29a	8568.9 ± 3.3	7815 ± 78
AP-F29b	11324.3 ± 16.6	8450 ± 85
AP-F29c	10890.5 ± 3.3	8170 ± 82
AP-F30a	10027 ± 2.3	8119 ± 81
AP-F30b	9011.3 ± 2.8	8066 ± 81
AP-F30c	11390.1 ± 2.8	8121 ± 81
AP-F31	8810.8 ± 9.7	8356 ± 84
AP-F32	11679.7 ± 3.3	10404 ± 104
AP-F33	7795.5 ± 8.9	6168 ± 62
3C-F1a	7171.6 ± 3.6	7042 ± 70
3C-F1b	2323 ± 3.3	2085 ± 21
3C-F1c	2274.3 ± 3.3	2516 ± 25
3C-F2a	8475.7 ± 2.3	4809 ± 48
3C-F2b	8533.8 ± 9.7	9756 ± 98

Table D.2 continued from previous page

3C-F2c	9798.2 ± 2.8	9266 ± 93
3C-F3a	6109.9 ± 2.8	6818 ± 68
3C-F3b	6012.6 ± 6.1	6603 ± 66
3C-F3c	5201.4 ± 3.3	6107 ± 61
3C-F4a	7175.7 ± 7.4	7587 ± 76
3C-F4b	7308.1 ± 3.3	7646 ± 76
3C-F4c	5920.7 ± 2.8	7176 ± 72
3C-F5a	6560.2 ± 20	6938 ± 69
3C-F5b	7182 ± 0.6	7044 ± 70
3C-F5c	7165.8 ± 26.8	6551 ± 66
NA-F1a	1153.6 ± 1.2	180 ± 2
NA-F1b	1215.8 ± 1.2	239 ± 2
NA-F1c	1193.8 ± 2	278 ± 3
NA-3C-F1a	4257.4 ± 1.4	2861 ± 29
NA-3C-F1b	4744.7 ± 1.1	3252 ± 33
NA-3C-F1c	4496.1 ± 6.3	3373 ± 34

Table D.3: Peroxide mass fraction and moles of peroxide functional groups per mass of particle given (as recommended in [71]) for the SOA samples. The triplicates of each condition were averaged, errors are given as the standard deviation. The different conditions used to generate the samples are also given.

SOA sample	peroxide mass fraction (assuming M_W 200 for peroxides)	moles of peroxide functional group per mass of particle (µmol/mg)	generation conditions
AP-F27	24.5% ± 1.8%	1.23 ± 0.09	low VOC - no RH
AP-F28	24.7% ± 1.0%	1.23 ± 0.05	high VOC - no RH
AP-F29	23.1% ± 3.0%	1.15 ± 0.15	low VOC - RH
AP-F30	22.2% ± 2.0%	1.11 ± 0.10	high VOC - RH
3C-F1	10.1% ± 5.4%	0.51 ± 0.27	low VOC - no RH
3C-F2	21.0% ± 1.5%	1.05 ± 0.07	high VOC - no RH
3C-F3	18.7% ± 1.1%	0.93 ± 0.05	low VOC - RH
3C-F4	19.6% ± 1.6%	0.98 ± 0.08	high VOC - RH
3C-F5	25.2% ± 1.7%	1.26 ± 0.09	max VOC, lamps, RH
NA-F1	15.1% ± 1.7%	0.76 ± 0.08	max VOC, lamps, RH
NA-3C-F1	21.6% ± 1.3%	1.08 ± 0.06	max VOC, lamps, RH

Appendix E

XCMS Code for Untargeted LC-MS Data Analysis

The following script was used in RStudio 2022.07.01 (Boston, MA, USA) for the untargeted peak detection of the LC-MS data in the studies presented in this work.

```
## set the working directory first
## ensure appropriate packages are initialised and number of cores set
if (!require("BiocManager", quietly = TRUE))
install.packages("BiocManager")

BiocManager::install("xcms")

require(xcms)
require(ggplot2)
require(reshape2)
require(multtest)
require(ggpubr)
require(ggsignif)
require(pls)
library(BiocParallel)
register(SerialParam())

register(bpstart(SnowParam(8)))

## set the working directory to where the mzML files are stored
setwd("LOCATION_OF_FILES")
```

```
## get the list of mzML files in the working directory
fileList <- list.files(setwd(getwd()), pattern = "mzML")

## import all raw data
raw_data <- readMSData(files = fileList,
mode = "onDisk")

## set the peak detection settings - use centWave as data is centroided
## settings should be relatively standard for Vanquish + Q Exactive Plus
cwp <- CentWaveParam(peakwidth = c(2, 45),
mzCenterFun = "wMean",
noise = 200,
prefilter = c(3, 500),
mzdiff = 0.0001,
verboseColumns = TRUE,
extendLengthMSW = TRUE,
ppm = 5)

## detect the peaks in the raw data
xdata <- findChromPeaks(raw_data, param = cwp)

chromPeakData(xdata)

## merge peaks which elute within three seconds of each other - this will
## be artefactual rather than real splitting, 5s is the minimum peak separation
## for isomers
## set parameters:
mpp <- MergeNeighboringPeaksParam(expandRt = 3)
## merge peaks:
xdata_pp <- refineChromPeaks(xdata, mpp)

## filter peaks by intensity parameter, lets try and set this to 5E7

pip <- FilterIntensityParam(threshold = 5E7)
xdata_pip <- refineChromPeaks(xdata, pip)
```

```
# plotChromPeakImage(xdata_pp)

## retention time correction (using obiwarp method)
## may not be needed so best to check once finished, see EIC plotting below
xdata_rtcorr <- adjustRtime(xdata_pp, param = ObiwarpParam(binSize = 0.1))

## optional - plot the retention time correction
plotAdjustedRtime(xdata_rtcorr)

## select a peak for visualisation of RT correction
## in this case cis-pinonic acid and isomers
## select mass range to extract:
mzr <- 183.10 + c(-0.005, 0.005)
## select retention time to extract, can be changed:
rtr <- c(700, 800)

## pull EIC data for raw, peak refined and RT adjusted data
chr_raw <- chromatogram(xdata, rt = rtr, mz = mzr)
chr_pp <- chromatogram(xdata_pp, mz = mzr, rt = rtr)
chr_adj <- chromatogram(xdata_rtcorr, rt = rtr, mz = mzr)

## you will need to import a csv file with sample information here
## ensure the file names are in the same order as the initial fileList
## add a column called "runType" with sample info or change the code
## to reflect the column needed
metadata <- read.csv("METADATA.csv")
xdata$ sample_group <- metadata$ storage_temp
xdata_pp$ sample_group <- metadata$ storage_temp
xdata_rtcorr$ sample_group <- metadata$ storage_temp


## create colour list for plotting
## you will need to add more colours if there are more than five sample groups
getColours <- c("#17253f",
"#e69138",
"#ff53dc",
```

```
"#204cee",
"#ffd966")

## name the colours - change "coating x" to whatever sample groups you have
group.colors <- c("coating 0" = getColours[1],
"coating 1" = getColours[2],
"coating 2" = getColours[3],
"coating 3" = getColours[4],
"QC" = getColours[5])

## plot the EICs, wait for the plots to be fully visualised (up to 15s)
plot(chr_raw)
plot(chr_pp)#, col = group.colors[xdata_pp$ sample_group])
plot(chr_adj)

## backup the initial data extraction
backup_xdata <- xdata

## select the processed data to take forward - may or may not be RT corrected
## change as appropriate
## here changed xdata_pp into xdata_pip
xdata <- xdata_pip



## set peak grouping parameters
pdp <- PeakDensityParam(sampleGroups = xdata$ sample_group,
bw = 5, binSize = 0.001, maxFeatures = 100)

## group the peaks
xdata_grouped <- groupChromPeaks(xdata, param = pdp)

## fill in the peaks which have zero values (may still have zeros at the end)
xdata_filled <- fillChromPeaks(xdata_grouped, param = ChromPeakAreaParam())

## knit up the data for csv export
final_ds <- featureValues(xdata_filled, filled = TRUE)
```

```
final_ds <- as.data.frame(final_ds)
res <- quantify(xdata_filled, value = "into")
final_features <- do.call(cbind, res@elementMetadata@listData)
final_features <- final_features[,-which(colnames(final_features) == 'peakidx')]
final_features <- as.data.frame(final_features)
dataWithFeatures <- cbind(final_features, final_ds)
dataWithFeatures <- as.data.frame(dataWithFeatures)
df <- apply(dataWithFeatures,2,as.character)
for(h in 1:ncol(dataWithFeatures))
dataWithFeatures[,h] <- as.character(dataWithFeatures[,h])


write.csv(pd, "EXPORTFILENAME.csv")

## remove some of the unhelpful features - solvent front and re-equilibration
outsideRTrange <- c(which(final_features[,4] < 120), which(final_features[,4] >
1560))
final_ds <- final_ds[-outsideRTrange,]
final_features <- final_features[-outsideRTrange,]
final_features <- as.data.frame(final_features)

## tidy the data for export
pd <- as.data.frame(t(final_ds))
# final_features <- final_features[,-c(7:9)]
colnames(pd) <- paste0(round(as.numeric(final_features$ mzmed), 4),
"/",
round(as.numeric(final_features$ rtmed), 2))
rownames(pd)[grep("mzML", rownames(pd))] <- gsub(".mzML", "", rownames(pd))

## write the csv file
write.csv(pd, "FINAL_EXPORT_FEATURES.csv")
```

List of Abbreviations

Abbreviation	Description
$^{\bullet}$NO3	Nitrate Radical
$^{\bullet}$OH	Hydroxyl Radical
3-Car	3-Carene
AAHP	α-Acyloxyalkyl Hydroperoxides
ACN	Acetonitrile
AGC	Automated Gain Control
AMS	Aerosol Mass Sepctrometry
a-Pin	α-Pinene
Aux	Pump Auxiliary Pump
BC	Black Carbon
BPC	Base Peak Chromatogram
B-Per	Benzoyl Peroxide
BrC	Brown Carbon
CI	Criegee Intermediate
C-trap	Curved Linear Trap
Cu-HP	Cumene Hydroperoxide
CUV	Cuvette
Cyt c	Cytochrome C
DMSO	Dimethyl Sulfoxide
EIC	Extracted Ion Chromatogram
ESI	Electrospray Ionization
FT-ICR	Fourier-Transform Ion-Cyclotron-Resonance
FTIR	Fourier Transform Infrared Spectroscopy
GC	Gas-Chromatography
GC/LC-MS	Gas-/Liquid-Chromatography coupled to Mass Spectrometry
GC-MS	Gas Chromatography coupled to Mass Spectrometry
GCxGC	Two-Dimensional Gas chromatography
HILIC	Hydrophilic Interaction Chromatography
HOMs	Highly Oxidized Multifunctional Molecules
HP	Hydrogen Peroxide
HPLC	High-Performance Liquid Chromatography
HPLC-CL	High-Performance Liquid Chromatography Chemiluminescence
HRMS	High Resolution Mass Spectrometry

Abbreviation	Description
HRP	Horseradish Peroxidase
HULIS	Humic-like Substances
HVASs	High-Volume Ambient Aerosol Samples
ICD	In-Column Derivatization
KI	Potassium Iodide
LC	Liquid-Chromatography
LLOD	Lower Limit of Detection
LPO	Liquid-Phase Ozonolysis
m/z	Mass-to-Charge Ratio
MBTCA	3-Methyl-1,2,3-Butanetricarboxylic Acid
mCPBA	3-Chloroperbenzoic Acid
MeCN	Acetonitrile
MeOH	Methanol
MS	Mass Spectrometry
M_W	Molecular Weight
Nap	Naphthalene
NMR	Nuclear Magnetic Resonance Spectroscopy
O_2^-	Superoxide Radical
O_3	Ozone
OA	Organic Aerosol
OCU	Organic Coating Unit
OFR	Oxidation Flow Reactor
OM	Organic Matter
OP	Oxidative Potential
PAH	Polycyclic Aromatic Hydrocarbons
PC	Principal Component
PCA	Principal Component Analysis
PCD	Post-Column Derivatization
PILS	Particle Into Liquid Sampler
PM	Particulate Matter
$PM_{2.5}$	Fine Particulate Matter
PMT	Photomultiplier Tube
POA	Primary Organic Aerosol
ppm	Parts per Million
R	Mass Resolving Power
RH	Relative Humidity

Abbreviation	Description
ROS	Reactive Oxygen Species
RPC	Reversed-Phase Chromatography
RT	Retention Time
SOA	Secondary Organic Aerosol
tB-HP	Tert-Butyl Hydroperoxide
TIC	Total Ion Current Chromatogram
TOF	Time-of-Flight
UHPLC	Ultrahigh-Performance Liquid Chromatography
UV-VIS	Ultraviolet-Visible Spectroscopy
VOC	Volatile Organic Compound

List of Figures

List of Tables